



**UNIVERSITÀ DI PARMA**

**UNIVERSITA' DEGLI STUDI DI PARMA**

**DOTTORATO DI RICERCA IN "SCIENZA  
E TECNOLOGIA DEI MATERIALI"**

**CICLO XXXV**

**UPPER RIM FUNCTIONALIZED CALIXARENES:  
FROM DISSIPATIVE CONTROL TO BIOLOGICAL  
APPLICATIONS**

Coordinatore:

Prof. Enrico Dalcanale

Tutor:

Prof. Alessandro Casnati

Dottorando: Francesco Rispoli

2019-2022

# Contents

List of abbreviations .....	I
Abstract .....	II-III

## **Chapter 1:**

### **Dissipative control of the fluorescence of a 1,3-dipyrenyl calix[4]arene in the cone conformation**

Introduction .....	1
1.1 Movement in molecular machines.....	1
1.2 Energy supply .....	2
1.3 Calix[n]arenes .....	5
1.4. Conformational behaviour of calix[4]arenes.....	6
1.5 State-of-the-art in controlling calix[4]arene geometry by means of chemical fuels .....	9
1.6 Aim of this work.....	12
Results and discussion.....	16
1.7 Synthesis.....	16
1.8 Spectroscopic characterization.....	20
1.9 <sup>1</sup> H NMR and fluorescence titration with TFA.....	22
1.10 <sup>1</sup> H NMR and fluorescence studies with chemical fuels 8 and 10 .....	25
1.11 Conclusions.....	33
Experimental part.....	36
1.12 General information.....	36

## **Chapter 2:**

### **Temporal control of the host-guest properties of a calix[6]arene receptor by the use of a chemical fuel**

Introduction .....	49
2.1 Out of equilibrium systems.....	49
2.2 Self-assembly and dissipative self assembly.....	50
2.3 Host-guest chemistry.....	52
2.4 Host-guest systems controlled in a dissipative way by means of chemical fuels.....	53
2.5 Calix[6]arenes as a host in supramolecular chemistry.....	56
2.6 Aim of tis work.....	59
Results and discussion.....	62
2.7 Synthesis.....	62
2.8 <sup>1</sup> H NMR titration between calix[6]arene 5 and N-methyl isoquinolinium trifluoromethansulfonato 7.....	63
2.9 <sup>1</sup> H NMR titration between calix[6]aren 5 and TFA.....	67
2.10 Operation of 5 under dissipative conditions.....	71
2.11 Conclusion.....	81
Experimental part.....	83
2.12 General information .....	83

## **Chapter 3:**

### **Zwitterionic calix[4]arenes for bacteria cell wall detection**

Introduction.....	93
-------------------	----

3.1 Bacteria and their cell wall.....	93
3.2 Bacteria Detection.....	94
3.3 Calixarene-based ligands for biochemical application.....	100
3.4 Zwitterionic calix[4]arene ligands.....	103
3.5 Attachment of amino acids to calix[4]arenes by Mannich reaction.....	106
3.6 Saturation transfer difference (STD) NMR to study molecular interactions.....	109
3.7 Aim of this work.....	112
<b>Results and discussion.....</b>	<b>116</b>
3.8 Synthesis.....	116
3.9 STD NMR experiments.....	126
3.9.1 On-cell STD NMR experiments with ligands 1,2 and 3.....	127
3.9.2 STD NMR experiments with ligands 1,2 and 3 and LPS.....	131
3.10 Conclusion.....	132
<b>Experimental part.....</b>	<b>135</b>
3.11 General information.....	135
3.12 Bacterial strains and media.....	135
3.13 On-cell STD NMR experiments.....	135

## **Chapter 4:**

### **Calix[4]arenes-based ligands for protein surface recognition**

Introduction.....	148
4.1 Proteins.....	148
4.2 Multivalency.....	149
4.3 X-ray crystallography as a technique for the study of protein-ligand interactions.....	153
4.4 Calixarene-based multivalent ligands for proteins .....	157
4.5 Aim of this work.....	166
<b>Results and discussion.....</b>	<b>169</b>
4.6 Target proteins.....	169
4.6.1 Ralstonia solanacearum lectin (RSL): Carbohydrate binding proteins (CBS).....	169
4.6.2 Dimethylated Ralstonia solanacearum lectin (RSL-KMe2).....	170
4.7 The ligands.....	171
4.7.1 p-methylsulfonatocalix[4]arene.....	171
4.7.2 Zwitterionic calix[4]arenes .....	173
4.8 Crystallization tests between zwitterionic calix[4]arenes and RSL.....	175
4.9 Conclusion.....	191
<b>Experimental part.....</b>	<b>193</b>
4.10 Protein production.....	193
4.11 Stock solutions of the ligands and proteins.....	193
4.12 NMR spectroscopy.....	193
4.13 General experiment for the crystallization tests.....	194
4.14 SDS-PAGE.....	194
4.15 General procedure for the dimethylation of lysine residues on.....	194
4.16 X-ray diffraction and structure determination.....	195

## LIST OF ABBREVIATIONS

The following list reports the significance of various abbreviations and acronyms present in this thesis. In the case of non standard acronyms, used in some part or abbreviate names of particular cases are not in the list, but reported in the chapters.

Ar: Aromatic

DCM: Dichloromethane ( $\text{CH}_2\text{Cl}_2$ )

DMF: Dimethylformamide

DMSO: Dymethyl sulfoxide

ESI-MS: Electron Spray Ionization Mass Spectroscopy

EtOAc: Ethyl Acetate

NMR: Nuclear Magnetic Resonance

NOE: Nuclear Overhauser Effect

TFA: Trifluoroacetic acid

TLC: Thin Layer Chromatography

UV-VIS: Ultraviolet-visible spectroscopy

EtOH: Ethanol

MeOH: Methanol

$\text{NEt}_3$ : Triethylamine

PBS: Phosphate-buffered saline

SDS: Sodium dodecyl sulfate

RSL: *Ralstonia solanacearum* lectin

## Abstract of this thesis

The present thesis deals with the synthesis of upper rim functionalised calixarenes and the study of their properties under dissipative conditions or in biological media for the recognition of protein and bacteria cell wall constituents. These two apparently distant topics, artificial machines under dissipative control and biomolecular recognition might merge, in a close future, in artificial systems whose recognition properties toward biomolecules is triggered by a chemical fuel.

The first chapter of this thesis studies artificial molecular machines whose functions depend on the conformational changes experienced by the macrocycles under dissipative conditions. Among the chemical stimuli used for the modulation of the conformational motion we used 2-cyano-2-phenylpropanoic acid or trichloroacetic acid as chemical fuels. They allow to change the status of the system for a certain time and when all the fuel is consumed, the system turns back to its original state. The presence of two pyrene nuclei in distal positions at the upper rim of the calixarenes, allows to combine the fuel triggered conformational motion with the switch off/on of the fluorophore. The possibility of modulating the conformation of this calix[4]arene-based molecular machine using trichloroacetic acid as chemical fuel has been studied and the proposed “conformational cycle” will be discussed.

In the second chapter it was demonstrated that the host–guest interaction of a trisaminocalix[6]arene receptor with N-methylisoquinolinium trifluoromethanesulfonate can be dissipatively driven by means of 2-cyano-2-(4'-chlorophenyl)propanoic acid used as the most convenient chemical fuel. When the fuel is added to a dichloromethane solution containing the inclusion complex, the host is induced to immediately release the guest in the bulk solution. Consumption of the fuel allows the guest to be re-uptaken by the host.

In the third chapter it is reported the progress done in the development of a new approach for the selective identification of different bacterial strains using supramolecular receptors based on calix[4]arenes decorated with zwitterionic amino acids at the upper rim. Amino acids are attached to the upper rim of calixarenes, preserving their zwitterionic structure, using the Mannich reaction. The screening of the recognition properties of these calixarenes towards different bacteria strains was achieved using on-cell STD NMR experiments. The zwitterionic calixarene receptors are able to selectively bind Gram-negative bacteria. It was also evidenced that the selective recognition possibly takes place via recognition of LPS present on the Gram-

negative bacteria cell wall. The rapid and on-site identification of bacteria strains and viruses, using cheap, abiotic and portable devices, is of great appeal and interest also because it will allow a timely selection of the most appropriate antibiotic class to treat the patient, thus avoiding the administration of useless or broad-spectrum antibiotics which are responsible for the continuous and fast growth of antimicrobial resistance (AMR).

The last part of this thesis deals with the screening of zwitterionic calix[4]arenes and the p-methylsulfonatocalix[4]arene as molecular glues for proteins. This work has been carried out in a six-month study period at the University of Galway (IE). Surface recognition is shown to drive protein assembly in the solid state only in the case of the p-methylsulfonatocalix[4]arene. The preliminary results of the crystal structure obtained by SOLEIL synchrotron in Paris between this ligand and RSL-KMe<sub>2</sub> is discussed.

# Chapter 1

## **Dissipative control of the fluorescence of a 1,3-dipyrenyl calix[4]arene in the cone conformation\***

\*Part of this chapter is published on: *Organic & Biomolecular Chemistry*, **20** (1), 132–138.  
<https://doi.org/10.1039/D1OB02096J>

# Introduction

## 1.1 Movement in Molecular Machines

In Nature, movement is one of the most important attributes of life and a key characteristic in many technological processes. In living organisms there are some extremely complex systems formed over billions of years of evolution, called motor proteins, which work in the cell like ordinary machines. The structure and the functioning of these systems have been clarified only in a small number of cases. While artificial movement is provided by engines powered by electrical energy or combustion, in living organisms it is caused by machines and motors of molecular size that usually exploit the energy of chemical fuels at ambient temperature to generate forces and finally execute work. Among the most important motor proteins, the best known are those of ATP,<sup>1</sup> the kinesin,<sup>2</sup> and myosin<sup>3</sup> families and the bacterial flagellar motors.<sup>4</sup> In the past few decades, thanks to the progress in different areas of science and to the inspiration given by these bio-nanodevices, chemists have developed artificial systems able to exhibit directionally controlled and stimuli-induced movement of their parts. During the past thirty years, chemists have developed, built, and investigated a large number of molecular devices by exploiting electronic, photonic and chemical inputs to stimulate supramolecular systems<sup>5-12</sup>. The scientific value of this field has been recognized in 2016 thanks to the award of the Nobel Prize in Chemistry to Jean-Pierre Sauvage, Fraser Stoddart and Ben Feringa.<sup>13</sup> The Nobel Committee recognized the potential of molecular machine for progress in several areas of technology and medicine with applications limited only by imagination.<sup>14</sup> The term “molecular machine” refers to an assembly of a discrete number of molecules or supramolecule system which is able to perform a mechanical movement in response to an external stimulus. The most significant features of the nanoworld regarding movement, is the fact that molecular-sized objects are subject to the random motion caused by thermal energy (Brownian motion). Such random thermal fluctuations could preclude the controlled precision typical of machines. Motor proteins, however, use an external chemical energy source to influence thermal agitation and make the movement in a given direction



more likely than that in other directions. This principle is illustrated in Figure 1. Initially, a more stable state is destabilized by an input that brings the system in a non-equilibrium condition.

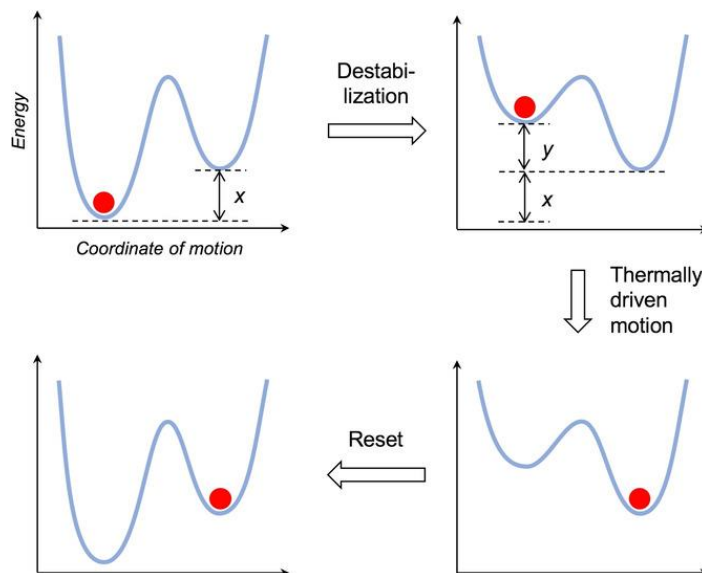


**Fig.1:** Schematic representation of the thermally driven motion of a system in relation to an energy input

After that, the thermal motion will push the system over the decreased barrier to reach the lower energy state. Hence, the thermal agitation causes the movement which is made directional by the input energy. Reset occurs when the energy input ends, or an opposite input is activated.<sup>15</sup> The study of motion in molecular machines is a fascinating topic and a promising field for a lot of applications.

## 1.2 Energy supply

As discussed in the previous paragraph, Brownian motion at thermal equilibrium cannot be exploited to achieve directed and controlled movement of a molecular machine. Thus, an external input of energy is necessary for a molecular machine to operate. Molecular machines are, like their macroscopic counterparts, characterized by:

- i. The type of energy input required to make them work
- ii. The type of movement (oscillatory, linear, rotatory...)
- iii. The function used monitor the movement
- iv. The possibility to repeat their movement

## v. The time taken to complete a cycle

The first point is probably the most important; one of the most obvious ways to supply energy to this kind of systems is through a reactant (“fuel”) that can perform an exergonic reaction. This is what happens in biomolecular machines<sup>16</sup> that usually are powered by ATP hydrolysis. In a molecular machine driven by chemical power, the fuel needs to be delivered where and when necessary. The reaction with the fuel will lead to the formation of wastes that could be accumulate in the reaction medium unless they are removed.

One more feature of chemically powered molecular machine is the way in which they utilize the fuel. After the reaction with the fuel, if the system has been brought into a new state of equilibrium, another reactant (“anti-fuel”) must be added to the solution to bring back the process and close the cycle as shown in Figure 2a. Hence, this operation requires the alternate addition of the two reactant and makes the working cycle operator dependent. In this case the machine is not capable of using the input of the fuel in autonomous way. This is what happen in artificial molecular machine developed until now which are, in fact, mechanical switches. An example of this kind of system is the paramagnetic [2]rotaxane shown in Figure 3a. This compound consists in two mechanically interlocked components: one nitroxide crown ether containing seven ethereal oxygen atoms and a cationic guest in which are present two different recognition sites, a dialkylammonium and 4-4'-bipyridinium site.<sup>17</sup>

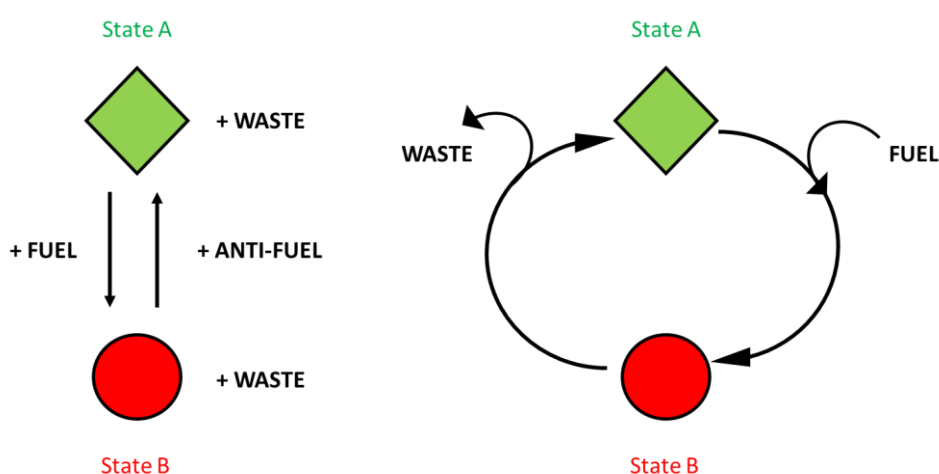


**Fig.2:** a) Schematic representation of molecular switches that use fuel and anti-fuel to change between two different equilibrium states. b) Autonomous chemically driven molecular machines that use the catalytic decomposition of the fuel to move between the two different states.

In this example, at the beginning (state A) the paramagnetic macrocycle is positioned at the ammonium site as a result of strong  $N^+ \cdots H \cdots O$  hydrogen bonds. The shuttling of the red macrocycle toward the secondary bipyridinium station is promoted by using an appropriate base, such as diisopropylethylamine. This base is strong enough to deprotonate the dialkylammonium site and, as a consequence, the platform loses affinity to this station and moves to the second one (State B) in which the complex is stabilized by charge-transfer interaction between the  $\pi$ -electron rich aromatic units of the paramagnetic macrocycle and the  $\pi$ -electron poor bipyridinium units. Upon addition of an acid, such as TFA, the ammonium sites are protonated again, allowing the return movement of the red macrocycle onto the preferred ammonium site. This motion can be repeated by the consecutive addition of a basic fuel and an acid anti-fuel. The one-shot addition of both these reactants to a solution containing the [2]rotaxane would lead to their annihilation.

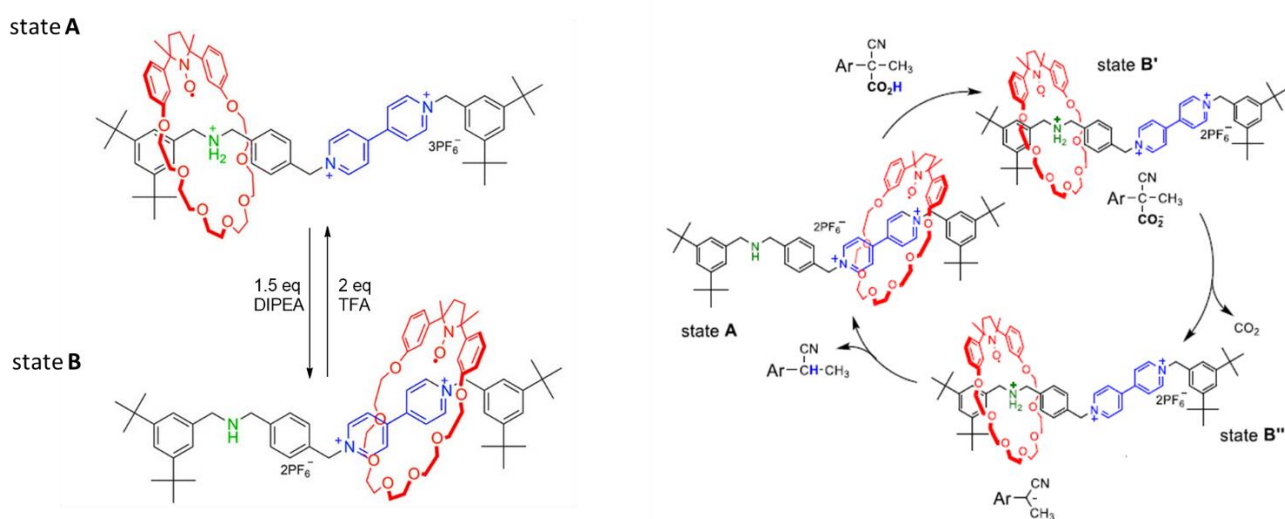


**Fig.3:** a) Shuttling of the paramagnetic macrocycle between the two different stations after addition of TFA to state A and after addition of DIPEA to state B. b) Schematic mechanism for the back-and-forth motions of paramagnetic rotaxane triggered by the chemical fuel 2-cyano-2-phenylpropanoic acids.

On the other hand, biomolecular machines are able to autonomously repeat their operation as long as the fuel is available Figure 2b. The reason why this is possible is because such systems use the fuel in a catalytic way; in fact, *state B* acts as catalyst for the fuel decomposition to waste. An example of an artificial supramolecular machine able to autonomously close the switching cycle with the addition of a single chemical fuel is shown in Figure 3b. The system

is the same [2]rotaxane shown above (Figure 3a) but in this case phenylpropionic acid is used to drive the switchable molecular shuttle.<sup>18</sup> When 1 equiv of acid fuel is added to the rotaxane in *state A*, the carboxylic acid donates a proton to the amine station and the red macrocycle shifts to the dialkylammonium station (*state B'*). The following decarboxylation produces the carbanion that, thanks to its high basicity, promptly re-extracts back the proton (*state B''*) and induces the crown ether to return to the initial bipyridinium station (*state A*). The [2]rotaxane thus acts as a catalyst for the base-promoted decarboxylation of the fuel and completes a mechanical switching cycle for each processed fuel molecule.

### 1.3 Calix[n]arenes

Metacyclophanes such as calixarenes, resorcinarenes, or pyrogalloarenes are a very interesting class of macrocyclic compounds. Their ability to act as receptors for a large variety of guest species, the easy way to tune their size, structure and functional groups attached make these scaffolds very promising in the field of supramolecular chemistry.<sup>19–28</sup> Among metacyclophanes, calixarenes are probably the most relevant for their use as components of molecular machine.

Calixarenes can be synthesized from the reaction between *para*-substituted phenol and formaldehyde in basic conditions. This family of macrocyclic compounds can have a variable number (between 4 and 20) of aromatic units linked by methylene bridges in *ortho* position. The most commonly used calixarenes, shown in Figure 4, are those made by 4–8 aromatic units and they can be synthesized by changing the solvent, the temperature, the base, and the ratio of the reactants used in the condensation reaction.<sup>29,30</sup>

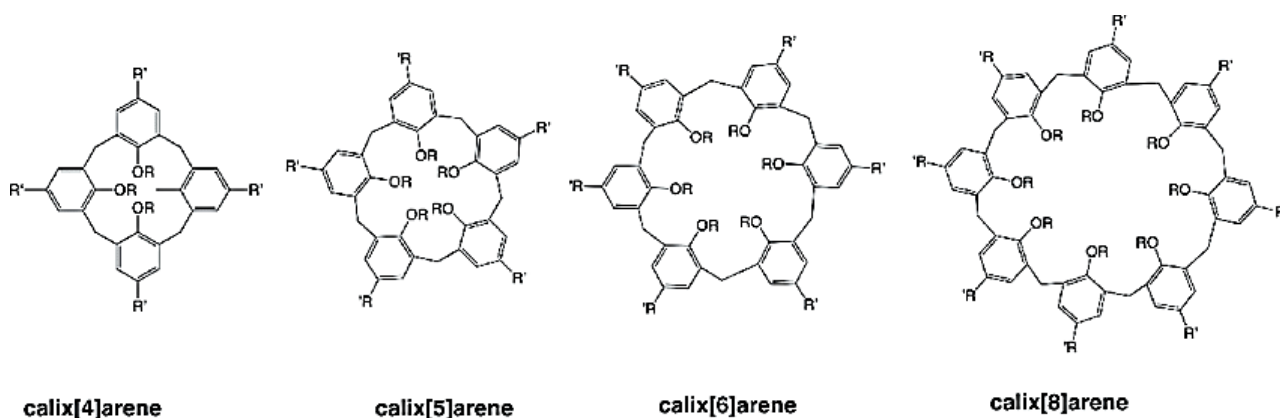


**Fig.4:** Calix[n]arenes with different valency ( $n=4,5,6$  and 8)

The term calixarenes was coined by Gutsche in 1978 and was inspired by the cup-like shape of the tetrameric derivative that resembles a Greek vase called *calyx krater*, in Latin. The suffix arene recalls the aromatic nature of the repeating units that form the macrocycle. As shown in Figure 5, it is possible to differentiate a lower rim, characterized by the presence of the hydroxyl groups, and an upper rim identified by the region containing the atoms *para* to the hydroxyl phenolic groups.

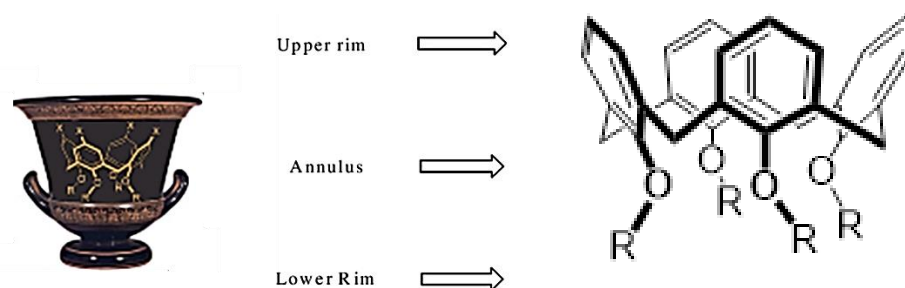


**Fig.5:** Example of *calyx krater* (left) Generic structure of a calix[4]arenes with indication of the lower and upper rim (right)

While calix[*n*]arenes with  $n > 5$  show high conformational mobility in solution, for the smaller homolog, calix[4]- and calix[5]arenes, the conformational behaviour is much more complicated. For the scope of this thesis we will restrict the discussion to the smaller calix[4]arenes, leaving the description of the conformational properties of calix[5]arenes to specialised literature.<sup>31-33</sup>

## 1.4 Conformational behaviour of calix[4]arenes

Calix[4]arenes have been widely used as abiotic scaffolds in Supramolecular Chemistry and most of their supramolecular properties depend on the conformational features of their scaffold. Tetrahydroxycalix[4]arenes, both at the solid state and in solution, are kept in a *cone* conformation by the establishment of a strong homodromic intramolecular hydrogen bond network between the phenolic hydroxyl groups. All the four phenolic aromatic nuclei form equal angles with the average plane defined by the four methylene bridge carbon atoms and a tridimensional  $\pi$ -rich cavity is well defined. The molecule has a  $C_{4v}$  symmetry, and this conformation is also named *regular cone*. Increasing the temperature, the rotations around

the C-C  $\sigma$ -bonds of the methylene bridges allow for a ring flipping (cone to cone inversion) as shown in Figure 6.

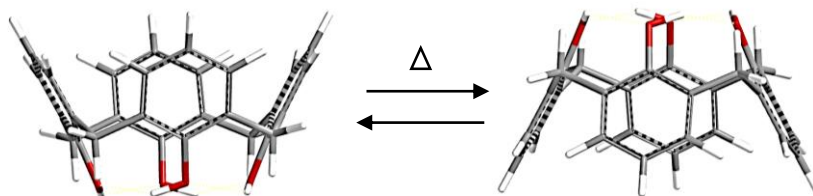


**Fig.6:** Ring flipping in Tetrahydroxycalix[4]arenes

When the hydroxy groups present at the lower rim are functionalised with R groups, in addition to the already mentioned *cone*, calix[4]arenes can exist also in three other limiting conformations identified as *partial cone*, *1,2-alternate* and *1,3-alternate*<sup>34</sup> characterized by different orientations of the aromatic rings, as shown in Figure 7. When R groups have a limited steric hindrance compared to the dimension of the calixarene annulus, *i.e.*  $R \leq \text{CH}_2\text{CH}_3$ , calix[4]arenes are conformationally mobile. On the other hand, when R groups larger than ethyl are introduced, the macrocycle can be locked into one (or a mixture) of the four conformations.

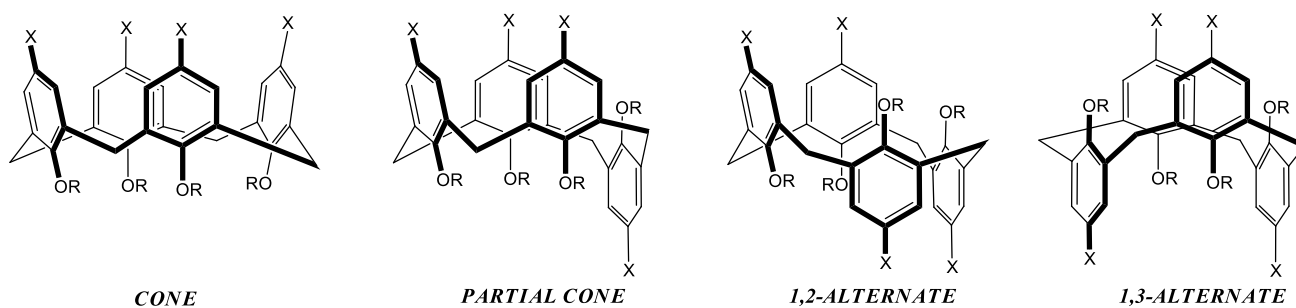


**Fig.7:** The four limiting conformations adopted by calix[4]arenes ( $R > \text{CH}_2\text{CH}_3$ )

The adopted conformation can be easily identified using  $^1\text{H}$  NMR spectroscopy, since each structure gives rise to a very typical pattern of signals for the protons of the methylene bridge. In fact, in the case of a *cone* calix[4]arene, these methylene groups are equivalent (being related by a  $C_{4v}$  symmetry axis) but the two protons of each bridge are diastereotopic as shown in Figure 8: taking the average plane of the annulus as a reference, one is nearly parallel and is called *equatorial*, while the other is nearly perpendicular and is called *axial*. These two protons thus show two doublets in the  $^1\text{H}$  NMR spectra with a typical geminal coupling

constant ( $J=13-16$  Hz). The *equatorial* protons are upfield shifted compared to the *axial* ones due to the shielding effect of the aromatic nuclei. On the other hand, in the *partial cone*, *1,2-alternate* and *1,3-alternate* conformations, some of the aromatic nuclei are oriented *anti* one to the other and the two protons of the bridge comprised among them are chemically equivalent giving rise to a singlet in the  $^1\text{H}$  NMR spectrum.

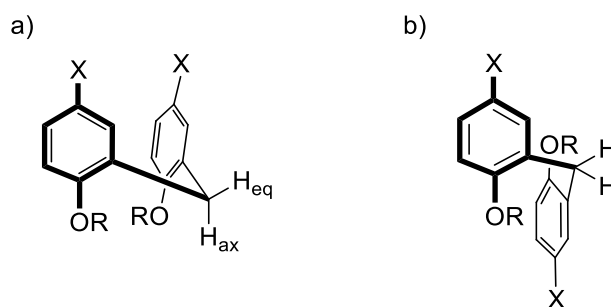


**Fig.8:** Proton disposition in the methylene bridges between two aromatic rings oriented a) *syn*, the same direction or b) *anti*, in opposite direction

A calix[4]arene blocked in the *cone* geometry, even if functionalized at the lower rim with four bulky R groups, can rapidly interconverts between two equally stable *pinched cone* conformations as a result of the swinging of the aromatic rings around the carbon atoms of the bridge. Consequentially, the *regular cone* conformation of  $C_{4v}$  symmetry, can be considered as the transition state of the interconversion between the two limiting *pinched cone* conformations, that are equally stable and have  $C_{2v}$  symmetry<sup>35</sup> as shown in Figure 9. The interconversion between these two limiting structures, often called “*breathing of the calix*”, is fast compared to the NMR timescale, thus the  $^1\text{H}$  NMR spectrum reflects the  $C_{4v}$  symmetry as an average between the  $C_{2v}$  *pinched cone* conformations. Moreover, when a tetraalkoxy calix[4]arene, is functionalized at the upper rim with two substituents in 1,3-distal positions, this equilibrium is usually fixed in one of the two possible *pinched* structures as a result of attractive or repulsive interactions between the upper rim distal substituents as shown in Figure 10.

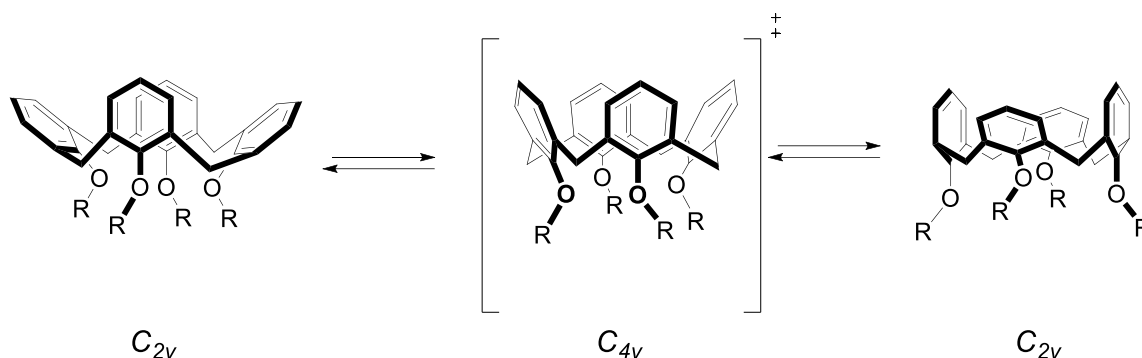


**Fig.9:** Residual mobility in the conformation of a cone calix[4]arene (“breathing of the calix”)

Typically, the conformation with the para-substituted aromatic rings pointing outwards is called *open pinched cone* conformation. On the other hand, in case of attractive interactions between the substituents, the two para-substituted aromatic rings come closer (nearly parallel each to the other) and the conformation adopted by the calix[4]arene is called “*closed pinched cone*” conformation.

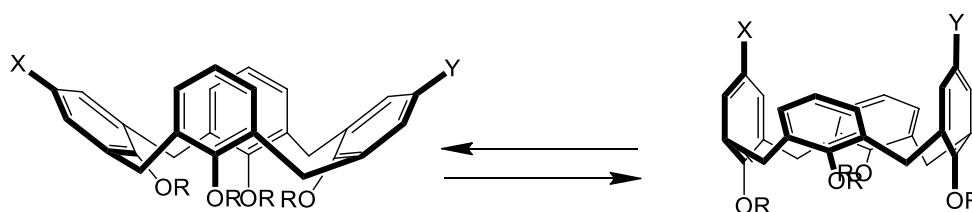


**Fig.10:** Open (left) and closed (right) pinched cone conformation of 1,3-para-substituted calix[4]arene

The ability to form intramolecular interactions among the para-substituents, the solvent used and the presence of potential guests may modulate the calix[4]arene *pinched cone* equilibrium towards the closed or open conformation.

## 1.5 State-of-the-art in controlling calix[4]arene geometry by means of chemical fuels

In nature, one of the most used tools to control chemical properties is the modulation of the conformation of complex molecular architectures. Among them, chemically induced conformational changes are employed to modify binding capability or catalytic activity in proteins. In case of man-made supramolecular systems, important examples of chemically induced conformational control of properties and reactivity have been reported, mainly based on molecular machines.<sup>36–52</sup> Among them, our attention was directed to systems that exploit a chemical fuel to drive a conformational change.<sup>53–66</sup> In these cases, the changes of the



conformation from *state A* to *state B* ( $A \rightarrow B$ ) and the variation of their chemical properties are carried on as long as the fuel is available. As soon as the fuel is exhausted, the system reverts to its original state ( $B \rightarrow A$ ) and chemical properties change again. In 2020, our research group, in collaboration with professor Di Stefano's group at the Roma University "La Sapienza", reported the use of a chemical fuel to conveniently control the conformational equilibrium of the diamino-calix[4]arene shown in Figure 11.<sup>67</sup>

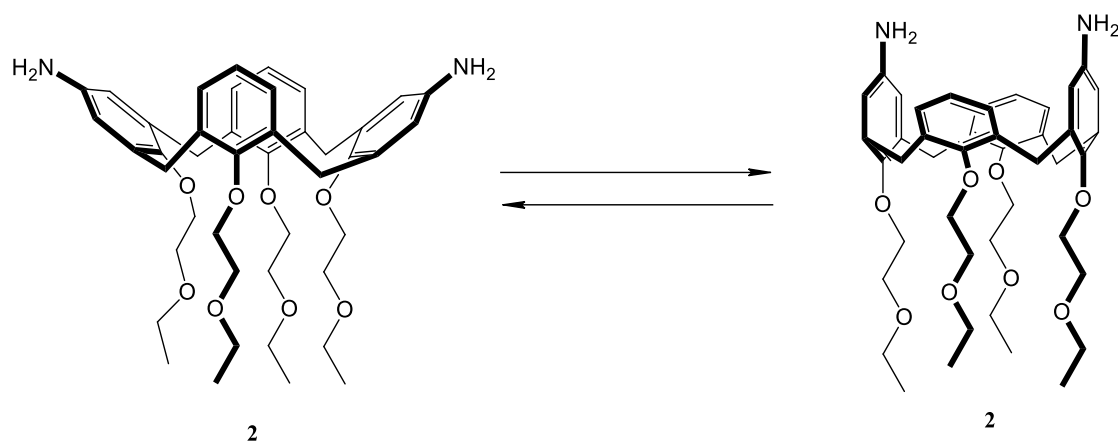


**Fig.11:** Conformational interconversion between the open and closed pinched cone conformation of 1,3-distal diaminocalix[4]arene (*unlocked state*)

As chemical fuel, it was employed the 2-cyano-2-phenylpropanoic acid and its derivatives, previously used as chemical fuels to control the movement of acid-base operated molecular machine.<sup>68-72</sup>

In the basic form, the so called "*unlocked*" state represented in Figure 11, calix[4]arene **2** is in a mobile situation where it is free to interconvert between the two nearly equally stable *pinched cone* conformations. In the presence of one equivalent of the acid fuel (**1**), monoprotection of compound **2** results in the conjugated acid  $2H^+$ . The intramolecular hydrogen bond forces the calixarene conformation in a "*locked*" state (*closed pinched cone*) with the two aniline rings convergent to share the proton as shown in Figure 12.

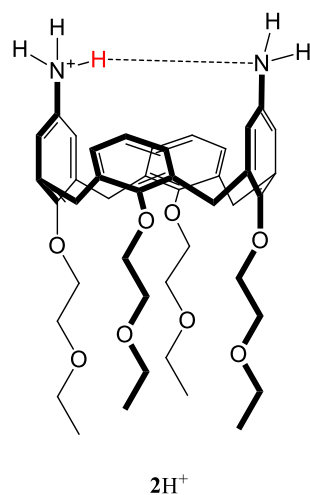


**Fig.12:** Intramolecular hydrogen bond in conjugated acid  $2H^+$  (locked state)

When the fuel is exhausted, the calixarene reverts to its original “unlocked” state. This design is illustrated in Figure 13

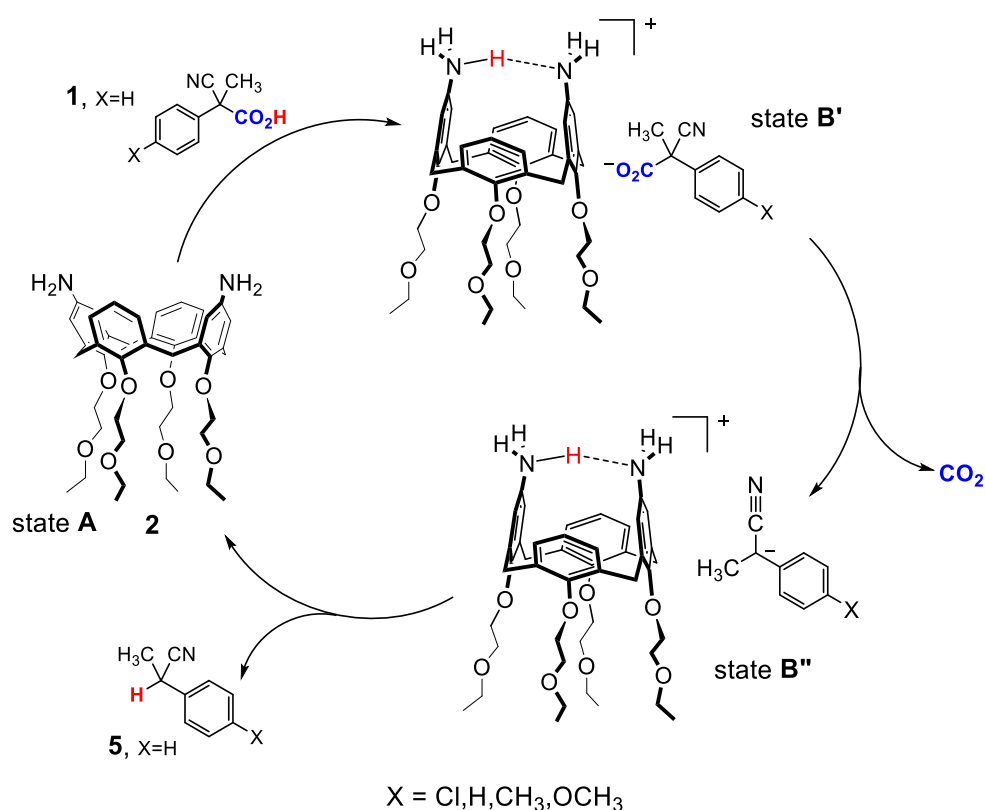


**Fig.13:** Proposed “conformational cycle” experienced by diaminocalix[4]arene **2** under the action of fuels

Addition of 1 mol equivalent of fuel **1**, H immediately causes a series of shifts in the  $^1\text{H}$  NMR spectrum, due to the protonation of **2** (Figure 14). In fact, aromatic signals marked in red (para unsubstituted) and blue (para-amino substituted) are shifted towards lower and higher fields, respectively. This proves the formation of an ion pair in the *state B'*, with the calixarene scaffold assuming a rigid *pinched-cone* conformation (“*locked*” state). In this conformation, the two amino functionalized aromatic rings are nearly parallel to each other as a consequence of the intramolecular hydrogen bond and experience the shielding effect of the other two ring facing outwards. From 3 minutes on, decarboxylation and fast back proton transfer regenerate the native unlocked cone conformation. At the end of the process ( $t = 245$  min), the solution only contains calixarene **2** in *state A* and the waste product **5**.

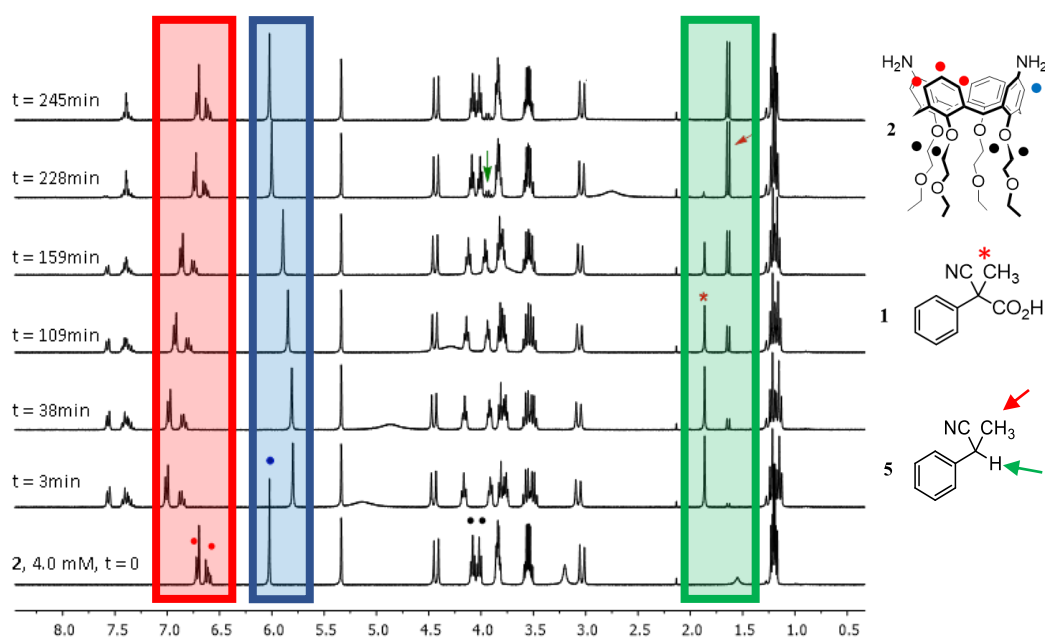


**Fig.14:**  $^1\text{H}$  NMR time-monitoring of the reaction between 4.0 mM **2** and 4.0 mM fuel **1**, H, in  $\text{CD}_2\text{Cl}_2$  at 25  $^\circ\text{C}$ . The bottom trace is the spectrum of 4.0 mM **2** taken before the addition of the fuel

## 1.6 Aim of this work

With the aim of studying the conformational locking/unlocking mechanism using chemical fuels we decided to synthesize compound **6**, similar to compound **2** but adorned with two additional pyrene units at the upper rim, as shown in Figure 15a.

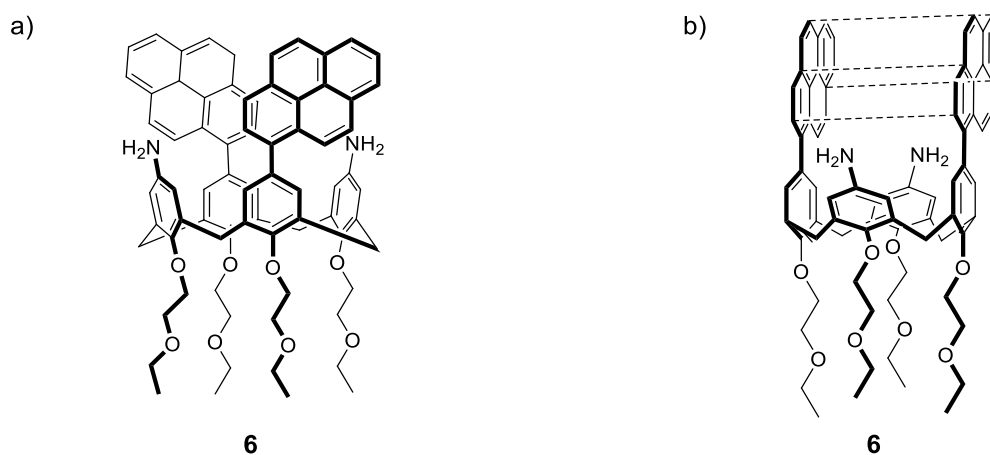


**Fig.15:** a) Chemical structure and b)  $\pi$ - $\pi$  interactions between pyrene functions of compound **6**

The two pyrene groups of compound **6** have the purpose of inserting a further conformational control mechanism as they could interact with each other through  $\pi$ - $\pi$  interactions and therefore block the conformation of the calix[4]arene as shown in Figure 15b. Moreover, the presence of the two pyrene functions would allow to study the conformational mechanism also through fluorescence spectroscopy. This is due to the fact that when the pyrenes are involved in the intramolecular interaction, the typical excimer emission band would appear in the fluorescence spectrum<sup>73</sup> as shown in Figure 16. The excimer fluorescence has a substantially longer wavelength than the monomer emission.

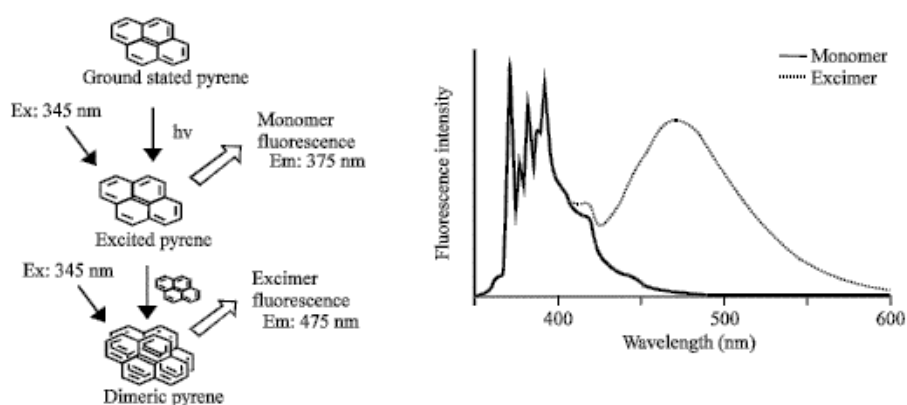


**Fig.16:** Interaction mechanism leading to the formation of an excimer (left). Typical fluorescence emission spectrum (right) of the pyrene monomer and excimer

Therefore, the idea behind our hypothesis is that when the calixarene conformation is “unlocked”, the two pyrene units are allowed to get close together and the fluorescence spectrum would be characterized by the excimer emission. On the other hand, the addition of a fuel acid would trigger a first conformational change to the “locked” pinched-cone structure.

In this state, the interactions between the two amino groups would prevail, and the two chromophores would be forced far apart, thus turning off the excimer fluorescence as shown in Figure 17.

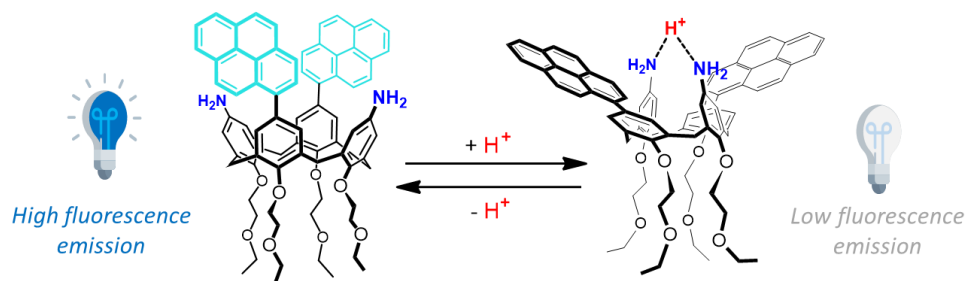


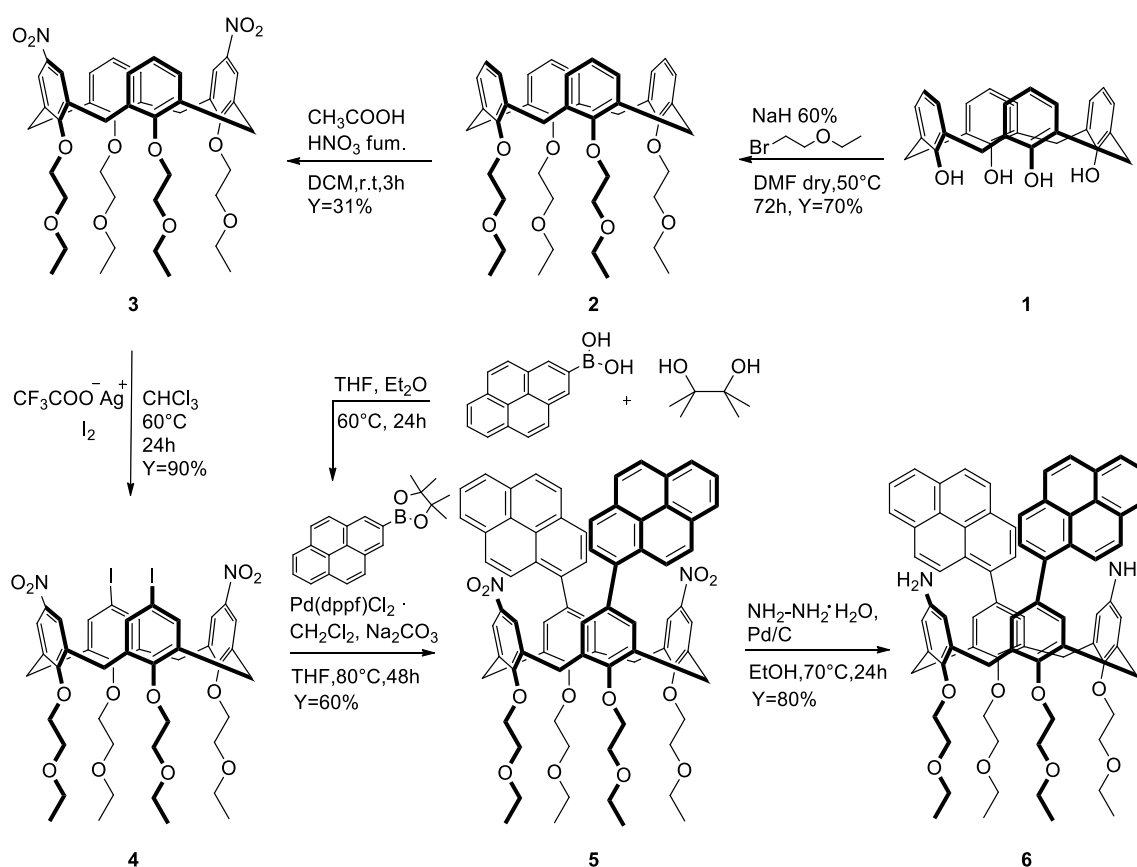
**Fig.17:** Schematic representation of the excimer formation in molecular machine **6**



# Results and Discussion

## 1.7 Synthesis

Calix[4]arene **6** was synthesized in five steps from tetrahydroxy calix[4]arene **1** (Scheme 1). The synthesis of compounds **1-4** are already known in literature and the described protocols were followed.<sup>74</sup>

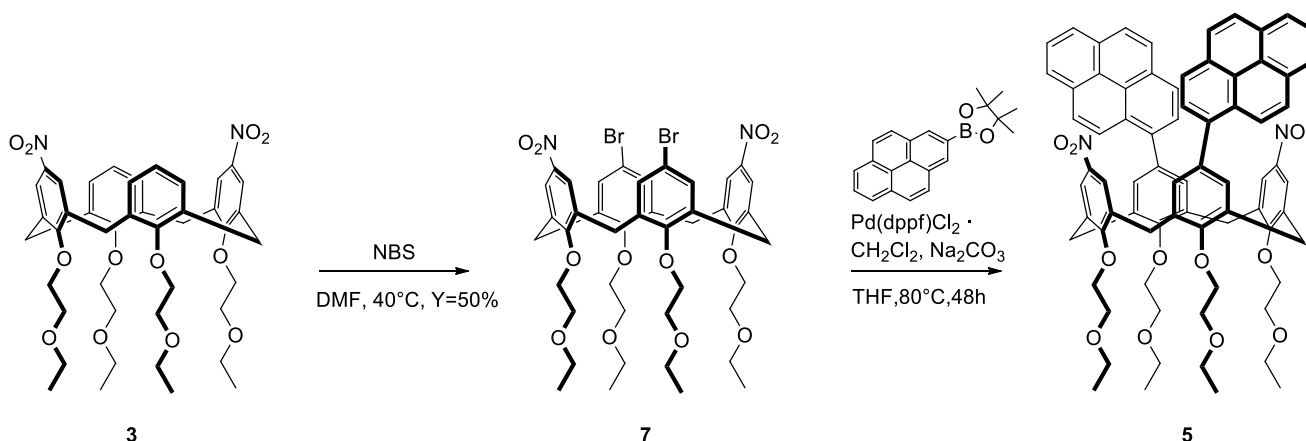


**Scheme 1:** Synthetic strategy for the synthesis of compound **6**

Starting from 25,26,27,28-tetrahydroxy calix[4]arene **1**, the first step was the alkylation of the hydroxyl groups, using NaH as a base for the deprotonation of the phenolic ring and 2-bromoethyl ethyl ether as alkylating agent. The four 2-ethoxyethoxy groups at the lower rim guarantee that the structure maintains its cone conformation ensuring also the solubility in a wide range of solvent. The second step was the nitration of compound **3**, using fuming  $\text{HNO}_3$  and acetic acid as nitrating agent. Due to the equivalence of the four reactive positions of the

upper rim of compound **2**, the nitration reaction leads to the formation of a mixture of different nitrated by-products. To minimize the formation of tri and tetra nitrated products, the reaction, monitored by TLC, was quenched after 3 hours. The crude product was then purified by a flash chromatography column to separate the unreacted reagent and the mono nitrated compound from the 1,3-dinitrated compound **3** and its regioisomer, the 1,2-dinitrated calixarene. Finally, the 1,3-distal dinitro compound was separated from the 1,2-vicinal by crystallization in methanol to give the pure compound **3** as colourless needles.

To attach the pyrene units at the calixarene upper rim we planned to exploit the Suzuki *cross-coupling* reaction. The first strategy tested for obtaining derivative **5**, illustrated in scheme 2, involved the use of compound **7** as a reagent. This derivative was prepared using NBS as a source of bromine in DMF.



**Scheme 2:** First strategy for the synthesis of compound **5**

Derivative **7** was then used as a substrate for the Suzuki reaction using the 4,4,5,5-tetramethyl-2-(pyren-1-yl)-1,3,2-dioxaborolane as coupling partner with Pd(dppf)Cl<sub>2</sub> as a catalyst. The reaction was carried out in refluxing toluene for 24 hours in an inert atmosphere to avoid oxidation of the catalyst. Unfortunately, the reaction did not lead to the obtainment of the desired product. In fact, <sup>1</sup>H-NMR analysis of the crude product revealed the presence of different species in solution, which could not be identified. To try to foster the Suzuki reaction it was decided to use a more reactive dihalogen calixarene and therefore we decided to synthesize the di-iodo compound **4**. The addition of iodine should increase the reactivity in oxidative addition compared to bromine. Compound **4** was then synthesized according to literature protocol. The reaction was performed using silver trifluoroacetate and I<sub>2</sub> in chloroform (Scheme 1). After heating at reflux for 24h, the reaction mixture was filtered to eliminate the AgI that forms during the reaction. After several washing with sodium



thiosulfate, the organic phase was dried to give **4** as a yellow solid in high yield. Derivative **4** was then used for the Suzuki reaction using the same conditions adopted for compound **7**. In a Schlenk tube, under argon atmosphere, Pd(dddpf)Cl<sub>2</sub>, compound **4** and 4,4,5,5-tetramethyl-2-(pyren-1-yl)-1,3,2-dioxaborolane were dissolved in THF. Then 1.35 mL of 2 M solution of Na<sub>2</sub>CO<sub>3</sub> was added and the reaction was stirred at 80 °C for 48 h. After purification by flash chromatography column compound **5** was obtained as a pale-yellow solid in a 60% yield. Calix[4]arene **5** was fully characterized by 1D <sup>1</sup>H and <sup>13</sup>C NMR, 2D (COSY, HSQC, NOESY) and ESI mass spectrometry. The <sup>1</sup>H NMR spectra at room temperature of **5** both in CDCl<sub>3</sub> (Figure 1) and in toluene-d<sub>8</sub>, are characterized by relatively sharp peaks for the calixarene protons and broad ones for the protons of the pyrenyl units, indicative of a hindered rotation of these groups around the calixarene-pyrene C-C bond. In this case, the calixarene **5** adopts in solution a pinched cone conformation with the aromatic calixarene nuclei bearing the fluorophores nearly parallel because of a strong π-π interaction between the two pyrenyl units. The signal of the protons ortho to the pyrenyl groups is high-field shifted (singlet at 6.83 ppm) due to the shielding effect of the nitro-substituted, outward-oriented aromatics (that give a singlet at 8.21 ppm).<sup>75,76</sup>

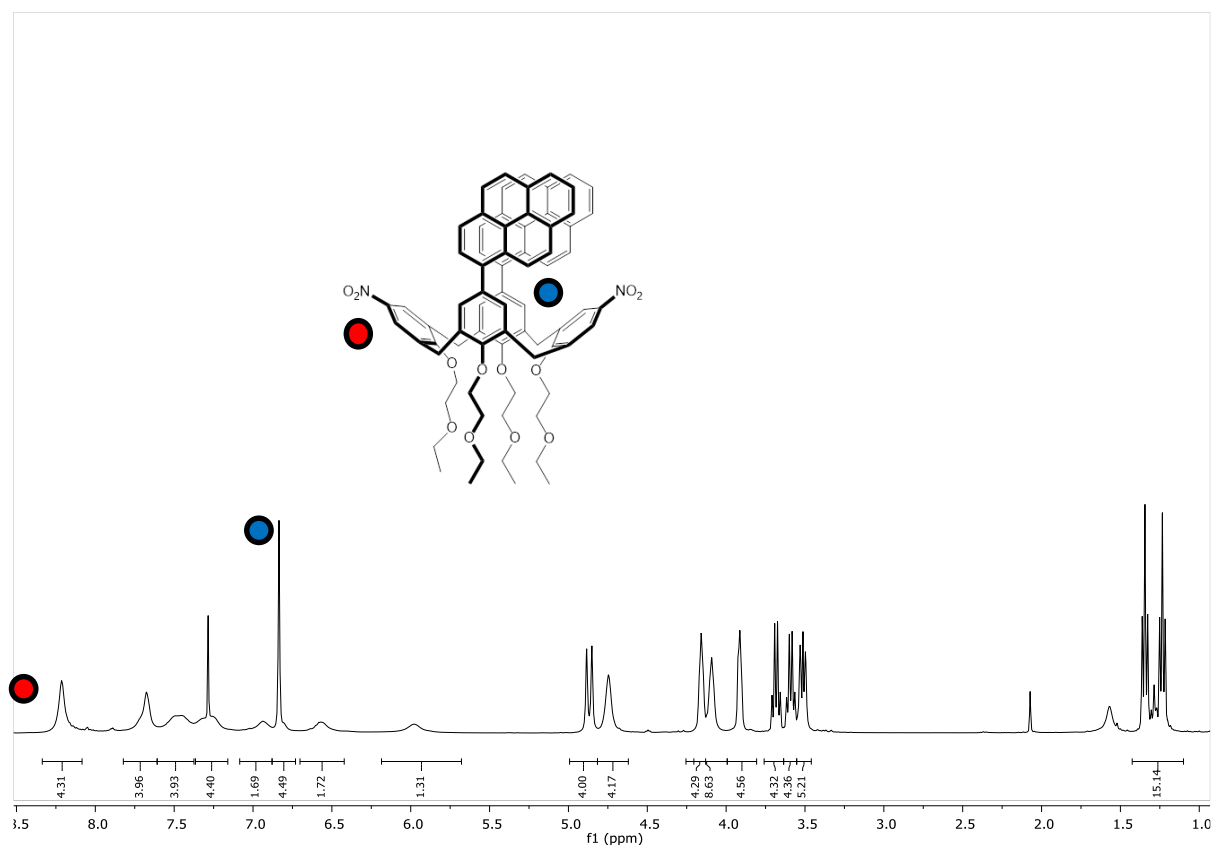
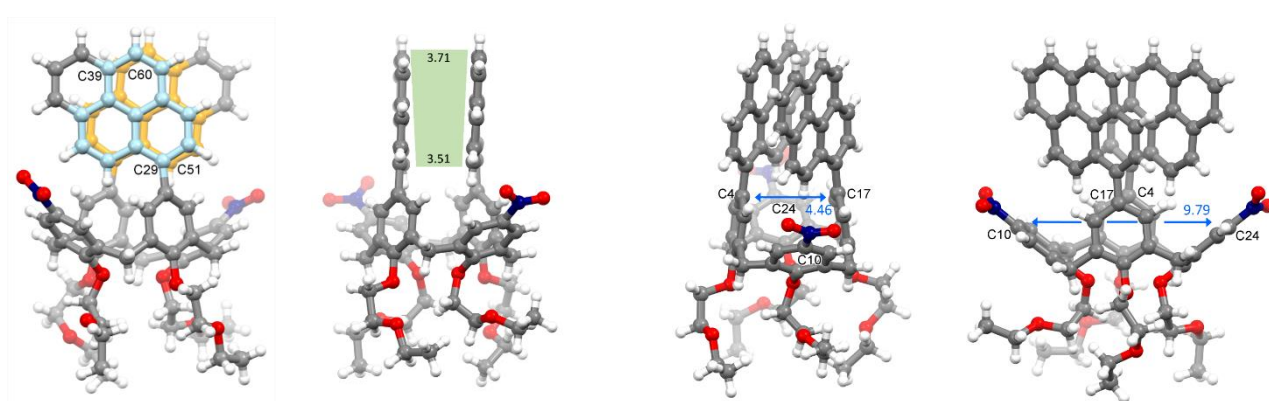


Fig. 1: <sup>1</sup>H NMR (400 MHz, CDCl<sub>3</sub>) of compound **5**

The XRD analysis performed on a single crystal of **5** grown from acetone displays a pinched cone conformation similar to that present in solution. The molecular structure (Figure 2) shows the partial  $\pi$ - $\pi$  stacking between the two aromatic fragments. The partial overlap involves three (colored in yellow and cyano) out of four aromatic rings of each pyrene moiety. The two pyrene units are slightly divergent with the closest contact between the C(29) and C(51) atoms (3.51 Å), whereas the longest one is between the C(39) and C(60) atoms (3.71 Å). The intramolecular distance between C(4) and C(17) is of 4.46 Å, whereas C(10) and C(24) are separated by 9.79 Å.



**Fig. 2:** XRD *solid state molecular structure of calix[4]arene 5*

The last step of the synthesis to obtain the final product **6** is the reduction of the two nitro group of derivatives **5**. The reaction was carried out in ethanol, using hydrazine hydrate as a source of hydrogen and Pd/C as a catalyst. The reaction was refluxed for 24 hours, and after filtration of the catalyst, the pure product was obtained with an 80% yield. Calix[4]arene **6** was fully characterized by 1D  $^1\text{H}$  and  $^{13}\text{C}$  NMR, 2D (COSY, HSQC, NOESY) and HR mass spectrometry. In the  $^1\text{H}$  NMR spectrum of **6** in different solvents ( $\text{CDCl}_3$ ,  $\text{CD}_2\text{Cl}_2$ ,  $\text{CD}_3\text{OD}$ ,  $\text{CH}_2\text{Cl}_2/\text{CH}_3\text{CN}$  (1:1) and toluene- $d_8$ ) the signals of the pyrene protons are always quite broad, while the calixarene peaks remain sharp, suggesting, also for this compound, the presence of a  $\pi$ - $\pi$  interaction between the pyrene units.

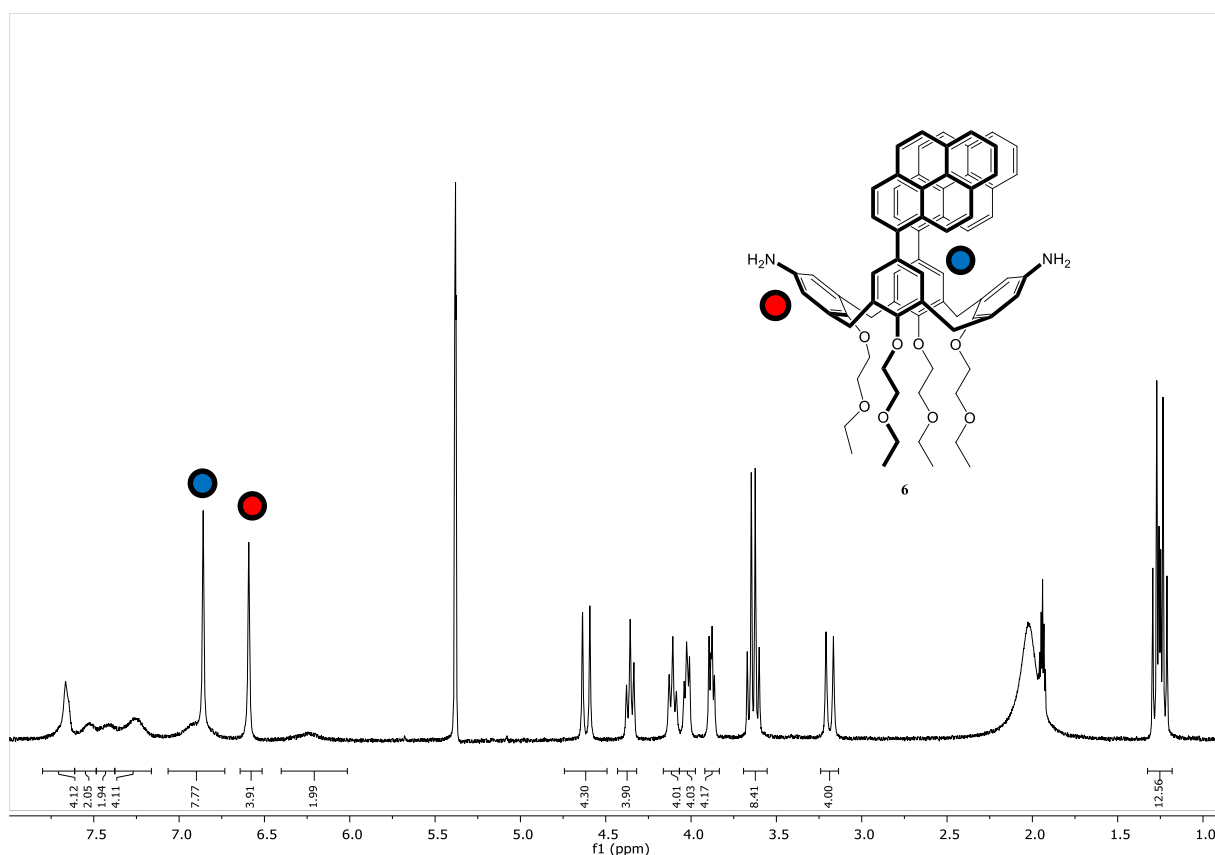


**Fig. 3:**  $^1\text{H}$  NMR (400MHz,  $\text{CD}_2\text{Cl}_2/\text{CH}_3\text{CN}$ ) of compound **6**

As expected, the main difference with the  $^1\text{H}$  NMR spectrum of compound **5** is the disappearance of the signal at 8.21 ppm ( $\text{ArNO}_2$ ) and appearance at higher fields (6.59 ppm) of the signal related to the protons ortho to the amine group ( $\text{ArNH}_2$ ) as a consequence of the  $\text{NO}_2$  to  $\text{NH}_2$  reduction.

## 1.8 Spectroscopic characterization

Calix[4]arenes **5** and **6** were studied by absorption and steady-state fluorescence spectroscopy. The absorption spectra were collected in  $\text{CHCl}_3$  while the fluorescence spectra in a 1/1 mixture of  $\text{CH}_2\text{Cl}_2/\text{CH}_3\text{CN}$  as shown in Figure 4. It is already known in the literature that nitroaromatic compounds are often used as fluorescence quenchers.<sup>77–80</sup> In the fluorescence emission spectrum of compound **5**, it can be seen that the excimer band is not present, probably due to an electron/charge transfer mechanisms.<sup>81–85</sup>

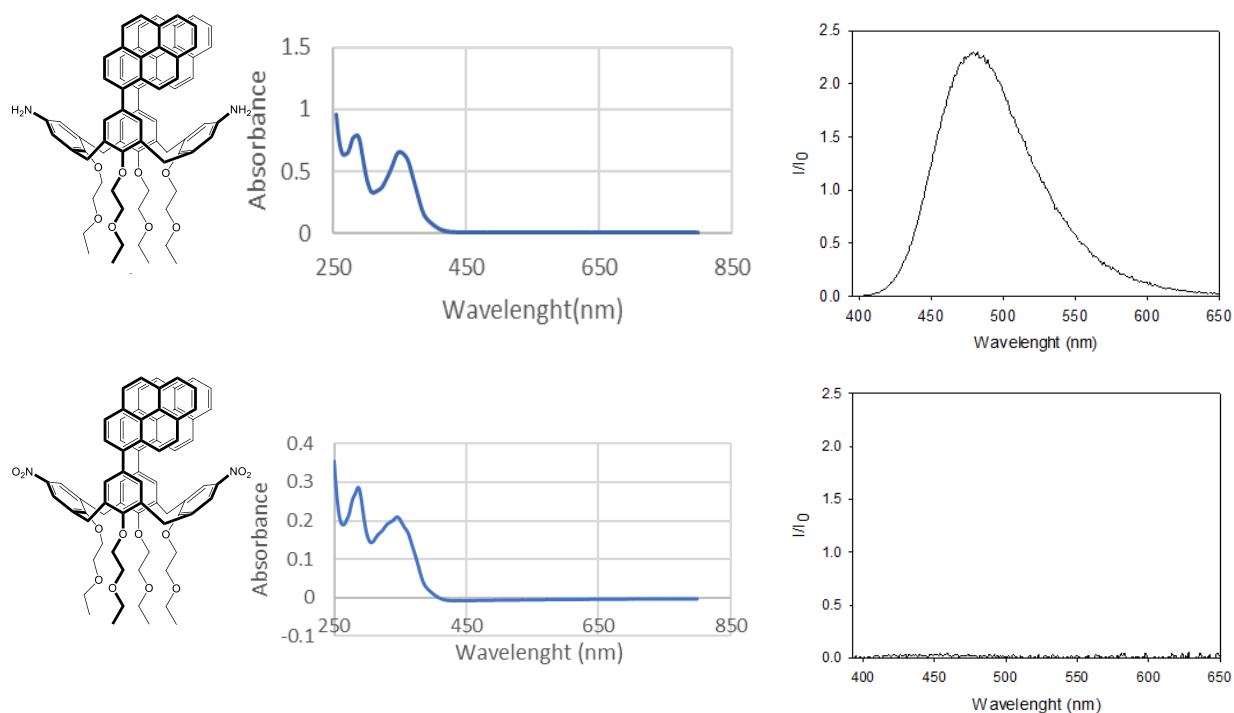


**Fig. 4:** Fluorescence (top right) and absorption (top left) spectra of  $5.0 \mu\text{M}$  **6** ( $\text{CH}_2\text{Cl}_2/\text{CH}_3\text{CN}$  1/1,  $25^\circ\text{C}$ ,  $\lambda_{\text{exc}} = 345 \text{ nm}$ , slit = 1 nm). Fluorescence (bottom right) and absorption (bottom left) spectra of  $5.0 \mu\text{M}$  **5**, ( $\text{CH}_2\text{Cl}_2/\text{CH}_3\text{CN}$  1/1,  $25^\circ\text{C}$ ,  $\lambda_{\text{exc}} = 353 \text{ nm}$ , slit = 1 nm).

The presence of a strong excimer band (Figure 4, top right) in the fluorescence spectrum of **6** confirms that the two pyrene units are close together and the calixarene conformation is in the unlocked state with the two pyrenyl moieties in close proximity. The comparison of the excitation spectra at the monomer and at the excimer emission wavelength can be used to investigate the origin of the pyrene dimer. If the spectra are identical, then the pyrene dimer is an excimer (a dimer formed in the excited state). If, on the contrary, one of the spectra is shifted, the dimer is already formed in the ground-state.

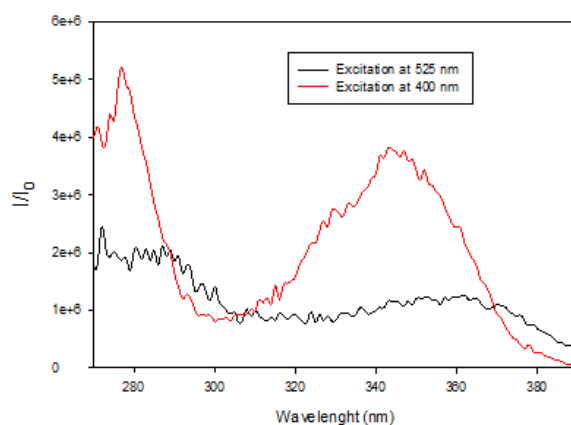


**Fig. 5:** Excitation spectra of  $2.50 \mu\text{M}$  **6** +  $2.50 \mu\text{M}$  TFA in  $\text{CH}_2\text{Cl}_2/\text{CH}_3\text{CN}$  1/1 monitored at 400 nm (red trace) and at 525 nm (black trace).

Some authors<sup>86,87</sup> consider the first dimer a “dynamic excimer” and the second a “static” one. The spectra in Figure 5 show that the excitation spectrum monitored at 525 nm is red-shifted with respect to that monitored at 400 nm, suggesting that the excimer band is emitted by a pyrene dimer formed at the ground-state (“static excimer”).

### 1.9 <sup>1</sup>H-NMR and fluorescence titration with TFA

The <sup>1</sup>H NMR titration of 2.0 mM **6** with TFA, illustrated in Figure 6, shows that the protonation of **6** initially causes an up-field shift of the signal related to the aromatic protons ortho to the NH<sub>2</sub> groups from 6.59 ppm to lower values, which is a characteristic feature of the “locked” pinched-cone conformation with the aniline rings slightly convergent.<sup>88</sup> One aniline N atom is protonated and the NH<sub>2</sub> group of the unprotonated aniline is intramolecularly H-bonded to the first one. On the contrary, the pyrene-substituted calixarene aromatics are downfield shifted and divergent. This unusual upfield shift of the protons ortho to the NH<sub>2</sub> upon catching the proton is due to the shielding effect that the divergent aromatic rings exert on the convergent ones. In addition, such protonation dramatically affects the aromatic signals of the pyrenyl moieties, which are shifted to lower fields and become sharper, suggesting a break-up of the  $\pi$ - $\pi$  interaction and a higher conformational freedom. Upon further addition of TFA (more than 2 mol equiv.), the signal of the NH<sub>2</sub>-substituted aromatic rings tends to shift downfield and becomes broader. On the contrary, the pyrene-substituted aromatic rings signal moves upfield even if much more slowly. Also, the pyrene signals are again slightly shifted to higher fields and become broader. These latest pieces of evidence point to a second protonation of the calixarene structure to give **6**H<sub>2</sub><sup>2+</sup> with one proton on each of the two amino groups, whose electrostatic repulsion brings again together the pyrenyl moieties.

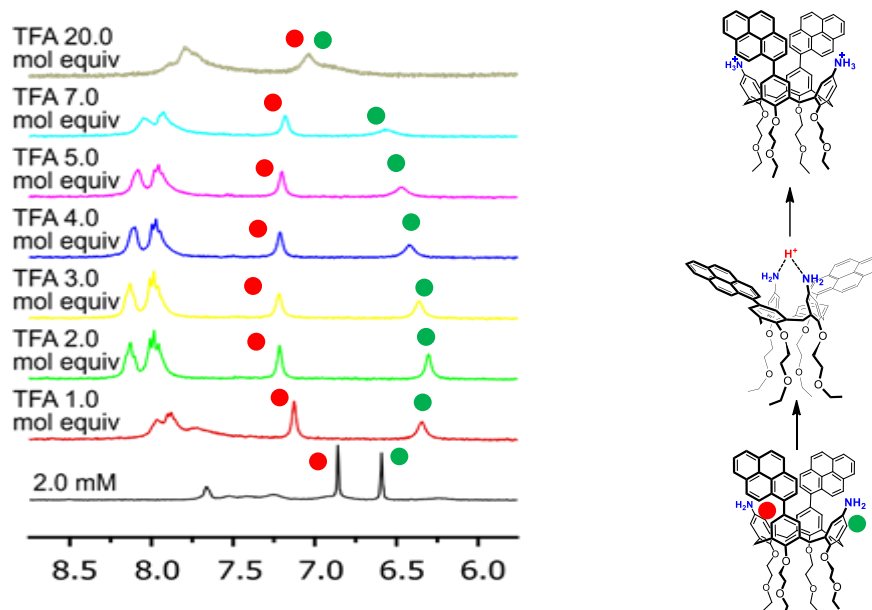


**Fig. 6:** Titration of 2.0 mM **6** with 1, 2, 3, 4, 5, 7 and 20 eq TFA. For clarity only the aromatic portion of the spectrum is shown ( $^1\text{H}$  NMR monitoring;  $\text{CD}_2\text{Cl}_2/\text{CD}_3\text{CN}$  1:1, 25 °C)

Fluorescence titration of 0.15 mM **6** with TFA in the same mixture of solvents, shown in Figure 7a ( $\lambda_{\text{exc}} = 385$  nm,  $\text{CH}_2\text{Cl}_2/\text{CH}_3\text{CN}$  1:1, 25 °C), shows a decrease of the excimer emission band at 475 nm and a corresponding increase of the band at 408 nm due to the monomeric emission of the pyrenyl units. These data confirm the formation of the mono-protonated form **6H<sup>+</sup>** in its pinched-cone conformation with the two pyrenyl units pointing far from each other. Conversely, the addition of a larger excess of TFA (up to 50 mol equiv., shown in Figure 7b), causes the excimer band at 475 nm to increase again. This confirms what observed also by  $^1\text{H}$  NMR: the protonation of both the amino groups to ammonium groups, causes a repulsion of the anilinium units that translates into a re-approaching of the pyrenyl groups.

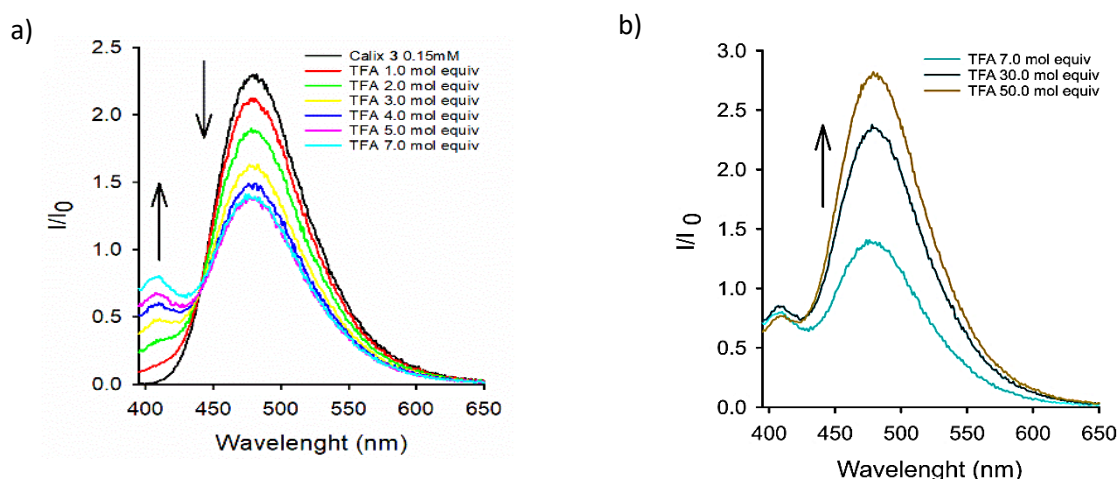


**Fig. 7:** a) Titration of 0.15 mM **6** with TFA (fluorescence monitoring,  $\lambda_{exc} = 385$  nm;  $CH_2Cl_2/CH_3CN$  1:1, 25 °C). b) Fluorescence spectra obtained after addition of further TFA (7, 30 and 50 mol equivs). The excimer bands again re-increases due to re-approaching of the pyrenyl groups.

To be certain that any disappearance of the excimer band is due to the conformation that **6** assumes with the protonation to  $6H^+$  and not to a possible quenching of the fluorescence by the trifluoroacetate ion, a base stronger than aniline such as triethylamine is added to the system **6** + 3 mol equiv TFA (Figure 8). After the addition of trimethylamine (3 mol equiv), the spectrum returns to that of the unprotonated **6**, thus excluding any quenching of fluorescence by the trifluoroacetate ion.

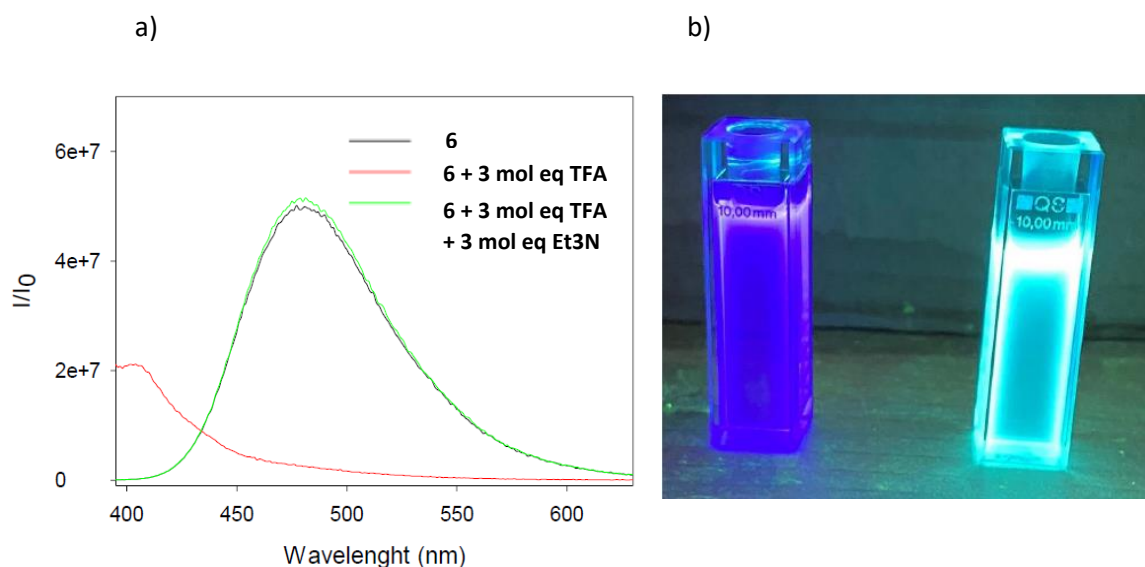


**Fig. 8:** a) Titration of 0.15 mM **6** (green), 0.15 mM **6** with 3 mol eq TFA (red) and 0.15 mM **6** with 3 mol eq TFA and 3 mol eq  $Et_3N$  (fluorescence monitoring,  $\lambda_{exc} = 385$  nm;  $CH_2Cl_2/CH_3CN$  1:1, 25 °C). b) Fluorescence emission under UV lamp of **6** + 3 eq TFA (violet) and **6** + 3 eq TFA + 3 eq  $Et_3N$  (cyan)

Compound **6** in the neutral state shows a fluorescence emission shifted towards a higher wavelength due to the presence of the excimer while, after addition of the acid, the protonated **6H<sup>+</sup>** shows a shift in the wavelength towards the violet. After the base addition to deprotonate the amino group, the fluorescence of the excimer returns as shown in Figure 8b.

### 1.10 <sup>1</sup>H NMR and fluorescence studies with chemical fuels **8** and **10**

Having demonstrated that the protonation with TFA is effective in producing the expected conformational variations of **6**, we then started to explore the use of a chemical fuel to achieve a temporal control of the conformation and fluorescence properties of calixarene **6**. Initially, 2-(4-chlorophenyl)-2-cyanopropanoic acid **8** was employed as the fuel as in the case of a previous work.<sup>88</sup> The addition of 2 mol equiv of fuel acid **8** to calixarene **6** was monitored by <sup>1</sup>H NMR from 3 minutes to more than 10 h (in Figure 9) and corroborated our hypothesis. The first spectrum (second trace from the bottom in Figure 9) recorded after 3 min showed shifts of the signals of the free calixarene **6** (first trace from the bottom in Figure 9) that closely resemble those observed in the titration with TFA, proving the formation of the monoprotonated form **6H<sup>+</sup>** and the adoption of the “locked” conformation. In the following 4-5 hours, no substantial variations can be detected in the spectra (traces 3-5 from the bottom in Figure 9) except for the building up of the signal belonging to the waste product **9** produced during the complete cycle (decarboxylation of the fuel and its protonation).



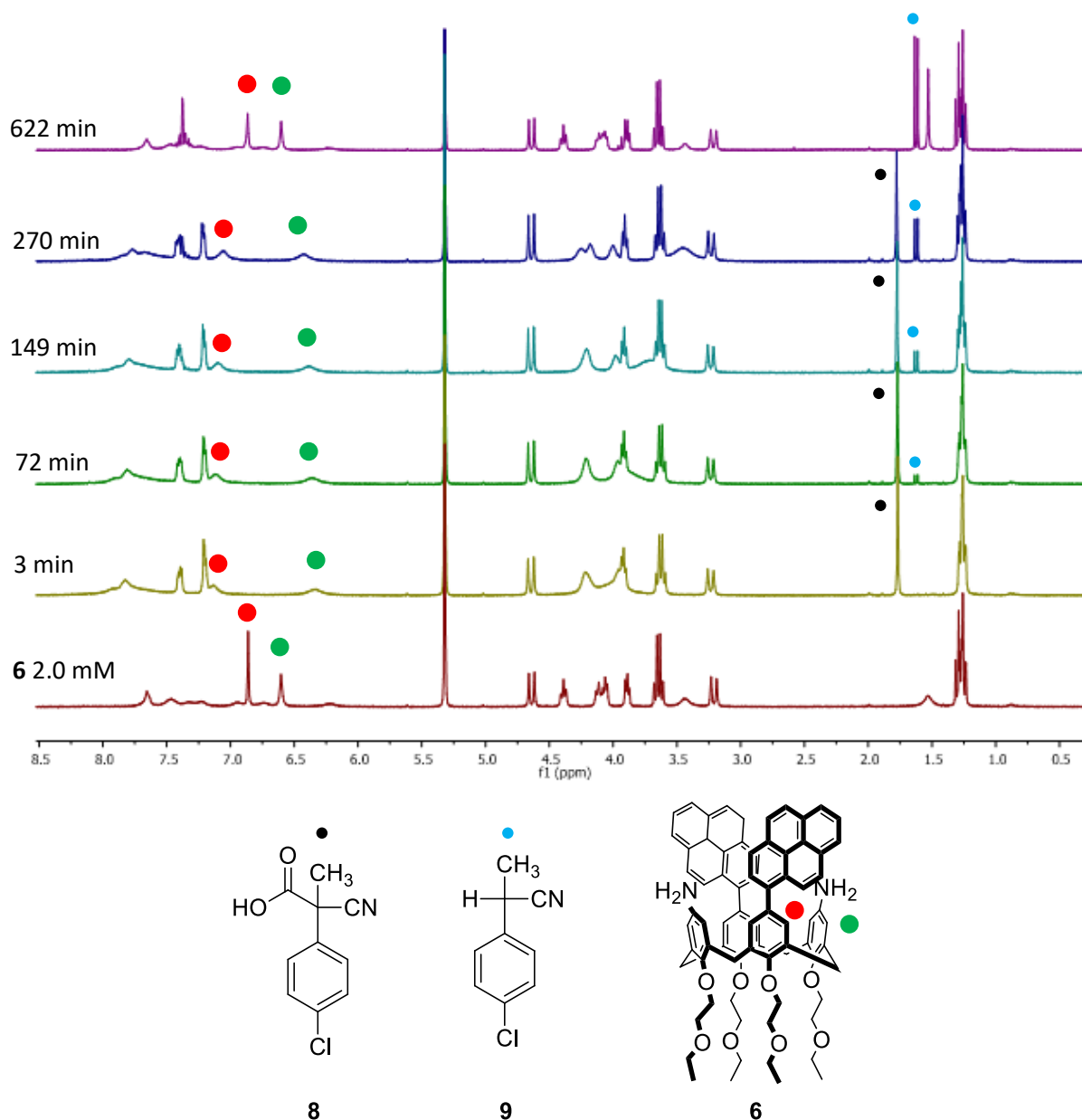


**Fig.9:**  $^1\text{H}$  NMR monitoring of the reaction between 4.0 mM of acid **8** and a 2.0 mM solution **6** (2 mol equiv), ( $\text{CD}_2\text{Cl}_2$ , 25 °C). The bottom trace is relative to 2.0 mM **6**, before the addition of the fuel. Following spectra were recorded after the addition of fuel, at the given reaction time, upward increasing.

The reaction between **8** and **6** is followed by monitoring the decrease of fuel concentration and increase of waste concentrations over time, as well as the chemical shift of the proton signals of the amino-substituted rings (Figure 10).

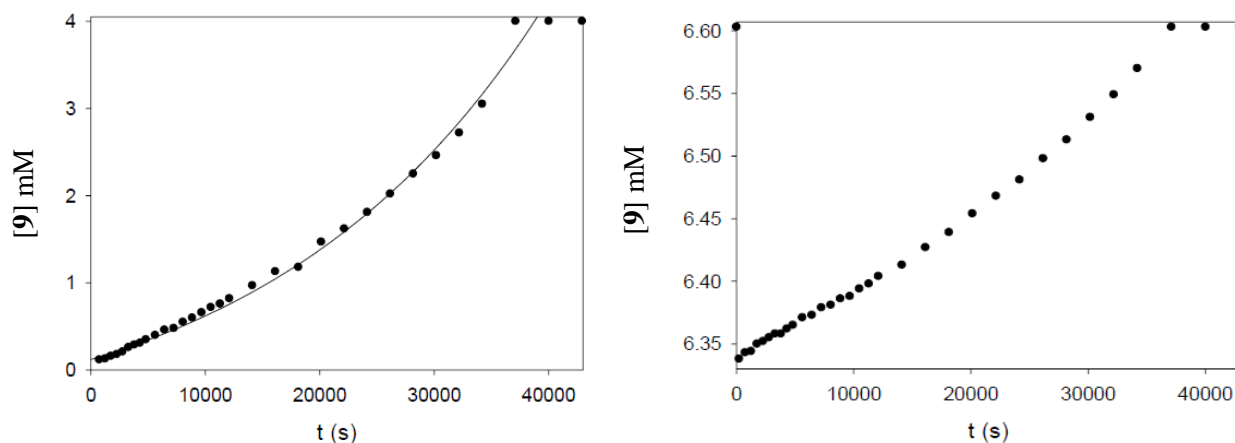


**Fig.10:** (a) Plot of the concentration of the waste product **5** vs. time as monitored by  $^1\text{H}$  NMR for the reaction between 2.0mM **6** and 2 mol equiv. of fuel **8**, in  $\text{CD}_2\text{Cl}_2$  at 25 °C. (b) Chemical shift variation, over the time, of the signals related to the protons of the substituted amino rings.

The kinetic profiles obtained from this first experiment are similar to those obtained with **11** in the previous work,<sup>89</sup> so that it can be assumed that the reaction mechanism is similar. Compared with the reaction conducted with the same calixarene:fuel ratio, in the case of the diamino calix[4]arene **11** the reaction is slower as shown in Figure 11. The fact that at the same calixarene:fuel ratio the complete cycle lasts longer in the case of **6** compared to **11** suggests that in the former case something in the system stabilizes the conjugate base of the fuel.

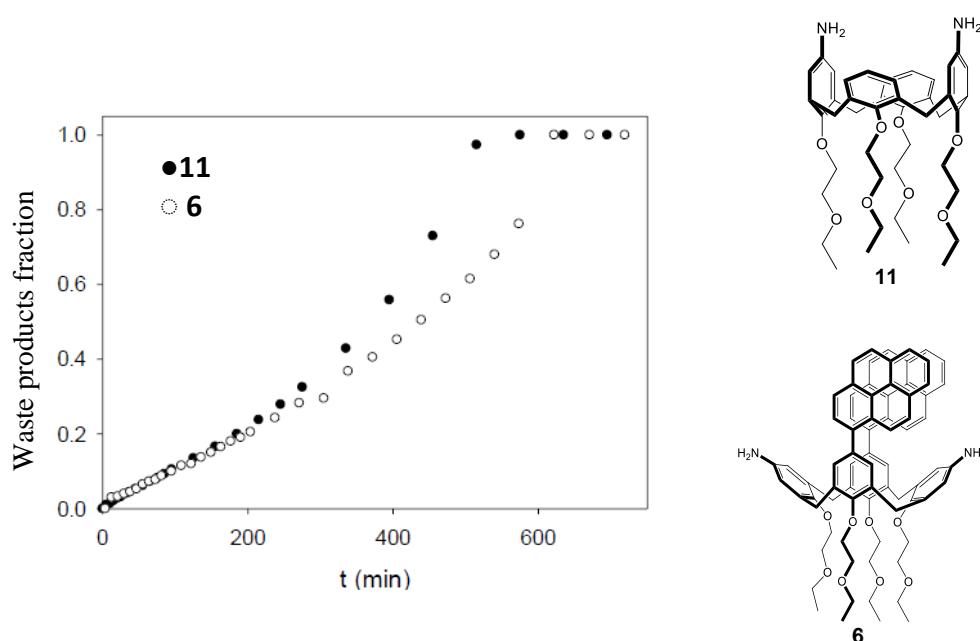


**Figure 11:** Comparison of waste products fractions produced over time using **11** and **6**

Comparing the  $^1\text{H}$  NMR spectra of the reaction between **8** and the two different calix[4]arene derivatives **6** and **11** (Figure 12), it can be seen that both the signals of the ArH and  $\text{CH}_3$  protons of the conjugate base of the fuel are shielded in case of calixarene **6** compared with the diaminocalix[4]arene **11**. This could be due to a stacking interaction of the aromatic portion of the fuel conjugate base with the pyrenyl substituents that stabilise the ion pair between **6** and **8**, slowing down the decarboxylative step.

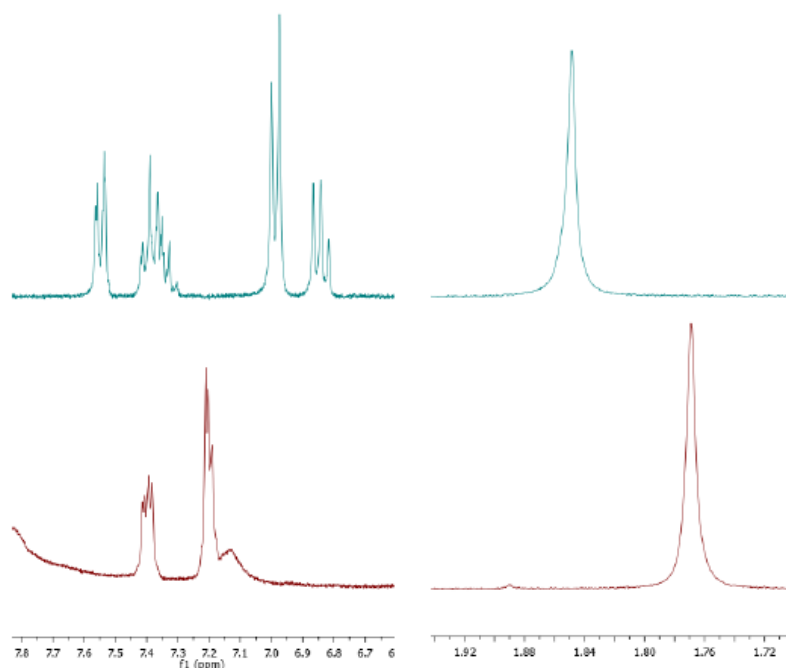


**Fig.12:** Comparison of fuel signals in the case of reaction mediated by **6** (bottom) and by calix[4]diamino **11** (top). Portion of the spectra of the ArH signals (left) and of the  $\text{CH}_3$  signals (right)

Unfortunately, while the  $^1\text{H}$  NMR monitoring of the reaction corroborated our hypothesis as shown in Figure 7, we were unable to observe the expected fluorescence quenching of the excimer emission during the reaction, probably due to an interposition of the aromatic portion of this fuel between the two pyrenyl moieties of **6**. This was confirmed by a new experiment between 4mM of fuel and 2mM of triethylamine using  $10^{-6}$  M calix[4]arene **6** as a fluorescence indicator. Since triethylamine is more basic than **6**, it should react with the fuel, promoting its decarboxylation. In the absence of interaction between **6** and the conjugate base of the fuel, it is expected that the fluorescence spectrum of **6** remains constant over time.

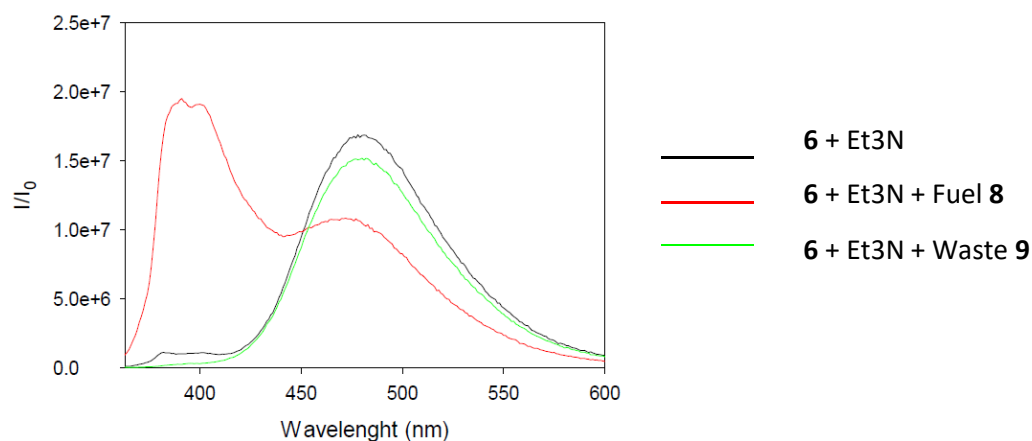


**Fig.12:** Fluorescence emission of **6** before (black), during (red) and after (green) the reaction between  $Et_3N$  and fuel **8**

As can be seen from Figure 12, the fluorescence emission of **6** changes when fuel **8** was added and only returns to its initial state at the end of the transformation of the fuel in the waste **9**. This supports the hypothesis of an interaction between the conjugated base of the fuel and calixarene **6** and therefore makes fuel **8** unsuitable to be used to monitor the reaction with calix[4]arene **6** by fluorescence. Moreover, since the fluorescence spectrum of **6** returns to its initial state at the end of the reaction, an interaction with the waste product **9** can be excluded. We then resorted to trichloroacetic acid **10** as an acid fuel, although it was found less manageable due to its deliquescence. The addition of 2.3 mol equiv of trichloroacetic acid to 2.0 mM **6**, shown in the second trace (5 min from the addition) of Figure 13, results in a series of shifts that closely resemble those observed in the titration of **6** with TFA or **8**. Indeed, in case of trichloroacetic acid, a larger separation of the calixarene aromatic signals (red and green stripes, Figure 13) and the down-field shift together with an increase of resolution of the pyrenyl signals are observed, proving the adoption of the “locked” pinched-cone conformation for **6**.

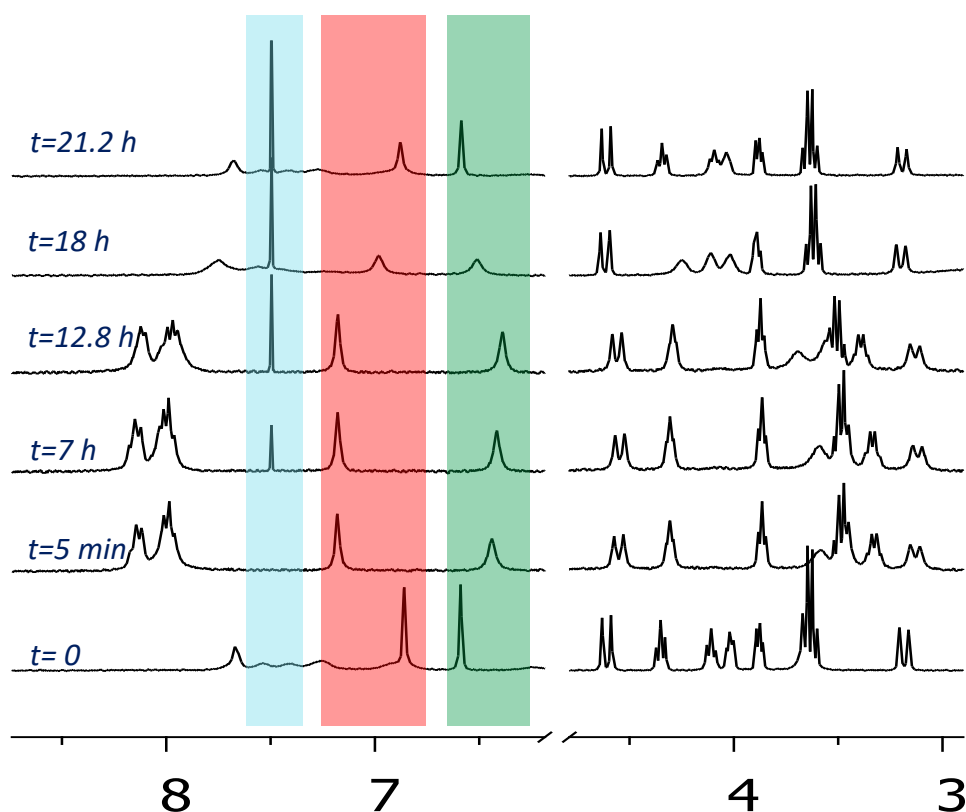


**Fig.13:**  $^1\text{H}$  NMR monitoring of the reaction between 2.0 mM **6** and 2.3 mol equiv of **10**. ( $\text{CD}_2\text{Cl}_2/\text{CD}_3\text{CN}$  1:1, 25 °C)

In the following 12–13 hours, no substantial variations can be detected in the  $^1\text{H}$  NMR spectrum except for the building up of the signal at 7.49 ppm corresponding to  $\text{CHCl}_3$  produced as a waste during the decarboxylation of **10** (blue stripe on Figure 13). From this point ( $t > 12$  h), all the signals corresponding to the calix[4]arene scaffold begin to revert to the initial chemical shift values and, at the end of the reaction, after 21 h, the  $^1\text{H}$  NMR spectrum turns to be superimposable to the initial one. This clearly demonstrates that the whole cycle  $\mathbf{A} \rightarrow \mathbf{B}' \rightarrow \mathbf{B}'' \rightarrow \mathbf{A}$  shown in Figure 14 has occurred. In other words, the “locked” pinched-cone structure persists as long as an excess of fuel is present.

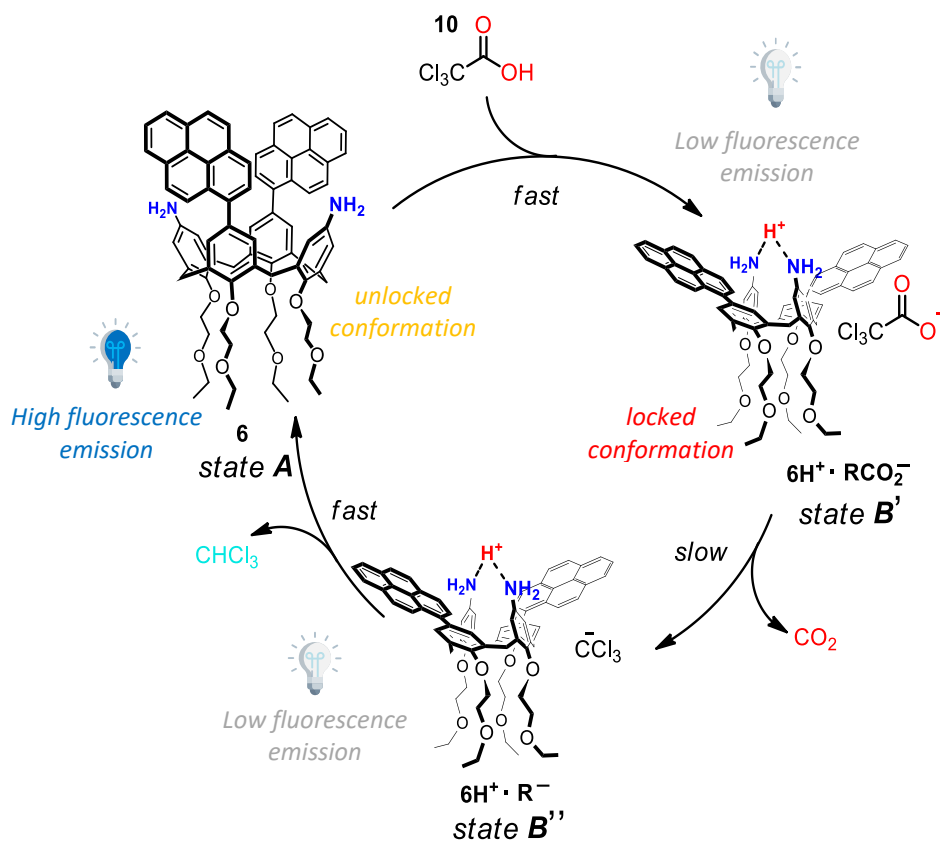


**Fig.14:** Expected conformational cycle of **6** controlled by means of chemical fuel **10**

The kinetics of the reaction between **10** and **6** were also followed by monitoring fuel and waste concentrations over time (Figure 15), as well as the chemical shift of the proton signals of the amino-substituted aromatic rings.

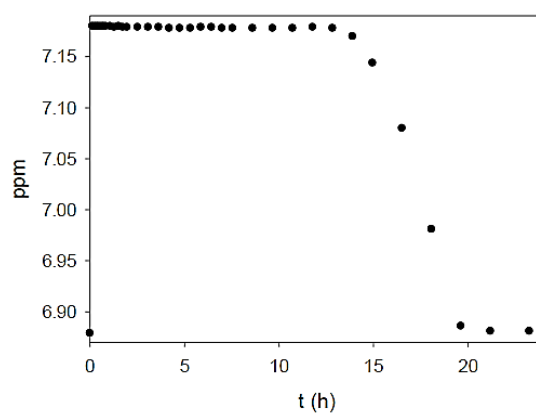


**Figure 15:** (a)  $^1\text{H}$  NMR monitoring of the reaction between 2.3 mol equiv. **10** catalysed by 2.0 mM **6**, ( $\text{CD}_2\text{Cl}_2$ , 25 °C). The chemical shift of the pyrenyl substituted aromatic rings of **6** vs time is reported.

The time in which the calix[4]arene scaffold remains in the “locked” state depends on the amount of the added fuel. In fact, the addition of 2.3 mol equiv. of fuel maintains the locked form for 13 h, while the presence of 4.0 mol equiv of fuel keeps the locked form for 32 h, as shown in Figure 16.

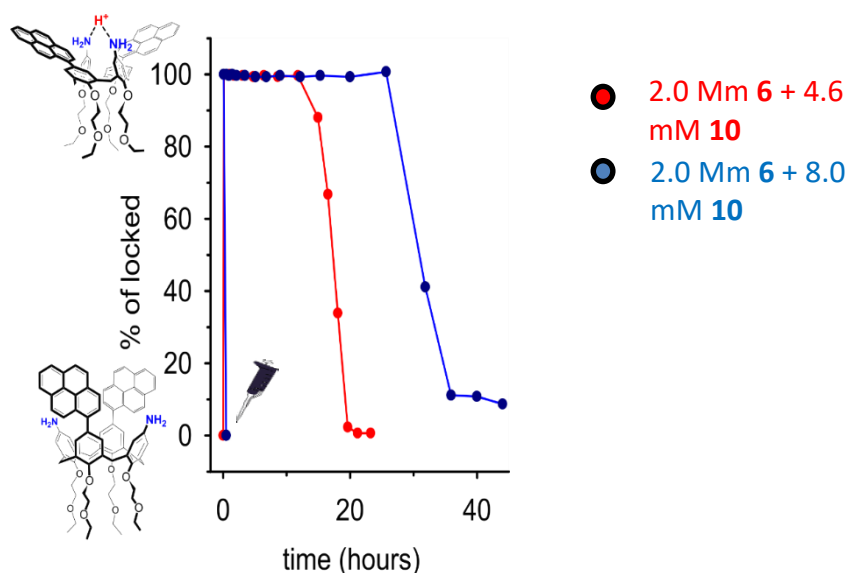


**Fig.16:** Percentage of **6** in its locked conformation in function of time for the reactions carried out in the presence of 2.3 mol equiv. (red trace) and 4.0 mol equiv. (blue trace) of **10**

Then, we monitored the reaction using a spectrofluorometer, recording over time the emission intensity at 475 nm ( $\lambda_{exc} = 385$  nm) of a 0.15 mM **6** solution ( $\text{CH}_2\text{Cl}_2/\text{CH}_3\text{CN}$  1:1 at 25 °C) to which 5.0 mol equiv. of fuel **10** were added. As shown in Figure 17a, after the addition, an immediate decrease of the intramolecular excimer fluorescence emission takes place, witnessing the unpairing of the pyrenyl moieties and the formation of the locked conformation. The reaction proceeds and, after approximately 3 h, the emission intensity at 475 nm is recovered as a result of the completion of the cycle  $A \rightarrow B' \rightarrow B'' \rightarrow A$  and, consequently, of the formation of pyrene-pyrene interactions. The observation that the reaction rate is faster at these concentrations (0.15 mM of **6**) than that observed at higher concentrations (2.00 mM of **6**,  $^1\text{H}$  NMR experiments), is likely due to a weaker ion pairing between  $\mathbf{6H}^+$  and  $\text{RCO}_2^-$  at more diluted concentrations, which destabilizes the  $\text{RCO}_2^-$  anion and facilitates the decarboxylation step. As a matter of fact, decarboxylation does not proceed at any extents if dichloromethane alone is used as a solvent instead of the mixture dichloromethane:acetonitrile 1:1, both at high and low concentrations, suggesting an important role of the solvent in influencing the ion pair character. Eventually, Fig. 17b shows that the system is robust and reversible. Four subsequent  $A \rightarrow B' \rightarrow B'' \rightarrow A$  cycles have

been achieved by means of four successive shots of fuel **10**, as witnessed by the loss and recovery of the fluorescence at 475 nm.

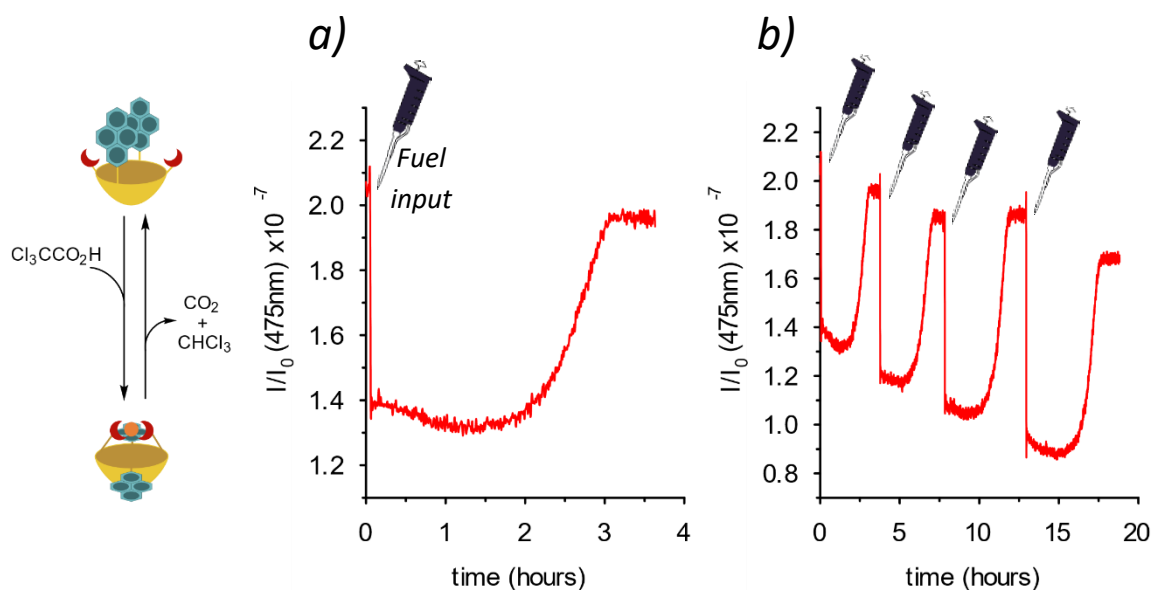


**Fig.17:** (a) Time course monitoring of the fluorescence emission at 475 nm ( $\lambda_{\text{exc}} = 385$  nm) before and after the addition of 5.0 mol equivs of **10** ( $\text{CH}_2\text{Cl}_2/\text{CH}_3\text{CN}$  1:1 at 25 °C). The cartoon on the left schematically shows the conformations relative to the high and to the low fluorescence emission. (b) Up to four dissipative conformational cycles were obtained by the subsequent addition of **10** ( $\text{CH}_2\text{Cl}_2/\text{CH}_3\text{CN}$  1:1 at 25 °C).

## 1.11 Conclusion

In this chapter, we have shown that the shape of calix[4]arene scaffold in its cone conformation can be temporary controlled by means of chemical fuels. In particular the cone 1,3-distal di pyrenyl calix[4]arene **6** offers a unique solution for this purpose. The basicity of the system is enhanced by the possibility of the two amino groups to share the proton in the conjugate acid. This basicity enhancement enables the calix[4]arene **6** to promote the decarboxylation of activated acids **10** and **8** which act as chemical fuels. During the decarboxylation reaction, the vast majority of the calixarene molecules persist in the closed pinched cone conformation with the two amino groups convergent and H-bonded each to the other, while the two pyrenyl group strongly divergent (locked state). The time spent by the calix[4]arene scaffold in the locked state can be regulated by controlling the amount of added fuel. A conformational cycle of calix[4]arene **6** in a dissipative fashion can be monitored by  $^1\text{H}$  NMR. With trichloroacetic acid **10** it was also possible to monitor the conformational cycle by means of fluorescence. Given the presence of the two pyrenyl units in the opposite positions of the upper rim of calix[4]arene **6** such control translates into the dissipative time-



modulation of the solution fluorescence. In no other systems for which the fluorescence due to the intramolecular excimer between two pyrenyl units is switched ON/OFF or *viceversa* was observed the operation under dissipative conditions.<sup>90,91</sup>

We believe that the possibility to fine-tune the conformational interconversion of the calixarene in a time-dependent fashion and without recurring to solvent changes opens the way to new perspectives in calixarene chemistry, ranging from molecular receptors to sensing devices whose active state could be switched on.



# Experimental Part

## 1.12 General information

All moisture sensitive reactions were carried out under nitrogen or argon atmosphere, using previously degassed solvents. Analytical TLC were performed using prepared plates of silica gel (Merck 60 F 254 on aluminium) and then, according to the functional groups present on the molecules, revealed with UV lights or using staining reagents. Merck silica gel 60 was used for flash chromatography (40-63  $\mu\text{m}$ ).  $^1\text{H-NMR}$  and  $^{13}\text{C-NMR}$  spectra were recorded on Bruker AV400 spectrometers and partially deuterated solvents were used as internal standards to calculate the chemical shifts ( $\delta$  values in ppm). All  $^{13}\text{C-NMR}$  spectra were performed with proton decoupling. Electrospray ionization (ESI) mass analysis were performed with a Waters single-quadrupole spectrometer in positive mode using MeOH or  $\text{CH}_3\text{CN}$  as solvents. High resolution mass spectra were recorded on a LTQ Orbitrap XL instrument in positive mode using MeOH as solvent. Melting points were determined on an Gallenkamp apparatus in closed capillaries. Absorption spectra were collected with a Perkin-Elmer Lambda 250 spectrophotometer on freshly prepared solutions at room temperature. Emission measurements were performed on diluted solutions (concentration  $\sim 10^{-6}\text{M}$ ) with a Fluoromax-3 Horiba Jobin-Yvon fluorometer. During the measurements the samples were thermostated at a temperature of 23  $^\circ\text{C}$

### Synthesis of 25,26,27,28-Tetra[2-(ethoxy)ethoxy]calix[4]arene (2)

Calix[4]arene (2.54 g, 5.41 mmol) was dissolved in dry DMF (76 ml) and cooled down to 0  $^\circ\text{C}$ . Sodium hydride (2.16 g of a 60% dispersion in oil, 54.1 mmol) was added portion wise and the mixture was stirred for 30 min under nitrogen atmosphere. 1-bromo-2-ethoxyethane (4g, 26 mmol) was then added portion wise and the mixture was allowed to warm up to r.t. After that time the mixture was warmed up to 80  $^\circ\text{C}$  and stirred overnight. The reaction was quenched with 1M HCl solution (100 ml), and the organic solvents were evaporated. The residue was dissolved in  $\text{CH}_2\text{Cl}_2$  (100 ml) and washed with an aq. sat. solution of  $\text{NH}_4\text{Cl}$  (100

ml). The organic layer was separated and washed with water, dried over  $\text{Na}_2\text{SO}_4$  and concentrated under reduced pressure. The obtained oil was treated with cold methanol and calix[4]arene **1** was obtained by crystallization as a white solid (2.13 g, 55%).  $^1\text{H-NMR}$  (400 MHz,  $\text{CDCl}_3$ ): 6.56 – 6.64 (m, 12H,  $\text{ArH}$ ). 4.50 (d, 4H,  $J = 13.4$  Hz,  $\text{Ar-CH}_{\text{ax}}\text{-Ar}$ ), 4.12 (t, 8H,  $J = 5.8$  Hz,  $\text{OCH}_2\text{CH}_2\text{O}$ ), 3.85 (t, 8H,  $J = 5.8$  Hz,  $\text{OCH}_2\text{CH}_2\text{O}$ ), 3.55 (q, 8H,  $J = 7.0$  Hz,  $\text{OCH}_2\text{CH}_3$ ), 3.15 (d, 4H,  $J = 13.4$  Hz,  $\text{Ar-CH}_{\text{eq}}\text{-Ar}$ ), 1.21 (t, 12H,  $J = 7.0$  Hz,  $\text{CH}_3$ ). The compound showed the same physico-chemical properties as those reported in literature.<sup>1</sup>

### Synthesis of 5,17-Dinitro-25,26,27,28-tetra[2(ethoxy)ethoxy]calix[4]arene (3).

To a solution of **2** (1 g, 1.40 mmol) in a mixture of  $\text{CH}_2\text{Cl}_2$ /acetic acid 17:1 (50 ml) was added nitric acid (5 ml, 70 mmol) at 0 °C under nitrogen atmosphere. The mixture was stirred for 2 h at 0 °C and 1 h at r.t. Water (100 ml) was added to the mixture, and it was extracted with  $\text{CH}_2\text{Cl}_2$  (2x100 ml). The organic layer was then washed with an aq. solution  $\text{K}_2\text{CO}_3$  (5%) until pH 7. The combined organic layers were dried over  $\text{Na}_2\text{SO}_4$  and concentrated under reduced pressure. The residue was purified by a silica gel flash column chromatography (hexane/AcOEt 9:1 to 7:3) to afford dinitrocalix[4]arene **3** which was further recrystallized in MeOH to give a colourless needles (0.350g, 31%).  $^1\text{H-NMR}$  (400 MHz,  $\text{CDCl}_3$ ): 7.66 (s, 4H,  $\text{ArH}$ ), 6.53–6.59. (m, 6H,  $\text{ArH}$ ), 4.58 (d, 4H,  $J = 13.7$  Hz  $\text{Ar-CH}_{\text{ax}}\text{-Ar}$ ), 4.30 (t, 8H,  $J = 5.1$  Hz,  $\text{OCH}_2\text{CH}_2\text{O}$ ), 4.07 (t, 4H,  $J = 5.2$  Hz,  $\text{OCH}_2\text{CH}_2\text{O}$ ), 3.83 (t, 4H,  $J = 5.1$  Hz,  $\text{OCH}_2\text{CH}_2\text{O}$ ), 3.78 (t, 4H,  $J = 5.2$  Hz,  $\text{OCH}_2\text{CH}_2\text{O}$ ), 3.54 (q, 8H,  $J = 7.0$  Hz,  $\text{OCH}_2\text{CH}_3$ ), 3.49 (q, 8H,  $J = 7.0$  Hz,  $\text{OCH}_2\text{CH}_3$ ); 3.25 (d, 4 H,  $J = 13.7$  Hz,  $\text{Ar-CH}_{\text{eq}}\text{-Ar}$ ), 1.21 (t, 6 H,  $J = 7.0$  Hz,  $\text{CH}_3$ ), 1.16 (t, 6 H,  $J = 7.0$  Hz,  $\text{CH}_3$ ). The compound showed the same physico-chemical properties as those reported in literature.<sup>92</sup>

### Synthesis of 5,17-diiodo-11,23-dinitro-25,26,27,28-tetrakis(2-ethoxyethoxy)calix[4]arene (4).

To a suspension of  $\text{CF}_3\text{COOAg}$  (0.370g, 1.7 mmol) in refluxing  $\text{CHCl}_3$ , (20mL) was added a solution of **2** (0.450g, 0.56mmol) in 10 mL of  $\text{CHCl}_3$  and the resulting suspension was refluxed for 15 min. Then iodine (0.430g, 1.7 mmol) was added until the purple colour was permanent. The reaction mixture was then refluxed for 24 h. After cooling to room temperature, the yellow precipitate was filtered over Celite and the solution was washed with

a 10% aq Na<sub>2</sub>S<sub>2</sub>O<sub>3</sub> (2x30mL), water (30mL), brine (30mL) and dried over Na<sub>2</sub>SO<sub>4</sub>. The solvent was removed under reduce pressure to give a yellow solid. The pure product **4** was obtain after a trituration in MeOH as a pale-yellow solid (0.6g, 99%). <sup>1</sup>H NMR (400 MHz, CDCl<sub>3</sub>) δ (ppm) 7.71 (s, 4H, ArH), 6.93 (s, 4H, ArH), 4.57 (d, 4H, J=13.7 Hz, ArCH<sub>ax</sub>-Ar), 4.32 (t, 4H, J=4.9 Hz, OCH<sub>2</sub>CH<sub>2</sub>O), 4.06 (t, 4H, J=4.7 Hz, OCH<sub>2</sub>CH<sub>2</sub>O), 3.81 (t, 4H, J=4.4 Hz, OCH<sub>2</sub>CH<sub>2</sub>O), 3.76 (t, 4H, J=5.3 Hz, OCH<sub>2</sub>CH<sub>2</sub>O), 3.54 (q, 4H, J=7 Hz, OCH<sub>2</sub>CH<sub>3</sub>), 3.48 (q, 4H, J=7 Hz, OCH<sub>2</sub>CH<sub>3</sub>), 3.25 (d, 4H, J=13.7 Hz ArCH<sub>eq</sub>-Ar), 1.22 (t, 6H, J=7 Hz, OCH<sub>2</sub>CH<sub>3</sub>), 1.15 (t, 6H, J=7 Hz, OCH<sub>2</sub>CH<sub>3</sub>). The compound showed the same physico-chemical properties as those reported in literature.<sup>92</sup>

#### **4,4,5,5-tetramethyl-2-(pyren-1-yl)-1,3,2-dioxaborolane (13)**

A mixture of commercially available 1-pyreneboronic acid (2g, 8 mmol) and pinacol (2.9 g, 24 mmol) in ether (40 mL) and tetrahydrofuran (10 mL) was stirred at 60°C for 24h. After the evaporation of solvent, the residue was purified by a silica gel flash column chromatography (hexane/AcOEt 20:1) affording **13** as a white solid (3g, 79%). <sup>1</sup>H NMR (400 MHz, CDCl<sub>3</sub>) δ (ppm) 8.98 (d, 1H, J=9.2 Hz, ArH), 8.44 (d, 1H, J=8 Hz, ArH), 8.09 (d, 1H, J=7.6 Hz, ArH), 8.05 (d, 1H, J=8 Hz, ArH), 8.04 (t, 2H, J=9.2 Hz, ArH), 7.96 (m, 2H, ArH), 7.87 (t, 1H, J=7.6 Hz, ArH), 1.37 (s, 12H, CH<sub>3</sub>). The compound showed the same physico-chemical properties as those reported in literature.<sup>93</sup>

#### **Synthesis of 5,17-(dipyren-1-yl)-11,23-dinitro-25,26,27,28-tetrakis(2-ethoxyethoxy)calix[4]arene (5)**

A mixture of calix [4]arene **4** (0.233 g, 0.22 mmol), 4,4,5,5-tetramethyl-2-(pyren-1-yl)-1,3,2-dioxaborolane (**13**) (0.160 g, 0.48 mmol) and [1,1'-bis(diphenylphosphino)ferrocene]dichloropalladium(II) (0.018 g, 0.022 mmol) was prepared under an argon atmosphere in a Schlenk tube. THF (5.2 mL) and 2 M Na<sub>2</sub>CO<sub>3</sub> (1.35 mL) were added sequentially, and the mixture was stirred at 80 °C for 2 days. After cooling, the reaction was quenched with distilled water. The crude product was extracted with dichloromethane (3 × 50 mL) and the combined organic phases were dried over anhydrous Na<sub>2</sub>SO<sub>4</sub> and evaporated under reduced pressure. Purification by column chromatography (silica gel, eluent: dichloromethane/ethyl acetate 95:5) yielded the pure product **5** as a light-yellow solid (0.161 g, 60%). Mp 247.7–248.2 °C. <sup>1</sup>H NMR (400 MHz, CDCl<sub>3</sub>) δ (ppm) 8.21 (4H, broad s, ArH),

7.68 (4H, broad s, ArH(Py)), 7.50 (4H, broad s, ArH(Py)), 7.25 (4H, broad s, ArH(Py)), 6.94 (2H, broad s, ArH(Py)), 6.84 (4H, broad s, ArH), 6.56 (2H, broad s, ArH (Py)), 5.98 (2H, broad s, ArH(Py)), 4.87 (4H, d, ArCHH<sub>eq</sub>Ar, J = 13.3 Hz) 4.75 (4H, broad s, OCH<sub>2</sub>CH<sub>2</sub>O), 4.15 (4H, broad s, OCH<sub>2</sub>CH<sub>2</sub>O), 4.08 (4H, broad s, OCH<sub>2</sub>CH<sub>2</sub>O), 3.91 (4H, br s, OCH<sub>2</sub>CH<sub>2</sub>O), 3.68 (4H, q, OCH<sub>2</sub>CH<sub>3</sub> J = 7.0 Hz), 3.59 (4H, q, OCH<sub>2</sub>CH<sub>3</sub>, J = 7.0 Hz), 3.53 (4H, d, ArCHH<sub>ax</sub>Ar, J = 13.3 Hz), 1.36 (6H, t, OCH<sub>2</sub>CH<sub>3</sub>, J = 6.5 Hz) 1.25 (6H, t, OCH<sub>2</sub>CH<sub>3</sub>, J = 7.0 Hz). <sup>13</sup>C NMR (100 MHz, CDCl<sub>3</sub>) δ 163.57, 154.04, 142.73, 138.17, 135.76, 135.08, 132.15, 131.23, 130.57, 129.60, 129.07, 126.62, 126.03, 125.52, 124.86, 124.21, 124.02, 123.07, 122.80, 77.24, 74.79, 73.81, 70.15, 69.65, 66.64, 66.31, 31.22, 15.37. ESI-MS: m/z calcd for C<sub>76</sub>H<sub>71</sub>N<sub>2</sub>O<sub>12</sub> [(5+H)<sup>+</sup>] 1203.38 found 1203.47 calcd for C<sub>76</sub>H<sub>69</sub>N<sub>2</sub>O<sub>12</sub>Na [(5+Na)<sup>+</sup>] 1225.36, found 1225.64, calcd for C<sub>76</sub>H<sub>69</sub>N<sub>2</sub>O<sub>12</sub>K [(5+K)<sup>+</sup>] 1241.47 found 1241.69.

### Synthesis of 5,17-(dipyren-1-yl)-11,23-diamino-25,26,27,28-tetrakis(2-ethoxyethoxy) calix[4]arene (6)

To a solution of calix[4]arene 5 (0.160 g, 0.133 mmol) in ethanol (15 mL), hydrazine hydrate (0.126 mL, 3.99 mmol) and a catalytic amount of Pd/C (10%) were added. The reaction mixture was refluxed for 24 h and quenched by catalyst filtration. The filtrate was evaporated under reduced pressure; the residue was dissolved with dichloromethane and washed with distilled water. The organic layer was separated, dried over Na<sub>2</sub>SO<sub>4</sub> and evaporated to dryness under reduced pressure to obtain the pure product as a light-yellow solid (0.121 g, 80%). Mp 180.7–181.2 °C. <sup>1</sup>H NMR (400 MHz, CD<sub>2</sub>Cl<sub>2</sub>/CH<sub>3</sub>CN) δ (ppm) 7.66 (4H, broad s, ArH(Py)), 7.53 (2H, broad s, ArH(Py)), 7.41 (2H, broad s, ArH(Py)), 7.25 (4H, broad s, ArH(Py)), 6.90 (4H, broad s, ArH(Py)), 6.86 (4H, s, ArH), 6.59 (4H, broad s, ArH), 6.25 (2H, s, ArH(Py)), 4.61 (4H, d, ArCHH<sub>eq</sub>Ar, J = 13.0 Hz), 4.36 (4H, t, OCH<sub>2</sub>CH<sub>2</sub>O, J = 8.6 Hz), 4.11 (4H, t, OCH<sub>2</sub>CH<sub>2</sub>O J = 8.6 Hz), 4.03 (4H, t, OCH<sub>2</sub>CH<sub>2</sub>O J = 6.2 Hz), 3.88 (4H, t, OCH<sub>2</sub>CH<sub>3</sub>, J = 6.2 Hz), 3.62 (8H, q, J = 9.3 Hz), 3.25 (4H, d, ArCHH<sub>ax</sub>Ar, J = 13.0 Hz), 1.27 (6H, t, OCH<sub>2</sub>CH<sub>3</sub>, J = 9.3 Hz), 1.23 (6H, t, OCH<sub>2</sub>CH<sub>3</sub>, J = 9.3 Hz). <sup>13</sup>C NMR (100 MHz, CD<sub>2</sub>Cl<sub>2</sub>) δ (ppm) 154.16, 150.40, 141.72, 137.44, 136.54, 134.57, 133.43, 130.71, 130.54, 129.80, 128.70, 126.83, 126.14, 125.71, 125.70, 124.69, 124.18, 123.99, 123.84, 123.63, 123.37, 123.06, 115.57, 74.54, 72.93, 70.22, 69.83, 66.48, 66.30, 31.04, 15.34, 15.16. HR-MS, m/z calculated for C<sub>76</sub>H<sub>75</sub>N<sub>2</sub>O<sub>8</sub> [(6+H)<sup>+</sup>] 1143.55179, found 1143.55037.

**Table 1. Crystal data and structure refinement for calixarene 5**

Empirical formula	C <sub>76</sub> H <sub>70</sub> N <sub>2</sub> O <sub>12</sub>
Formula weight	1203.34
Temperature/K	150.0
Crystal system	triclinic
Space group	P-1
a/Å	14.238(3)
b/Å	14.993(3)
c/Å	15.638(2)
$\alpha$ /°	70.194(7)
$\beta$ /°	85.592(7)
$\gamma$ /°	77.672(8)
Volume/Å <sup>3</sup>	3068.1(9)
Z	2
$\rho_{\text{calc}}$ /cm <sup>3</sup>	1.303
$\mu$ /mm <sup>-1</sup>	0.709
F(000)	1272.0
Crystal size/mm <sup>3</sup>	0.11 × 0.03 × 0.03
Radiation	CuK $\alpha$ ( $\lambda$ = 1.54178 Å)
2 $\theta$ range for data collection/°	7.18 to 136.48
Index ranges	-17 ≤ h ≤ 16, -18 ≤ k ≤ 18, -18 ≤ l ≤ 18
Reflections collected	37030
Independent reflections	11007 [R <sub>int</sub> = 0.1530, R <sub>sigma</sub> = 0.1346]
Data/restraints/parameters	11007/37/843
Goodness-of-fit on F <sup>2</sup>	1.017
Final R indexes [I ≥ 2 $\sigma$ (I)]	R <sub>1</sub> = 0.0790, wR <sub>2</sub> = 0.1737
Final R indexes [all data]	R <sub>1</sub> = 0.1757, wR <sub>2</sub> = 0.2211
Largest diff. peak/hole / e Å <sup>-3</sup>	0.28/-0.34

## References

- (1) von Ballmoos, C.; Cook, G. M.; Dimroth, P. Unique Rotary ATP Synthase and Its Biological Diversity. *Annu Rev Biophys* **2008**, *37* (1), 43–64. <https://doi.org/10.1146/annurev.biophys.37.032807.130018>.
- (2) Gould, G. W.; Lippincott-Schwartz, J. New Roles for Endosomes: From Vesicular Carriers to Multi-Purpose Platforms. *Nat Rev Mol Cell Biol* **2009**, *10* (4), 287–292. <https://doi.org/10.1038/nrm2652>.
- (3) Foth, B. J.; Goedecke, M. C.; Soldati, D. New Insights into Myosin Evolution and Classification. *Proceedings of the National Academy of Sciences* **2006**, *103* (10), 3681–3686. <https://doi.org/10.1073/pnas.0506307103>.
- (4) Minamino, T.; Imada, K. The Bacterial Flagellar Motor and Its Structural Diversity. *Trends Microbiol* **2015**, *23* (5), 267–274. <https://doi.org/10.1016/j.tim.2014.12.011>.
- (5) Balzani, V.; Credi, A.; Venturi, M. Molecular Logic Circuits. *ChemPhysChem* **2003**, *4* (1), 49–59. <https://doi.org/10.1002/cphc.200390007>.
- (6) Erbas-Cakmak, S.; Leigh, D. A.; McTernan, C. T.; Nussbaumer, A. L. Artificial Molecular Machines. *Chem Rev* **2015**, *115* (18), 10081–10206. <https://doi.org/10.1021/acs.chemrev.5b00146>.
- (7) Balzani, V.; Credi, A.; Raymo, F. M.; Stoddart, J. F. Artificial Molecular Machines. *Angewandte Chemie* **2000**, *39* (19), 3348–3391. [https://doi.org/10.1002/1521-3773\(20001002\)39:19<3348::AID-ANIE3348>3.0.CO;2-X](https://doi.org/10.1002/1521-3773(20001002)39:19<3348::AID-ANIE3348>3.0.CO;2-X).
- (8) Nitschke, J. R. The Nature of the Mechanical Bond. From Molecules to Machines By Carson J. Bruns and J. Fraser Stoddart. *Angewandte Chemie International Edition* **2017**, *56* (1), 39–39. <https://doi.org/10.1002/anie.201611682>.
- (9) J. Wang. *Nanomachines—Fundamentals and Applications*,; RSC Publishing: cambridge, 2012.
- (10) A. P. de Silva. *Molecular Logic-Based Computation*; Royal Society of Chemistry: Cambridge, 2012. <https://doi.org/10.1039/9781849733021>.
- (11) Balzani, V., C. A. V. M. *Molecular Devices and Machines: Concepts and Perspectives for the Nanoworld*, second edition.,; 2008.
- (12) Wegner, H. A. Molecular Switches. Second Edition. Edited by Ben L. Feringa and Wesley R. Browne. *Angewandte Chemie International Edition* **2012**, *51* (10), 2281–2281. <https://doi.org/10.1002/anie.201108931>.
- (13) Stylios, G. K. There Is Plenty of Room at the Bottom, R.P. Feynman. *International Journal of Clothing Science and Technology* **2013**, *25* (5). <https://doi.org/10.1108/IJCST-06-2013-0067>.
- (14) Peplow, M. The Tiniest Lego: A Tale of Nanoscale Motors, Rotors, Switches and Pumps. *Nature* **2015**, *525* (7567), 18–21. <https://doi.org/10.1038/525018a>.
- (15) Baroncini, M.; Casimiro, L.; de Vet, C.; Groppi, J.; Silvi, S.; Credi, A. Making and Operating Molecular Machines: A Multidisciplinary Challenge. *ChemistryOpen* **2018**, *7* (2), 169–179. <https://doi.org/10.1002/open.201700181>.
- (16) von Ballmoos, C.; Cook, G. M.; Dimroth, P. Unique Rotary ATP Synthase and Its Biological Diversity. *Annu Rev Biophys* **2008**, *37* (1), 43–64. <https://doi.org/10.1146/annurev.biophys.37.032807.130018>.
- (17) Bleve, V.; Franchi, P.; Konstanteli, E.; Gualandi, L.; Goldup, S. M.; Mezzina, E.; Lucarini, M. Synthesis and Characterisation of a Paramagnetic [2]Rotaxane Based on a Crown Ether-Like



- Wheel Incorporating a Nitroxide Motif. *Chemistry - A European Journal* **2018**, *24* (5), 1198–1203. <https://doi.org/10.1002/chem.201704969>.
- (18) Franchi, P.; Poderi, C.; Mezzina, E.; Biagini, C.; di Stefano, S.; Lucarini, M. 2-Cyano-2-Phenylpropanoic Acid Triggers the Back and Forth Motions of an Acid–Base-Operated Paramagnetic Molecular Switch. *J Org Chem* **2019**, *84* (14), 9364–9368. <https://doi.org/10.1021/acs.joc.9b01164>.
- (19) Sanabria Español, E.; Maldonado Villamil, M.; Estesó, M. Á.; Vargas, E. F. Volumetric and Acoustic Properties of Two Sodium Sulfonateresorcin[4]Arenes in Water and Dimethylsulfoxide. *J Mol Liq* **2018**, *249*, 868–876. <https://doi.org/10.1016/j.molliq.2017.11.060>.
- (20) Castillo-Aguirre, A.; Rivera-Monroy, Z.; Maldonado, M. Selective O-Alkylation of the Crown Conformer of Tetra(4-Hydroxyphenyl)Calix[4]Resorcinarene to the Corresponding Tetraalkyl Ether. *Molecules* **2017**, *22* (10), 1660. <https://doi.org/10.3390/molecules22101660>.
- (21) Maldonado, M.; Sanabria, E.; Batanero, B.; Estesó, M. Á. Apparent Molal Volume and Viscosity Values for a New Synthesized Diazoted Resorcin[4]Arene in DMSO at Several Temperatures. *J Mol Liq* **2017**, *231*, 142–148. <https://doi.org/10.1016/j.molliq.2017.01.093>.
- (22) Yang, F.; Guo, H.; Vicens, J. Mini-Review: Calixarene Liquid Crystals. *J Incl Phenom Macrocycl Chem* **2014**, *80* (3–4), 177–186. <https://doi.org/10.1007/s10847-014-0394-6>.
- (23) Tero, T.-R.; Nissinen, M. A Perspective to Resorcinarene Crowns. *Tetrahedron* **2014**, *70* (6), 1111–1123. <https://doi.org/10.1016/j.tet.2013.12.057>.
- (24) Velásquez-Silva, A.; Cortés, B.; Rivera-Monroy, Z. J.; Pérez-Redondo, A.; Maldonado, M. Crystal Structure and Dynamic NMR Studies of Octaacetyl-Tetra(Propyl)Calix[4]Resorcinarene. *J Mol Struct* **2017**, *1137*, 380–386. <https://doi.org/10.1016/j.molstruc.2017.02.059>.
- (25) Casas-Hinestroza, J.; Maldonado, M. Conformational Aspects of the O-Acetylation of C-Tetra(Phenyl)Calixpyrogallol[4]Arene. *Molecules* **2018**, *23* (5), 1225. <https://doi.org/10.3390/molecules23051225>.
- (26) Sanabria, E.; Estesó, M.; Pérez-Redondo, A.; Vargas, E.; Maldonado, M. Synthesis and Characterization of Two Sulfonated Resorcinarenes: A New Example of a Linear Array of Sodium Centers and Macrocycles. *Molecules* **2015**, *20* (6), 9915–9928. <https://doi.org/10.3390/molecules20069915>.
- (27) Sanabria, E.; Estesó, M. Á.; Vargas, E.; Maldonado, M. Experimental Comparative Study of Solvent Effects on the Structure of Two Sulfonated Resorcinarenes. *J Mol Liq* **2018**, *254*, 391–397. <https://doi.org/10.1016/j.molliq.2018.01.111>.
- (28) Wenzel, T. J. Calixarenes and Calix[4]Resorcinarenes as Chiral NMR Solvating Agents. *J Incl Phenom Macrocycl Chem* **2014**, *78* (1–4), 1–14. <https://doi.org/10.1007/s10847-013-0325-y>.
- (29) Placido Neri; Jonathan L. Sessler; Mei-Xiang Wang. *Calixarenes and Beyond*; Neri, P., Sessler, J. L., Wang, M.-X., Eds.; Springer International Publishing: Cham, 2016. <https://doi.org/10.1007/978-3-319-31867-7>.
- (30) Lassaad Baklouti; Jack Harrowfield; Jacques Vicens. *Calixarenes in the Nanoworld*; Vicens, J., Harrowfield, J., Baklouti, L., Eds.; Springer Netherlands, 2007. <https://doi.org/10.1007/978-1-4020-5022-4>.
- (31) Arnaud-Neu, F.; Fuangwasdi, S.; Notti, A.; Pappalardo, S.; Parisi, M. F. Calix[5]Arene-Based Molecular Vessels for Alkylammonium Ions. *Angewandte Chemie International Edition* **1998**,

- 37 (1–2), 112–114. [https://doi.org/10.1002/\(SICI\)1521-3773\(19980202\)37:1/2<112::AID-ANIE112>3.0.CO;2-O](https://doi.org/10.1002/(SICI)1521-3773(19980202)37:1/2<112::AID-ANIE112>3.0.CO;2-O).
- (32) Biali, S. E.; Böhmer, V.; Columbus, I.; Ferguson, G.; Grüttner, C.; Grynszpan, F.; Paulus, E. F.; Thondorf, I. Conformational Studies of Calix[5]Arenes Containing a Single Alkanediyl Bridge †. *Journal of the Chemical Society, Perkin Transactions 2* **1998**, No. 10, 2261–2270. <https://doi.org/10.1039/a803470b>.
- (33) Thondorf, I.; Brenn, J. Conformations of Calix[5]Arenes—a Molecular Mechanics Study. *Journal of the Chemical Society, Perkin Transactions 2* **1997**, No. 11, 2293–2300. <https://doi.org/10.1039/a702967e>.
- (34) C David Gutsche. *Calixarenes*; Royal Society of Chemistry: Cambridge, 2008. <https://doi.org/10.1039/9781847558190>.
- (35) Arduini, A.; Fabbi, M.; Mantovani, M.; Mirone, L.; Pochini, A.; Secchi, A.; Ungaro, R. Calix[4]Arenes Blocked in a Rigid Cone Conformation by Selective Functionalization at the Lower Rim. *J Org Chem* **1995**, 60 (5), 1454–1457. <https://doi.org/10.1021/jo00110a055>.
- (36) Lim, J. Y. C.; Yuntawattana, N.; Beer, P. D.; Williams, C. K. Ioselective Lactide Ring Opening Polymerisation Using [2]Rotaxane Catalysts. *Angewandte Chemie* **2019**, 131 (18), 6068–6072. <https://doi.org/10.1002/ange.201901592>.
- (37) de Bo, G.; Leigh, D. A.; McTernan, C. T.; Wang, S. A Complementary Pair of Enantioselective Switchable Organocatalysts. *Chem Sci* **2017**, 8 (10), 7077–7081. <https://doi.org/10.1039/C7SC02462B>.
- (38) Eichstaedt, K.; Jaramillo-Garcia, J.; Leigh, D. A.; Marcos, V.; Pisano, S.; Singleton, T. A. Switching between Anion-Binding Catalysis and Aminocatalysis with a Rotaxane Dual-Function Catalyst. *J Am Chem Soc* **2017**, 139 (27), 9376–9381. <https://doi.org/10.1021/jacs.7b04955>.
- (39) Semwal, S.; Choudhury, J. Switch in Catalyst State: Single Bifunctional Bi-State Catalyst for Two Different Reactions. *Angewandte Chemie International Edition* **2017**, 56 (20), 5556–5560. <https://doi.org/10.1002/anie.201702142>.
- (40) Mittal, N.; Pramanik, S.; Paul, I.; De, S.; Schmittel, M. Networking Nanoswitches for ON/OFF Control of Catalysis. *J Am Chem Soc* **2017**, 139 (12), 4270–4273. <https://doi.org/10.1021/jacs.6b12951>.
- (41) Kwan, C.-S.; Chan, A. S. C.; Leung, K. C.-F. A Fluorescent and Switchable Rotaxane Dual Organocatalyst. *Org Lett* **2016**, 18 (5), 976–979. <https://doi.org/10.1021/acs.orglett.5b03700>.
- (42) Galli, M.; Lewis, J. E. M.; Goldup, S. M. A Stimuli-Responsive Rotaxane-Gold Catalyst: Regulation of Activity and Diastereoselectivity. *Angewandte Chemie International Edition* **2015**, 54 (46), 13545–13549. <https://doi.org/10.1002/anie.201505464>.
- (43) Beswick, J.; Blanco, V.; de Bo, G.; Leigh, D. A.; Lewandowska, U.; Lewandowski, B.; Mishiro, K. Selecting Reactions and Reactants Using a Switchable Rotaxane Organocatalyst with Two Different Active Sites. *Chem Sci* **2015**, 6 (1), 140–143. <https://doi.org/10.1039/C4SC03279A>.
- (44) Blanco, V.; Carlone, A.; Hänni, K. D.; Leigh, D. A.; Lewandowski, B. A Rotaxane-Based Switchable Organocatalyst. *Angewandte Chemie* **2012**, 124 (21), 5256–5259. <https://doi.org/10.1002/ange.201201364>.
- (45) Kwamen, C.; Niemeyer, J. Functional Rotaxanes in Catalysis. *Chemistry – A European Journal* **2021**, 27 (1), 175–186. <https://doi.org/10.1002/chem.202002876>.

- (46) Wang, J.; Feringa, B. L. Dynamic Control of Chiral Space in a Catalytic Asymmetric Reaction Using a Molecular Motor. *Science (1979)* **2011**, *331* (6023), 1429–1432. <https://doi.org/10.1126/science.1199844>.
- (47) Baroncini, M.; Silvi, S.; Credi, A. Photo- and Redox-Driven Artificial Molecular Motors. *Chem Rev* **2020**, *120* (1), 200–268. <https://doi.org/10.1021/acs.chemrev.9b00291>.
- (48) Baroncini, M.; Casimiro, L.; de Vet, C.; Groppi, J.; Silvi, S.; Credi, A. Making and Operating Molecular Machines: A Multidisciplinary Challenge. *ChemistryOpen* **2018**, *7* (2), 169–179. <https://doi.org/10.1002/open.201700181>.
- (49) van Dijk, L.; Tilby, M. J.; Szpera, R.; Smith, O. A.; Bunce, H. A. P.; Fletcher, S. P. Molecular Machines for Catalysis. *Nat Rev Chem* **2018**, *2* (3), 0117. <https://doi.org/10.1038/s41570-018-0117>.
- (50) Pizzolato, S. F.; Collins, B. S. L.; van Leeuwen, T.; Feringa, B. L. Bifunctional Molecular Photoswitches Based on Overcrowded Alkenes for Dynamic Control of Catalytic Activity in Michael Addition Reactions. *Chemistry - A European Journal* **2017**, *23* (25), 6174–6184. <https://doi.org/10.1002/chem.201604966>.
- (51) Blanco, V.; Leigh, D. A.; Marcos, V. Artificial Switchable Catalysts. *Chem Soc Rev* **2015**, *44* (15), 5341–5370. <https://doi.org/10.1039/C5CS00096C>.
- (52) Erbas-Cakmak, S.; Leigh, D. A.; McTernan, C. T.; Nussbaumer, A. L. Artificial Molecular Machines. *Chem Rev* **2015**, *115* (18), 10081–10206. <https://doi.org/10.1021/acs.chemrev.5b00146>.
- (53) Biagini, C.; di Stefano, S. Abiotic Chemical Fuels for the Operation of Molecular Machines. *Angewandte Chemie International Edition* **2020**, *59* (22), 8344–8354. <https://doi.org/10.1002/anie.201912659>.
- (54) Biagini, C.; Capocasa, G.; del Giudice, D.; Cataldi, V.; Mandolini, L.; di Stefano, S. Controlling the Liberation Rate of the *in Situ* Release of a Chemical Fuel for the Operationally Autonomous Motions of Molecular Machines. *Org Biomol Chem* **2020**, *18* (20), 3867–3873. <https://doi.org/10.1039/D0OB00669F>.
- (55) Biagini, C.; Capocasa, G.; Cataldi, V.; del Giudice, D.; Mandolini, L.; di Stefano, S. The Hydrolysis of the Anhydride of 2-Cyano-2-phenylpropanoic Acid Triggers the Repeated Back and Forth Motions of an Acid–Base Operated Molecular Switch. *Chemistry – A European Journal* **2019**, *25* (66), 15205–15211. <https://doi.org/10.1002/chem.201904048>.
- (56) Biagini, C.; Fielden, S. D. P.; Leigh, D. A.; Schaufelberger, F.; Di Stefano, S.; Thomas, D. Dissipative Catalysis with a Molecular Machine. *Angewandte Chemie* **2019**, *131* (29), 9981–9985. <https://doi.org/10.1002/ange.201905250>.
- (57) Biagini, C.; Fielden, S. D. P.; Leigh, D. A.; Schaufelberger, F.; Di Stefano, S.; Thomas, D. Dissipative Catalysis with a Molecular Machine. *Angewandte Chemie International Edition* **2019**, *58* (29), 9876–9880. <https://doi.org/10.1002/anie.201905250>.
- (58) Franchi, P.; Poderi, C.; Mezzina, E.; Biagini, C.; di Stefano, S.; Lucarini, M. 2-Cyano-2-Phenylpropanoic Acid Triggers the Back and Forth Motions of an Acid–Base-Operated Paramagnetic Molecular Switch. *J Org Chem* **2019**, *84* (14), 9364–9368. <https://doi.org/10.1021/acs.joc.9b01164>.
- (59) Shi, Q.; Chen, C.-F. Step-by-Step Reaction-Powered Mechanical Motion Triggered by a Chemical Fuel Pulse. *Chem Sci* **2019**, *10* (8), 2529–2533. <https://doi.org/10.1039/C8SC05469J>.

- (60) Biagini, C.; Di Pietri, F.; Mandolini, L.; Lanzalunga, O.; Di Stefano, S. Photoinduced Release of a Chemical Fuel for Acid–Base-Operated Molecular Machines. *Chemistry – A European Journal* **2018**, *24* (40), 10122–10127. <https://doi.org/10.1002/chem.201800474>.
- (61) Ghosh, A.; Paul, I.; Adlung, M.; Wickleder, C.; Schmittel, M. Oscillating Emission of [2]Rotaxane Driven by Chemical Fuel. *Org Lett* **2018**, *20* (4), 1046–1049. <https://doi.org/10.1021/acs.orglett.7b03996>.
- (62) Biagini, C.; Albano, S.; Caruso, R.; Mandolini, L.; Berrocal, J. A.; di Stefano, S. Variations in the Fuel Structure Control the Rate of the Back and Forth Motions of a Chemically Fuelled Molecular Switch. *Chem Sci* **2018**, *9* (1), 181–188. <https://doi.org/10.1039/C7SC04123C>.
- (63) Erbas-Cakmak, S.; Fielden, S. D. P.; Karaca, U.; Leigh, D. A.; McTernan, C. T.; Tetlow, D. J.; Wilson, M. R. Rotary and Linear Molecular Motors Driven by Pulses of a Chemical Fuel. *Science (1979)* **2017**, *358* (6361), 340–343. <https://doi.org/10.1126/science.aao1377>.
- (64) Wilson, M. R.; Solà, J.; Carlone, A.; Goldup, S. M.; Lebrasseur, N.; Leigh, D. A. An Autonomous Chemically Fuelled Small-Molecule Motor. *Nature* **2016**, *534* (7606), 235–240. <https://doi.org/10.1038/nature18013>.
- (65) Berrocal, J. A.; Biagini, C.; Mandolini, L.; Di Stefano, S. Coupling of the Decarboxylation of 2-Cyano-2-Phenylpropanoic Acid to Large-Amplitude Motions: A Convenient Fuel for an Acid-Base-Operated Molecular Switch. *Angewandte Chemie* **2016**, *128* (24), 7111–7115. <https://doi.org/10.1002/ange.201602594>.
- (66) Berrocal, J. A.; Biagini, C.; Mandolini, L.; Di Stefano, S. Coupling of the Decarboxylation of 2-Cyano-2-Phenylpropanoic Acid to Large-Amplitude Motions: A Convenient Fuel for an Acid-Base-Operated Molecular Switch. *Angewandte Chemie International Edition* **2016**, *55* (24), 6997–7001. <https://doi.org/10.1002/anie.201602594>.
- (67) del Giudice, D.; Spatola, E.; Cacciapaglia, R.; Casnati, A.; Baldini, L.; Ercolani, G.; di Stefano, S. Time Programmable Locking/Unlocking of the Calix[4]Arene Scaffold by Means of Chemical Fuels. *Chemistry – A European Journal* **2020**, *26* (65), 14954–14962. <https://doi.org/10.1002/chem.202002574>.
- (68) Biagini, C.; Capocasa, G.; Cataldi, V.; del Giudice, D.; Mandolini, L.; di Stefano, S. The Hydrolysis of the Anhydride of 2-Cyano-2-phenylpropanoic Acid Triggers the Repeated Back and Forth Motions of an Acid–Base Operated Molecular Switch. *Chemistry – A European Journal* **2019**, *25* (66), 15205–15211. <https://doi.org/10.1002/chem.201904048>.
- (69) Biagini, C.; Capocasa, G.; del Giudice, D.; Cataldi, V.; Mandolini, L.; di Stefano, S. Controlling the Liberation Rate of the *in Situ* Release of a Chemical Fuel for the Operationally Autonomous Motions of Molecular Machines. *Org Biomol Chem* **2020**, *18* (20), 3867–3873. <https://doi.org/10.1039/D0OB00669F>.
- (70) Goswami, A.; Saha, S.; Elramadi, E.; Ghosh, A.; Schmittel, M. Off-Equilibrium Speed Control of a Multistage Molecular Rotor: 2-Fold Chemical Fueling by Acid or Silver(I). *J Am Chem Soc* **2021**, *143* (36), 14926–14935. <https://doi.org/10.1021/jacs.1c08005>.
- (71) Ghosh, A.; Paul, I.; Schmittel, M. Multitasking with Chemical Fuel: Dissipative Formation of a Pseudorotaxane Rotor from Five Distinct Components. *J Am Chem Soc* **2021**, *143* (14), 5319–5323. <https://doi.org/10.1021/jacs.1c01948>.
- (72) Berrocal, J. A.; Biagini, C.; Mandolini, L.; Di Stefano, S. Coupling of the Decarboxylation of 2-Cyano-2-Phenylpropanoic Acid to Large-Amplitude Motions: A Convenient Fuel for an Acid-Base-Operated Molecular Switch. *Angewandte Chemie International Edition* **2016**, *55* (24), 6997–7001. <https://doi.org/10.1002/anie.201602594>.

- (73) Förster, Th. Excimers. *Angewandte Chemie International Edition in English* **1969**, 8 (5), 333–343. <https://doi.org/10.1002/anie.196903331>.
- (74) Timmerman, P.; Verboom, W.; Reinhoudt, D. N.; Arduini, A.; Grandi, S.; Sicuri, A. R.; Pochini, A.; Ungaro, R. Novel Routes for the Synthesis of Upper Rim Amino and Methoxycarbonyl Functionalized Calix[4]Arenes Carrying Other Types of Functional Groups. *Synthesis (Stuttg)* **1994**, 1994 (02), 185–189. <https://doi.org/10.1055/s-1994-25435>.
- (75) Tosi, I.; Segado Centellas, M.; Campioli, E.; Iagatti, A.; Lapini, A.; Sissa, C.; Baldini, L.; Cappelli, C.; Di Donato, M.; Sansone, F.; Santoro, F.; Terenziani, F. Excitation Dynamics in Hetero-Bichromophoric Calixarene Systems. *ChemPhysChem* **2016**, 17 (11), 1686–1706. <https://doi.org/10.1002/cphc.201501065>.
- (76) Lazzarotto, M.; Sansone, F.; Baldini, L.; Casnati, A.; Cozzini, P.; Ungaro, R. Synthesis and Properties of Upper Rim C-Linked Peptidocalix[4]Arenes. *ChemInform* **2010**, 33 (5), no-no. <https://doi.org/10.1002/chin.200205066>.
- (77) Goodpaster, J. v.; McGuffin, V. L. Fluorescence Quenching as an Indirect Detection Method for Nitrated Explosives. *Anal Chem* **2001**, 73 (9), 2004–2011. <https://doi.org/10.1021/ac001347n>.
- (78) Chen, M.; Chen, D.; Chou, P. Fluorescent Chromophores Containing the Nitro Group: Relatively Unexplored Emissive Properties. *Chempluschem* **2021**, 86 (1), 11–27. <https://doi.org/10.1002/cplu.202000592>.
- (79) Zhao, C.-X.; Liu, T.; Xu, M.; Lin, H.; Zhang, C.-J. A Fundamental Study on the Fluorescence-Quenching Effect of Nitro Groups in Tetraphenylethene AIE Dyes with Electron-Withdrawing Groups. *Chinese Chemical Letters* **2021**, 32 (6), 1925–1928. <https://doi.org/10.1016/j.ccllet.2021.02.008>.
- (80) Dhingra, D.; Bhawna; Pandey, A.; Pandey, S. Fluorescence Quenching by Nitro Compounds within a Hydrophobic Deep Eutectic Solvent. *J Phys Chem B* **2020**, 124 (20), 4164–4173. <https://doi.org/10.1021/acs.jpcc.0c02231>.
- (81) Joseph R. Lakowicz. Instrumentation for Fluorescence Spectroscopy. In *Principles of Fluorescence Spectroscopy*; Springer US: Boston, MA, 2006; pp 27–61. [https://doi.org/10.1007/978-0-387-46312-4\\_2](https://doi.org/10.1007/978-0-387-46312-4_2).
- (82) Panja, S. K.; Dwivedi, N.; Saha, S. Tuning the Intramolecular Charge Transfer (ICT) Process in Push–Pull Systems: Effect of Nitro Groups. *RSC Adv* **2016**, 6 (107), 105786–105794. <https://doi.org/10.1039/C6RA17521J>.
- (83) Zobel, J. P.; Nogueira, J. J.; González, L. Mechanism of Ultrafast Intersystem Crossing in 2-Nitronaphthalene. *Chemistry - A European Journal* **2018**, 24 (20), 5379–5387. <https://doi.org/10.1002/chem.201705854>.
- (84) Valeur, B. Molecular Fluorescence. In *digital Encyclopedia of Applied Physics*; Wiley-VCH Verlag GmbH & Co. KGaA: Weinheim, Germany, 2009; pp 477–531. <https://doi.org/10.1002/3527600434.eap684>.
- (85) Hurley, R.; Testa, A. C. Photochemical  $n \rightarrow \pi^*$  Excitation of Nitrobenzene. *J Am Chem Soc* **1966**, 88 (19), 4330–4332. <https://doi.org/10.1021/ja00971a005>.
- (86) Kim, S. K.; Bok, J. H.; Bartsch, R. A.; Lee, J. Y.; Kim, J. S. A Fluoride-Selective PCT Chemosensor Based on Formation of a Static Pyrene Excimer. *Org Lett* **2005**, 7 (22), 4839–4842. <https://doi.org/10.1021/ol051609d>.

- (87) Winnik, F. M. Photophysics of Preassociated Pyrenes in Aqueous Polymer Solutions and in Other Organized Media. *Chem Rev* **1993**, *93* (2), 587–614. <https://doi.org/10.1021/cr00018a001>.
- (88) del Giudice, D.; Spatola, E.; Cacciapaglia, R.; Casnati, A.; Baldini, L.; Ercolani, G.; di Stefano, S. Time Programmable Locking/Unlocking of the Calix[4]Arene Scaffold by Means of Chemical Fuels. *Chemistry – A European Journal* **2020**, *26* (65), 14954–14962. <https://doi.org/10.1002/chem.202002574>.
- (89) del Giudice, D.; Spatola, E.; Cacciapaglia, R.; Casnati, A.; Baldini, L.; Ercolani, G.; di Stefano, S. Time Programmable Locking/Unlocking of the Calix[4]Arene Scaffold by Means of Chemical Fuels. *Chemistry – A European Journal* **2020**, *26* (65), 14954–14962. <https://doi.org/10.1002/chem.202002574>.
- (90) Deng, Y.; Lai, S. K.-M.; Kong, L.; Au-Yeung, H. Y. Fine-Tuning of the Optical Output in a Dual Responsive Catenane Switch. *Chemical Communications* **2021**, *57* (23), 2931–2934. <https://doi.org/10.1039/D1CC00310K>.
- (91) Jarolímová, Z.; Vishe, M.; Lacour, J.; Bakker, E. Potassium Ion-Selective Fluorescent and PH Independent Nanosensors Based on Functionalized Polyether Macrocycles. *Chem Sci* **2016**, *7* (1), 525–533. <https://doi.org/10.1039/C5SC03301B>.
- (92) Timmerman, P.; Verboom, W.; Reinhoudt, D. N.; Arduini, A.; Grandi, S.; Sicuri, A. R.; Pochini, A.; Ungaro, R. Novel Routes for the Synthesis of Upper Rim Amino and Methoxycarbonyl Functionalized Calix[4]Arenes Carrying Other Types of Functional Groups. *Synthesis (Stuttg)* **1994**, *1994* (02), 185–189. <https://doi.org/10.1055/s-1994-25435>.
- (93) Sabine Seifert, Dr. David Schmidt, Dr. Kazutaka Shoyama, Prof. Dr. Frank Würthner Base-Selective Five- versus Six-Membered Ring Annulation in Palladium-Catalyzed C–C Coupling Cascade Reactions: New Access to Electron-Poor Polycyclic Aromatic Dicarboximides. *Angewandte Chemie - International Edition*, **2017**, vol. 56, # 26, p. 7595 - 7600



# Chapter 2

## **Temporal control of the host-guest properties of a calix[6]arene receptor by the use of a chemical fuel\***

\*Part of this chapter is published on: *J. Org. Chem.* 2022, **87**, 5, 3623–3629.  
<https://doi.org/10.1021/acs.joc.2c00050>



# Introduction

## 2.1 Out of equilibrium systems

The majority of man-made materials are in equilibrium, which means that the forward and backward rates of assembly and bond formation are balanced. Under equilibrium conditions, we understand and can control the properties of current materials or even create new materials with new functions.<sup>1</sup> Out-of-equilibrium structures and materials can exist when there is a net exchange of matter and energy with their surroundings (dissipative system). Life and living systems are in thermodynamically unstable status and thus cannot exist in equilibrium. The smallest organizational unit that expresses life characteristics is a cell.<sup>2</sup> Cells develop, divide, procreate, interact with their environment, and adjust its status to changes taking place around it.<sup>3</sup> These characteristics need a constant supply of energy, that enters the cell in the form of high-energy nutrients; when the energy supply stops, death occurs. The energy released during nutrient breakdown is used to create lipids, peptides, carbohydrates and nucleic acids. These substances then self-assemble in a thermodynamically controlled manner to create the fundamental cell structures, such as membranes, proteins, and the genome. Importantly, energy is also required for the synthesis of molecules with high chemical potentials, such as acetyl-CoA, NADH, and ATP, which act as the chemical fuels for the biological engine.<sup>4</sup> These molecules are transformed into waste molecules with lower chemical potentials, and the energy released from these molecules drives molecular pumps and motors, causing sustained concentration gradients and directional movement signs of a non-equilibrium system.<sup>5,6</sup> Chemical fuels also control the self-assembly processes in time and space, directly contributing to the structural organization of the cell.<sup>7,8</sup> Chemical fuels also enable the formation of high-energy structures, which is another indication of the non-equilibrium nature of life, through a direct coupling of self-assembly processes and energy dissipation. Nature can make considerable use of high-energy transient self-assembly structures capable of performing work via dissipative processes. While the out-of-equilibrium nature of these structures confers unique features on the resulting biological materials, the creation of

equivalent man-made out-of-equilibrium supramolecular materials is still in its early stages. Implementing this type of non-equilibrium process in synthetic systems is certain to have a dramatic impact on the fields of chemistry, materials science, and synthetic biology, leading to novel dissipative structures capable of converting and storing chemical energy. Supramolecular chemistry is fast advancing into uncharted area in which the composition of a dynamic system is dictated not by the relative thermodynamic stabilities of the components, but by the components ability to occupy high-energy states through energy-dissipating processes. This capability means that such systems may store and transfer energy, bringing us one step closer to replicating the amazing features of living systems in synthetic ones.<sup>9</sup> This progress has resulted in energy-driven molecular machines,<sup>10-13</sup> materials,<sup>14,15</sup> pattern formation<sup>16,17</sup> and chemical reactivity<sup>18</sup> demonstrating the broad range of possibilities afforded by out-of-equilibrium chemistry. For this reason, a great effort is nowadays devoted to the design of artificial machineries that operate under dissipative conditions, that is until the stimulus (fuel) is present.<sup>19</sup> A number of dissipative systems have been recently developed in the fields of self-assembly,<sup>20-22</sup> DNA-based systems,<sup>23-25</sup> molecular machines and pumps,<sup>26-28</sup> and host-guest chemistry,<sup>29,30</sup> with a clear predominance of the first category.

## 2.2 Self-assembly and dissipative self-assembly

Self-assembly process is common and essential to life. The term self-assembly refers to the spontaneous and independent arrangement of unconnected parts into formal structures and has become a powerful method for developing intelligent and useful materials. The smallest biological unit of life, the cell, for example, is made up of multiple self-assembling building parts that work together to create a sophisticated and useful system. Phospholipids and proteins are combined to form the complete cell wall, a semipermeable barrier that protects the cell and controls trans-cellular communication. Self-assembly has become also the most effective method for creating artificial molecular nanostructures during the past few decades. It has enabled significant advancements in the domains of materials chemistry and nanotechnology<sup>31</sup> as well as the creation of novel diagnostic and catalytic systems. Molecular self-assembly is the direct result of non-covalent interactions between individual molecules, such as electrostatic interactions, hydrogen bonds,  $\pi$ - $\pi$  interactions or hydrophobic effects and it is thermodynamically favoured because these interactions are strong enough to overcome the loss of entropy brought on by the organization of the building components. Often, the

reversibility of these systems ensures that the self-assembled state is dynamic and that there will always be interchange with unassembled building blocks. Self-assembly is a particularly versatile and attractive method for the creation of novel artificial functional systems due to the dynamic nature of the self-assembled state, its spontaneity, and the fact that it is thermodynamically favourable. Although there are many successful artificial materials based on self-assembly, these structures cannot compete with the extremely complex and sophisticated architectures found in natural systems. Many self-assembly processes are associated with an energy-consuming process and these processes are defined as dissipative self-assembly.<sup>7,32</sup> Nature takes advantage of dissipative self-assembly to gain temporal control over the chemical functions linked with the assembled state<sup>33,34</sup>.

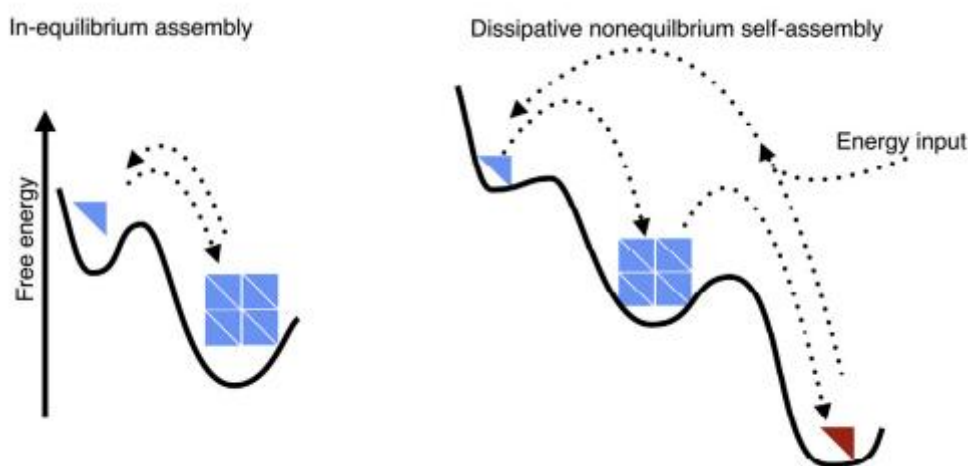


**Fig.1** Thermodynamic energy landscape of (a) equilibrium self-assembly, (b) dissipative self-assembly. Blue colour denotes building-blocks and assemblies at thermodynamic minimum, whereas red one denotes entities at lower energies<sup>35</sup>

In terms of the thermodynamic description of the assemblies, there are two categories of molecular self-assembly: equilibrium self-assembly and out-of-equilibrium self-assembly.<sup>36</sup> When equilibrium self-assembly occurs, the system does not produce or consume any Gibbs free energy since the created structures are at thermodynamic minimum (Figure 1). Dissipative self-assembly results in the formation of inherently unstable assemblies that can only be kept in a steady condition by a steady stream of energy. Then, by means of irreversible entropy-producing processes, this energy is lost (Figure 1). There is currently a strong interest to implement the same principle in synthetic systems, with the ultimate goal of creating intelligent materials and devices capable of performing different functions based on stimuli provided in the form of energy.<sup>37,38</sup> In recent years, this has led to the development of various

chemical systems that require energy to self-assemble into functional structures.<sup>39</sup> The most frequent way of supplying energy to these systems is in the form of physical stimuli such as light<sup>14,40,41</sup> but also electrical current<sup>42</sup>, ultrasound<sup>43m</sup> or, alternatively, by changing the pH.<sup>44,45</sup>

### 2.3 Host-guest chemistry

Supramolecular Chemistry<sup>46,47</sup> concepts and methodologies have been regarded as useful tools for assembling the components of nanodevices and thus for the development of nanotechnologies.<sup>48,49</sup> Supramolecular chemistry is a discipline of chemistry that focuses on chemical systems made of a finite number of molecular subunits or components that spontaneously assemble through non-covalent interactions. Unlike classical chemistry, which focuses on the manipulation of covalent bonds, supramolecular chemistry takes advantage of reversible non-covalent interactions between distinct chemical species, either charged or neutral, in the solid, liquid, or gas phase. Although these interactions are very weak, they may create stable supramolecular complexes when they work together, making them a potent tool for organizing chemical species in space to give the aggregates specialized functionalities. These aggregates have brand-new characteristics and capabilities that set them apart from the single components.<sup>48,50,51</sup> One of the core ideas of supramolecular chemistry is molecular recognition. It results in the development of *host-guest* complexes and is based on the geometrical and electrical complementarity between the species involved. According to this definition, a *host* is a chemical compound that has convergent binding sites, whereas a *guest* has complementary and divergent binding sites. The *host* is typically, but not always, a big molecule or aggregation, such as an enzyme with a central hole or cavity or a synthetic macrocycle. The *guest* might be a neutral species, an ion pair, a cation, an anion, or a more complex molecule. The free energy gain, caused by intermolecular interactions that lead to aggregation, drives complex development. When compared to their acyclic counterparts, complexes generated by macrocyclic hosts have an extra stability due to what is known as the macrocyclic effect.<sup>52</sup> This impact is related not only to the guest binding by many sites, but also to their pre-organization. Complementarity between the host and the guest in terms of binding affinity is another important criterion for modelling and creating Host-Guest complexes. To be efficient, a host must supplement the guest binding sites with a precise arrangement of its own binding activities. Based on this, supramolecular chemistry concepts and methodologies may be useful tools for tuning the reactivity and desirable features of the

guests.<sup>53</sup> Nature makes considerable use of supramolecular chemistry to utilize a wide range of biological activities.

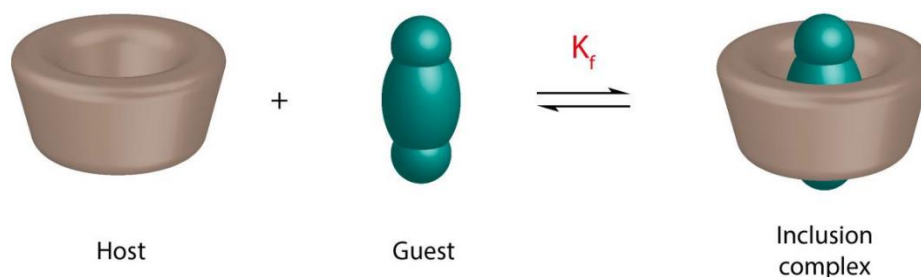


**Fig.2** Schematic representation of the formation of a Host-guest complex

Enzymes, in particular, are excellent examples of supramolecular catalysts and how intermolecular interactions may direct a process down the proper paths.

In recent decades, there has been a lot of interest in using *Host-Guest* chemistry to produce novel supramolecular devices and machine prototypes. Countless instances of operational devices and molecular level machines equipped with specific functionalities have been created by employing well-defined and shaped molecules exploring the concepts of the "bottom-up approach".<sup>54,55</sup>

## 2.4 Host-guest system controlled in a dissipative way by means of chemical fuel

The first examples of how chemical fuels control the host-guest properties are starting to emerge in the literature. In 2015, Nitschke et al.<sup>29</sup> described a self-assembled cage made of porphyrin building blocks and Cu(I)-metal ions that dissociated when triphenylphosphine ( $\text{PPh}_3$ ) was added.

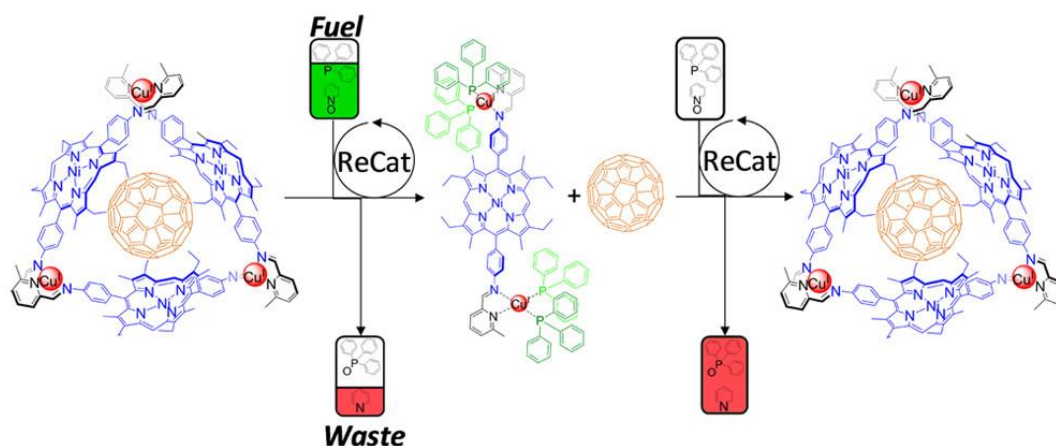


**Fig 3:** Transient displacement of fullerene from a molecular cage driven by triphenylphosphine<sup>29</sup>

This happened because heteroleptic N,P-complexes formed preferentially with Cu(I) (Figure 3). However, when PPh<sub>3</sub> was introduced under oxidative conditions (with pyridine N-oxide as an oxidant and the oxo-transfer catalyst ReCat as an accelerator), it was gradually oxidised to triphenylphosphine oxide, which no longer coordinated Cu(I). As a result, the system restored to its assembled condition. By introducing a new batch of PPh<sub>3</sub>, a new cycle can be started. Transient dissociation of the cage occurred because the oxidation rate is much slower compared to rate of the ligand exchange. The approaches described above enable time-dependent regulation of guest binding and rotaxane production, and they have the potential to be coupled to even more complex responses, such as those displayed by molecular machines.<sup>56</sup> The ability to incorporate time delays into complex molecular systems is important in the context of designing intricate responses, as demonstrated by examples from both natural systems and artificial systems.<sup>57</sup>

In 2016, Di Stefano et al.<sup>58</sup> introduced, for the first time, the use of a particular class of chemical fuel, carboxylic acid activated by electronwithdrawing groups in alpha positions,<sup>19</sup> able to trigger cycles of motion of molecular machines by a single pulse (see also Chapter 1). Among the different machines studied by this group, the one reported in 2021<sup>30</sup> shown that nitroacetic acid (O<sub>2</sub>NCH<sub>2</sub>CO<sub>2</sub>H) can be conveniently used to control the pH of a water solution over time and consequently the uptake/release of a guest from a host cavity. Time-programmable sequences of the type pH1(high)-pH2(low)-pH3(high) can be obtained, where both the magnitude of the initial pH jump and the time necessary for the subsequent pH rise can be predictably controlled by prudent reagent concentration selection. Subsequent additions of nitroacetic acid can produce pH1(high)-pH2(low)-pH3(high) sequences. As a proof of concept, the nitroacetic acid-driven pH1(high)-pH2(low)-pH3(high) time-programmed sequence was applied to the well-known host-guest pH dependent interaction between alpha-cyclodextrin and p-aminobenzoic acid, which can be easily monitored using a spectrofluorometer.<sup>59</sup> The protonation state of p-aminobenzoic acid can be easily controlled by adjusting the solution pH. In the presence of excess of alpha-cyclodextrin, the zwitterionic form of p-aminobenzoic acid, is firmly bound by the cyclodextrin cavity, resulting in a high fluorescence emission (Figure 4).<sup>59</sup>

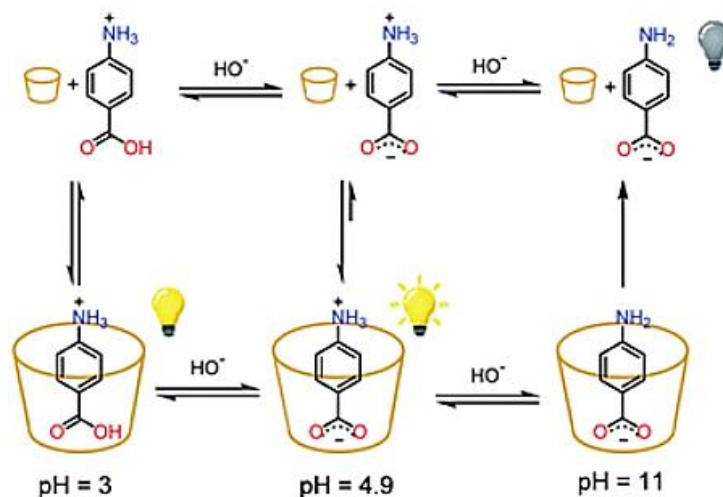


**Fig.4:** State of charge of *p*-aminobenzoic acid at different pHs and corresponding affinity for  $\alpha$ -cyclodextrin.<sup>30</sup>

When the acid is positively charged (lower pH), the host-guest interactions weaken and the guest is partially released, resulting in a mild quenching of fluorescence emission (Figure 4). Binding is even less strong for the negatively charged form of *p*-aminobenzoic acid (high pH), and emission is noticeably less effective (Figure 4). Thus, fluorescence fluctuations are mostly caused by the extent to which the acid is incorporated into cyclodextrin.

Another example of dissipative host-guest complex formation driven by chemical fuels was reported by Schmitt et al.<sup>60</sup> in which the design of the pseudorotaxane-based rotor included a 3-fold complete self-sorted library of dynamic patterns. The five-component rotor is based on the association/dissociation of the pyridyl head of the pseudorotaxane rotator arm between two zinc(II) porphyrin stations. The addition of TFA or 2-cyano-2-phenylpropanoic acid as a chemical fuel to a zinc release mechanism and the loose rotor components allowed the liberated zinc(II) ions and protons to function in concert, establishing the rotor via the development of a heteroleptic zinc complex and a pseudorotaxane linkage (Figure 5).

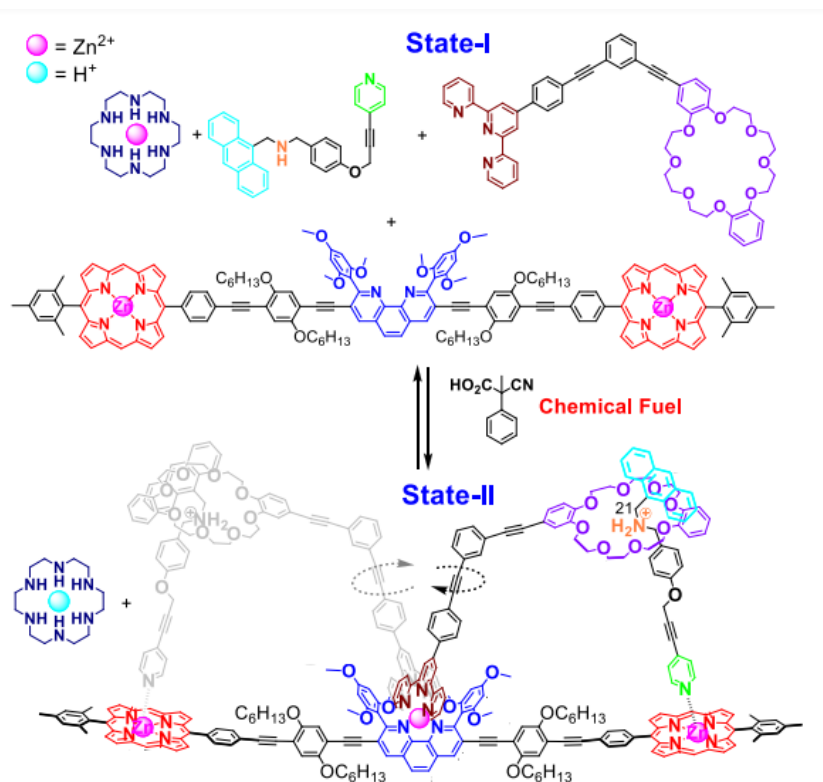


**Fig.5:** Representation of the pseudorotaxane rotor studied by Schmittl driven by chemical fuels<sup>60</sup>

The dissipative device was successfully pulsed three times with chemical fuel. Because of the dual role of the fuel acid, two kinetically separate processes were involved in both the out-of-equilibrium assembly and disassembly of the rotor, emphasizing the difficult issues in chemical fuel multitasking.

## 2.5 Calix[6]arenes as a host in supramolecular chemistry

In the previous chapter it was shown that calix[4]arenes are suitable scaffold for the construction of molecular machine. In addition, they have demonstrated to be versatile for the construction of selective receptors for cation<sup>61</sup> and neutral molecules.<sup>62,63</sup>



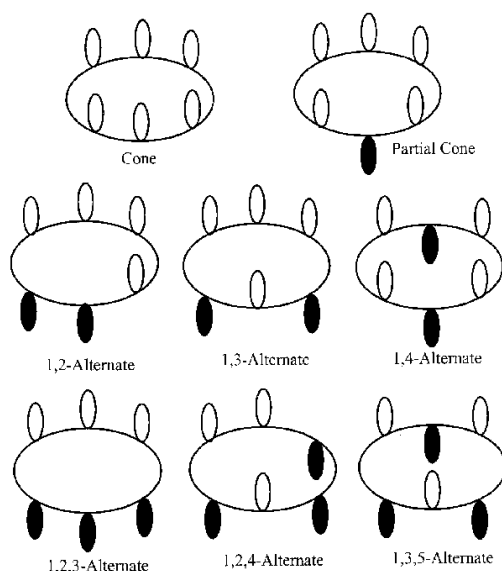


**Fig.6:** The limiting conformations of calix[6]arene. White ellipse denotes benzyl ring is up, black means down.<sup>108</sup>

Calix[6]arenes have received less attention as molecular building block for *host-guest* chemistry, mainly because it is more difficult to control their conformation but also because the reaction to functionalize the upper and lower rim are often more difficult and sometimes impossible. The control of the conformation of calix[6]arenes scaffold has been a major target over recent years. The functionalization at the phenolic groups with large substituents is not sufficient to restrict the conformational motion in *p*-tert-butylcalix[6]arenes because Reinhoudt *et al.*<sup>64</sup> and others have shown that also the tert-butyl groups can rotate through the annulus in these larger macrocycles. To make this class of macrocycle suitable for their use as a molecular receptor a strategy is to rigidify them in a cone shape structure. C. David Gutsche's primary objective for developing calixarene chemistry was to use these macrocyclic structures as molecular baskets to build enzyme analogues.<sup>65</sup> The technique relied on a calix[6]arene that was covalently capped at the lower rim to limit its conformational mobility and functionalized at the upper rim by catalytic protein residue mimics. Although this study did not achieve the anticipated catalytic promises, it inspired Gutsche and others to devise novel ways for selectively functionalizing a calix[6]arene core. Inspired by this work, many research groups have tried to develop calix[6]arenes as molecular receptors. Rigidified calix[6]arenes have been studied as receptor for cations<sup>66,67</sup> (organic and inorganic), anions<sup>68</sup> and neutral molecule.<sup>69</sup> Among the most active research group in this field, the one of Reinaud and Jabin *et al.*<sup>70</sup> described the synthesis and characterization of two new calix[6]arene-based

ligand represented in Figure 7. Both compounds are capped by a trenamide core at the upper rim that prevents the uptake/release exchange of guest molecules through the upper rim and one of them presents three imidazole residues at the lower rim. The first important consequence of covalent capping is the resultant limited conformational freedom and the freezing of the cone conformation.

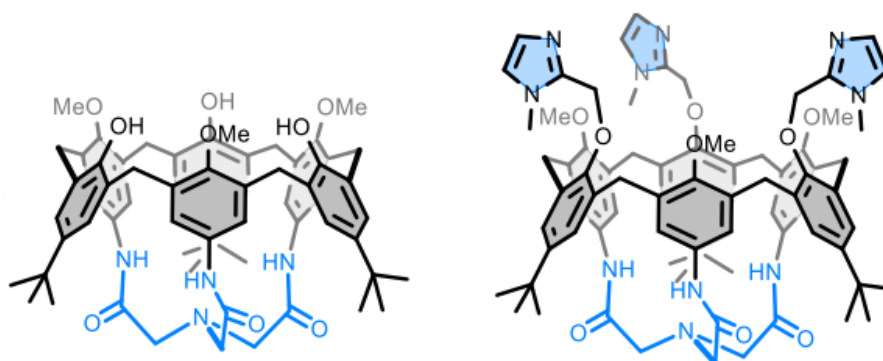


**Fig.7:** structure of the novel calix[6]arene ligand developed by Reinaud, Jabin *et al.*

The trenamide tripod can bind a metal ion like  $Zn^{2+}$  where the metal ion is coordinated to the three carbonyl groups of the amide functions. The  $Zn^{2+}$  ion preferentially binds at the lower rim even when the trisimidazole groups are present. Guest ligand exchange must then take place via a metal ion decoordination/recoordination mechanism. The upper rim capping modifies and rigidifies the calixarene conformation, which strengthens metal ion coordination at the lower rim. This results in a selective metallo-receptor able to discriminate the size of primary amines, being able to readily bind  $EtNH_2$  but not  $PrNH_2$ . As a result, the cavity covalent capping does not forbid ligand exchange, but imposes a drastic selectivity change on guest binding. The increased rigidity of the receptor, however, weakens the host-guest interactions, precluding important induced-fit behaviours that are at work in the parent, upper rim opened, funnel complex.

In 2000 Arduini *et al.*<sup>71</sup> discovered that a guest with axial symmetry and appropriate chemical information, such as N,N'-4,4'-bipyridinium salt, can thread the calix[6]arene annulus to create supramolecular interlocked system, namely a pseudorotaxane.<sup>72-75</sup> In this work they reported the first example of a calix[6]arene being utilized as a wheel in the generation of pseudorotaxanes and rotaxanes. This calixarene host is characterized by the presence of three phenylureido groups at the upper rim and three methoxy groups and three octyloxy chains in alternate positions at the lower rim. This tris-(N-phenylureido)calix[6]arene in a solution of

weakly polar solvents (chloroform, dichloromethane, benzene or toluene), assumes a cone conformation on the NMR time scale.

The chosen guests for the formation of the pseudorotaxane complex was *N,N'*-4,4'-bispyridinium salt functionalised with two octyl chains (Figure 8). Thus, this calix[6]arene was shown to be able to take up viologen salts in weakly polar solvents and form pseudorotaxane structures, with an apparent association constant  $\log K \sim 6\div 7$ , as estimated using UV/vis measurements.<sup>76</sup>

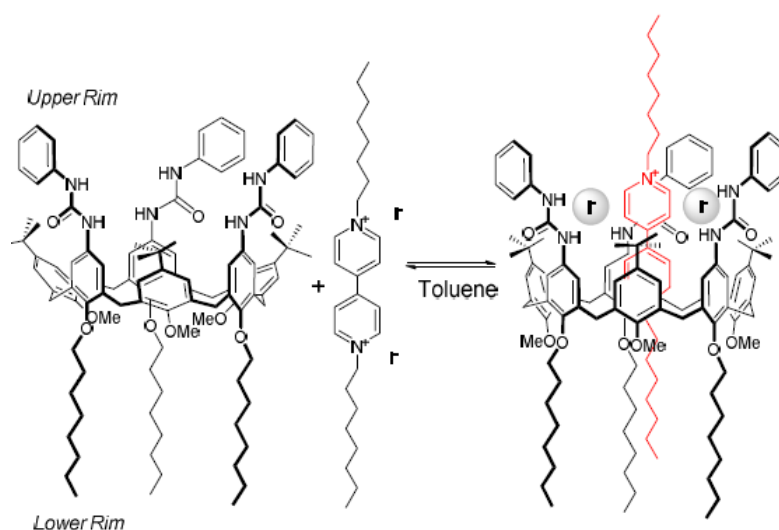
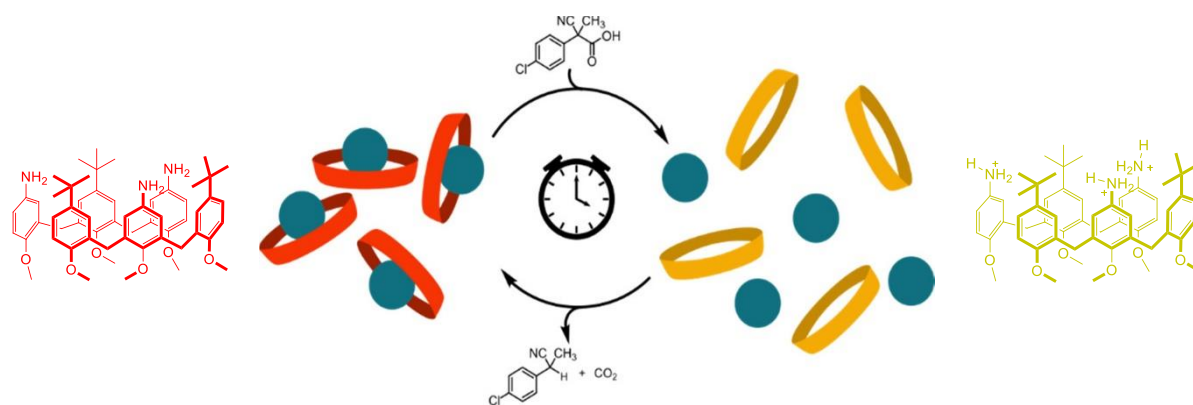


**Fig.8:** Formation of a pseudo-rotaxane in weakly polar solvents (toluene) for a triphenylureido calix[6]arene-based wheel and an *N,N'*-dioctyl viologen axle

A plethora of non-covalent intermolecular interactions hold this complex together. The wheel and axle are kept together by the cooperative action of  $\pi$ - $\pi$ , CH- $\pi$  and charge transfer (CT) interactions, but the formation of six hydrogen bonds between the three phenylureido groups of the host and the two counteranions (iodide) of the salt is particularly important in stabilizing the complex.

## 2.6 Aim of this work

Taking inspiration from all the works shown in the previous sections, we planned to exploit the chemical fuels to trigger the uptake/release of guests inside the preorganized cavity of a calix[6]arene scaffold. As already explained, calix[6]arenes are floppier and less organized than the calix[4]arene scaffold but their cavity is larger and potentially more suitable to host small guest molecules.<sup>77,78</sup>



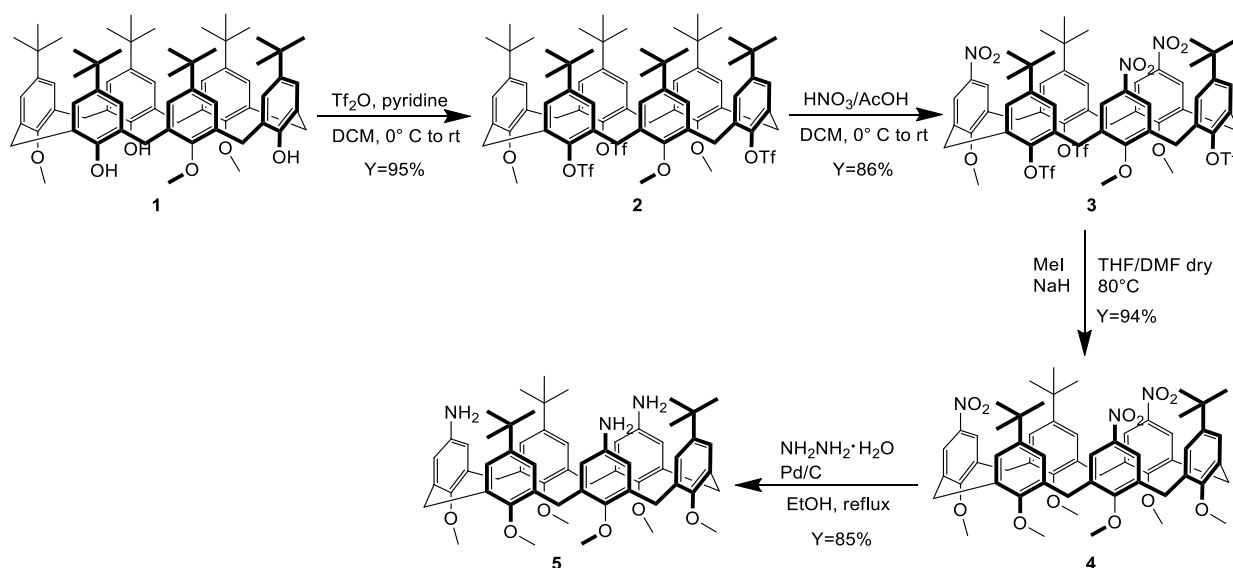
Moreover, the purpose is to drive and temporally control the host-guest complexation between host **5** where three alternate aromatic moieties are functionalized with three amine groups and a suitable guest molecule by means of carboxylic acid fuels under dissipative conditions.



# Results and Discussion

## 2.7 Synthesis

The triamino-hexamethoxycalix[6]arene **5** was obtained in a few steps from the known 1,3,5-trimethoxycalix[6]arene (Scheme 1) following the already know protocol. The synthetic strategy relies on the regioselective introduction of three nitro groups at the upper rim of calix[6]arene scaffold obtained thanks to the different reactivity of methylated phenols compared to triflated ones (regioselective nitration from **2** to **3** in Scheme 1).



**Scheme 1:** Synthesis of compound **5**

Although the regioselective nitration has been also carried out on compound **1**<sup>79</sup>, thanks to the higher reactivity of phenols compared to anisoles,<sup>80</sup> the yields of 1,3,5-trinitrocalix[6]arene are low and its purification from differentially nitrated products quite difficult. For this reason, it was devised to increase the difference in nucleophilicity of the two aromatic nuclei and to sulphonate the three free hydroxyl groups of **1**, using pyridine as a base and triflic anhydride, to obtain compound **2**. The reaction was carried out in dichloromethane and the triflic anhydride was added dropwise at 0 °C. After 24 h the reaction was quenched with 1M HCl and the organic phase was evaporated to dryness. The pure

product was obtained with a yield of 95% after trituration in acetonitrile. Electron-withdrawing groups, such as triflate, connected to the phenol O atoms of **2**, deactivate the corresponding aromatic units of the calix[6]arene toward electrophilic attacks, thus allowing a highly selective ipso-nitration at the upper rim of the anisole units. Compound **2** was then nitrated to obtain **3** by using fuming HNO<sub>3</sub> and acetic acid as nitrating agent. To a solution of **2** in dichloromethane the two acids were added dropwise at 0 °C and the reaction was left to return to room temperature. After 6h the reaction was quenched with water and the organic phase was separated and evaporated to dryness. Pure compound **3** was obtained after purification by flash chromatography with an 86% yield. To increase the stability of our final host molecule to hydrolysis, we decided to replace the triflic groups with methyl groups. Therefore, we reacted a mixture of compound **3** and iodomethane as methylated agent in a Schlenk tube in THF/DMF. This allowed the simultaneous removal of triflates and insertion of the methyl groups. The reaction was heated to 80 °C for 5h, then quenched with water and the organic products were extracted in dichloromethane. The crude product was then purified by a chromatography column to give pure **4** with a 94% yield. Finally, product **4** was reduced to the triamino-hexamethoxy calix[6]arene **5** using hydrazine as a source of hydrogen and Pd supported on carbon as catalyst. The reaction was carried out in refluxing ethanol for 24h. After catalyst filtration the pure product **5** was obtained in 85% yield.

## 2.8 <sup>1</sup>H NMR titration between calix[6]arene **5** and N-methyl isoquinolinium trifluoromethanesulfonate **7**

To investigate the potential host ability of compound **5** we registered a series of <sup>1</sup>H NMR spectra of 1:1 mixture of **5** and alkylammonium ions in CD<sub>2</sub>Cl<sub>2</sub> solution. It is in fact well known that calixarenes, thanks to their electron-donating cavities form complexes with quaternary ammonium ions thanks to cation- $\pi$  interactions.<sup>81,82</sup> We noticed significant shifts of the host only in the presence of N-methyl-isoquinolinium trifluoromethanesulfonate **7**. Therefore, the calix[6]arene **5** was titrated with **7** by <sup>1</sup>H NMR and the most significant portion of the resulting spectra, 300 MHz in CD<sub>2</sub>Cl<sub>2</sub> at 25 °C, are reported in Figure 1. Trace *a*, spectrum of the free host **5**, presents two singlets at 3.0 and 3.6 ppm corresponding to the methoxy groups of the two different anisole nuclei and a singlet at 3.8 ppm due to the 12 protons of the methylene bridges. The presence of a single singlet for the protons of the methylene bridges indicates that calix[6]arene **5** is conformationally flexible<sup>83</sup>, due to a fast

rotation of the aromatic rings around the methylene hinges on the NMR time-scale. Singlets at 6.0 ppm and 7.2 ppm are due to the aromatic protons of the rings bearing the amino and *t*-butyl groups (*a* and *b* in Figure 1), respectively.

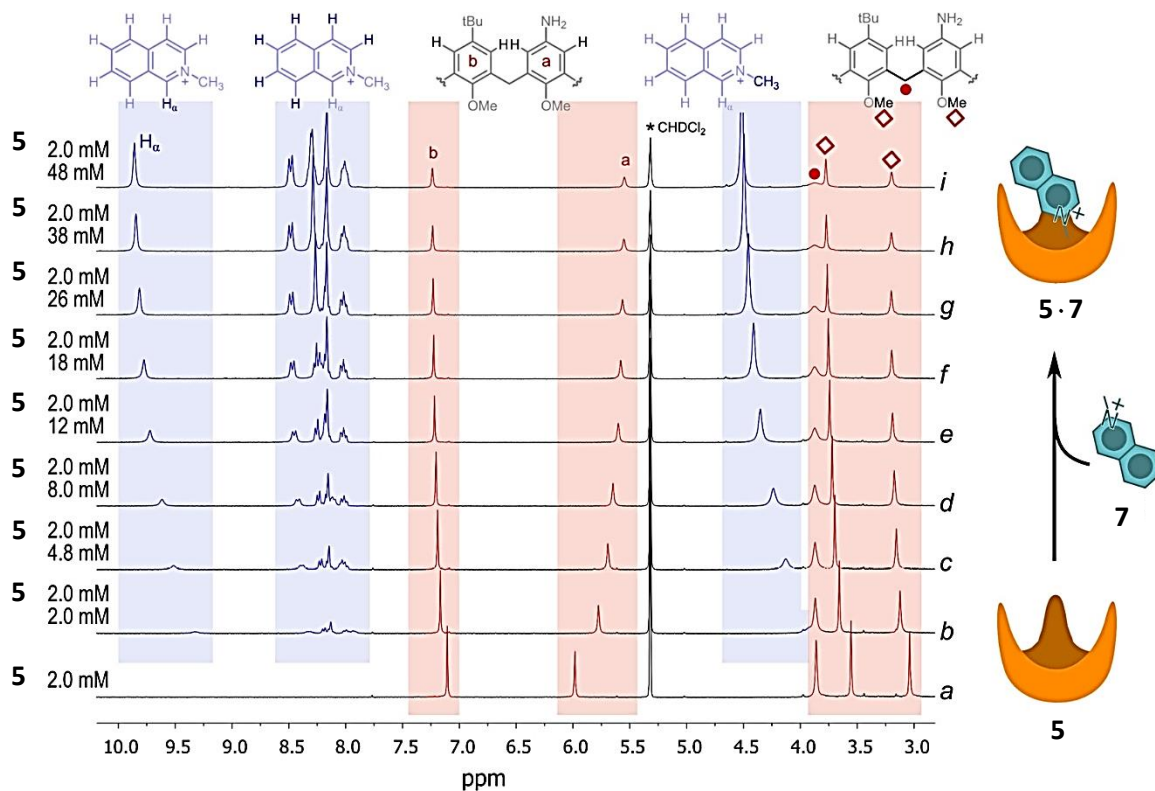


**Fig 1.** Titration of 2.00 mM calix[6]arene **5** (light red areas) with **7** (light blue areas), in  $CD_2Cl_2$  at 25 °C. Trace **a** is related to 2.00 mM calix[6]arene **5**; traces **b–i** are related to the same calixarene solution to which a solution of increasing amount of guest **7** and 2mM host **5** was added (to maintain the concentration of **5** constant along the titration).

The presence of a single set of signals for the protons of host and guest along the titration indicates the presence of a fast exchange regime with the complex on the NMR timescale. For this reason, the shape and multiplicity of the methylene bridge protons, which are expected to change in the complex, only broaden upon complex formation



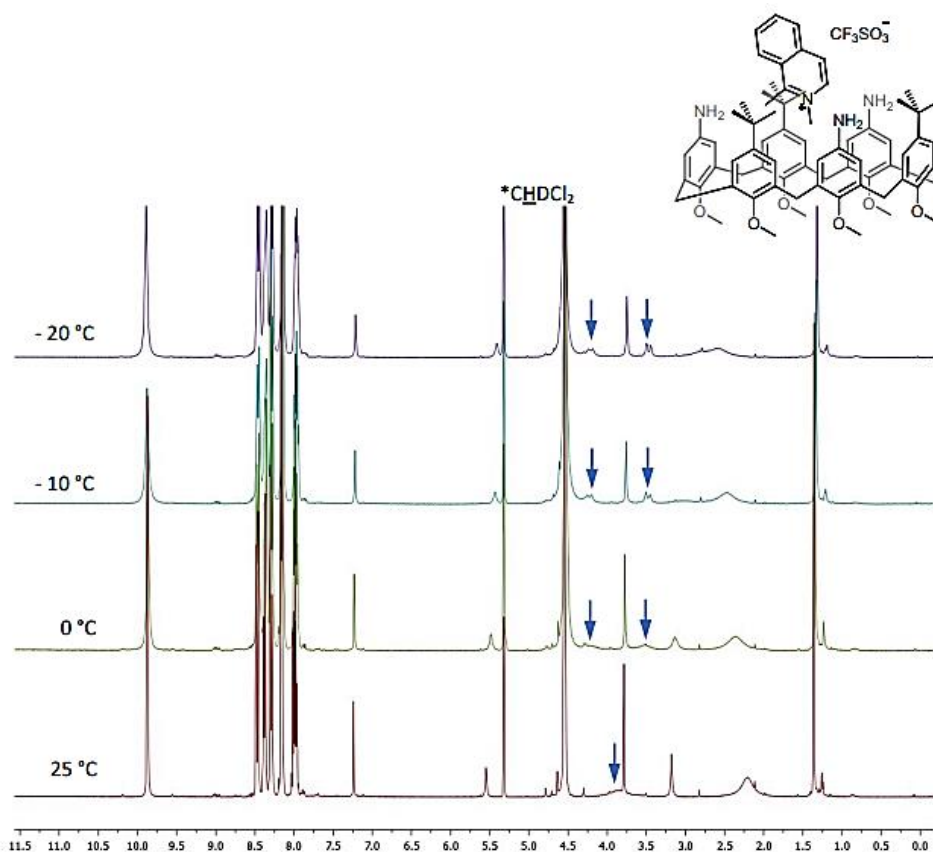


**Fig.2**  $^1\text{H}$  NMR spectra ( $\text{CD}_2\text{Cl}_2$ , 300 MHz) of 2.00 mM **5** + 100 mM **7** (approximately 98% complex **5**•**7**, vide infra for  $K_{\text{ass}}$  determination) at different temperature. Blue arrows show the splitting of the signals belonging to the methylene bridges upon cooling.

Upon increasing the concentration of guest **7**, the aromatic singlets of the calixarene aromatic protons *a* and *b* diverge. In the meantime, the methoxy signals are downfield shifted, and the singlet related to the methylene bridges becomes broader and broader, due to a rigidification of the structure when guest **7** is hosted inside **5**. This loss of conformational flexibility is confirmed by the low-temperature spectra of **5** in presence of a 50-fold molar excess of **7**, with the appearance, at  $-10\text{ }^\circ\text{C}$ , of two doublets for the diastereotopic methylene protons (see blue arrows in Figure 2), typical of a more rigid cone conformation of the calixarene.<sup>84</sup> At the same temperature, in the absence of the guest, the methylene protons give only a slightly broadened singlet.

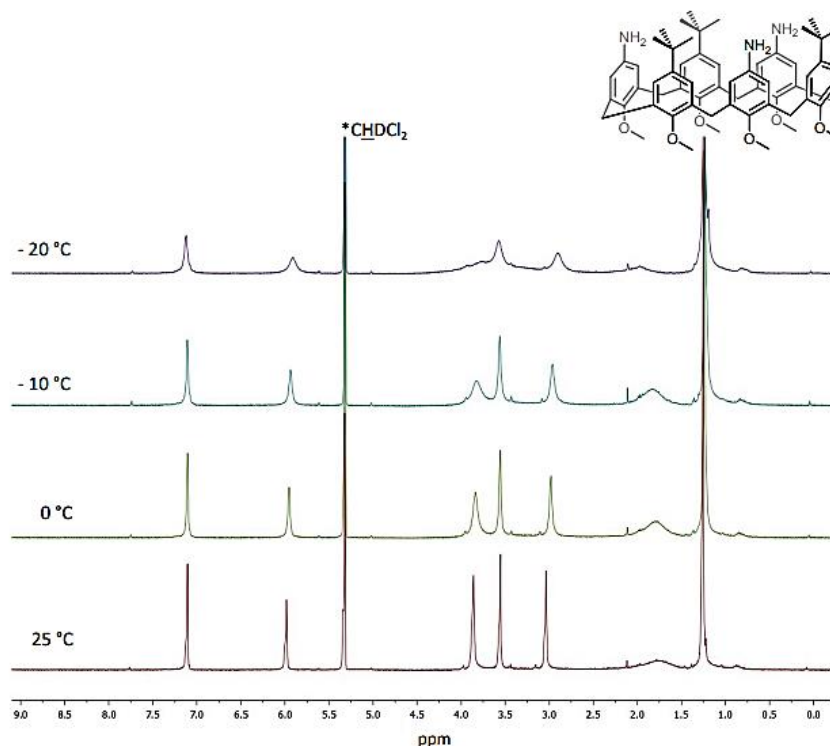
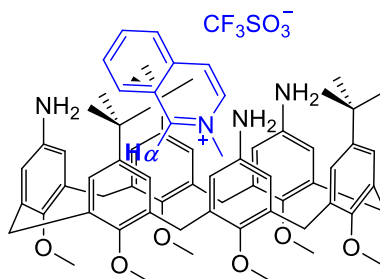


**Fig.3.**  $^1\text{H}$  NMR spectra ( $\text{CD}_2\text{Cl}_2$ , 300 MHz) of 2.00 mM **5** at different temperatures.

Interestingly, along the titration of **5** with **7**, a significant shift of the signals of the guest **7** is also observed. In the first point of the titration (see Figure 1, trace *b*), when added titrant **7** is equimolar to calix[6]arene host **5**, the percentage of added **7** complexed to **5** is significant (38% according to  $K_{\text{ass}}$ ). Inclusion of guest **7** into the aromatic cavity of host **5** is proved by the marked shielding effect observed on the signals of the guest upon complexation. Under the above-mentioned conditions, a 0.68 ppm up-field shift is observed on the signal of the methyl group of the guest ( $\delta = 4.61$  ppm is the chemical shift of the methyl group of uncomplexed **7**, and  $\delta = 3.93$  ppm is the observed chemical shift in trace *b*). Among the aromatic signals related to **7**, that of the alpha proton ( $\text{H}_\alpha$ ) is the most upfield shifted (it is found at 9.30 ppm in trace *b* of Figure 1 as a broad singlet and at 9.95 ppm in uncomplexed **7** as a sharper singlet) indicating that the inclusion must occur as depicted in Scheme 2



**Scheme 2.** Schematic representation of the host-guest complex between **5** and **7**

The fit of the experimental points obtained in the titration of **5** with **7** with a 1:1 binding isotherm gives a binding constant  $K_{\text{ass}}$  of  $500 \pm 30 \text{ M}^{-1}$  with a very nice agreement of the experimental data with the calculated ones.

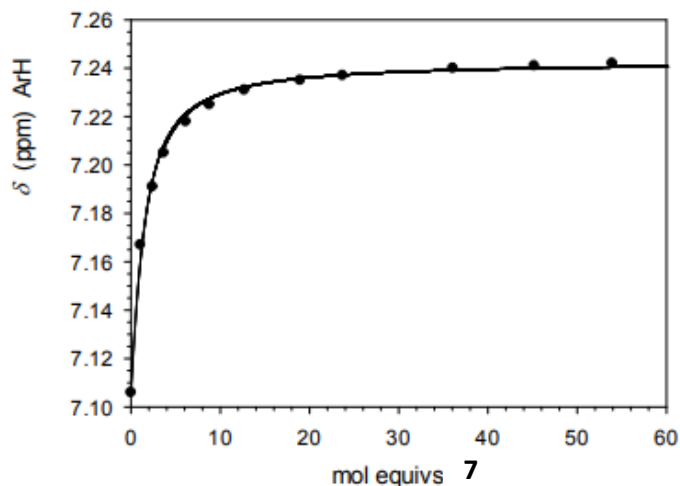


**Fig.4:**  $^1\text{H-NMR}$  ( $\text{CD}_2\text{Cl}_2$ , 300 MHz, 25 °C) titration of a 2.0 mM **5** solution with an increasing concentration of **7**. The chemical shift of the signal of the aromatic protons ortho to the *t*-Bu substituted is plotted vs. added molar equiv of **7**. The curve is a 1:1 binding isotherm calculated with the best fitted values  $K_{\text{ass}} = 500 \text{ M}^{-1}$ , and  $\delta_{\text{complex}} = 7.24 \text{ ppm}$ .

## 2.9 $^1\text{H}$ NMR titration between calix[6]arene **5** and TFA

Next, we tested the basic properties of calix[6]arene **5** by titration with trifluoroacetic acid (TFA). Addition of the first molar equiv of TFA to a 2.00 mM solution of **5** causes a general downfield shift of all signals due to the protonation of one of the three amino groups as shown in Figure 5. Further significant variations are observed when a second and a third molar equiv of TFA are added to the solution. In the latter case, most of the signals related to **5** appear broader, and some of them begin to show multiplicity as a consequence of an increased conformational rigidity (red box Figure 5).

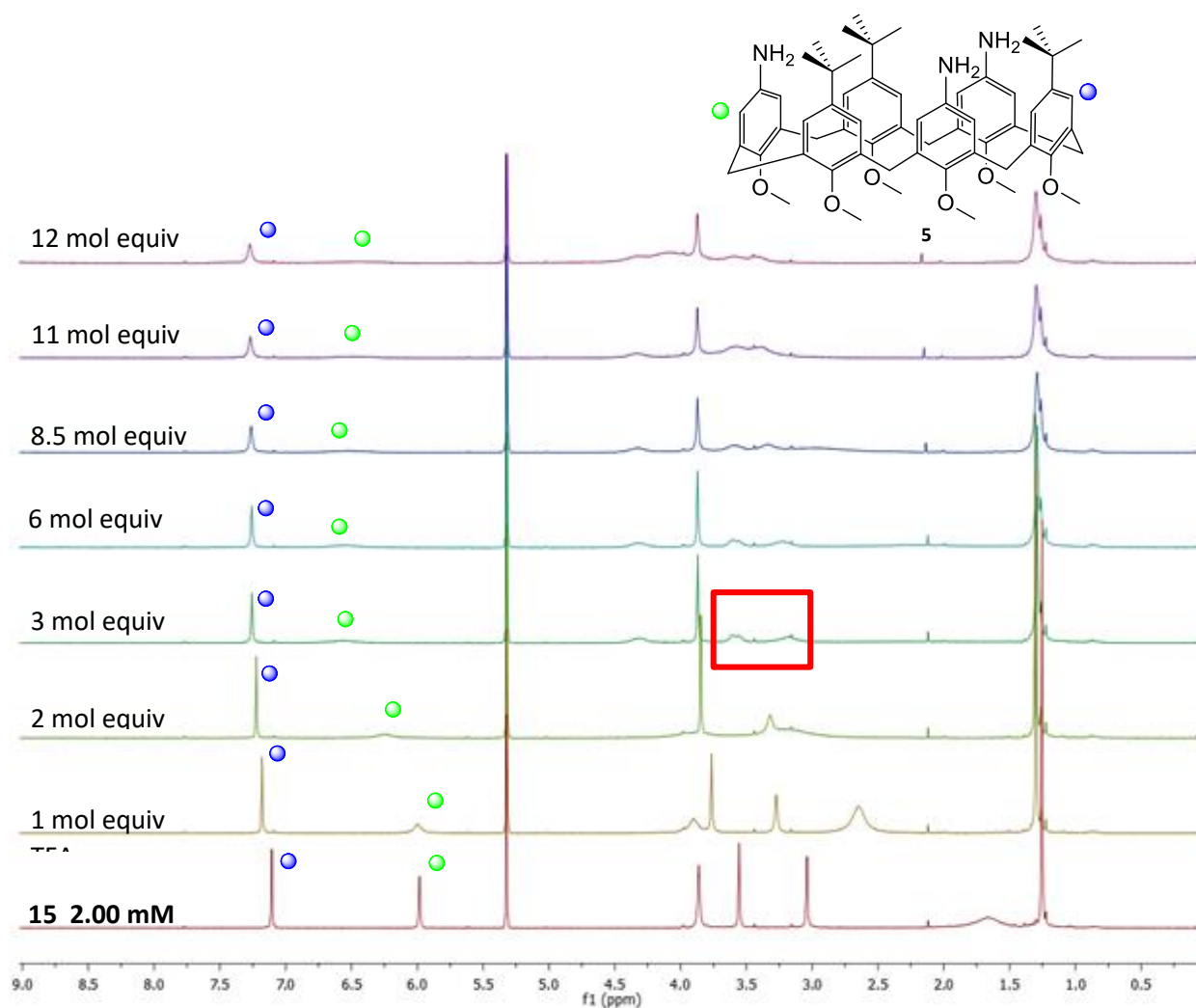


**Fig.5:**  $^1\text{H}$  NMR titration of the calix[6]arene **5** with TFA, ( $\text{CD}_2\text{Cl}_2$ ,  $25^\circ\text{C}$ ). From bottom to top: spectrum of 2.00 mM **5**, and spectra registered after the addition of increasing amounts of TFA, as reported.

$^1\text{H}$  NMR spectra (see Figures 5) do not seem to change significantly upon subsequent additions of TFA (up to 12 molar equiv). A definite assessment of the protonation degree of **5** after the addition of 3 or more molar equiv of TFA is not easy.

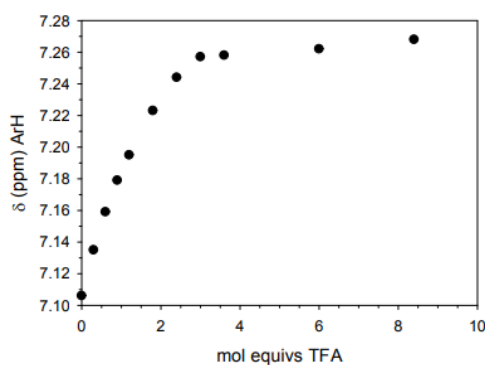
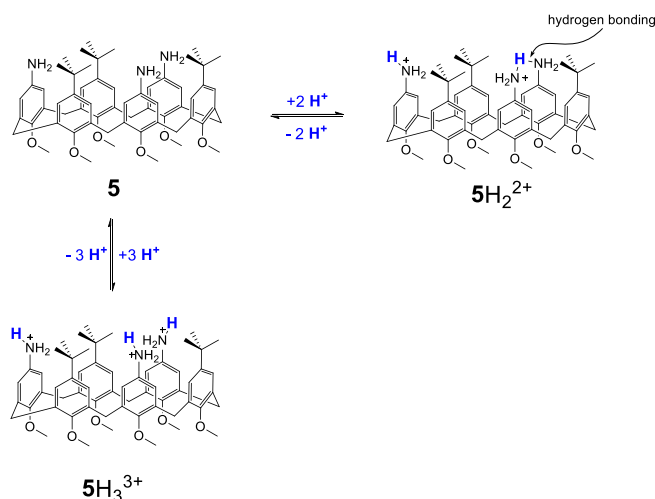


**Fig.6.** Plot of the chemical shift of the *t*-Bu substituted aromatic rings signal on increasing the amount of TFA

Doubly protonated  $5H_2^{2+}$  with one of the two protons on one of the three amino groups and the other shared between the remaining two amino groups (see Figure 4), or, alternatively, a triply protonated form ( $5H_3^{3+}$ ) with one proton on each of the amino groups, could be formed. However, the doubly protonated state  $5H_2^{2+}$  seems to be more probable considering the following arguments. First, in strict analogy to what was observed in the case of the monoprotonated form of diaminocalix[4]arene shown in a previous work,<sup>85</sup> the monoprotonated form  $5H^+$  obtained by the addition of one molar equiv of TFA to **5** is not deprotonated to any extent by the addition of excess p-anisidine (up to 20 molar equiv) as shown in Figure 7 proving that **5** has a much more basic character than p-anisidine probably due to the chance given to two amino groups to share the proton (in the presence of 1 molar equiv of TFA, the proton could be also shared by all the three amino groups).



**Scheme 3.** Protonation equilibria involving calix[6]arene **5** in excess of TFA.

An additional clue in favour of the  $5H_2^{2+}$  hypothesis in the presence of 3 or more molar equiv of TFA, comes from the pattern of the methylene bridge signals of the  $^1H$  NMR spectrum obtained under these conditions (see Figure 5). They appear as two broad doublets, a typical feature of an almost blocked or slowly interconverting cone conformation. Such conformation is hardly ascribable to a triprotonated  $5H_3^{3+}$  structure, which would adjust to keep the three positive groups as far as possible but is fully compatible with the  $5H_2^{2+}$  form in which the two protons can be rapidly scrambled among the three amino groups.

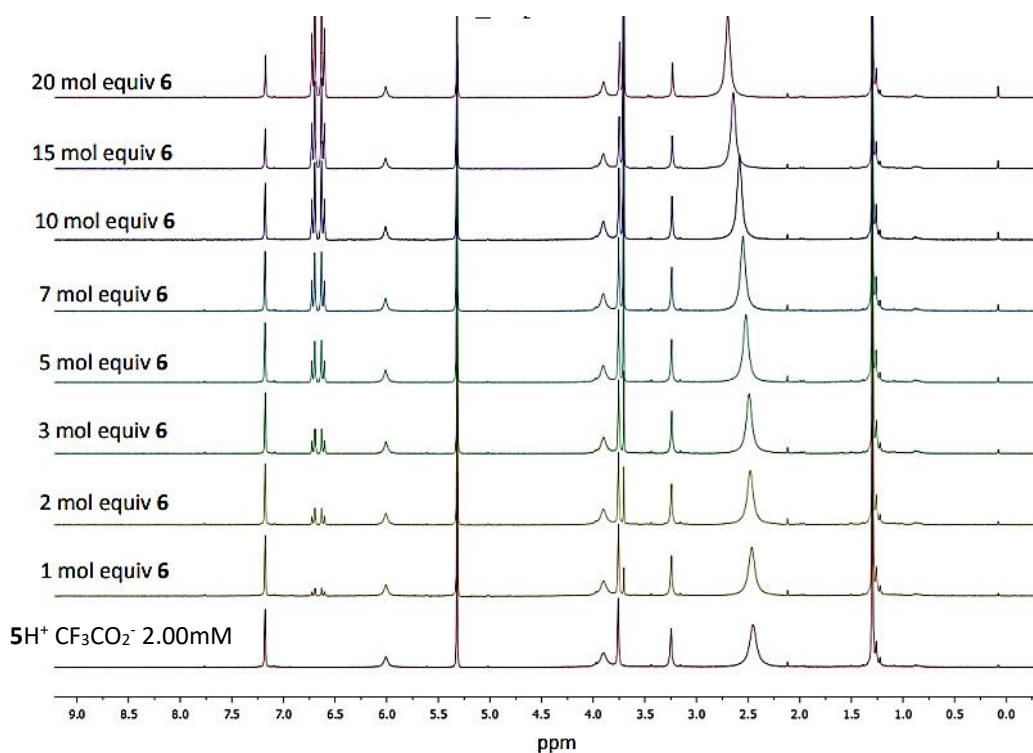


**Fig.7**  $^1\text{H}$  NMR ( $\text{CD}_2\text{Cl}_2$ , 300 MHz, 25 °C) titration of  $5\text{H}^+ \cdot \text{CF}_3\text{CO}_2^-$  (2.00 mM **5** + 2.00 mM TFA) with *p*-anisidine **6**. From bottom to top: spectrum of 2.00 mM  $5\text{H}^+ \cdot \text{CF}_3\text{CO}_2^-$ , and spectra registered after the addition of increasing amounts of *p*-anisidine **6**.

We then tested the effect of protonation on the binding ability of **5** toward N-methylisoquinolinium triflate **7** (Figure 8). Trace *a* is the  $^1\text{H}$  NMR spectrum of a  $\text{CD}_2\text{Cl}_2$  solution of 2.00 mM **5** and 6.00 mM **7**. Under these conditions, 70% **5** is in the form of **5**•**7** complex. The addition of 3 molar equiv of TFA causes the complete expulsion of guest **7** from host **5** as can be seen in the resulting trace *b* of Figure 8. Trace *b* is indeed the sum of the  $^1\text{H}$  NMR spectrum of **7** (trace *c*) and that of **5** + 3 molar equiv of TFA (trace *d*). The reason is probably electrostatic in nature: once host **5** is protonated, it loses any affinity for the positively charged N-methylisoquinolinium.

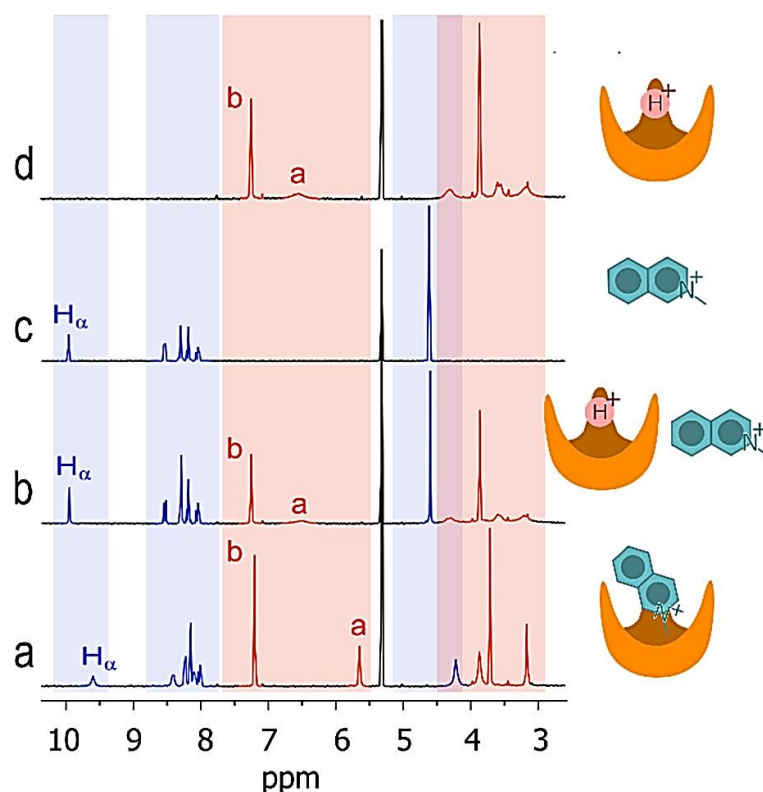


**Fig 8.** Effect of protonation on the binding ability of **5** (light red) toward *N*-methylisoquinolinium triflate **7** (light blue). (a) 2.00 mM **5** and 6.00 mM **7**; (b) 2.00 mM **5** and 6.00 mM **7** and 6.00 mM TFA; (c) 6.00 mM **7**; (d) 2.00 mM **5** and 6.00 mM TFA. CD<sub>2</sub>Cl<sub>2</sub>, 25 °C Signal labelling as in Figure 1.

## 2.10 Operation of **5** under dissipative conditions

We then investigated if calix[6]arene **5** is able to promote the decarboxylation of the fuel acids. As expected, it was found that the decarboxylation of acid **8d** (the most activated among 2-cyano-2-phenylpropanoic acids) promoted by **5** occurs in relatively quick times (the reaction is complete within 6.2 h in CD<sub>2</sub>Cl<sub>2</sub> at 25 °C). In the latest years, activated carboxylic acids like 2-cyano-2-phenylpropanoic acid<sup>86,87</sup> **8a** and its derivatives (**8b–d**),<sup>88,89</sup> trichloroacetic acid,<sup>90</sup> and nitroacetic acid<sup>91</sup> (Chart 1) have been conveniently used as chemical fuels to drive whole cycles of motion of molecular machines, both switches and motors. Among 2-cyano-2-phenylpropanoic acid derivatives (**8a–d**, see Chart 1), 2-cyano-2-(4'-chlorophenyl)propanoic acid **8d** was chosen because its decarboxylation is promoted by calixarene **5** in convenient times: it is over within 6.2 h under the adopted conditions, thus being complete within one work day. The reaction is slower and less convenient with acids **8a–c**. Decarboxylation of nitroacetic acid is instead too fast to be experimentally convenient under the adopted conditions. Eventually, we prefer to use 2-cyano-2-phenylpropanoic acid derivatives (**8a–d**) rather than trichloroacetic acid for practical convenience. All 2-cyano-2-

phenylpropanoic acid derivatives are easy-to-handle solids. Conversely, trichloroacetic acid is a deliquescent, hard to handle and weigh solid. We always find very difficult the preparation of a trichloroacetic acid stock solution, as already explain in the first chapter of this thesis, with an exactly known concentration.

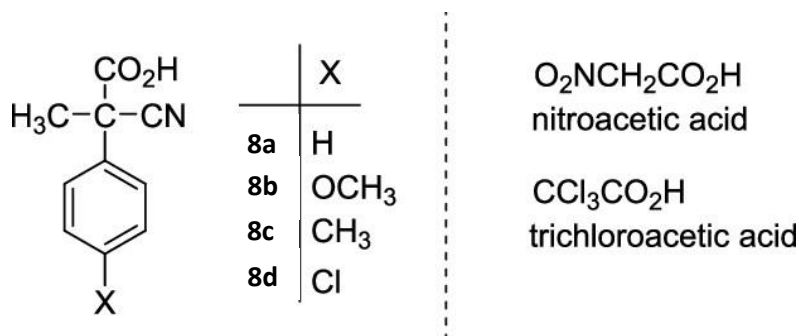


**Chart 1.** Activated carboxylic acids employed for the operation of molecular machines.

To an initial 2.00 mM solution of **5** (trace *a*, Figure 9), fuel **8d** (3 molar equiv) is added and **5** is immediately protonated (trace *b*, Figure 9). Decarboxylation starts and, within 6.2 h (371 min, trace *f*), the singlet at 1.75 ppm (green box in Figure 9) due to the methyl group of the deprotonated form of **8d**, is transformed into the doublet at 1.60 (red box in Figure 9) ppm belonging to the waste product. The typical quartet at 3.95 ppm of the benzylic proton of the waste product also appears

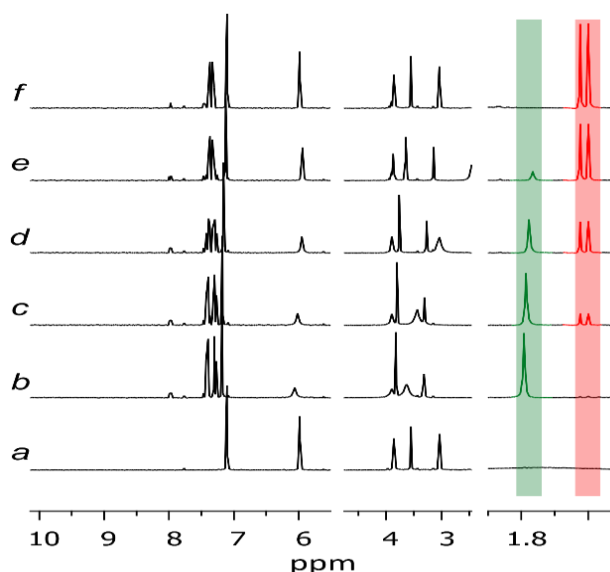


**Fig.9:** Reaction between 2.00 mM **5** and 6.00 mM **8d** (3 molar eq.) in CD<sub>2</sub>Cl<sub>2</sub> at 25 °C followed by <sup>1</sup>H NMR; trace *a* was recorded before addition of **8d**, traces *b*, *c*, *d*, *e* and *f* were recorded from 6 to 371 min



Contextually, calix[6]arene **5** returns to its original nonprotonated form demonstrating the perfect reversibility of the process. Interestingly, the reaction does not occur to any extent within the same time delay when p-anisidine (6.00 mM) is added instead of **5**, strongly pointing to the sharing of the proton between two of the three amino groups in  $5H^+$  as a reason for the increased basicity of **5**.

The same experiment of decarboxylation of the fuel was then repeated in the presence of 2.00 mM calixarene **5** and guest **7** (1:1 ratio).

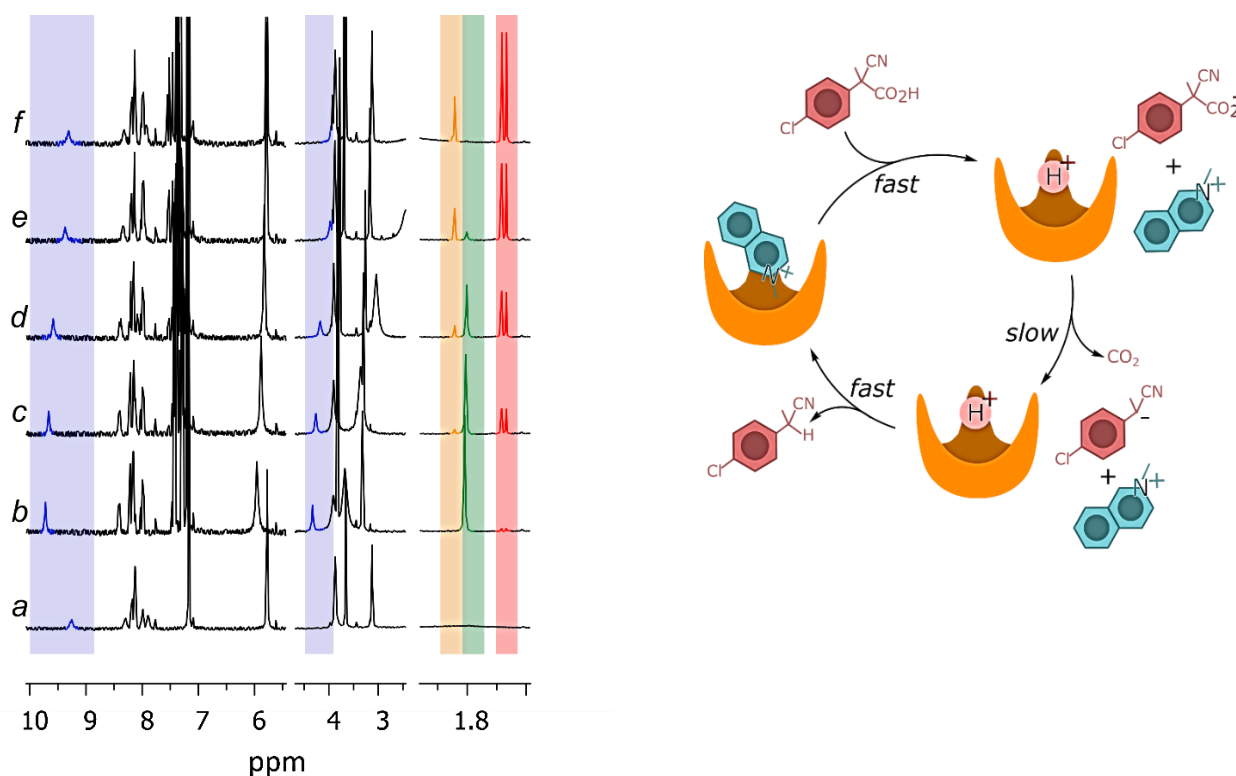


**Fig.10** Reaction between 2.00 mM **5** and 6.00 mM **8d** in the presence of 2.00 mM **7** in  $CD_2Cl_2$  at 25 °C followed by <sup>1</sup>H NMR; trace a was recorded before addition of **8d**. Traces b, c, d, e and f were recorded from 6 to 177 minutes. Schematic cartoon representing the release–reuptake  $5\cdot 7 \rightarrow 5H^+ + 7 \rightarrow 5\cdot 7$  dissipative cycle driven by fuel **8d** (left).

Under these conditions, 38% **5** is engaged in the formation of complex **5**•**7** (trace a, Figure 10). Now, fuel **8d** is added (3 molar equiv with respect to **5**), host **5** is immediately protonated, and guest **7** is released into the bulk solution (trace b, Figure 10). Decarboxylation of the deprotonated form of **8d** slowly occurs, **5** is contextually deprotonated again, and **7** is re-uptaken by host **5** (traces c–f, Figure 10). Thus, a release-and-reuptake cycle of guest **7** from and into host **5** has been realized under dissipative conditions. No difference of the chemical shift of the <sup>1</sup>H NMR signals of the fuel waste product is apparent in the presence or absence of calixarene **5** in all its protonation states, reasonably excluding any inclusion of the waste

product into **5**. Little (in no case higher than 0.020 ppm) differences are observed for the signals of the protonated or deprotonated forms of fuel **8d** in the presence or absence of **5**, reasonably excluding inclusion in the calixarene cavity also in this case. The process can be satisfactorily reiterated as shown by Figure 11, where four subsequent cycles triggered by four successive additions of fuel **8d** are monitored by following the variation of the chemical shift of the methyl group of **7** over the time.

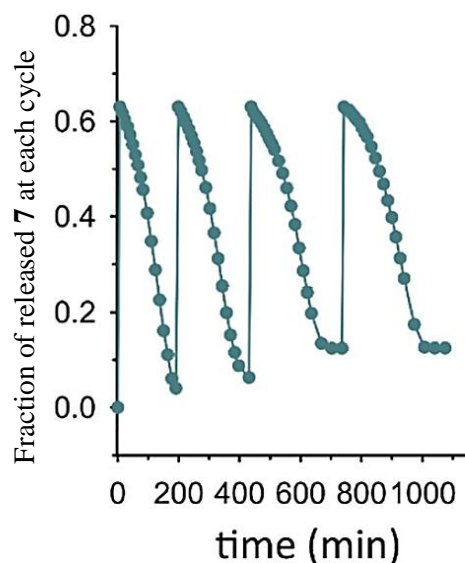


**Fig.11** Four subsequent  $5 \cdot 7 \rightarrow 5H^+ + 7 \rightarrow 5 \cdot 7$  dissipative cycles triggered by four successive additions of fuel **8d** (in each cycle, 3 mol equiv of **8d** were added to an equimolar 2.00 mM solution of **5** and **7**).

Unexpectedly, during this release–reuptake experiment (Figure 10), a second waste product accounting for about 25% of **8d** (Figure 10, trace *f*, yellow singlet at 1.95 ppm to be compared with the red doublet at 1.60 ppm) appears among the reaction products. Peroxide **9** in Figure 12 was tentatively proposed as this unexpected waste product. It does not form in the absence of **7** (Figure 9).

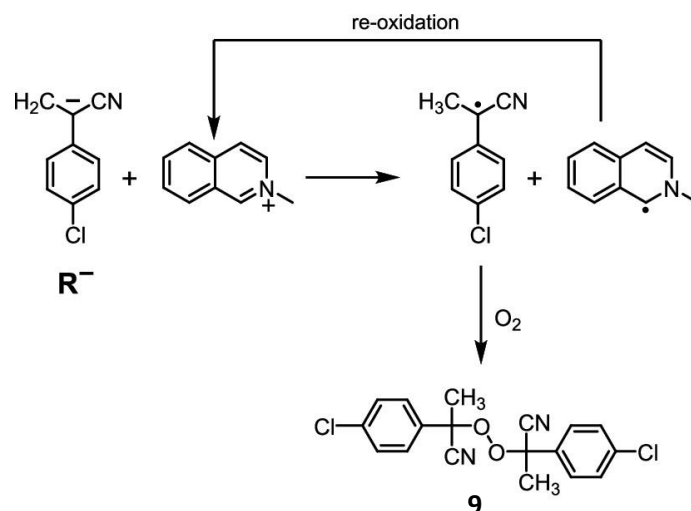


**Fig.12** Proposed mechanistic pathway to peroxide **9**.

Furthermore, the formation of **9** is not seen when the same reaction is carried out in the presence of guest **7** but substituting **5** with  $\text{Et}_3\text{N}$  (a base able to promote the decarboxylation of **8d**). In other words, it is only formed when calix[6]arene **5** and N-methylisoquinolinium triflate are both present in the reaction mixture. We hypothesize that this is due to the oxidation of the carbanion of the decarboxylated fuel by **7**,<sup>92,93</sup> immediately followed by oxygen capture, see Figure 12. The resulting N-methylisoquinoline radical must be then re-oxidized to N-methylisoquinolinium (very likely by  $\text{O}_2$ ) since the latter is found untouched at the end of each cycle. The identification of the waste co-product **9** was quite puzzling. First of all, the product was eluted through a Pasteur pipette by column chromatography carried out on the solution of the  $^1\text{H}$  NMR experiment described in Figure 10. The Figure 13 shows the  $^1\text{H}$  NMR of the fraction containing tiny amounts of **9**.

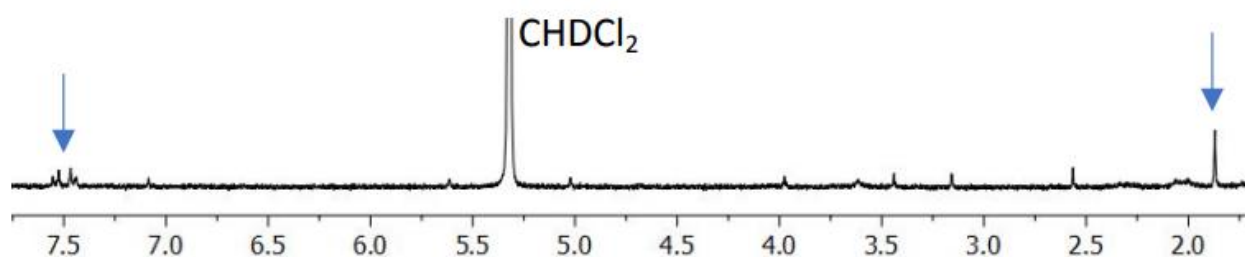


**Fig.13**  $^1\text{H}$  NMR (300MHz,  $\text{CD}_2\text{Cl}_2$ , 25 °C) of peroxide **9**

The AB system centred at 7.5 ppm and the singlet at 1.80 ppm belong to compound **9**. The same signals are easily found for example in the top spectrum of Figure 10. This spectrum compares well with the spectrum simulated for the peroxide **9** shown in Figure 14.

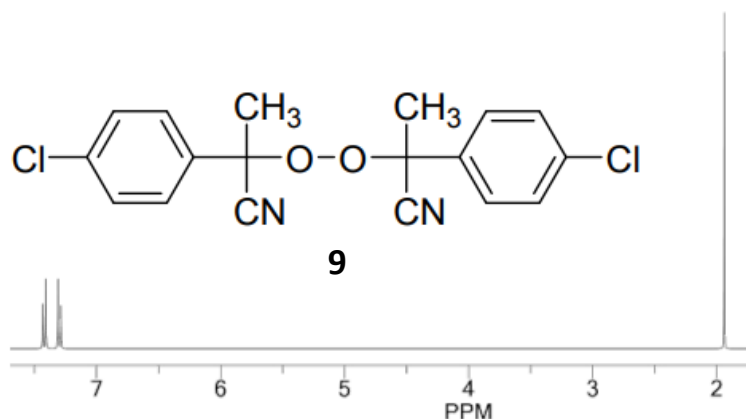


**Fig.14:** Simulation of the  $^1\text{H}$  NMR spectrum of peroxide **9**

When the above  $\text{CD}_2\text{Cl}_2$  solution was subjected to MS analysis, we found the same mass spectra that is obtained for p-chloroacetophenone (Figure 15). This fact can be justified by the loss of cyanogen in the injector of the mass spectrometer according to the mechanism illustrated below.

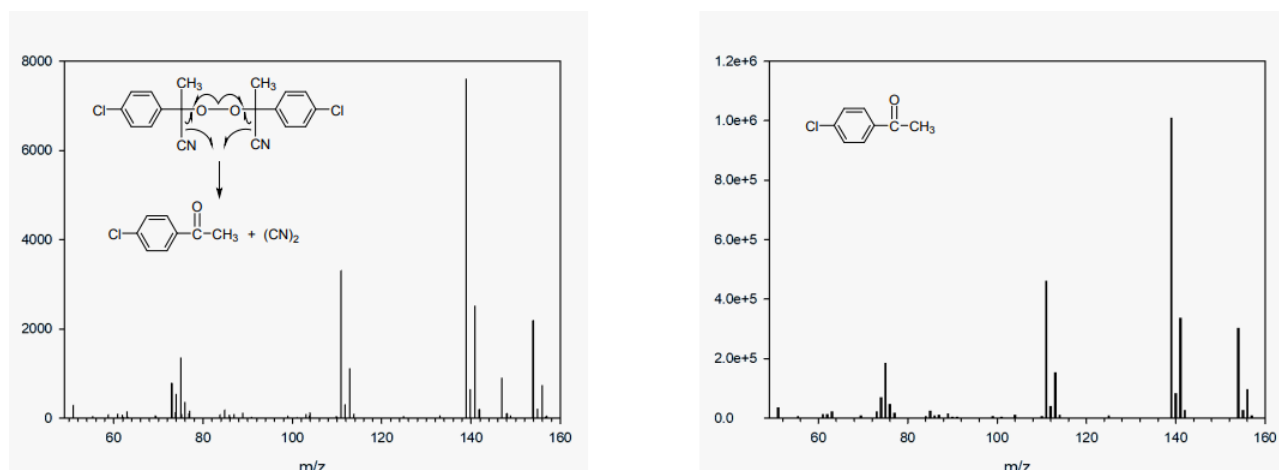
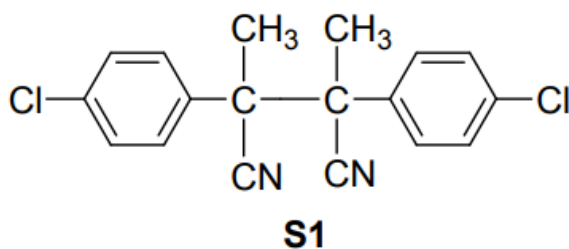


**Fig.15:** Comparison between MS spectra of **9** and p-chloroacetophenone

However, the structure of the waste coproduct is certainly not that of p-chloroacetophenone whose methyl group signal is found at 2.56 ppm ( $^1\text{H}$  NMR in  $\text{CD}_2\text{Cl}_2$ ). Oxidation to a radical species of a carbanion similar to that reported in Figure 12 by aromatic quaternary salts and subsequent capture of  $\text{O}_2$ , is well documented.<sup>94</sup> Furthermore, structure S1 deriving by the

direct coupling of two just formed carbon radicals can be excluded since it is known<sup>95</sup> that the methyl groups of the possible diastereoisomers (a couple of enantiomers and the meso compound) have slightly different absorption at <sup>1</sup>H NMR (we should observe two singlets around 1.8 ppm and not one only).



The above considerations, together with the findings that the contribution of the collateral pathway definitely decreases when:

- i) exclusion of O<sub>2</sub> from the solution was attempted through freeze-pump-thaw cycles operated on the NMR tube (passing from 25% to 15%)
- ii) higher excesses of fuel **8d**, 10.5 mM (5.25 mol equiv) and 18.4 mM (9.2 mol equiv) were added (passing from 25 to 15 and 10%, respectively. See Figure 15 and 16) were employed

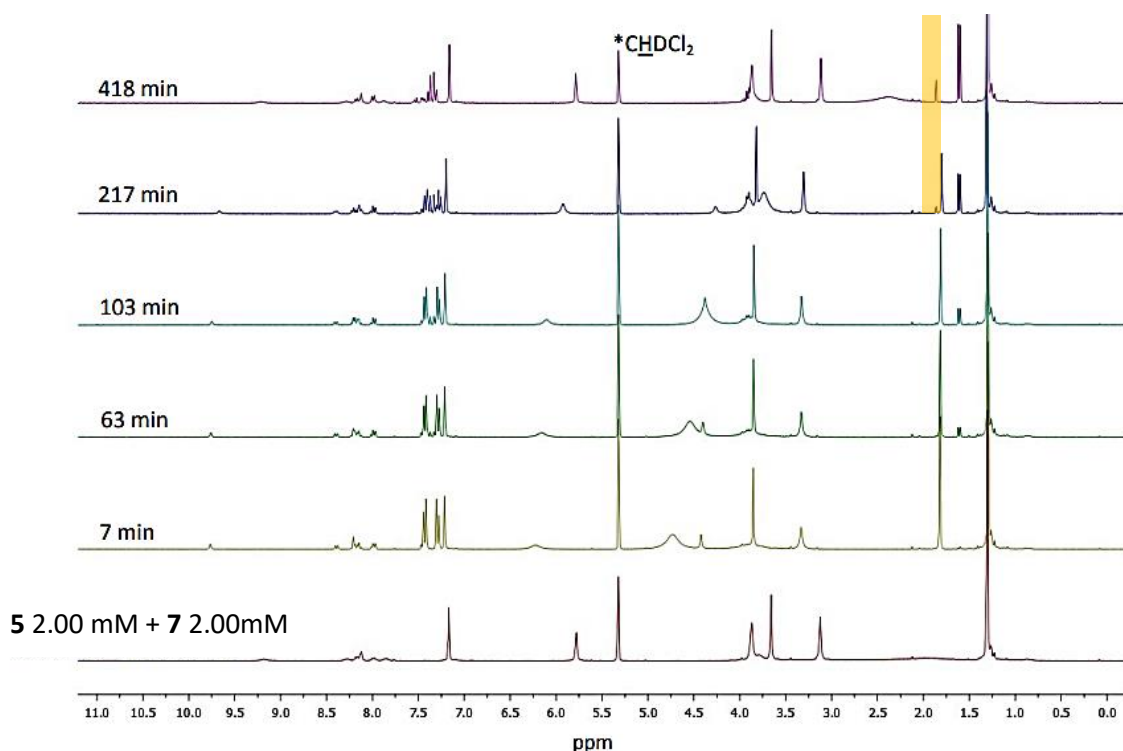


**Fig.15**  $^1\text{H}$  NMR monitoring ( $\text{CD}_2\text{Cl}_2$ , 300 MHz, 25 °C) of the decarboxylation of 10.5 mM **8d** catalysed by 2.0 mM **5** in the presence of 2.00 mM **8d**. The bottom trace is relative to 2.00 mM **5** + 2.00 mM **7**, before the addition of **8d**. Following spectra were recorded after the addition of acid **8d**, at the given reaction time, upward increasing. Signal belonging to by-product **9** is highlighted in the orange box

From the comparison of the spectra shows in Figures 15 and 16, it can be seen that after the addition of 10.5mM and 18.2mM of **8d**, respectively, the guest is released into solution as expected. As can be seen from the orange boxes in the two spectra (Figure 15 and 16), the intensity of the signal belonging to the by-product **9** decreases in the case where a larger amount of fuel equivalents was used.

These two experiments strongly points to the peroxide **9** as the structure of the waste co-product This collateral pathway is somewhat facilitated by calix[6]arene **5**. A hypothetical, tentative explanation is that calixarene **5** may favour the electron transfer between carbanion  $\text{R}^-$  and **7** by complexing the transient ion pair  $\text{7}\cdot\text{R}^-$  and properly orienting the two species in close proximity.

Eventually, time control of the dissipative release–reuptake cycle could be achieved by varying the amount of fuel **8d** added in the solution.

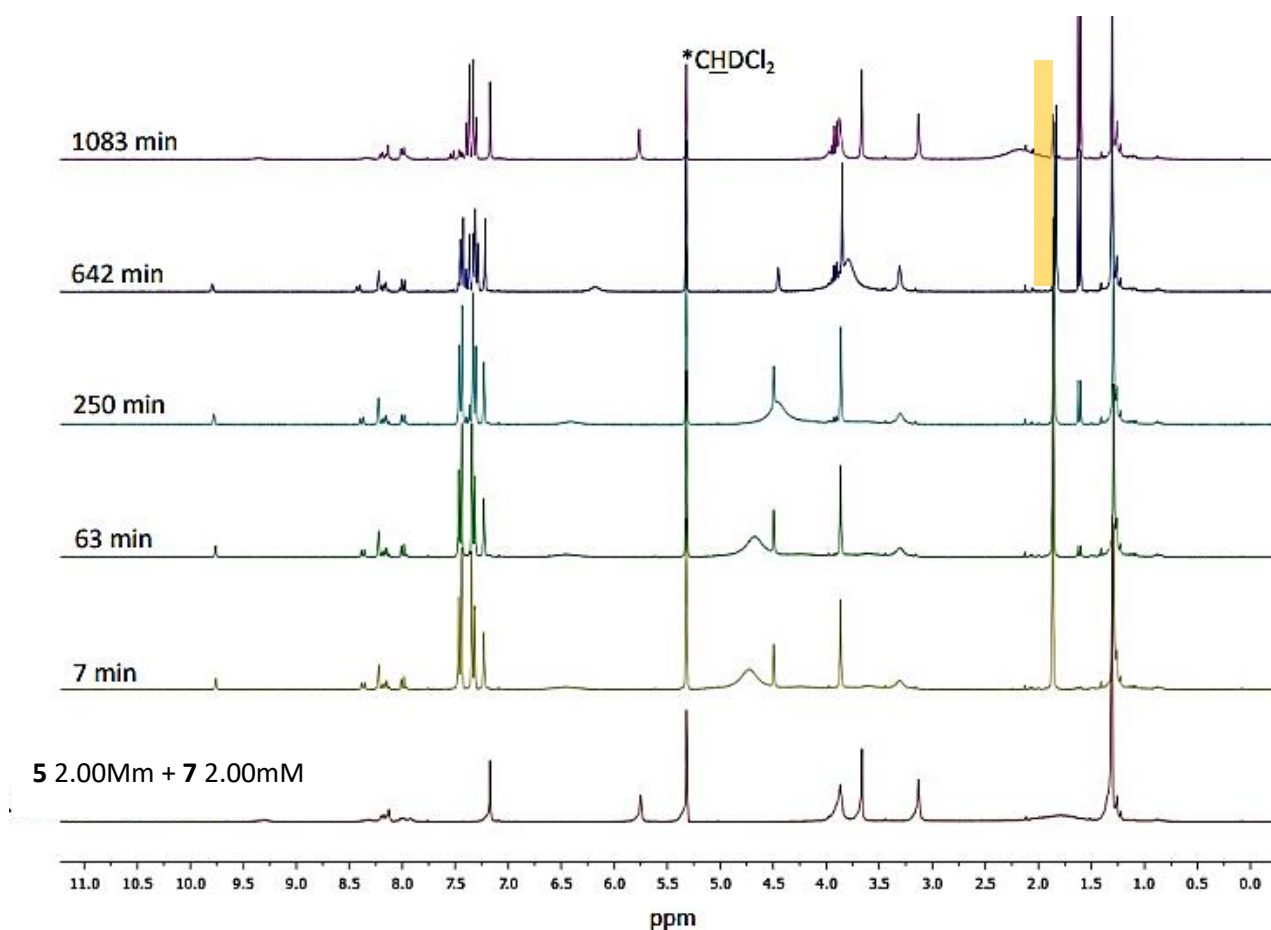


**Fig.16**  $^1\text{H}$  NMR monitoring ( $\text{CD}_2\text{Cl}_2$ , 300 MHz, 25 °C) of the decarboxylation of 18.2 mM **8d** catalysed by 2.0 mM **5** in the presence of 2.00 mM **7**. The bottom trace is relative to 2.00 mM **5** + 2.00 mM **7**, before the addition of **8d**. Following spectra were recorded after the addition of acid **8d**, at the given reaction time, upward increasing. Signal belonging to by-product **9** is highlighted in the orange box

Figure 17 shows three experiments where increasing amounts of fuel **8d** were added to mixtures of **5** (2.0 mM) and **7** (2.0 mM). The percentage of **7** temporarily escaped from **5** and the time spent outside increase on increasing the amount of the fuel added. When 3 molar equiv of **8d** are added (6.0 mM, Figure 17, yellow points), 63% of the guest is released by the host, and the reuptake process takes 150 min. When 5.25 molar equiv of **8d** are added (10.5 mM, Figure 17, orange points), 75% of **7** is released and reuptake takes 300 min. Eventually, when 9.2 molar equiv of **8d** are added (18.4 mM, Figure 17, azure points), 85% of **7** is released and reuptake takes more than 900 min. In other words, the higher the fuel excess, the longer the time needed to consume such excess, the longer the time spent by the host in the unloaded state.

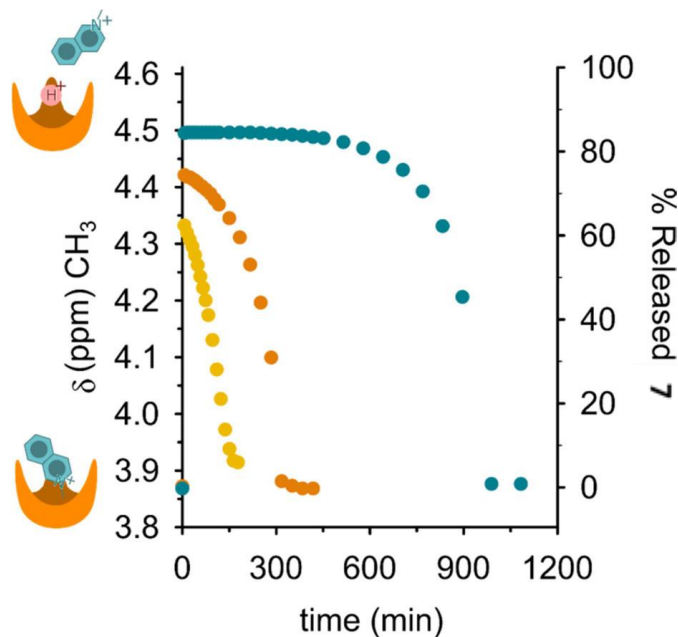


**Fig.17** Time-controlled dissipative  $5\cdot 7 \rightarrow 5H^+ + 7 \rightarrow 5\cdot 7$  cycles triggered by increasing amounts of fuel **8d** ( $CD_2Cl_2$ ,  $25\text{ }^\circ C$ ). In all experiments, equimolar amounts of **5** and **7** were used ( $2.0\text{ mM}$ ) while concentration of **8d** was varied. The advancement degree of the reaction over time (right axis) was calculated as  $[(\delta - 3.87)/(4.61 - 3.87) \times 100]$ , where  $\delta$  is the chemical shift of the N-methylisoquinolium methyl signal (left axis) observed at a given reaction time,  $4.61$  is the chemical shift of the methyl signal of uncomplexed N-methylisoquinolium, and  $3.87$  is the chemical shift of the N-methylisoquinolium methyl signal under the initial conditions, that is, when  $38\%$  complex  $5\cdot 7$  formation is observed (which corresponds to  $0.76\text{ mM } 5\cdot 7$ )

The particular shape of the kinetic profiles in Figure 17 after the exhaustion of excess fuel is probably due to an autocatalytic path involving deprotonated **5** itself as the catalyst. Such complex mechanism has been studied in detail in the simpler case of diaminocalix[4]arene.<sup>85</sup> In that case, it was shown that the fact that the rate of the autocatalytic process does not slow down on decreasing the substrate (fuel) concentration, with the consequent presence of a cusp just before the final plateau, can be explained considering the autocatalytic path to be kinetically zero order with respect to the substrate itself.

The observation of a pseudo zero-order substrate dependency for an autocatalytic reaction occurring in homogeneous solution can arise due to one of two possible mechanisms:

- (i) the autocatalyst is involved in a rate-limiting process preceding the reaction with the substrate;
- (ii) the substrate is involved in a strong pre-equilibrium binding that saturates a catalytic species present in minute amounts, the resulting complex then reacts with the autocatalyst in the rate-limiting product formation. In this case, the autocatalyst



is the calixarene in its neutral form and the substrate is the fuel acid. However, if mechanism i) were operating, the rate of the autocatalytic process would be independent of the nature of the fuel. Nevertheless, in the case of diaminocalix[4]arene<sup>85</sup> investigation of the kinetics of the reaction with different fuels (2-cyano-2-phenylpropanoic acids, differently substituted at the aromatic ring) showed that the rate of the autocatalytic process is fuel-dependent, thus ruling out mechanism i), and leaving mechanism ii) as a viable option.

The presence of minute amounts of cationic impurities in dichloromethane was shown to be likely responsible for such bizarre kinetic behaviour.

## 2.11 Conclusion

In this chapter the host-guest interaction between calix[6]arene **5** and N-methylisoquinolinium triflate **7** was shown. This assembly can be dissipatively driven by fuel acid **8d**. The addition of the fuel into a solution containing the complex **5•7** causes the temporary release of guest **7** by the host into the bulk. The former is re-uptaken by the latter once the fuel is exhausted. The amount of released guest and the duration of the unloaded state can be controlled at will by a fine modulation of the quantity of added fuel. Thus, the fully abiotic host-guest couple (**5•7**) described above is capable of operating under dissipative conditions (out of equilibrium, as long as the fuel is present), which are typical, operative conditions of systems with life-like properties.

A possible development of the present work could be the design of systems where the dissipative complex dissociation gives rise to a secondary effect. The temporal control of catalytic activity may be, for example, obtained in case the guest is a catalyst of a given reaction.<sup>96</sup>



# Experimental Part

## 2.12 General information

All moisture sensitive reactions were carried out under nitrogen or argon atmosphere, using previously degassed solvents. Analytical TLC were performed using prepared plates of silica gel (Merck 60 F 254 on aluminium) and then, according to the functional groups present on the molecules, revealed with UV lights or using staining reagents. Merck silica gel 60 was used for flash chromatography (40-63  $\mu\text{m}$ ).  $^1\text{H-NMR}$  and  $^{13}\text{C-NMR}$  spectra were recorded on Bruker AV400 spectrometers and partially deuterated solvents were used as internal standards to calculate the chemical shifts ( $\delta$  values in ppm). All  $^{13}\text{C-NMR}$  spectra were performed with proton decoupling. Electrospray ionization (ESI) mass analysis were performed with a Waters single-quadrupole spectrometer in positive mode using MeOH or  $\text{CH}_3\text{CN}$  as solvents.

### Synthesis of the 38,40,42-trimethoxy-*p-tert*-butylcalix[6]arene-37,39,41-triol (**1**)

To a suspension of *p-tert*-butylcalix[6]arene (3g, 3.08mmol) and  $\text{K}_2\text{CO}_3$  (1.28g, 9.26mmol) in dry acetone (200mL)  $\text{CH}_3\text{I}$  (1.53mL, 24.7mmol) was added and the solution was stirred at the reflux temperature for 24h. The mixture was filtered, and the filtrate was concentrated under reduce pressure to dryness. The residue was dissolved in chloroform and washed with 1M HCl solution (3 x 100mL), water (50mL) dried over anhydrous  $\text{Na}_2\text{SO}_4$  and concentrated under reduce pressure to give a crude product which was purified by a silica gel flash column chromatography (hexane/ tetrahydrofuran 95:5) to afford **1** as a white solid (0.8g, 26%).  $^1\text{H NMR}$  (400 MHz,  $\text{CDCl}_3$ )  $\delta$  (ppm) 7.04 (s, 6H, ArH), 6.93 (s, 6H, ArH), 3.91 (broad s, 6H, Ar-CH<sub>2</sub>-Ar), 3.49 (s, 9H, OCH<sub>3</sub>), 1.23 (s, 27H, C(CH<sub>3</sub>)<sub>3</sub>), 1.04 (s, 27H, C(CH<sub>3</sub>)<sub>3</sub>). The compound showed the same physico-chemical properties as those reported in literature.<sup>97</sup>

### Synthesis of the 38,40,42-Trimethoxy-37,39,41-tristriflate-*p-tert*-butylcalix[6]arene (**2**).

To a solution of **1** (1.5g, 1.48 mmol) in dry dichloromethane (75mL), pyridine (1.05mL, 1.3mmol) and trifluoromethanesulfonic anhydride (1.1mL, 6.54 mmol) were successively added dropwise under a nitrogen atmosphere at 0 °C. After cooling to room temperature, the

resulting solution was quenched with 30 mL of a 1M aqueous solution of HCl. The organic phase was separated, washed with brine (30mL), dried over Na<sub>2</sub>SO<sub>4</sub> and concentrated under reduce pressure. The crude product was purified by precipitation in acetonitrile to give **2** as a white solid (1.9g, 95%). <sup>1</sup>H NMR (400 MHz, CDCl<sub>3</sub>) δ (ppm) 7.27 (s, 6H, ArH), 6.80 (s, 6H, ArH), 4.33 (broad s, 6H, Ar-CH<sub>ax</sub>-Ar), 3.69 (broad s, 6H, Ar-CH<sub>eq</sub>-Ar), 2.41 (s, 9H, OCH<sub>3</sub>), 1.35 (s, 27H, C(CH<sub>3</sub>)<sub>3</sub>), 0.87 (s, 27H, C(CH<sub>3</sub>)<sub>3</sub>). The compound showed the same physico-chemical properties as those reported in literature.<sup>97</sup>

### **Synthesis of the 38,40,42-Trimethoxy-37,39,41-tristriflate-11,23,35-trinitro-5,17,29-tri-*tert*-butylcalix[6]arene (3)**

To a solution of **2** (1.47g, 1.04mmol) in dichloromethane (100mL) a (1/1) mixture of fuming nitric acid and glacial acetic acid (13 mL) was slowly added at 0 °C. The reaction mixture was then warmed to r.t. and stirred for 6h. The resulting solution was poured into 120 mL of iced water. The organic layer was separated, and the aqueous layer was extracted with dichloromethane (30 mL). The organic layer was washed with distilled water until the solution reach pH=7, dried over anhydrous Na<sub>2</sub>SO<sub>4</sub> and concentrated under reduce pressure to give a crude product which was purified by a silica gel flash column chromatography (hexane/dichloromethane 60:40) to afford **3** as a white solid (1.2g, 84%). <sup>1</sup>H NMR (400 MHz, CDCl<sub>3</sub>) δ (ppm) 7.85 (s, 6H, ArH), 7.01 (s, 6H ArH), 4.10 (s, 12H, Ar-CH<sub>2</sub>-Ar), 3.33 (s, 9H, OCH<sub>3</sub>), 1.12 (s, 27H, C(CH<sub>3</sub>)<sub>3</sub>). The compound showed the same physico-chemical properties as those reported in literature.<sup>98</sup>

### **Synthesis of the 37,38,39,40,41,42-hexamethoxy-11,23,35-trinitro-5,17,29-tri-*tert*-butyl calix[6]arene (4).**

In a (1/1) mixture of N,N-dimethylformamide and tetrahydrofuran (15 mL) under a nitrogen atmosphere, calixarene **3** (1g, 0.73mmol) and sodium hydride (60% wt. in mineral oil, 435 mg, 0.0109 mol) were added in a Schlenk pressure tube. Then iodomethane was slowly added (800 μL, 0.0131 mol) and the mixture was warmed to 80°C and stirred for 5h. After cooling to r.t the reaction was quenched with water (25mL). The solvent was concentrated under reduce pressure and the residue dissolved in dichloromethane (50mL). The organic layer was separated and washed with distilled water (4 x 30mL), dried over anhydrous Na<sub>2</sub>SO<sub>4</sub> and concentrated under reduce pressure. The crude product was purified by a silica gel flash

column chromatography (dichloromethane/cyclohexane 70/30) to yield **4** as a white solid (700mg, 93%). <sup>1</sup>H NMR (400 MHz, CDCl<sub>3</sub>) δ (ppm) 7.83 (s, 6H, ArH), 7.04 (s, 6H, ArH), 3.97 (s, 12H, Ar-CH<sub>2</sub>-Ar), 3.43 (s, 9H OCH<sub>3</sub>), 3.14 (s, 9H, OCH<sub>3</sub>), 1.21 (s, 27H, C(CH<sub>3</sub>)<sub>3</sub>). The compound showed the same physico-chemical properties as those reported in literature.<sup>98</sup>

**Synthesis of the 37,38,39,40,41,42-hexamethoxy-11,23,35-triamino-5,17,29-tri-tert-butyl calix[6]arene (5).**

To a suspension of calix[4]arene **4** (0.140 g, 0.133 mmol) in ethanol (15 mL), hydrazine hydrate (0.46 mL, 9. mmol) and a catalytic amount of Pd/C (10%) were added. The reaction mixture was refluxed for 24 h and quenched by catalyst filtration. The filtrate was evaporated under reduced pressure; the residue was dissolved with dichloromethane and washed with distilled water. The organic layer was separated, dried over anhydrous Na<sub>2</sub>SO<sub>4</sub> and evaporated to dryness under reduced pressure to obtain the pure product **5** as a white solid (0.1 g, 80%). <sup>1</sup>H NMR (400 MHz, CDCl<sub>3</sub>) δ (ppm) 7.08 (s, 6H, ArH), 6.01 (s, 6H, ArH), 3.89 (s, 12H, Ar-CH<sub>2</sub>-Ar), 3.59 (s, 9H, OCH<sub>3</sub>), 3.06 (s, 9H, OCH<sub>3</sub>), 1.12 (s, 27H, C(CH<sub>3</sub>)<sub>3</sub>). The compound showed the same physico-chemical properties as those reported in literature.<sup>98</sup>

## References

- (1) Philip A. Gale; J. Steed. *Supramolecular Chemistry*; Gale, P. A., Steed, J. W., Eds.; John Wiley & Sons, Ltd: Chichester, UK, 2012. <https://doi.org/10.1002/9780470661345>.
- (2) Ornes, S. How Nonequilibrium Thermodynamics Speaks to the Mystery of Life. *Proceedings of the National Academy of Sciences* **2017**, *114* (3), 423–424. <https://doi.org/10.1073/pnas.1620001114>.
- (3) Vella, F. Molecular Biology of the Cell (Third Edition). *Biochem Educ* **1994**, *22* (3), 164. [https://doi.org/10.1016/0307-4412\(94\)90059-0](https://doi.org/10.1016/0307-4412(94)90059-0).
- (4) Walsh, C. T.; Tu, B. P.; Tang, Y. Eight Kinetically Stable but Thermodynamically Activated Molecules That Power Cell Metabolism. *Chem Rev* **2018**, *118* (4), 1460–1494. <https://doi.org/10.1021/acs.chemrev.7b00510>.
- (5) Schliwa, M.; Woehlke, G. Molecular Motors. *Nature* **2003**, *422* (6933), 759–765. <https://doi.org/10.1038/nature01601>.
- (6) Astumian, R. D. Thermodynamics and Kinetics of Molecular Motors. *Biophys J* **2010**, *98* (11), 2401–2409. <https://doi.org/10.1016/j.bpj.2010.02.040>.
- (7) Karsenti, E. Self-Organization in Cell Biology: A Brief History. *Nat Rev Mol Cell Biol* **2008**, *9* (3), 255–262. <https://doi.org/10.1038/nrm2357>.
- (8) Wedlich-Söldner, R.; Betz, T. Self-Organization: The Fundament of Cell Biology. *Philosophical Transactions of the Royal Society B: Biological Sciences* **2018**, *373* (1747), 20170103. <https://doi.org/10.1098/rstb.2017.0103>.
- (9) Grzybowski, B. A.; Huck, W. T. S. The Nanotechnology of Life-Inspired Systems. *Nat Nanotechnol* **2016**, *11* (7), 585–592. <https://doi.org/10.1038/nnano.2016.116>.
- (10) Erbas-Cakmak, S.; Fielden, S. D. P.; Karaca, U.; Leigh, D. A.; McTernan, C. T.; Tetlow, D. J.; Wilson, M. R. Rotary and Linear Molecular Motors Driven by Pulses of a Chemical Fuel. *Science (1979)* **2017**, *358* (6361), 340–343. <https://doi.org/10.1126/science.aao1377>.
- (11) Cheng, C.; McGonigal, P. R.; Schneebeil, S. T.; Li, H.; Vermeulen, N. A.; Ke, C.; Stoddart, J. F. An Artificial Molecular Pump. *Nat Nanotechnol* **2015**, *10* (6), 547–553. <https://doi.org/10.1038/nnano.2015.96>.
- (12) Koumura, N.; Zijlstra, R. W. J.; van Delden, R. A.; Harada, N.; Feringa, B. L. Light-Driven Monodirectional Molecular Rotor. *Nature* **1999**, *401* (6749), 152–155. <https://doi.org/10.1038/43646>.
- (13) Kassem, S.; van Leeuwen, T.; Lubbe, A. S.; Wilson, M. R.; Feringa, B. L.; Leigh, D. A. Artificial Molecular Motors. *Chem Soc Rev* **2017**, *46* (9), 2592–2621. <https://doi.org/10.1039/C7CS00245A>.
- (14) Ikegami, T.; Kageyama, Y.; Obara, K.; Takeda, S. Dissipative and Autonomous Square-Wave Self-Oscillation of a Macroscopic Hybrid Self-Assembly under Continuous Light Irradiation. *Angewandte Chemie International Edition* **2016**, *55* (29), 8239–8243. <https://doi.org/10.1002/anie.201600218>.
- (15) van Rossum, S. A. P.; Tena-Solsona, M.; van Esch, J. H.; Eelkema, R.; Boekhoven, J. Dissipative Out-of-Equilibrium Assembly of Man-Made Supramolecular Materials. *Chem Soc Rev* **2017**, *46* (18), 5519–5535. <https://doi.org/10.1039/C7CS00246G>.
- (16) Foy, J. T.; Li, Q.; Goujon, A.; Colard-Itté, J.-R.; Fuks, G.; Moulin, E.; Schiffmann, O.; Dattler, D.; Funeriu, D. P.; Giuseppone, N. Dual-Light Control of Nanomachines That Integrate Motor and Modulator Subunits. *Nat Nanotechnol* **2017**, *12* (6), 540–545. <https://doi.org/10.1038/nnano.2017.28>.
- (17) Grzybowski, B. A.; Stone, H. A.; Whitesides, G. M. Dynamic Self-Assembly of Magnetized, Millimetre-Sized Objects Rotating at a Liquid–Air Interface. *Nature* **2000**, *405* (6790), 1033–1036. <https://doi.org/10.1038/35016528>.
- (18) Göstl, R.; Hecht, S. Controlling Covalent Connection and Disconnection with Light. *Angewandte Chemie International Edition* **2014**, *53* (33), 8784–8787. <https://doi.org/10.1002/anie.201310626>.

- (19) Biagini, C.; di Stefano, S. Abiotic Chemical Fuels for the Operation of Molecular Machines. *Angewandte Chemie International Edition* **2020**, *59* (22), 8344–8354. <https://doi.org/10.1002/anie.201912659>.
- (20) della Sala, F.; Neri, S.; Maiti, S.; Chen, J. L.-Y.; Prins, L. J. Transient Self-Assembly of Molecular Nanostructures Driven by Chemical Fuels. *Curr Opin Biotechnol* **2017**, *46*, 27–33. <https://doi.org/10.1016/j.copbio.2016.10.014>.
- (21) Ragazzon, G.; Prins, L. J. Energy Consumption in Chemical Fuel-Driven Self-Assembly. *Nat Nanotechnol* **2018**, *13* (10), 882–889. <https://doi.org/10.1038/s41565-018-0250-8>.
- (22) Kariyawasam, L. S.; Hossain, M. M.; Hartley, C. S. The Transient Covalent Bond in Abiotic Nonequilibrium Systems. *Angewandte Chemie International Edition* **2021**, *60* (23), 12648–12658. <https://doi.org/10.1002/anie.202014678>.
- (23) Del Grosso, E.; Ragazzon, G.; Prins, L. J.; Ricci, F. Fuel-Responsive Allosteric DNA-Based Aptamers for the Transient Release of ATP and Cocaine. *Angewandte Chemie* **2019**, *131* (17), 5638–5642. <https://doi.org/10.1002/ange.201812885>.
- (24) del Grosso, E.; Prins, L. J.; Ricci, F. Transient DNA-Based Nanostructures Controlled by Redox Inputs. *Angewandte Chemie International Edition* **2020**, *59* (32), 13238–13245. <https://doi.org/10.1002/anie.202002180>.
- (25) Mariottini, D.; del Giudice, D.; Ercolani, G.; di Stefano, S.; Ricci, F. Dissipative Operation of PH-Responsive DNA-Based Nanodevices. *Chem Sci* **2021**, *12* (35), 11735–11739. <https://doi.org/10.1039/D1SC03435A>.
- (26) Feng, Y.; Ovalle, M.; Seale, J. S. W.; Lee, C. K.; Kim, D. J.; Astumian, R. D.; Stoddart, J. F. Molecular Pumps and Motors. *J Am Chem Soc* **2021**, *143* (15), 5569–5591. <https://doi.org/10.1021/jacs.0c13388>.
- (27) Amano, S.; Fielden, S. D. P.; Leigh, D. A. A Catalysis-Driven Artificial Molecular Pump. *Nature* **2021**, *594* (7864), 529–534. <https://doi.org/10.1038/s41586-021-03575-3>.
- (28) Feng, L.; Qiu, Y.; Guo, Q.-H.; Chen, Z.; Seale, J. S. W.; He, K.; Wu, H.; Feng, Y.; Farha, O. K.; Astumian, R. D.; Stoddart, J. F. Active Mechanisorption Driven by Pumping Cassettes. *Science (1979)* **2021**, *374* (6572), 1215–1221. <https://doi.org/10.1126/science.abk1391>.
- (29) Wood, C. S.; Browne, C.; Wood, D. M.; Nitschke, J. R. Fuel-Controlled Reassembly of Metal–Organic Architectures. *ACS Cent Sci* **2015**, *1* (9), 504–509. <https://doi.org/10.1021/acscentsci.5b00279>.
- (30) del Giudice, D.; Spatola, E.; Valentini, M.; Bombelli, C.; Ercolani, G.; di Stefano, S. Time-Programmable pH: Decarboxylation of Nitroacetic Acid Allows the Time-Controlled Rising of pH to a Definite Value. *Chem Sci* **2021**, *12* (21), 7460–7466. <https://doi.org/10.1039/D1SC01196K>.
- (31) P.A. Gale; J.W. Steed. *Self-Assembly and Supramolecular Devices (Supramolecular Chemistry: From Molecules to Nanomaterials)*, Wiley.; 2012; Vol. 5.
- (32) Fialkowski, M.; Bishop, K. J. M.; Klajn, R.; Smoukov, S. K.; Campbell, C. J.; Grzybowski, B. A. Principles and Implementations of Dissipative (Dynamic) Self-Assembly. *J Phys Chem B* **2006**, *110* (6), 2482–2496. <https://doi.org/10.1021/jp054153q>.
- (33) Rizzoli, S. O. Synaptic Vesicle Recycling: Steps and Principles. *EMBO J* **2014**, *33* (8), 788–822. <https://doi.org/10.1002/embj.201386357>.
- (34) Saibil, H. Chaperone Machines for Protein Folding, Unfolding and Disaggregation. *Nat Rev Mol Cell Biol* **2013**, *14* (10), 630–642. <https://doi.org/10.1038/nrm3658>.
- (35) Grötsch, R. K.; Boekhoven, J. Unique Properties of Supramolecular Biomaterials through Nonequilibrium Self-Assembly. In *Self-assembling Biomaterials*; Elsevier, 2018; pp 235–250. <https://doi.org/10.1016/B978-0-08-102015-9.00012-5>.
- (36) Whitesides, G. M.; Grzybowski, B. Self-Assembly at All Scales. *Science (1979)* **2002**, *295* (5564), 2418–2421. <https://doi.org/10.1126/science.1070821>.

- (37) Ragazzon, G.; Baroncini, M.; Silvi, S.; Venturi, M.; Credi, A. Light-Powered Autonomous and Directional Molecular Motion of a Dissipative Self-Assembling System. *Nat Nanotechnol* **2015**, *10* (1), 70–75. <https://doi.org/10.1038/nnano.2014.260>.
- (38) Wilson, M. R.; Solà, J.; Carlone, A.; Goldup, S. M.; Lebrasseur, N.; Leigh, D. A. An Autonomous Chemically Fuelled Small-Molecule Motor. *Nature* **2016**, *534* (7606), 235–240. <https://doi.org/10.1038/nature18013>.
- (39) Cheng, C.; McGonigal, P. R.; Liu, W.-G.; Li, H.; Vermeulen, N. A.; Ke, C.; Frascioni, M.; Stern, C. L.; Goddard III, W. A.; Stoddart, J. F. Energetically Demanding Transport in a Supramolecular Assembly. *J Am Chem Soc* **2014**, *136* (42), 14702–14705. <https://doi.org/10.1021/ja508615f>.
- (40) Klajn, R.; Wesson, P. J.; Bishop, K. J. M.; Grzybowski, B. A. Writing Self-Erasing Images Using Metastable Nanoparticle “Inks.” *Angewandte Chemie International Edition* **2009**, *48* (38), 7035–7039. <https://doi.org/10.1002/anie.200901119>.
- (41) Zhao, H.; Sen, S.; Udayabhaskararao, T.; Sawczyk, M.; Kučanda, K.; Manna, D.; Kundu, P. K.; Lee, J.-W.; Král, P.; Klajn, R. Reversible Trapping and Reaction Acceleration within Dynamically Self-Assembling Nanoflasks. *Nat Nanotechnol* **2016**, *11* (1), 82–88. <https://doi.org/10.1038/nnano.2015.256>.
- (42) Krabbenborg, S. O.; Veerbeek, J.; Huskens, J. Spatially Controlled Out-of-Equilibrium Host-Guest System under Electrochemical Control. *Chemistry - A European Journal* **2015**, *21* (27), 9638–9644. <https://doi.org/10.1002/chem.201501544>.
- (43) Pappas, C. G.; Mutasa, T.; Frederix, P. W. J. M.; Fleming, S.; Bai, S.; Debnath, S.; Kelly, S. M.; Gachagan, A.; Ulijn, R. v. Transient Supramolecular Reconfiguration of Peptide Nanostructures Using Ultrasound. *Mater Horiz* **2015**, *2* (2), 198–202. <https://doi.org/10.1039/C4MH00223G>.
- (44) Heuser, T.; Weyandt, E.; Walther, A. Biocatalytic Feedback-Driven Temporal Programming of Self-Regulating Peptide Hydrogels. *Angewandte Chemie International Edition* **2015**, *54* (45), 13258–13262. <https://doi.org/10.1002/anie.201505013>.
- (45) Heuser, T.; Steppert, A.-K.; Molano Lopez, C.; Zhu, B.; Walther, A. Generic Concept to Program the Time Domain of Self-Assemblies with a Self-Regulation Mechanism. *Nano Lett* **2015**, *15* (4), 2213–2219. <https://doi.org/10.1021/nl5039506>.
- (46) Steed, J. W.; Atwood, J. L. *Supramolecular Chemistry*, 3rd ed.; Wiley, Ed.; 2013.
- (47) Lehn, J.-M. Perspectives in Supramolecular Chemistry—From Molecular Recognition towards Molecular Information Processing and Self-Organization. *Angewandte Chemie International Edition in English* **1990**, *29* (11), 1304–1319. <https://doi.org/10.1002/anie.199013041>.
- (48) Credi, A.; Silvi, S.; Venturi, M. Photochemically Driven Molecular Devices and Machines. In *Supramolecular Chemistry*; John Wiley & Sons, Ltd: Chichester, UK, 2012. <https://doi.org/10.1002/9780470661345.smc196>.
- (49) Teo, B. K.; Sun, X. H. From Top-Down to Bottom-Up to Hybrid Nanotechnologies: Road to Nanodevices. *J Clust Sci* **2006**, *17* (4), 529–540. <https://doi.org/10.1007/s10876-006-0086-5>.
- (50) Lehn, J.-M. Supramolecular Chemistry—Scope and Perspectives Molecules, Supermolecules, and Molecular Devices (Nobel Lecture). *Angewandte Chemie International Edition in English* **1988**, *27* (1), 89–112. <https://doi.org/10.1002/anie.198800891>.
- (51) Philip, D. *Supramolecular Chemistry: Concepts and Perspectives*. By J.-M. Lehn, VCH, Weinheim 1995, x, 271 Pp., Softcover, DM 58.00, ISBN 3-527-2931 1-6. *Advanced Materials* **1996**, *8* (10), 866–868. <https://doi.org/10.1002/adma.19960081029>.
- (52) Gordon A. Melson. *Coordination Chemistry of Macrocyclic Compounds*; Plenum Press.; New York, 1979.
- (53) Maiti, B.; Abramov, A.; Pérez-Ruiz, R.; Díaz Díaz, D. The Prospect of Photochemical Reactions in Confined Gel Media. *Acc Chem Res* **2019**, *52* (7), 1865–1876. <https://doi.org/10.1021/acs.accounts.9b00097>.



- (54) Stoddart, J. F. Molecular Machines. *Acc Chem Res* **2001**, *34* (6), 410–411. <https://doi.org/10.1021/ar010084w>.
- (55) Balzani, V.; Credi, A.; Venturi, M. The Bottom-Up Approach to Molecular-Level Devices and Machines. *Chemistry - A European Journal* **2002**, *8* (24), 5524–5532. [https://doi.org/10.1002/1521-3765\(20021216\)8:24<5524::AID-CHEM5524>3.0.CO;2-J](https://doi.org/10.1002/1521-3765(20021216)8:24<5524::AID-CHEM5524>3.0.CO;2-J).
- (56) Coskun, A.; Banaszak, M.; Astumian, R. D.; Stoddart, J. F.; Grzybowski, B. A. Great Expectations: Can Artificial Molecular Machines Deliver on Their Promise? *Chem. Soc. Rev.* **2012**, *41* (1), 19–30. <https://doi.org/10.1039/C1CS15262A>.
- (57) Elledge, S. J. Cell Cycle Checkpoints: Preventing an Identity Crisis. *Science (1979)* **1996**, *274* (5293), 1664–1672. <https://doi.org/10.1126/science.274.5293.1664>.
- (58) Berrocal, J. A.; Biagini, C.; Mandolini, L.; Di Stefano, S. Coupling of the Decarboxylation of 2-Cyano-2-Phenylpropanoic Acid to Large-Amplitude Motions: A Convenient Fuel for an Acid-Base-Operated Molecular Switch. *Angewandte Chemie International Edition* **2016**, *55* (24), 6997–7001. <https://doi.org/10.1002/anie.201602594>.
- (59) Shaomin, S.; Yu, Y.; Jinghao, P. Study on Molecular Recognition of Para-Aminobenzoic Acid Species by  $\alpha$ -,  $\beta$ - and Hydroxypropyl- $\beta$ -Cyclodextrin. *Anal Chim Acta* **2002**, *458* (2), 305–310. [https://doi.org/10.1016/S0003-2670\(02\)00066-1](https://doi.org/10.1016/S0003-2670(02)00066-1).
- (60) Ghosh, A.; Paul, I.; Schmittel, M. Multitasking with Chemical Fuel: Dissipative Formation of a Pseudorotaxane Rotor from Five Distinct Components. *J Am Chem Soc* **2021**, *143* (14), 5319–5323. <https://doi.org/10.1021/jacs.1c01948>.
- (61) Arnaud-Neu, F.; Fanni, S.; Guerra, L.; McGregor, W.; Ziat, K.; Schwing-Weill, M.-J.; Barrett, G.; McKervey, M. A.; Marrs, D.; Seward, E. M. Cation Complexation by Chemically Modified Calixarenes. Part 7. Transport of Alkali Cations by p-Tert-Butylcalix[n]Arene Esters and Amides. *Journal of the Chemical Society, Perkin Transactions 2* **1995**, No. 1, 113. <https://doi.org/10.1039/p29950000113>.
- (62) Gutsche, C. D.; See, K. A. Calixarenes. 27. Synthesis, Characterization, and Complexation Studies of Double-Cavity Calix[4]Arenes. *J Org Chem* **1992**, *57* (16), 4527–4539. <https://doi.org/10.1021/jo00042a038>.
- (63) Murakami, H.; Shinkai, S. Metal-Induced Conversion of a ‘Closed’ Receptor to an ‘Open’ Receptor on a p-Tert-Butylcalix[4]Arene Diamide Derivative; Fluorescence Detection of a Molecular Recognition Process. *J. Chem. Soc., Chem. Commun.* **1993**, No. 20, 1533–1535. <https://doi.org/10.1039/C39930001533>.
- (64) van Duynhoven, J. P. M.; Janssen, R. G.; Verboom, W.; Franken, S. M.; Casnati, A.; Pochini, A.; Ungaro, R.; de Mendoza, J.; Nieto, P. M. Control of Calix[6]Arene Conformations by Self-Inclusion of 1,3,5-Tri-O-Alkyl Substituents: Synthesis and NMR Studies. *J Am Chem Soc* **1994**, *116* (13), 5814–5822. <https://doi.org/10.1021/ja00092a036>.
- (65) Gutsche, C. D. *Calixarenes in the Nanoworld*; Vicens, J., Harrowfield, J., Baklouti, L., Eds.; Springer Netherlands, 2007. <https://doi.org/10.1007/978-1-4020-5022-4>.
- (66) Casnati, A.; Jacopozzi, P.; Pochini, A.; Ugozzoli, F.; Cacciapaglia, R.; Mandolini, L.; Ungaro, R. Bridged Calix[6]Arenes in the Cone Conformation: New Receptors for Quaternary Ammonium Cations. *Tetrahedron* **1995**, *51* (2), 591–598. [https://doi.org/10.1016/0040-4020\(94\)00918-K](https://doi.org/10.1016/0040-4020(94)00918-K).
- (67) Shinkai, S.; Koreishi, H.; Ueda, K.; Arimura, T.; Manabe, O. Molecular Design of Calixarene-Based Uranophiles Which Exhibit Remarkably High Stability and Selectivity. *J Am Chem Soc* **1987**, *109* (21), 6371–6376. <https://doi.org/10.1021/ja00255a023>.
- (68) Cai, R.; Hashimoto, K.; Itoh, K.; Kubota, Y.; Fujishima, A. Photokilling of Malignant Cells with Ultrafine TiO<sub>2</sub> Powder. *Bull Chem Soc Jpn* **1991**, *64* (4), 1268–1273. <https://doi.org/10.1246/bcsj.64.1268>.
- (69) Casnati, A.; Minari, P.; Pochini, A.; Ungaro, R. Conformational Freezing of P-Tert-Butylcalix[6]Arene in the Cone Structure by Selective Functionalization at the Lower Rim:

- Synthesis of New Preorganized Ligands. *J Chem Soc Chem Commun* **1991**, No. 19, 1413. <https://doi.org/10.1039/c39910001413>.
- (70) Nyssen, N.; Ajami, D.; Ardelean, A.; Desroches, F.; Li, J.; Luhmer, M.; Reinaud, O.; Jabin, I. Closing a Calix[6]Arene-Based Funnel Zn<sup>2+</sup> Complex at Its Large Rim Entrance: Consequences on Metal Ion Affinity and Host–Guest Properties. *J Org Chem* **2021**, *86* (17), 12075–12083. <https://doi.org/10.1021/acs.joc.1c01418>.
- (71) Arduini, A.; Giorgi, G.; Pochini, A.; Secchi, A.; Ugozzoli, F. Anion Allosteric Effect in the Recognition of Tetramethylammonium Salts by Calix[4]Arene Cone Conformers. *J Org Chem* **2001**, *66* (25), 8302–8308. <https://doi.org/10.1021/jo016035e>.
- (72) Arduini, A.; Orlandini, G.; Secchi, A.; Credi, A.; Silvi, S.; Venturi, M. Calixarene Threading by Viologen-Based Axles. In *Calixarenes and Beyond*; Springer International Publishing: Cham, 2016; pp 761–781. [https://doi.org/10.1007/978-3-319-31867-7\\_29](https://doi.org/10.1007/978-3-319-31867-7_29).
- (73) Bazzoni, M.; Terenziani, F.; Secchi, A.; Cera, G.; Jabin, I.; de Leener, G.; Luhmer, M.; Arduini, A. Tuning the Fluorescence Through Reorientation of the Axle in Calix[6]Arene-Based Pseudorotaxanes. *Chemistry – A European Journal* **2020**, *26* (14), 3022–3025. <https://doi.org/10.1002/chem.201905500>.
- (74) Arduini, A.; Ciesa, F.; Fragassi, M.; Pochini, A.; Secchi, A. Selective Synthesis of Two Constitutionally Isomeric Oriented Calix[6]Arene-Based Rotaxanes. *Angewandte Chemie International Edition* **2005**, *44* (2), 278–281. <https://doi.org/10.1002/anie.200461336>.
- (75) Bazzoni, M.; Andreoni, L.; Silvi, S.; Credi, A.; Cera, G.; Secchi, A.; Arduini, A. Selective Access to Constitutionally Identical, Orientationally Isomeric Calix[6]Arene-Based [3]Rotaxanes by an Active Template Approach. *Chem Sci* **2021**, *12* (18), 6419–6428. <https://doi.org/10.1039/D1SC00279A>.
- (76) Arduini, A.; Calzavacca, F.; Pochini, A.; Secchi, A. Unidirectional Threading of Triphenylureidocalix[6]Arene-Based Wheels: Oriented Pseudorotaxane Synthesis. *Chemistry - A European Journal* **2003**, *9* (3), 793–799. <https://doi.org/10.1002/chem.200390089>.
- (77) Arduini, A.; Ferdani, R.; Pochini, A.; Secchi, A.; Ugozzoli, F. Calix[6]Arene as a Wheel for Rotaxane Synthesis. *Angewandte Chemie* **2000**, *39* (19), 3453–3456. [https://doi.org/10.1002/1521-3773\(20001002\)39:19<3453::AID-ANIE3453>3.0.CO;2-I](https://doi.org/10.1002/1521-3773(20001002)39:19<3453::AID-ANIE3453>3.0.CO;2-I).
- (78) Arduini, A.; Domiano, L.; Ogliosi, L.; Pochini, A.; Secchi, A.; Ungaro, R. Self-Assembled Hydrogen-Bonded Molecular Cages of Calix[6]Arenetricarboxylic Acid Derivatives. *J Org Chem* **1997**, *62* (22), 7866–7868. <https://doi.org/10.1021/jo9704826>.
- (79) Casnati, A.; Minari, P.; Pochini, A.; Ungaro, R. Conformational Freezing of P-Tert-Butylcalix[6]Arene in the Cone Structure by Selective Functionalization at the Lower Rim: Synthesis of New Preorganized Ligands. *J Chem Soc Chem Commun* **1991**, No. 19, 1413. <https://doi.org/10.1039/c39910001413>.
- (80) Casnati, A.; Domiano, L.; Pochini, A.; Ungaro, R.; Carramolino, M.; Oriol Magrans, J.; M. Nieto, P.; López-Prados, J.; Prados, P.; de Mendoza, J.; G. Janssen, R.; Verboom, W.; N.Reinhoudt, D. Synthesis of Calix[6]Arenes Partially Functionalized at the Upper Rim. *Tetrahedron* **1995**, *51* (46), 12699–12720. [https://doi.org/10.1016/0040-4020\(95\)00826-T](https://doi.org/10.1016/0040-4020(95)00826-T).
- (81) Talotta, C.; Gaeta, C.; Neri, P. *Endo*-Complexation of Alkylammonium Ions by Calix[4]Arene Cavity: Facilitating Cation– $\pi$  Interactions through the Weakly Coordinating Anion Approach. *J Org Chem* **2014**, *79* (20), 9842–9846. <https://doi.org/10.1021/jo5016689>.
- (82) Iuliano, V.; Talotta, C.; Gaeta, C.; Hickey, N.; Geremia, S.; Vatsouro, I.; Kovalev, V.; Neri, P. Influence of *Exo*-Adamantyl Groups and *Endo*-OH Functions on the Threading of Calix[6]Arene Macrocycle. *J Org Chem* **2020**, *85* (19), 12585–12593. <https://doi.org/10.1021/acs.joc.0c01769>.

- (83) Zahim, S.; Wickramasinghe, L. A.; Evano, G.; Jabin, I.; Schrock, R. R.; Müller, P. Calix[6]Azacryptand Ligand with a Sterically Protected Tren-Based Coordination Site for Metal Ions. *Org Lett* **2016**, *18* (7), 1570–1573. <https://doi.org/10.1021/acs.orglett.6b00410>.
- (84) Gutsche, C. D.; Bauer, L. J. Calixarenes. 14. The Conformational Properties of the Ethers and Esters of the Calix[6]Arenes and the Calix[8]Arenes. *J Am Chem Soc* **1985**, *107* (21), 6059–6063. <https://doi.org/10.1021/ja00307a039>.
- (85) del Giudice, D.; Spatola, E.; Valentini, M.; Bombelli, C.; Ercolani, G.; di Stefano, S. Time-Programmable PH: Decarboxylation of Nitroacetic Acid Allows the Time-Controlled Rising of PH to a Definite Value. *Chem Sci* **2021**, *12* (21), 7460–7466. <https://doi.org/10.1039/D1SC01196K>.
- (86) Biagini, C.; Capocasa, G.; Cataldi, V.; del Giudice, D.; Mandolini, L.; di Stefano, S. The Hydrolysis of the Anhydride of 2-Cyano-2-phenylpropanoic Acid Triggers the Repeated Back and Forth Motions of an Acid–Base Operated Molecular Switch. *Chemistry – A European Journal* **2019**, *25* (66), 15205–15211. <https://doi.org/10.1002/chem.201904048>.
- (87) Biagini, C.; Di Pietri, F.; Mandolini, L.; Lanzalunga, O.; Di Stefano, S. Photoinduced Release of a Chemical Fuel for Acid–Base-Operated Molecular Machines. *Chemistry – A European Journal* **2018**, *24* (40), 10122–10127. <https://doi.org/10.1002/chem.201800474>.
- (88) Berrocal, J. A.; Biagini, C.; Mandolini, L.; Di Stefano, S. Coupling of the Decarboxylation of 2-Cyano-2-Phenylpropanoic Acid to Large-Amplitude Motions: A Convenient Fuel for an Acid-Base-Operated Molecular Switch. *Angewandte Chemie International Edition* **2016**, *55* (24), 6997–7001. <https://doi.org/10.1002/anie.201602594>.
- (89) Biagini, C.; Albano, S.; Caruso, R.; Mandolini, L.; Berrocal, J. A.; di Stefano, S. Variations in the Fuel Structure Control the Rate of the Back and Forth Motions of a Chemically Fuelled Molecular Switch. *Chem Sci* **2018**, *9* (1), 181–188. <https://doi.org/10.1039/C7SC04123C>.
- (90) Spatola, E.; Rispoli, F.; del Giudice, D.; Cacciapaglia, R.; Casnati, A.; Marchiò, L.; Baldini, L.; di Stefano, S. Dissipative Control of the Fluorescence of a 1,3-Dipyrenyl Calix[4]Arene in the Cone Conformation. *Org Biomol Chem* **2022**, *20* (1), 132–138. <https://doi.org/10.1039/D1OB02096J>.
- (91) Erbas-Cakmak, S.; Fielden, S. D. P.; Karaca, U.; Leigh, D. A.; McTernan, C. T.; Tetlow, D. J.; Wilson, M. R. Rotary and Linear Molecular Motors Driven by Pulses of a Chemical Fuel. *Science (1979)* **2017**, *358* (6361), 340–343. <https://doi.org/10.1126/science.aao1377>.
- (92) Mariottini, D.; del Giudice, D.; Ercolani, G.; di Stefano, S.; Ricci, F. Dissipative Operation of PH-Responsive DNA-Based Nanodevices. *Chem Sci* **2021**, *12* (35), 11735–11739. <https://doi.org/10.1039/D1SC03435A>.
- (93) del Giudice, D.; Tavani, F.; di Berto Mancini, M.; Fratello, F.; Busato, M.; Oliveira De Souza, D.; Cenesi, F.; Lanzalunga, O.; di Stefano, S.; D’Angelo, P. Two Faces of the Same Coin: Coupling X-Ray Absorption and NMR Spectroscopies to Investigate the Exchange Reaction Between Prototypical Cu Coordination Complexes. *Chemistry – A European Journal* **2022**, *28* (4). <https://doi.org/10.1002/chem.202103825>.
- (94) Franchi, P.; Poderi, C.; Mezzina, E.; Biagini, C.; di Stefano, S.; Lucarini, M. 2-Cyano-2-Phenylpropanoic Acid Triggers the Back and Forth Motions of an Acid–Base-Operated Paramagnetic Molecular Switch. *J Org Chem* **2019**, *84* (14), 9364–9368. <https://doi.org/10.1021/acs.joc.9b01164>.

- (95) Masataka Ohoka, \*; Tsuyoshi Kojitanii. Reaction of Nitriles with Thionyl Chloride in the Presence of Hydrogen Chloride. Formation of Sulfinyl and Sulfenyl Chlorides and Phenyl Cyanosulfine. *J. Org. Chem* **1975**, *40* (24), 3540–3544.
- (96) Li, G.; Trausel, F.; Helm, M. P.; Klemm, B.; Brevé, T. G.; Rossum, S. A. P.; Hartono, M.; Gerlings, H. H. P. J.; Lovrak, M.; Esch, J. H.; Eelkema, R. Tuneable Control of Organocatalytic Activity through Host–Guest Chemistry. *Angewandte Chemie International Edition* **2021**, *60* (25), 14022–14029. <https://doi.org/10.1002/anie.202102227>.
- (97) Casnati, A.; Minari, P.; Pochini, A.; Ungaro, R. Conformational Freezing of P-Tert-Butylcalix[6]Arene in the Cone Structure by Selective Functionalization at the Lower Rim: Synthesis of New Preorganized Ligands. *J Chem Soc Chem Commun* **1991**, No. 19, 1413. <https://doi.org/10.1039/c39910001413>.
- (98) Nyssen, N.; Ajami, D.; Ardelean, A.; Desroches, F.; Li, J.; Luhmer, M.; Reinaud, O.; Jabin, I. Closing a Calix[6]Arene-Based Funnel Zn<sup>2+</sup> Complex at Its Large Rim Entrance: Consequences on Metal Ion Affinity and Host–Guest Properties. *J Org Chem* **2021**, *86* (17), 12075–12083. <https://doi.org/10.1021/acs.joc.1c01418>.



# Chapter 3

**Zwitterionic calix[4]arene for  
bacteria cell wall detection**

# Introduction

## 3.1 Bacteria and their cell wall

Bacteria are small single cell organisms and millions of bacteria exist in the human body. The majority of bacteria are harmless to humans and are necessary for the production of vitamins, the death of sick cells, and play an important role in digestive tract.<sup>1</sup> However, certain bacteria have the capability to result in fatal illnesses. For instance, the World Health Organization (WHO) listed a few pathogens that might be particularly harmful to human health.<sup>2</sup> Additionally, due to the overuse of antibiotics, multidrug-resistant pathogenic bacteria are becoming a significant global issue.<sup>3</sup> Thus, identifying bacterial strains is crucial for treating bacterial illnesses and for targeting antibiotics. The first barrier that an antibacterial agent must overcome is the cell wall.<sup>4</sup> The cell wall complex polymers provide bacteria with strength and a barrier to the outside world, allowing them to survive in a variety of conditions, including the human body. Bacteria may be divided into three main groups based on their cell surface composition: Gram-positive, Gram-negative and mycobacteria.<sup>5-7</sup> Gram-positive bacteria are distinguished by thicker, more cross-linked peptidoglycans and the absence of an outer membrane.<sup>8</sup> Gram-negative bacteria, on the other hand, have a thin layer of peptidoglycan (PG) wall and an outer membrane composed of lipoproteins such as phospholipids and lipopolysaccharide (LPS).<sup>9</sup> In mycobacteria cell wall peptidoglycan is covalently attached to arabinogalactan, which is then bonded to mycolic acids. An outermost capsule made of polysaccharides, proteins, and lipids surrounds the top section of this cell wall and interacts with free lipids.<sup>10</sup>

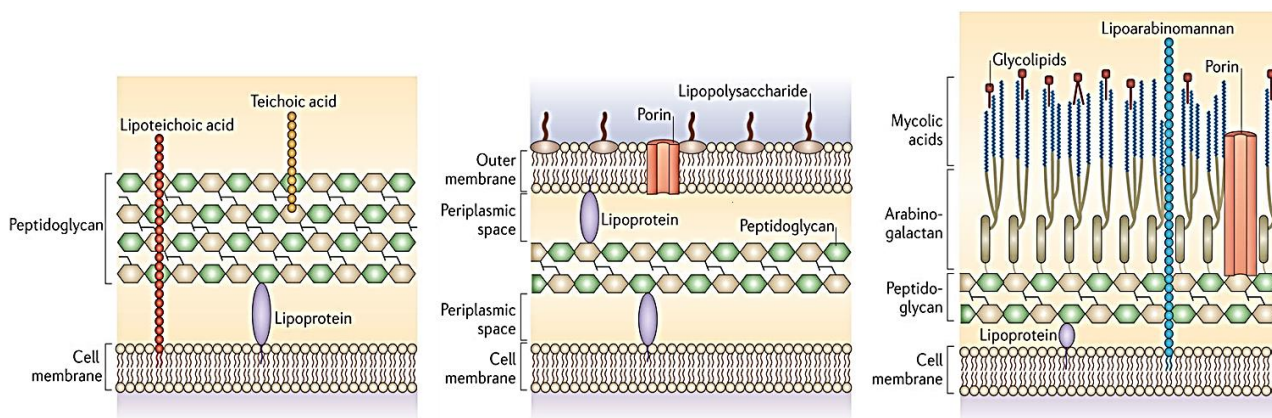


**Fig1** Structural features of the cell wall of Gram-positives, Gram-negatives, and mycobacteria.<sup>4</sup>

Teichoic acid represents 60% of the wall of Gram-positive bacteria, is obtained by the polymerisation of glycerol or ruitol, and is rich in phosphoric diesters. Lipopolysaccharides (LPS) and lipooligosaccharides (LOS) make up 75% of the cell wall of Gram-negative bacteria, exposing the polysaccharide chain, while the core, the so-called Lipid A, has two saccharide residues with negatively charged phosphate groups in the form of monoester. In mycobacteria, on the other hand, the molecular pattern is hydrophobic, due to chains of mycolic acid, a fatty acid belonging to the homologous series of C60-C90  $\alpha$ -alkyl- $\beta$ -hydroxy long-chain fatty acids

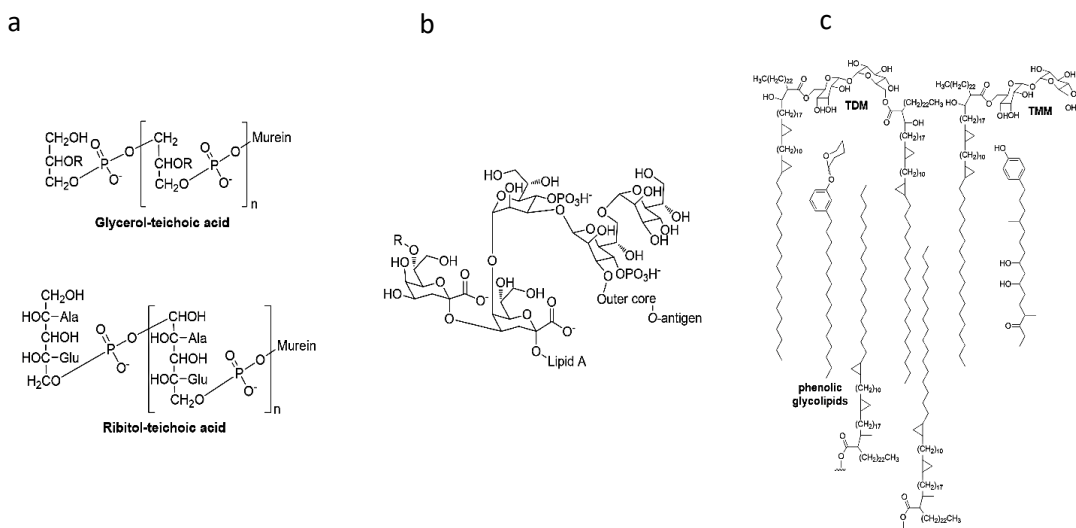


**Fig.2** Molecular patterns characteristic of the cell walls of Gram-positive bacteria (Teichoic acids) (a), Gram-negative bacteria (internal face of LPS) (b) and mycobacteria (Mycolic acid and glycolipids) (c).<sup>7</sup>



### 3.2 Bacteria Detection

The key control point in the prevention of illnesses caused by harmful bacteria is monitoring.<sup>11</sup> Effective detection procedures are required to limit this impact and have been developed throughout time through the use of traditional microbiological approaches.<sup>12,13</sup> These conventional procedures have been in use for almost a century and are still widely utilized for this sort of detection.<sup>14</sup> These traditional procedures nearly entirely rely on the employment of particular agar medium lines to isolate, cultivate, and count live cells in samples. The conventional sample technique normally comprises bacteria culture and isolation, followed by confirmation by biochemical and serological assays, which can take up from five to seven days to obtain a verified result for a specific organism.<sup>15</sup> Some of the most common methods for confirming pathogen presence are culture and colony counting methods, as well as the polymerase chain reaction (PCR).<sup>16</sup> For both selectivity and dependability, these techniques have often been analytically concrete.<sup>17</sup>

#### -PCR

The polymerase chain reaction (PCR) is a nucleic acid amplification technology that was created in the 1980s and is commonly used to identify microorganisms.<sup>18</sup> In general, the approach is designed for the isolation, amplification, and quantification of a short DNA sequence that includes the genetic material of the target microorganisms.<sup>18</sup>

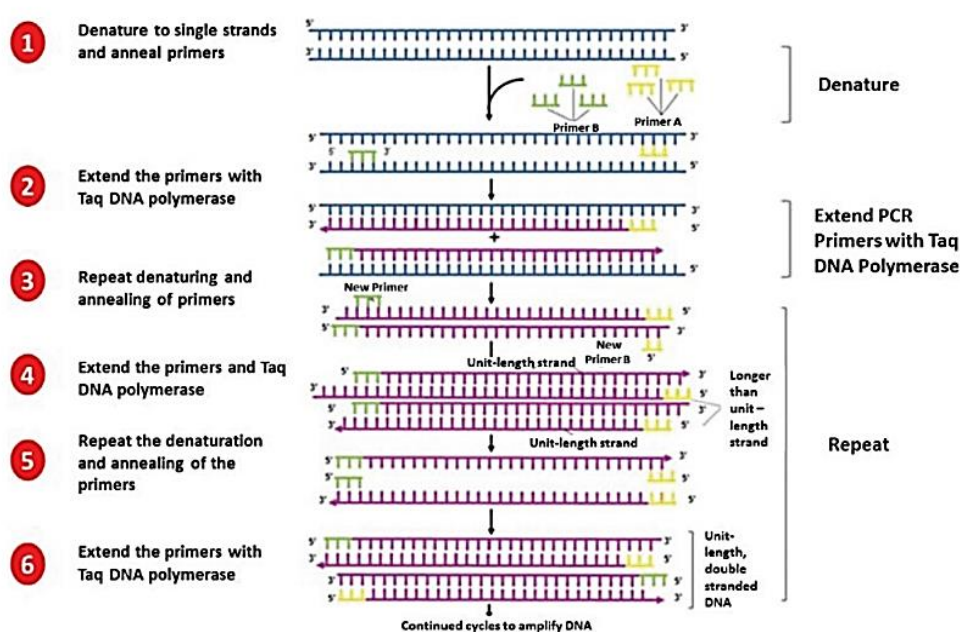
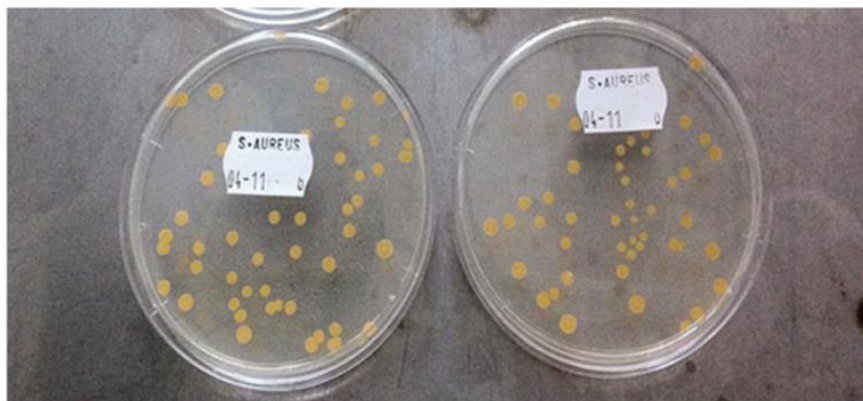


Fig.3: Schematic representation of a PCR cycle.<sup>19</sup>

Some examples of developed PCR methods for bacterial quantification are real-time PCR, multiplex PCR and reverse transcriptase PCR. PCR is much less time-consuming than other conventional techniques utilising culture and plating. PCR usually takes anywhere between 5 and 24 hours to produce a result but this is dependent on the specific PCR variation and excludes enrichment stages.<sup>20</sup> Figure 3 depicts the fundamental stages of PCR, which include denaturation, primer annealing, and primer extension.<sup>21</sup> To denature the targeted double-stranded DNA, different synthesis cycles are conducted and heat over the melting point of DNA is used. Following purification, DNA is extended using primers and a thermostable polymerisation enzyme. As a result, each new double-stranded DNA serves as a target for the next cycle, resulting in exponential amplification. A polymerase enzyme extends the primers from 5' to 3' to overlap the copies of the original template. Subsequent detection of the amplified sequence is performed through gel electrophoresis.<sup>22</sup> One of the most evident disadvantages of PCR methods is the inability to distinguish between viable and non-viable cells.<sup>23</sup> This is due to the fact that DNA is always present, whether the cell is alive or dead. To address this lack of discrimination, reverse transcriptase PCR (RT-PCR) was devised, which is capable of distinguishing live cells.<sup>24</sup> Because PCR is so sensitive, contamination of the material might yield false DNA readings. Prior sequencing data are necessary for generating primers, which allows the approach to identify only the presence or absence of recognized infections or genes. Furthermore, the primers employed might be annealed with comparable DNA as well as the target DNA, giving inaccurate results. Furthermore, erroneous nucleotides might be improperly integrated by PCR, producing misleading results. With the significant growth in research to discover, measure, and characterize the human microbiome, unique human-associated genetic markers have been created to decrease false positives and enhance the capacity to target species related to the host.

### **-Colony counting and culturing**

Until recently, attempts to discover and identify organisms relied heavily on in vitro techniques. This is the most established approach for detecting bacteria and is based on directly growing and plating the organisms.



**Fig.4:** Photograph of the *S. aureus* culture and plating process

Microbial culture has opened up a world of microscopic life detection, with Robert Koch first conveying the guidelines, known as Koch's postulates.<sup>25</sup> Koch's postulates are a set of ground principles that establish if a particular organism has the ability to cause illness. One of the guidelines specifies that a bacterium must be demonstrated to be disease ready by being able to grow outside of the human body. Bacterial colony counting may be accomplished using a variety of techniques. The traditional counting method is simple to use, but aseptic procedures must be strictly followed to prevent contamination. First, a targeted bacterium culture should be diluted and grown in a plate. Then the total colony forming units (CFUs) are calculated using a proper equation. The bulk of traditional tests for bacteria detection use culture-based techniques. Due to their reliability in effectiveness, sensitivity, and variety of application bases, they are the fundamental tools utilized for detection around the world. Beyond these benefits, the conventional culture techniques for pathogen detection need a significant quantity of laboratory supplies, consumables, and time. Unfortunately, it takes a lot of training for laboratory staff to compile and evaluate findings, which makes widespread, non-specialist use challenging.

### **-Biosensors**

A biosensor<sup>26,27</sup> is an analytical tool that combines a biological element with a physicochemical detector and is used to identify small chemicals or large biomolecules. An appealing method for the precise identification of bacteria is optical transducers.<sup>28</sup> The measurement may be sensitive to changes in thickness when the cells connect to the receptors on the transducer surface since optical transducers may pick up even the tiniest variations in refractive index.<sup>29</sup> The benefit of biosensors is that they can analyse samples quickly and do

not require the transportation of samples to a bio-medical laboratory for pathogen diagnosis. Due of their ease of use, colorimetric sensors are the most widely used type of these sensors. Without the need of any additional instruments, the infections are plainly visible with the naked eye by changing colour.

Despite several breakthroughs, it is still difficult to construct receptors that can selectively distinguish between structurally identical species.<sup>30</sup> The interaction of matrix compounds, calibration techniques, the need for dependable and low maintenance functioning over long periods of time, sterilization (especially for clinical applications), reproducible fabrication of numerous sensors, the ability to manufacture the biosensor at a competitive price, disposable format, and a clearly defined market are some of the technical challenges facing the development of biosensors. There is no biosensor system available today that offers the same bacterial specificity as the plate culture approach, which is a critical requirement in today's market. Obviously, improving the specificity of biosensor systems and including all of the best properties into a single bacterial biosensor device is a difficult task. This is the primary reason for the delayed market penetration of biosensors.

### **-Supramolecular sensors**

Supramolecular chemistry has drawn inspiration from highly specific host-guest interactions found in nature over the last few decades, and as a result, supramolecular chemists are mimicking and exploiting such interactions in the design and development of supramolecular synthetic receptors and sensors.<sup>31,32</sup> Traditional sensing assays like the indicator spacer receptor approach (ISR) involving covalent connections between the signal unit and the binding site are rarely employed to provide productive results in a shorter amount of time with great selectivity, sensitivity, and application (Figure 5a). Researchers have developed innovative methods to get around this issue making use of a variety of non-covalent interactions.<sup>33,34</sup>

Indicator displacement assays (IDAs), a competitive sensing displacement assay in supramolecular analytical chemistry, are the most well-liked of the different contemporary sensing assays (Figure 5b).<sup>35</sup> In this displacement assay, the indicator binds to the receptor (host) reversibly and forms a supramolecular ensemble via intermolecular interactions such as H-bonding, electrostatic interactions, coordinate bonding, stacking interactions,

hydrophobic effect, and so on, depending on the solvent system and the appropriate geometry, charge, and hydrophobicity of an indicator.<sup>36–38</sup>

Following that, the addition of a competitive analyte (guest) causes the indicator to be displaced from the host, resulting in a modified optical response if the indicator binding affinity with the receptor is less than that of the analyte with the same receptor. The supramolecular ensembles created in the competitive IDA technique, either between the receptor and the chosen indicator or between the receptor and the target analyte, are kinetically reversible and correspond to the intended system's thermodynamic minimum via association and dissociation processes.<sup>39</sup> The IDA method has several advantages over traditional sensing techniques. First and foremost, this assay does not rely on synthesis and employs non-covalent/supramolecular linkages between the indicator and the receptor. Second, these supramolecular connections allow for the use of multiple indicators with the same receptor, allowing for the tuning of sensitivity or selectivity. Third, this well-known sensing approach works equally well in both aqueous and organic liquids.<sup>40</sup>

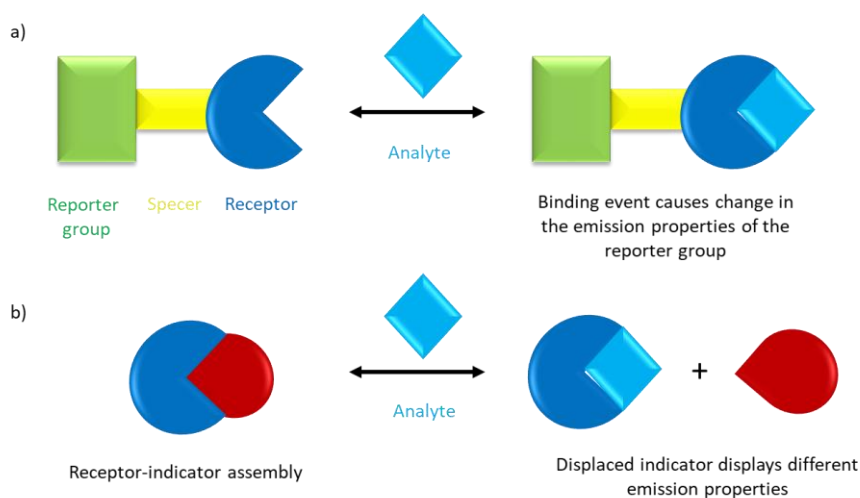


**Fig.5:** The working principles of luminescent sensors based on the receptor-spacer-reporter (ISR) approach (a) and the indicator displacement (IDA) approach (b).

Rotello et al.<sup>41</sup> in 2008, demonstrated that noncovalent conjugates of gold nanoparticles and poly(paraphenyleneethynylene) (PPE) successfully identify bacteria with high selectivity and within minutes. Interactions between nanoparticles and bacteria release the bound fluorescent polymer from the gold-nanoparticle quencher, allowing the polymer fluorescence to be activated. The identification of the different bacteria is made possible by the use of LDA (linear discriminant analysis), a quantitative statistical method used in pattern recognition.

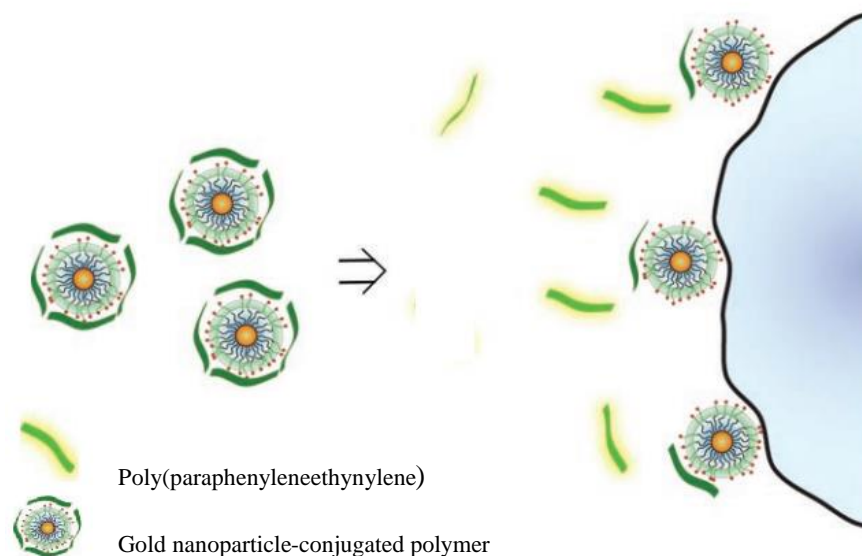


**Fig.6:** Schematic representation of the nanoparticle–conjugated polymer sensor array.<sup>41</sup>

As shown in Figure 6, cationic gold nanoparticles are initially linked to an anionic PPE in aqueous solution to produce complexes that quench fluorescence. The anionic PPE is released in the presence of bacteria, whose surfaces are always negatively charged. Fluorescence is thus restored as a result of the existence of free PPE after the addition of bacteria to the nanoparticle-PPE conjugate. In this work, p-conjugated polymer provides the molecular wire effect<sup>42</sup> and multivalency to assist in the efficient creation of signals during the sensing process. Functional patches (charged residues and hydrophobic regions) are common on the wall of cells and microorganisms hence this approach may be used to identify a variety of microorganisms. Using this method, they can also discern all twelve microorganisms, which contain both Gram-positive and Gram-negative species.

### 3.3 Calixarene-based ligands for biochemical application

Many calixarene-based compounds are being developed for biological purposes.<sup>43–47</sup> The unique conformational properties, functionality, low toxicity, and low cost make calixarene-based compounds a valuable candidate for biochemical application. One of the most important properties of calixarenes is their ability to spatially direct functional groups or other small ligating units in order to create desired interactions with biological components of interest (e.g., proteins, cell surfaces). Examples include calixarene-based glycoclusters for trypanocidal activity,<sup>48</sup> guanidinium functionalized calixarenes for antibacterial activity<sup>49,50</sup>,

and polyanionic calix[4]arenes or anti-HIV activity.<sup>51</sup> In our research group we have already investigated guanidinium-functionalised calixarenes (Figure 7, left) as potential cell transfection agents.<sup>52–55</sup> In these studies the upper-rim or lower-rim functionalized guanidino-calixarenes were first used to demonstrate their ability to interact with DNA and transfect cells. The lower-rim substituted guanidinium calixarenes are efficient cell transfection agents with reduced cytotoxicity compared to the upper-rim derivatives.

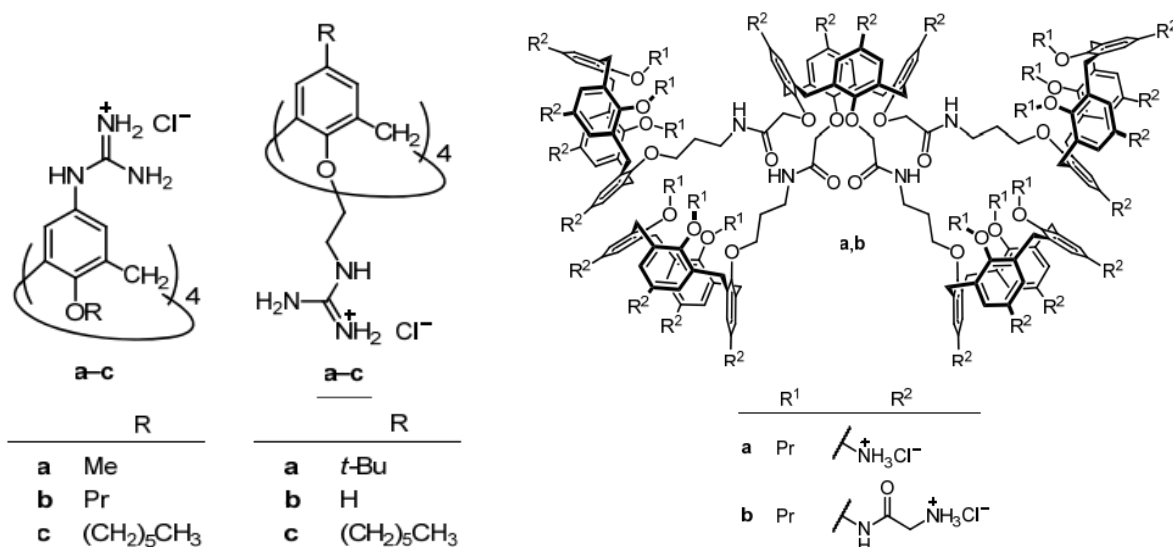


**Fig.7:** Guanidinium functionalized calixarenes and “multicalixarene” for biological application

Similar to this, Lalor et al.<sup>56</sup> proposed dendritic calixarenes with ammonium functionalization as possible gene delivery systems (Figure 7, right). These researchers discovered that the “multicalixarenes” bonded to DNA (by balancing the DNA negative charges) and were not hazardous to the human cells used in the study. More recently, Sansone et al demonstrated that calixarenes functionalised with arginine residues are extremely potent agents able to transfect several cell lines with DNA,<sup>57</sup> miRNA<sup>58</sup> and even artificial nucleic acids such as PNA.<sup>59</sup>

Calixarenes have been, however, also used for other biological applications. Kenek et al.<sup>60</sup> used carbohydrate-functionalized calix[4]arenes (glycocalixarenes) as natural killer cell stimulants to elicit a response to tumor cells.

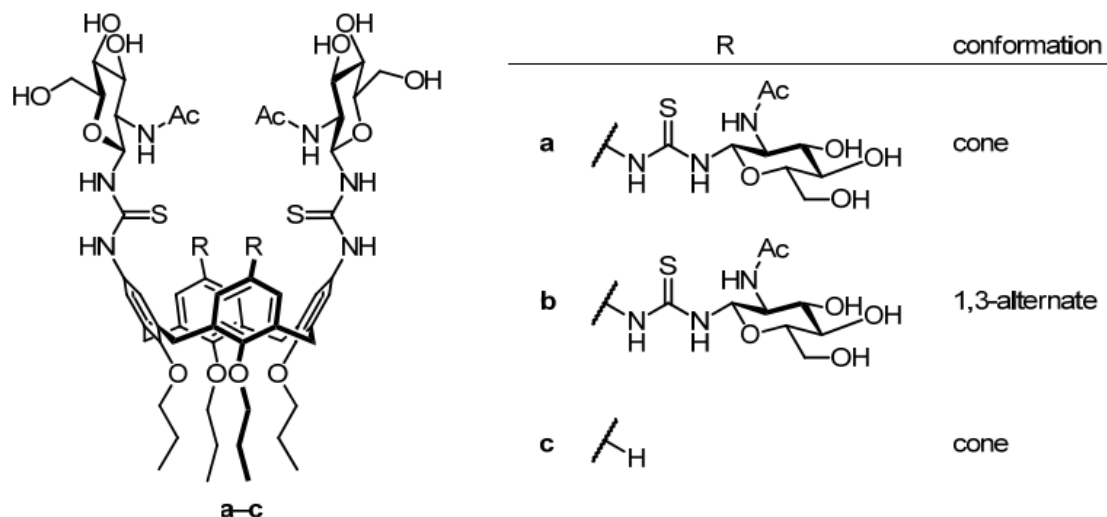


**Fig.8:** carbohydrate-functionalized calix[4]arenes for biological applications

The calixarenes in Figure 8, which were comparable to the dendritic octaglycan previously studied by the authors,<sup>61</sup> performed better than the monomeric sugar unit detached from the macrocycle. The tetrasubstituted calix[4]arene performed better than the 1,3-alternate conformer and the bis-substituted. Thus, carbohydrate multivalency seems to play an important role in the binding to natural killer cells.

Guo et al.<sup>62</sup> studied the potential biosensor properties of a variety of sulfonate-functionalized calixarenes (Figure 9) towards acetylcholine. The authors selected to use commercially available tetrasulfonato calixarenes and a fluorescent dye, lucigenin, in an Indicator Displacement Assay.

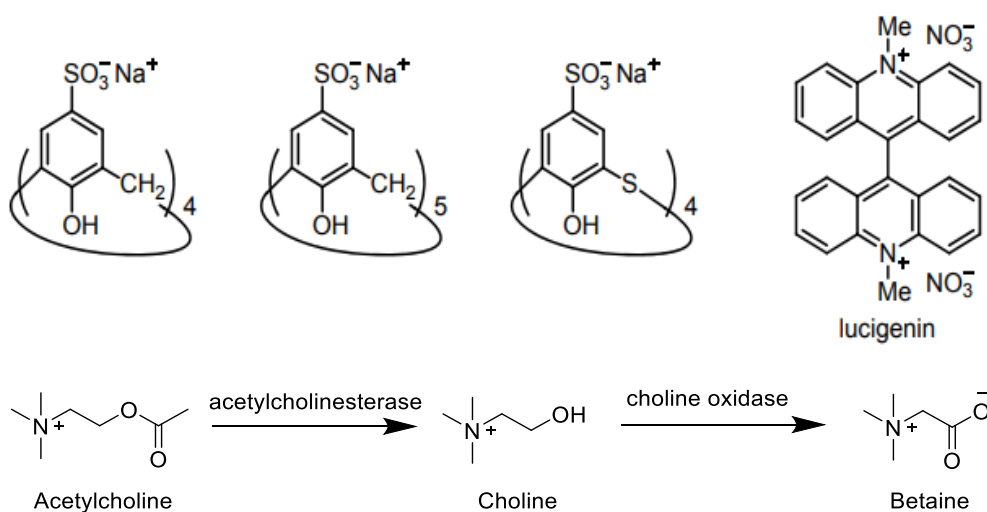


**Fig. 9:** calixarenes investigated as potential sensors with fluorescence probe, lucigenin (up), the acetylcholine hydrolysis of acetylcholine to choline followed by oxidation to betaine (down)



When a strong competitor, like acetylcholine, is present, the dye is displaced from the calixarenes cavity, resulting in a luminous reaction, while no displacement and hence no fluorescence raised from the samples when choline was transformed to the weaker binding betaine. The authors claimed that such a molecule may be used to monitor acetylcholinesterase (an enzyme implicated in Alzheimer's disease) during Alzheimer's dementia therapy.

### 3.4 Zwitterionic calix[4]arene ligands

A zwitterion (or inner salt, formerly dipolar ion) is a molecule, macromolecule or a peptide with the same number of cationic and anionic functional groups. Zwitterions have been used in a wide range of topologies intended for biological purposes (Figure 10). Zwitterionic inner salts as protein chaperones and stabilizers,<sup>63</sup> zwitterionic polymer-protein conjugates,<sup>64</sup> zwitterion-conjugated surfaces,<sup>65</sup> zwitterionic nanoparticles,<sup>66</sup> hydrogels,<sup>67</sup> and liposomes are some of these architectures.<sup>68</sup>

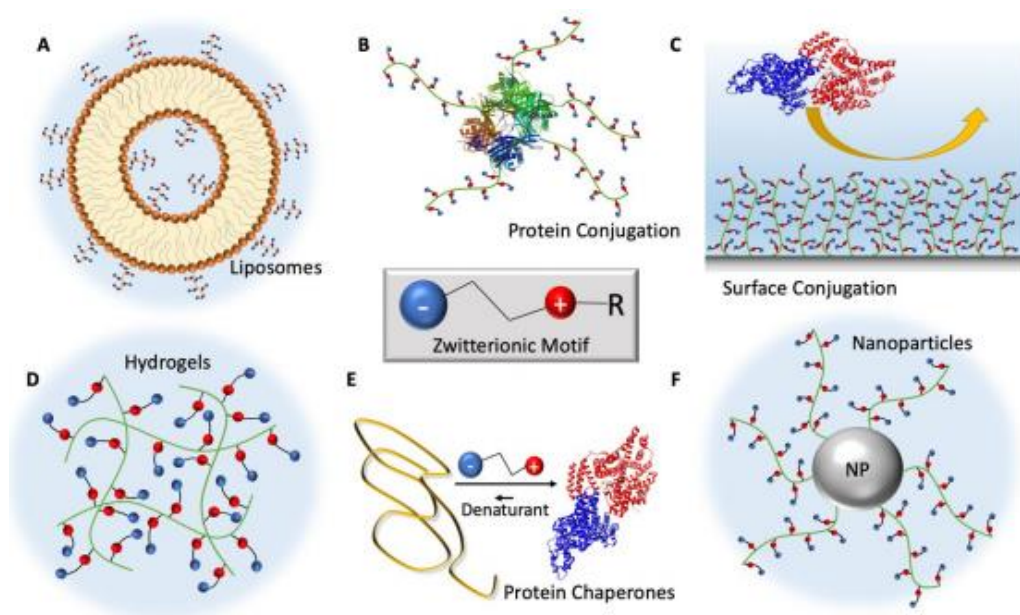


**Fig.10:** Schematic representation of different architectures in which zwitterionic moieties have been applied in biological systems. These include liposomes (a), zwitterionic polymer–protein conjugates (b), zwitterion-conjugated surfaces (c), hydrogels (d), zwitterionic inner salts as protein chaperones and stabilizers (e), and zwitterionic nanoparticles (f).<sup>63</sup>

In literature are present numerous examples that involved functionalised calixarene with positive or negative charged residues, but the employment of calixarene bearing zwitterionic groups is not common.

In 2018 Mocerino et al.<sup>69</sup> described the proline-functionalised calix[4]arene that operates as a hydrogelator, but only in the presence of particular anions, with the gel characteristics fine-tuned by altering the associated cation. Furthermore, the gels are stable throughout a pH range of 0-7 and may be dismantled reversibly by raising the pH above 7. The proline functionalised calixarene is significantly water soluble (up to 500 g/L).

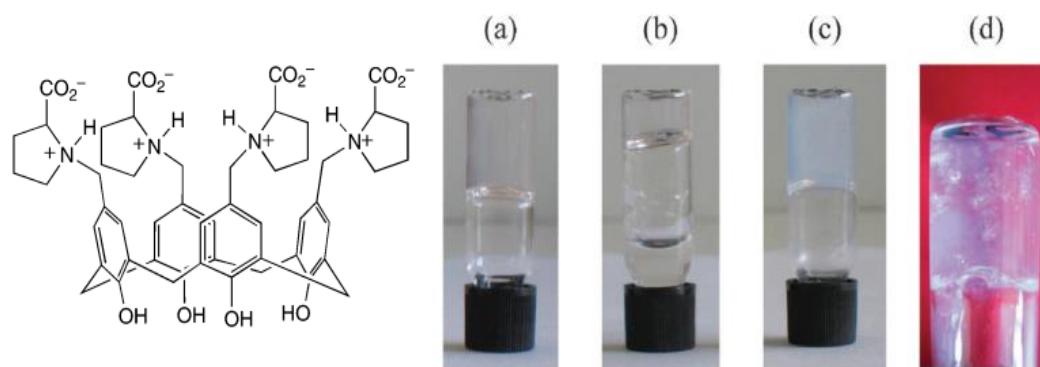


**Fig 11:** Gel formation of 0.2 M of proline-functionalised calix[4]arene solutions, and salts. (a) LiCl, 1.26 M, stable gel, (b) NaCl, 1.26 mol M, incomplete gel, (c) La(NO<sub>3</sub>)<sub>3</sub>, 0.01 M, stable translucent gel, and (d) NaI, 0.10 M, transient gel.<sup>69</sup>

Zhang et al.<sup>70</sup> demonstrated that proline-functionalised calix[4]arene, in the presence of basic amino acids, will also form hydrogels in neutral to acidic conditions. The results reveal that distinct amino acids result in different distinct hydrogel backbones (Figure 12), which could be detected using a combination of atomic force microscopy, transmission electron microscopy, and scanning electron microscopy. Furthermore, all the generated low molecular weight hydrogels are thermoreversible, with the gel-to-sol transition temperature ( $T_{gel}$ ) dependent on calixarene concentration, giving these hydrogels the capacity to entrap and release model dye molecules.

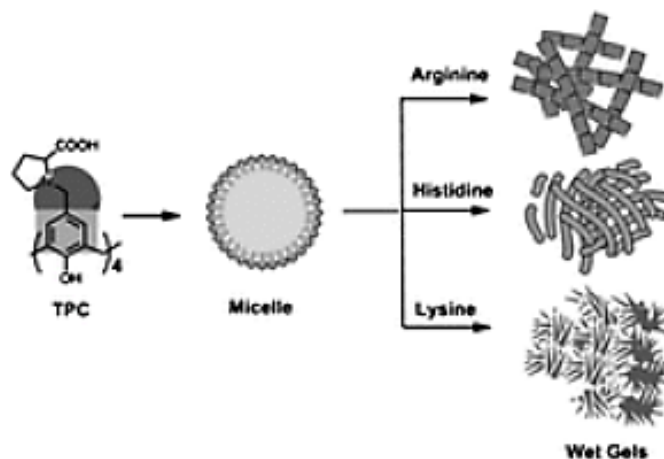


**Fig 12:** Schematic illustration of gel generation from proline-functionalised calix[4]arene induced by basic amino acids.<sup>70</sup>

Recently Yilmaz et al.<sup>71</sup> studied the synthesis of upper rim- and lower rim-functionalized L-proline-based calix[4]arene derivatives and the assessment of their cytotoxic ability for human cancerous cells.

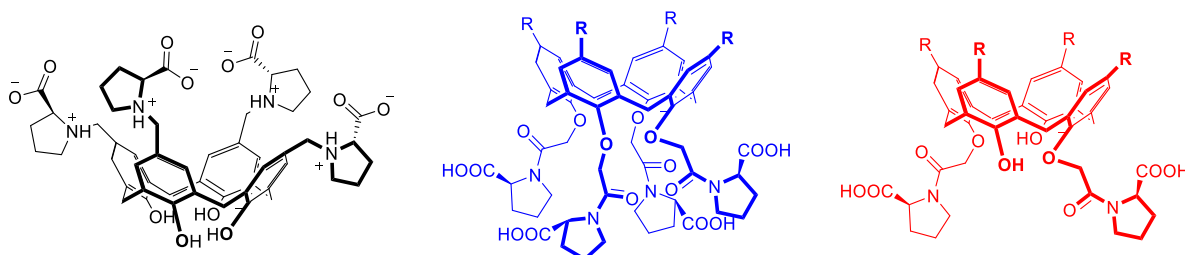


**Fig.13:** The structure of L-proline based calix[4]arene derivatives in Yilmaz study

The lower rim L-proline derivative (blue in Figure 13) was shown to be the most toxic for human CRC (DLD-1) and lung cancer (A549) cells. In addition, several substances demonstrated dose-dependent proliferation of various human malignant cells, including liver, prostate, lung, and colorectal carcinomas.

In 2016, Mocerino et al.<sup>72</sup>, demonstrated that chiral proline-modified calix[4]arenes prevent the assembly of the human papillomavirus 16 L1 pentamer. The effect of L- and D-Proline modified calix[4]arenes (Figure 14) on the assembly of HPV 16 L1 pentamer (L1-p) was examined in this study. Matrix-Assisted Laser Desorption/Ionization, Time of Flight Mass Spectrometry (MALDI-TOF-MS) and Nuclear Magnetic Resonance (NMR) were used to explore the mechanism of action using model peptides, which demonstrated that the binding was targeting the basic residues at the L1 interface. The trypsin digestion studies and

molecular simulations performed on the full-length L1 pentamer confirmed this. The substantial differences in energy and shape reported by molecular simulations explain the binding disparity of L- and D- Proline modified calix[4]arenes to L1 pentamer, and thus their selective suppression of L1-p production.

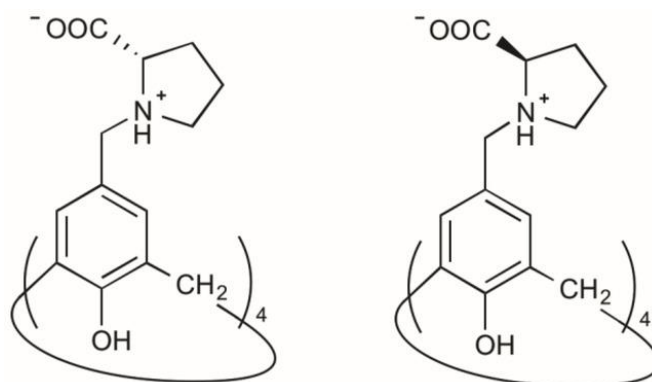


**Fig.14:** Structure of the L- and D- Proline modified calix[4]arenes derivative in Mocerino study [72]

L- and D-Proline modified calix[4]arenes indeed binds to the positively charged residues (Arg and Lys) and therefore protects it from trypsin degradation when allowed to interact with glutathione S-transferase fused L1 (GST-L1). In addition, the comparison of grey values in SDS-PAGE pages indicated that L- Proline calix[4]arene provided a better protection than D- Proline calix[4]arene, which can be attributed to the enantiomeric differences in binding to GST-L1.

The current discovery opens the way for the development of enantioselective and cost-effective inhibitors as novel anti-HPV drugs, which might then be expanded to other viruses using the same chemical mechanism.

### 3.5 Attachment of amino acids to calix[4]arenes by Mannich reaction

Different strategies have been used to obtain amino acid functionalised calixarene but only a few of these allow the amino acid to retain its zwitterionic character. The two classical approaches often used for attach an amino acid to a calixarene scaffold are: the N-linked and the C-linked approach. Using these two approaches will result in the formation of a new amide bond between calixarene and amino acid. The C-linked approach utilises an appropriately functionalised calixarene at the upper edge with amino groups that will then be exploited in

the formation of the amide bond with the amino acids carboxyl groups. Vice versa the N-linked approach differs in that the new amide bond is formed from the carboxylic group on the calixarenic scaffold and the amino group of the amino acid.

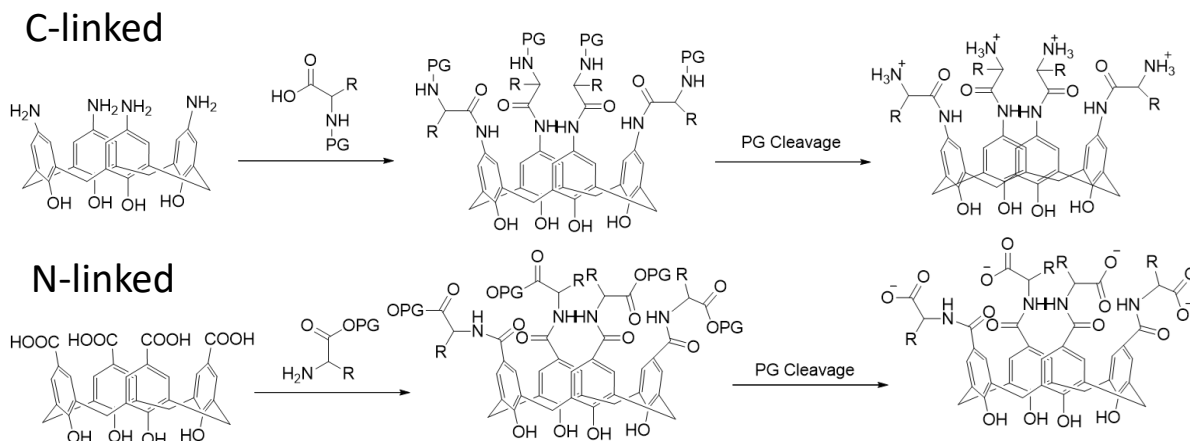


**Fig.15:** Schematic representation of the N-linked and C-linked approach

Amines and amino acids can be connected to the upper rim of calixarenes through a methylene group in cases when an amide is not desired. General approaches include the Mannich reaction and halomethylation followed by a nucleophilic substitution of the halide at the upper rim of calixarenes.<sup>73</sup> Functionalization of calixarenes at the upper-rim has been achieved via halomethylation and nucleophilic substitution. Yang et al<sup>73</sup>. studied the nucleophilic replacement of bromomethylated calix[4]arene by a number of nucleophiles including minor alcohols (e.g. MeOH), thiols (e.g. PhSH), and carboxylic acids (e.g. AcOH).

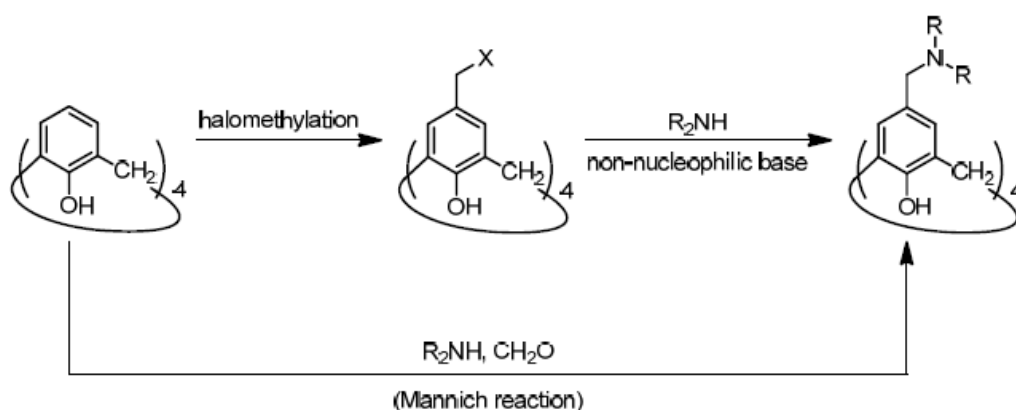


**Fig.16:** General scheme for attaching amino acids to calixarenes via methylene linkage.

This method required two different step and several purifications of the products using chromatography and sometimes the yield of the entire process is low. Another convenient

method to obtain amino functionalized zwitterionic calixarenes is through the Mannich<sup>74,75</sup> reaction. The Mannich reaction occurs when a C-H activated molecule (such as phenol or ketone), a primary or secondary amine, and a non-enolizable aldehyde react together. The Mannich reaction is not restricted to amines. Agababyan et al.<sup>76</sup> shown that amino acids may be employed as the amine component in a variety of Mannich reaction. In the past, calixarenes and secondary amines were used to create Mannich bases (Figure 17) by Gutsche and Nam.<sup>77</sup> This approach was expanded to functionalized calixarenes with substances based on the piperazine ring.<sup>78,79</sup>

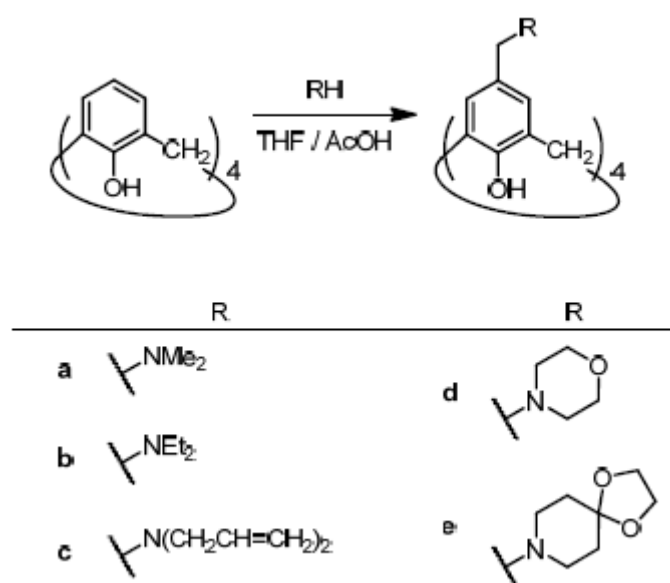


**Fig.17:** Selected calix[4]arene Mannich bases prepared by Gutsche and Nam.

Additionally, Gutsche and Nam discovered that by quaternarization of the Mannich adducts in Figure 17 with methyl iodide (without alkylating the phenols), it was possible to substitute the ammonium moiety by a nucleophile (passing through a p-quinonemethide as intermediate). A Mannich reaction may easily functionalize calix[4]arenes at the upper-rim in a single step when they lack substituents at the position para to the phenol. Ogden et al.<sup>80</sup> attached proline to the calix[4]arene by the Mannich reaction in good yield. In order to evaluate how macrocycle size and as a consequence, the spatial arrangement of the proline moieties influenced the self-assembly properties of such motifs calix[5]arene and calix[6]arene scaffolds was also tested.<sup>81</sup> While using calix[5]arene scaffold, the reaction resulted in the product being obtained, even if in lower yields than the calix[4]arene, with the calix[6]arene, under the same conditions, the product was not formed. This was suspected to

be a result of the lower solubility of the partially substituted calix[6]arene in the tetrahydrofuran-water solvent system. The dipropoxy calix[4]arene in Figure 18 was also subjected to the Mannich reaction with proline in an effort to selectively functionalize calix[4]arene with proline moieties, but this failed to give any products; the starting material was recovered.<sup>82</sup>

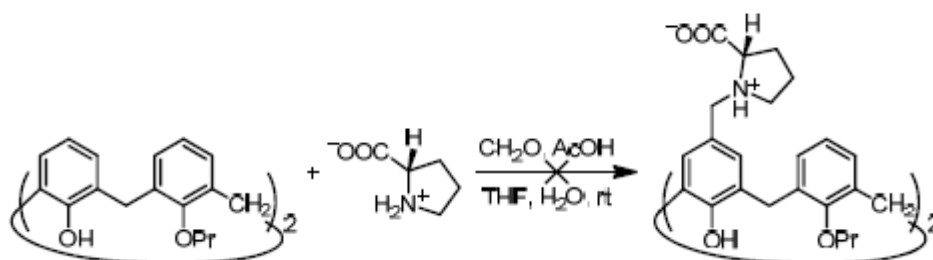


**Fig.18:** Mannich reaction on 1,3-dipropoxycalix[4]arene

This suggested that for the Mannich reaction to occur efficiently, the para Ar-H needed to be activated by the hydrogen bonding between nearby phenolic molecules. This is in line with Gutsche theory<sup>83</sup>, which postulated that under Mannich conditions, the higher acidity of the free phenol calixarenes led to a higher reactivity of the para aromatic position.

### 3.6 Saturation transfer difference (STD) NMR to study molecular interactions

NMR spectroscopy is a unique tool for studying molecular interactions in solution, and it has become a crucial technique for characterizing molecular recognition events and obtaining information on the interactions of small ligands with physiologically relevant macromolecules<sup>84</sup> (proteins or nucleic acids). Ligand-based NMR screening and NMR determination of a ligand binding conformation are critical tools in the rational drug-discovery process. For many years, the saturation transfers difference NMR (STD-NMR) experiment has been utilized to describe ligand-receptor complexes. The Nuclear Overhauser Effect (NOE) and the measurement of ligand resonance signals are at the heart of the STD-NMR experiment. It can be used as a screening strategy, to discover lead structures, or to find ligand moieties critical for binding. In the STD-NMR literature, the term binding epitope is widely used to define the hydrogens of the ligand that are closest to the protein following binding.<sup>85</sup> The STD-NMR experiment relies on the fact that, for a weak-binding ligand (dissociation constant,  $K_D$ , ranging from  $10^{-8}$  mol L<sup>-1</sup> to  $10^{-3}$  mol L<sup>-1</sup>), there is exchange

between the bound and the free ligand state. An STD experiment implies subtracting a spectrum in which the protein was selectively saturated (on-resonance spectrum obtained by irradiating at a region of the spectrum that contains only resonances of the receptor/protein such as 0 ppm to 1 ppm) with signal intensities  $I_{SAT}$  from one without protein saturation (off-resonance spectrum) with signal intensities  $I_0$ . Only the signals of the ligand(s) that got saturation transfer from the protein (through spin diffusion and/or nuclear Overhauser effect<sup>86</sup>) appear in the difference spectrum ( $I_{STD} = I_0 - I_{SAT}$ ).

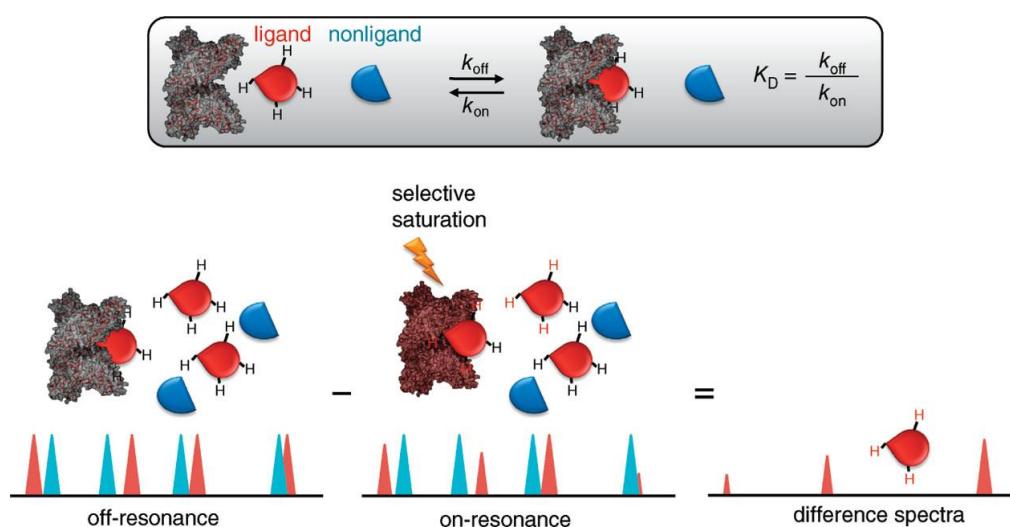


**Fig. 19:** The STD-NMR experiment scheme. Intermolecular transfer of magnetization from the receptor to the bound small molecule is enabled by the interchange of free and bound ligand.<sup>87</sup>

Other substances that could be present but do not bind to the receptor will not experience saturation transfer; their signals will be equally strong on the on-resonance and off-resonance spectra as a result, and after subtraction, no signals from the nonbinding small molecule will show up in the difference spectrum. It is possible to quantify the difference in intensity brought on by saturation transfer ( $I_{STD} = I_0 - I_{SAT}$ ), which serves as a sign of binding. Only the signals of the hydrogen atoms that are in close contact with the protein ( $\leq 5 \text{ \AA}$ ) and receive magnetization transfer will show up in the difference spectrum for a molecule that binds to the receptor. Of those, the hydrogen atoms closest to the protein will have stronger signals due to a more effective saturation transfer. The last 10 years have seen considerable use of STD NMR spectroscopy to investigate receptor-ligand interactions.<sup>88–93</sup> By utilizing samples containing platelets or entire cells and liquid state NMR spectroscopy, this method has also been utilized to analyse molecular recognition events involving membrane receptors and their



ligands.<sup>94,95</sup> This approach allowed the fundamental issues caused by the tremendous difficulty of isolating and keeping individual membrane receptors in solution with the right folding and the necessary functioning to be solved, at least in some specific circumstances. However, cells generated from solid tissues have a significant propensity to aggregate, making it difficult or impossible to use STD NMR investigations on them. In fact, these cells are only in suspension for a short period of time, which results in the capture of extremely poor STD spectra. In light of these considerations, Nicotra et al.<sup>96</sup> in 2011 develop a robust NMR methodology to study the interaction between cell membrane proteins and ligands by directly employing whole, vital cells. They considered it would be crucial to have access to a technique unaffected by limitations associated with the original tissue characteristics. As a result, the use of high-resolution magic angle spinning (HR-MAS) NMR methods with rotation at a relatively high speed has been investigated. This approach aims to keep the cells in the sample "active window."

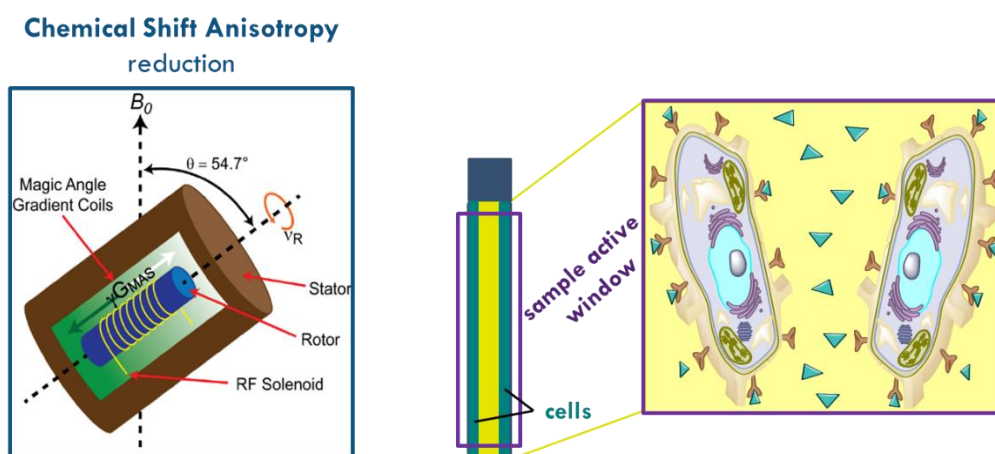


**Fig.20:** Schematic representation of HR-MAS STD experiment. Due to the centrifugal force, cells distribute along the internal walls of the MAS rotor and remain in the sample active window.<sup>96</sup>

Indeed, when a regular liquid state NMR probe is used, cells tend to settle to the bottom of the NMR tube instead of dispersing along the internal walls of the MAS rotor and forming a homogeneous layer that is visible through visual inspection of the rotor insert after spectrum acquisition and replicates cell disposition on tissue surface<sup>97</sup>. The rotor walls, in contrast to the tube bottom, fit inside the detecting zone of an HR-MAS probe. As a result, every ligand that dissociates from its receptor is immediately detectable in the rotor cell-free central core. When a sample is placed in a tube, the ligand must diffuse from the bottom of the tube, where the pellet settles, to the "active window."

### 3.7 Aim of this work

Antimicrobial resistance (AMR) is one of the major threats of the last century. The availability of fast, economical, and selective methods for the identification of bacterial strains is therefore a topic of great interest since it will rapidly allow a timely selection of the most appropriate antibiotic class to treat the patient. The aim of this project is to create chemical tools that are stimuli-responsive and intelligent, allowing for the quick identification of bacterial species *in vitro* through the molecular identification of whole bacterial cells and/or small molecules (microbial metabolites) produced by bacteria under normal and pathological circumstances.

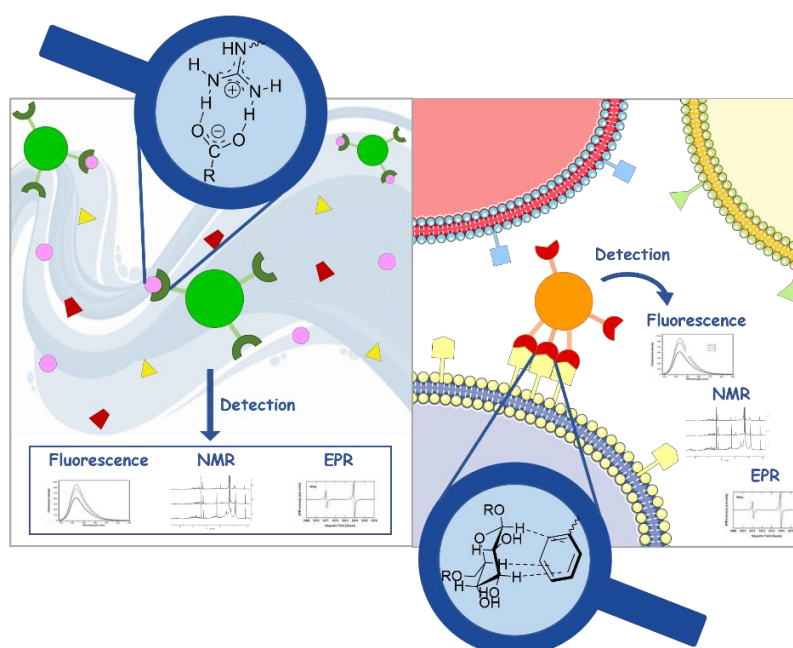
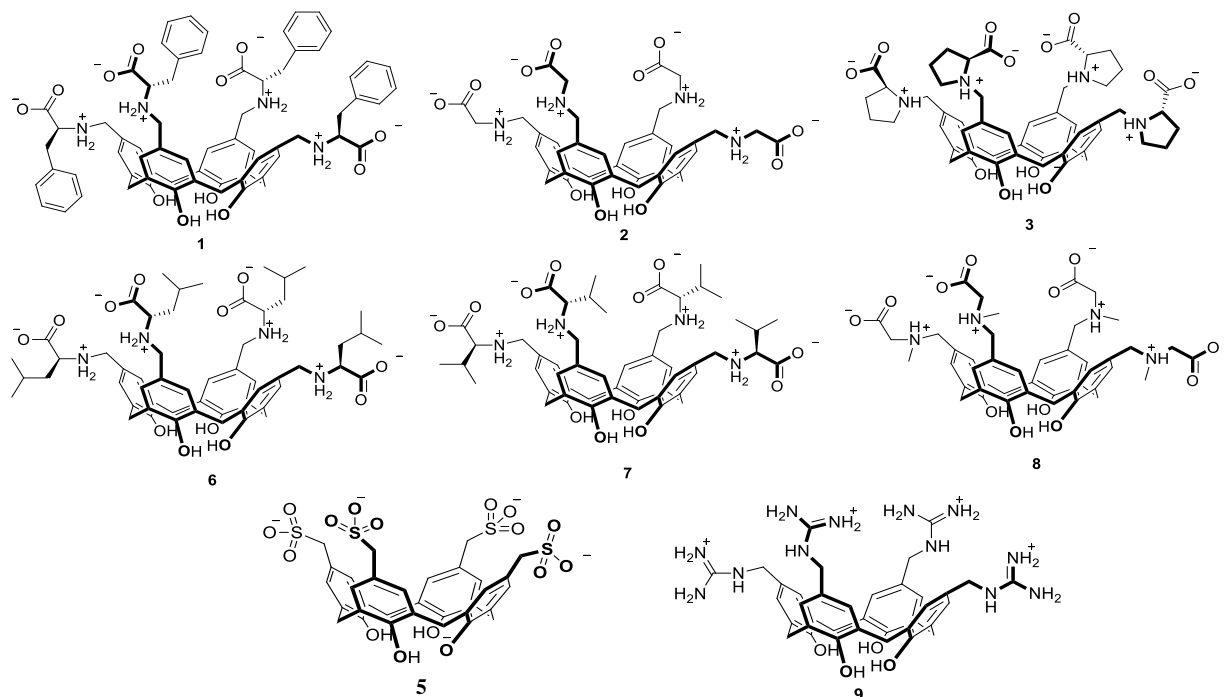


**Fig.21:** Representation of nanosensor for the detection of bacteria metabolite (left) and of bacteria cell wall (right)

Recognition of the target relies on molecular receptors, such as calix[n]arenes. Interactions established between receptor and analyte may include electrostatic interactions, hydrogen bonds, hydrophobic effects, dispersive forces, and generally all the necessary non-covalent interactions typical of supramolecular chemistry. Each nanosensor must, through appropriate functionalization and as a result of interaction with the target, cause a signal modulation so that the analyte can be detected by the chosen technique. Advanced NMR techniques, such as NMR chemosensing, STD-NMR, EPR techniques and fluorescent indicator displacement assays (IDA) will be used to screen the different nanostructures, and to select the most promising ones for further development.

With the aim of testing different family of calix[4]arenes ligand for the bacteria wall targeting we decided to synthesize the calixarenes shown in Scheme 1. These ligands were selected and designed with the aim of testing different interacting groups and different charged calix[4]arenes.



**Scheme 1:** Structure of the ligands studied in this chapter for bacteria wall recognition

The different bacterial classes differ in their cell wall composition. These molecular patterns are different for the different class of bacteria and the ligands have been functionalized with different functional group and different charges.

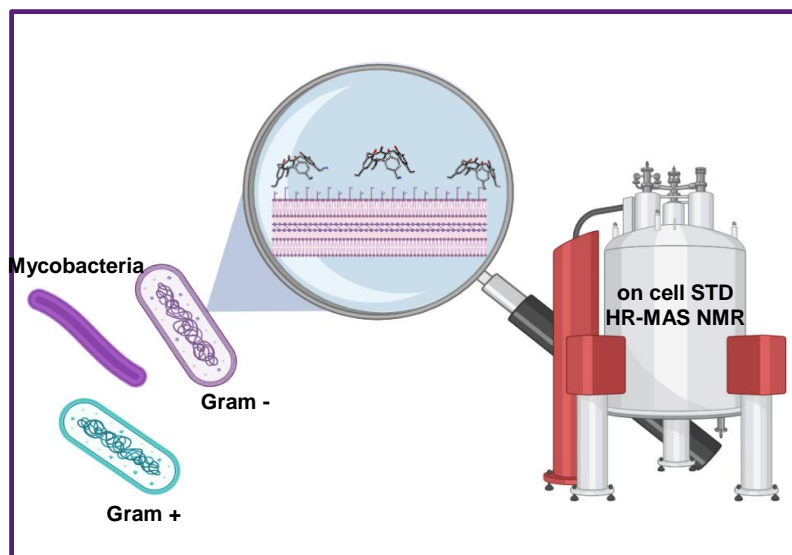


**Fig.22:** Schematic representation of the aim of this work.<sup>96</sup>

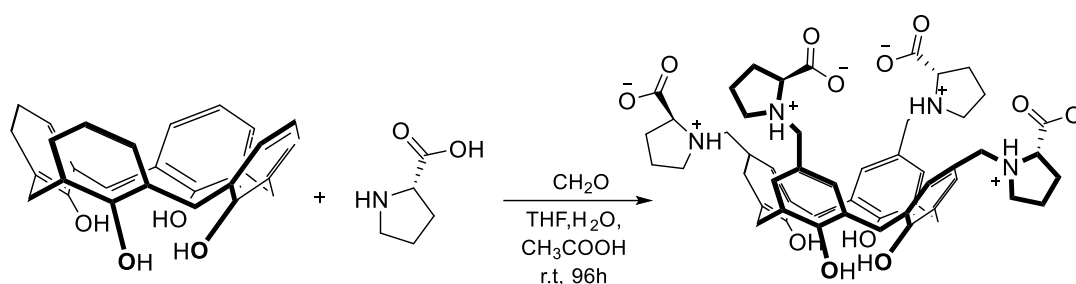
The screening of the recognition properties of these calixarenes towards different bacteria strains were studied using on-cell STD NMR experiments by professor Airoidi group from University Milano Bicocca.



# Results and Discussion

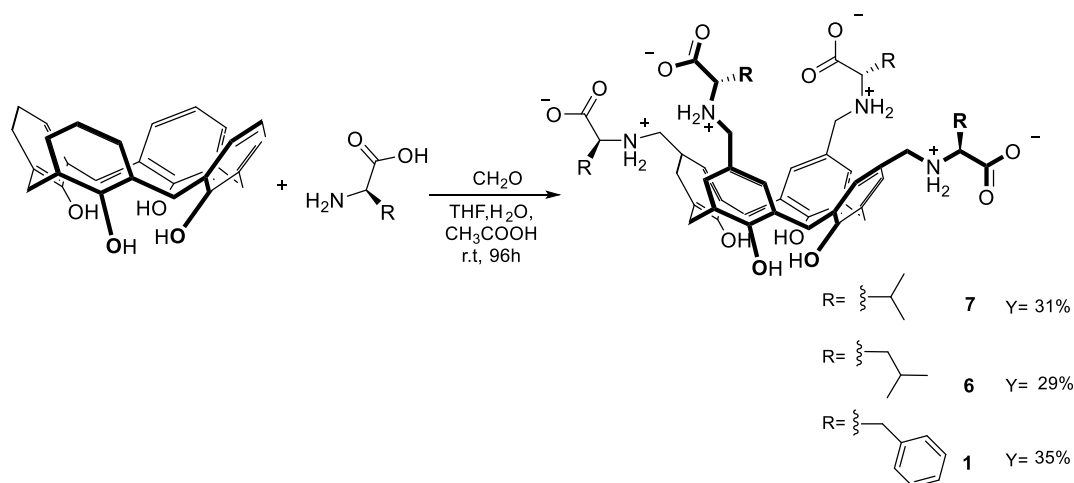
## 3.8 Synthesis

The guanidino derivatives **9** and the methylsulfonato derivative **5** were already available in our laboratory since previously synthesised by a master degree student,<sup>98</sup> while **3** was synthesized as reported in the literature.<sup>99</sup>



**Scheme 1:** Synthetic strategy for the synthesis of compound **3**

Proline is added to the upper rim of calix[4]arene in a single step by reaction with formaldehyde in acetic acid and secondary amine. The reaction was monitored via ESI-MS until the signals related to partial functionalization intermediates disappear. After 96h the predominant signal was that related to the molecular ion of **3** and its sodium adduct. The solution was then concentrated under reduced pressure, and the precipitate formed was filtered and triturated with acetone. The pure product is obtained after recrystallization in an ethanol/water/acetone mixture (1:1:2). Calix[4]arene **3** has also a very high solubility in water which was estimated to be approximately 0.5 g/mL. Since the Mannich reaction provided a relatively easy access to amino acid functionalized calix[4]arenes, other amino acids were investigated. Following this same synthetic procedure, we were able to synthesize also derivative **1**, **6** and **7**.



**Scheme 2:** Synthesis of compounds **1**, **6** and **7**

Again, the reaction was monitored by ESI-MS analysis of the crude reaction mixture. In the case of compound **1** after 96h it is still possible to see from the ESI-MS analysis (Figure 1) the presence of the di- and tri-substituted intermediate even after several additions of the reagents. The reaction mixture was then concentrated under reduced pressure. The solid formed was filtered and washed with water to remove traces of acetic acid and the unreacted amino acid. Calix[4]arene **1** is then obtained pure after trituration in THF and then methanol with a 35% yield.

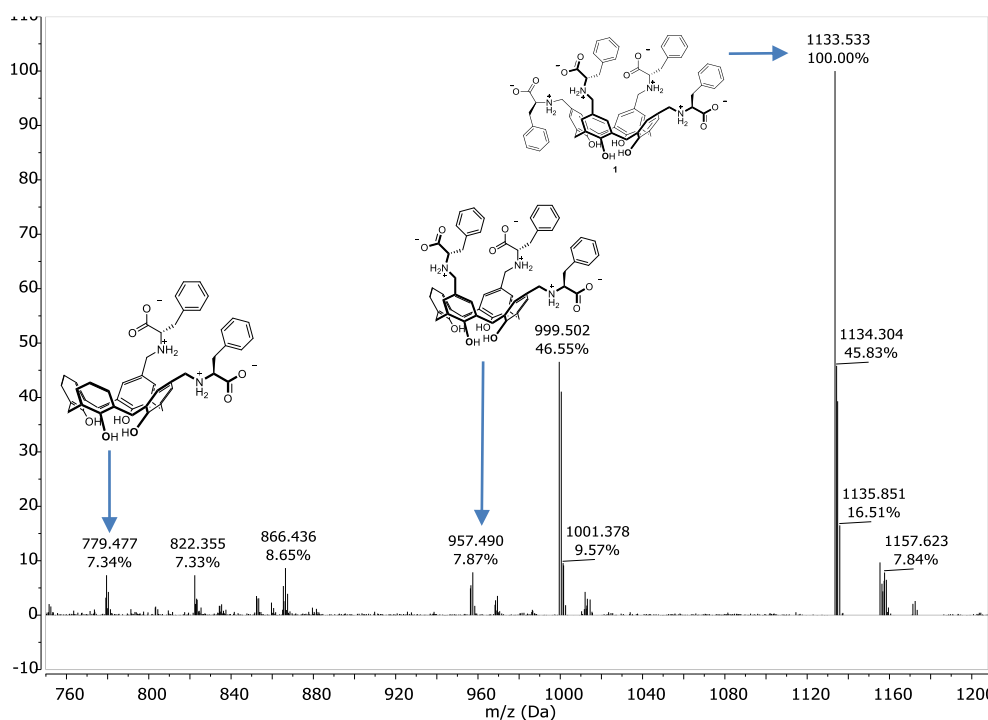


**Fig. 1:** ESI-MS spectrum after 96h of the reaction mixture to obtain **1**. The analysis confirms the presence of the product **1** and its intermediates.

In the case of compounds **6** and **7**, however, ESI-MS analysis performed on the crude after 96h still shows the presence of intermediates (Figure 2 and 3). As also in the case of **1**, the presence of several unknown species with molecular weights similar to the intermediates, probably formed due to some secondary reaction, was also noted. From ESI-MS analyses conducted on successive reactions, it was found that the intensity of signals related to these by-products increases with increasing reaction times. Then after 96h the suspended solid was filtered and washed with water to remove traces of acid. Compound **6** was triturated in methanol to remove unreacted leucine and finally with THF in an attempt to solubilize any traces of intermediates. The product was then obtained pure in 29% yield. Compound **7** also precipitates from the reaction environment and this precipitate was filtered and washed with water. The resulting solid was then triturated in methanol and then acetone and obtained pure with a yield of 31%.

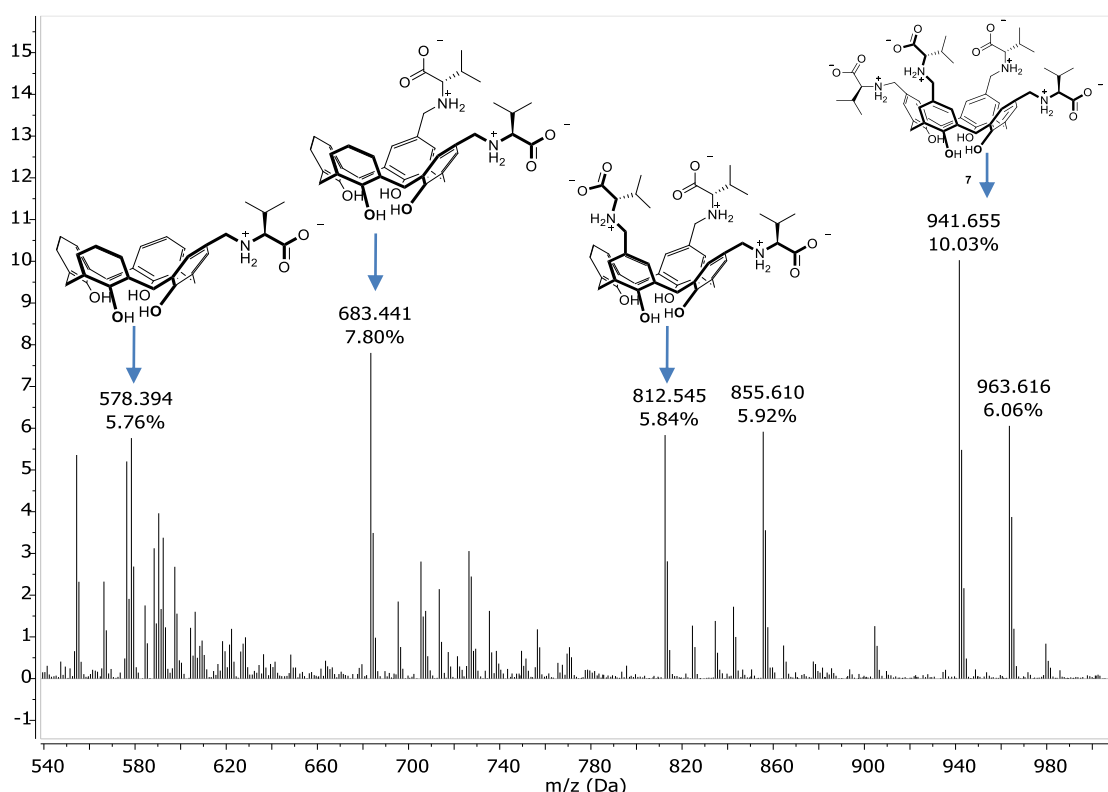


**Fig. 2:** ESI-MS spectrum after 96h of the reaction mixture to obtain **7**. The analysis confirms the presence of the product **7** and the partially functionalised intermediates.

Unlike **3**, these three derivatives are sparingly soluble in water. This is probably due to the greater hydrophobic character of valine, leucine and phenylalanine compared to proline. To



analyze by ESI-MS the crude reaction samples are solubilized by addition of 1M NaOH solution until the suspended solid is completely soluble and then diluted with methanol. Compounds **1**, **6**, and **7** were fully characterised by 1D  $^1\text{H}$  and  $^{13}\text{C}$  NMR, 2D (COSY, HSQC) and ESI mass spectrometry. Stacked  $^1\text{H}$ -NMR spectra of compounds **1**, **6** and **7** are shown in Figure 4. Due to their poor solubility in neat water, these compounds were characterised as sodium salts after the addition of a 20  $\mu\text{L}$  of a solution of NaOD in  $\text{D}_2\text{O}$  (40 %w/v) to a suspension of these compounds in  $\text{D}_2\text{O}$ . The addition of the base allowed complete solubilisation of what was the insoluble residue at neutral pH. At this pH the four carboxylic moieties and at least one phenol ring of this compounds are deprotonated improving the solubility in water.

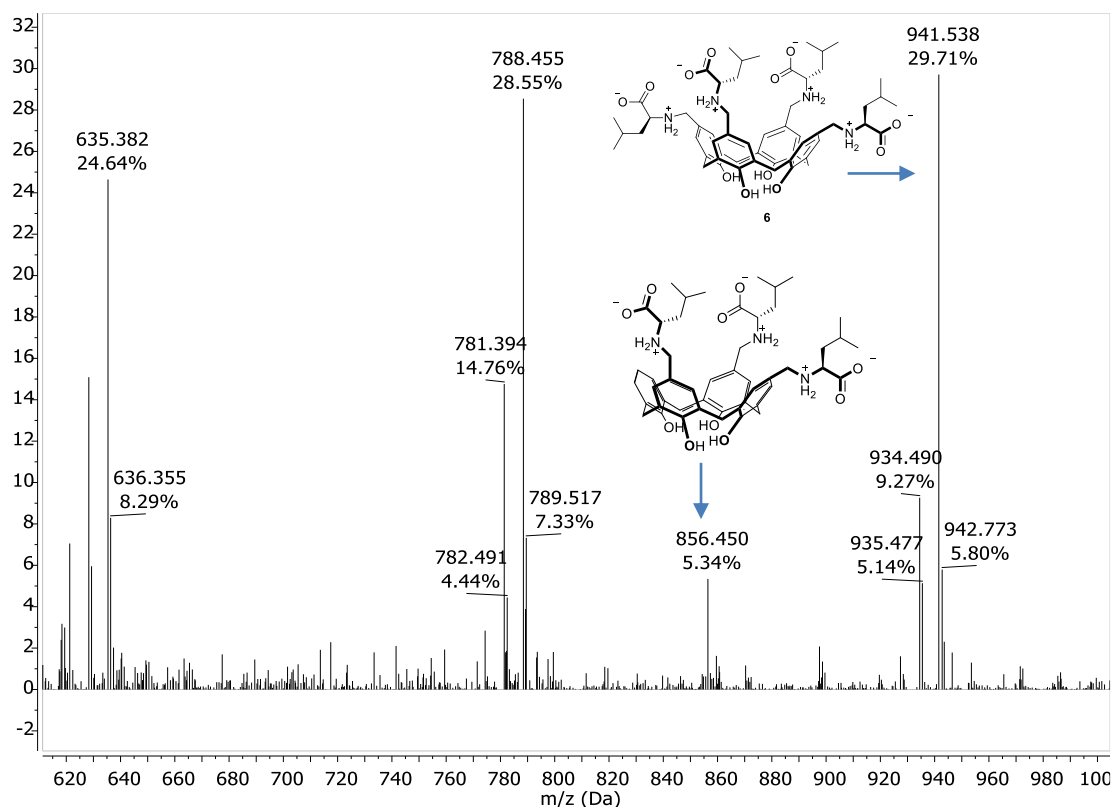


**Fig. 3:** ESI-MS spectrum after 96h of the reaction mixture to obtain **6**. The analysis confirms the presence of the product **6**, some intermediated and by-products.

The  $^1\text{H}$ -NMR spectra of **6** and **7** are obviously very similar since leucine has only one additional methylene group in its side chain compared with valine. In fact, as can be seen from the NMR spectrum, the signal related to the proton bound to the chiral carbon of the amino acids at about 2.6 ppm changes from doublet in valine to triplet in leucine.

Furthermore, the presence of a unique enlarged singlet signal related to the aromatic protons of calix[4]arene at about 6.9 ppm confirms that only the tetra functionalized product was obtained.

In all three spectra it is possible to observe the two broadened signals related to the protons of the axial methylene bridges of calixarene at about 4.2 ppm and those related to the equatorial protons at about 3.2 ppm overlapped by the signal of newly formed methylene between the calix[4]arene and the amino acids. In the spectrum of **1**, it can be seen that the signals relating to the aromatic protons of phenylalanine are broadened and overlap with the calixarene signal. By analysing the integral of the aromatics proton and normalising the signal relating to the benzyl CH<sub>2</sub> of phenylalanine it was possible to confirmed the obtainment of the product.

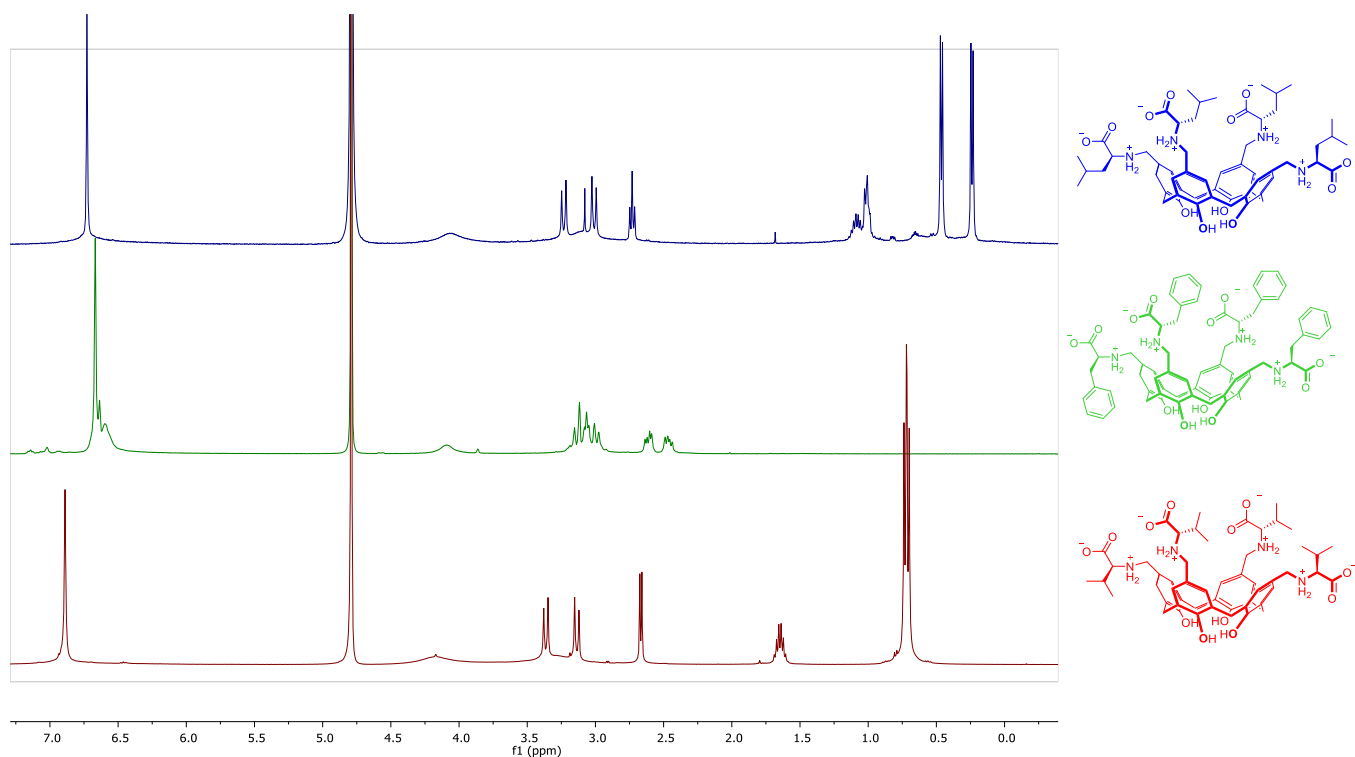
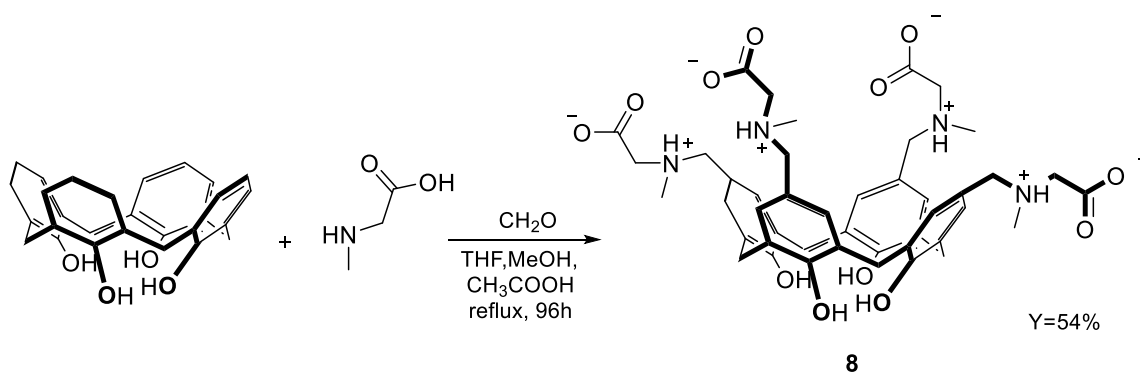


**Fig. 4:** Stacked <sup>1</sup>H-NMR (450 μL D<sub>2</sub>O+20 μL NaOD, 400MHz, 25°C) of compounds **7** (red), **6** (blue) and **1** (green)

The presence of only a signal for the Ar-CH<sub>2</sub>-Ar carbon atoms, in the <sup>13</sup>C-NMR spectra of these compound, around 31 ppm indicate that these calix[4]arenes derivative are in cone conformation at room temperature<sup>100</sup> (calix[4]arenes in the partial cone or 1,3-alternate conformations have <sup>13</sup>C chemical shifts at ~37 ppm). Indeed, this chemical shift is compatible also with a calixarene structure rapidly interconverting between the two inverted cone

conformations, as is indeed expected. Cone conformation is certainly preferred because of the presence of an array of H-bonds between the phenolic OH groups and the deprotonate phenoxide O<sup>-</sup> atom which is known to be present already from pH > 4. In fact, it is was determined that the first deprotonation constant K<sub>a</sub> in calix[4]arenes might be as low as 10<sup>-3.3</sup> M.<sup>101</sup>

In an attempt to obtain highly water-soluble calix[4]arenes derivatives, the classical procedure was also applied to amino acids with polar side groups such as tyrosine, lysine, aspartic acid and glutamic acid. Unfortunately, using these amino acids, the reaction does not lead to the formation of the desired product, as also confirmed by the ESI-MS analysis, and at the end of the process only the starting reagents are recovered.



**Scheme 3:** Synthesis of compound **8**

This is probably due to the higher polarity of these amino acids which makes them less soluble in the reaction solvent. The procedure reported in the literature was then varied but the reaction did not lead to the desired products even when changing the solvent mixture of the reaction to more polar solvents such as DMF or 1,4-dioxane or heating the reactions to reflux. Supposing that the higher water solubility (and higher yields) of **3** compared to **1**, **6** and **7** might be related to the presence of a tertiary amine in the structure, we also tested the reaction with sarcosine (N-methylglycine), that possesses, as proline, a secondary amine in place of the primary amine of phenylalanine, valine and leucine. An effort to synthesize the sarcosine functionalized calix[4]arene **8** using the same chemical conditions as for **3** (Scheme 1 and 2) failed to produce a Mannich adduct: only the starting calix[4]arene was recovered. However, when the solvent system was changed to tetrahydrofuran-methanol (1:1) to increase the solubility of the reactants and the reaction solution was heated at reflux, the expected product **8** was produced in 54% yield (Scheme 3).

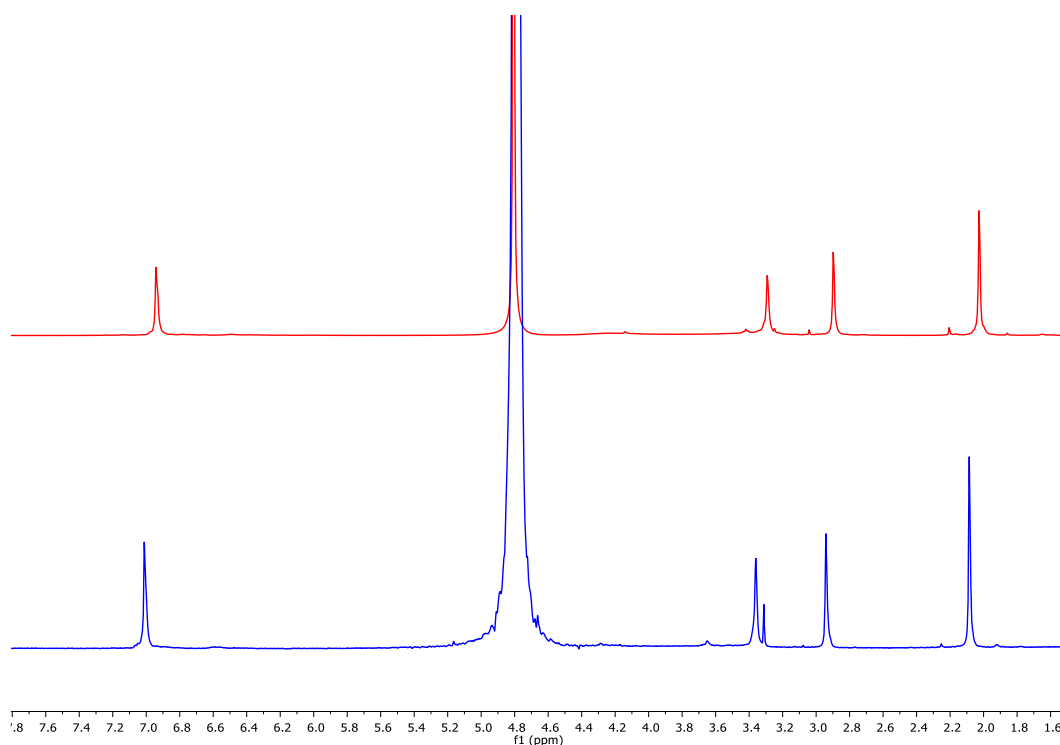


**Fig. 5:** Stacked  $^1\text{H}$ -NMR (400MHz, 25°C) of compounds **8** in  $\text{D}_2\text{O}$  before in presence of a solid precipitate (top) and after, clear solution (bottom) the addition of 20  $\mu\text{L}$  of NaOD.

Upon cooling to room temperature the product precipitated as a white solid from the reaction solution. The  $^1\text{H}$  NMR spectrum of the  $\text{D}_2\text{O}$ -soluble component was consistent with the desired product **8**: a singlet for the calixarene Ar-H, a singlet for the N-methyl group and two singlets for the  $\text{CH}_2$  groups of the  $\text{NCH}_2\text{CO}$  group and of the  $\text{ArCH}_2\text{N}$  between the calix[4]arene and the sarcosine. Also, in this case, the presence of only a signal for Ar- $\text{CH}_2$ -Ar around 31.5 ppm, in the  $^{13}\text{C}$ -NMR spectra of this compound, indicates that these calix[4]arenes are mainly present in a cone conformation. After the addition of a 20  $\mu\text{L}$  of NaOD solution, the entire solid is solubilized. The two NMR spectra, before and after addition of NaOD in Figure 5 show no significant differences in signal composition, demonstrating the homogeneity of product **8**. Finally, as supposed, the water solubility of this compound is not significantly lower than that of compound **3**.

Following the “classical” procedure (THF/ $\text{H}_2\text{O}$ ,  $\text{CH}_3\text{COOH}$ ) we were able to observe the formation of the product and its intermediates by ESI-MS analysis also when glycine was used as amino acid in the Mannich reaction. Unfortunately, the crude reaction mixture is difficult to purify because contains several by-products with a higher molecular weight than

the **2** (Figure 6). and despite different triturations in different solvents of the solid precipitated by the reaction, attempts to obtain the pure product **2** were unsuccessful (Figure 7).

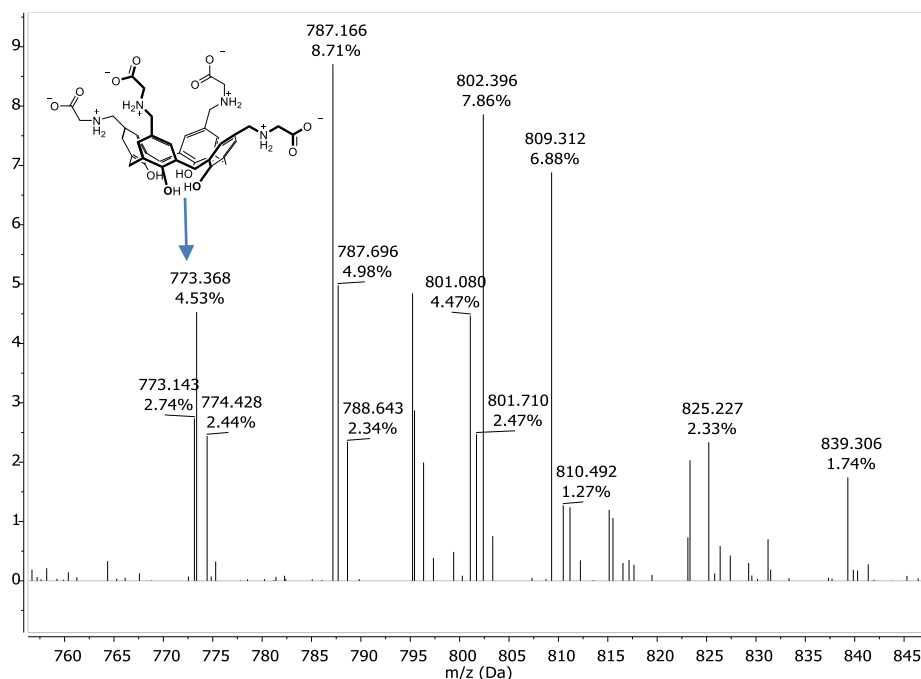


**Fig. 6:** ESI-MS spectrum after 96h of the “classical” Mannich reaction with Glycine. The analysis confirms the presence of the product but there are also by-products with much higher molecular weights.

Following the “classical” procedure (THF/H<sub>2</sub>O, CH<sub>3</sub>COOH) we were able to observe the formation of the product and its intermediates by ESI-MS analysis also when glycine was used as amino acid in the Mannich reaction. Unfortunately, the crude reaction mixture is difficult to purify because contains several by-products with a higher molecular weight than the **2** (Figure 6). and despite different triturations in different solvents of the solid precipitated by the reaction, attempts to obtain the pure product **2** were unsuccessful (Figure 7).

Resorcinarenes<sup>102</sup> have also been used as the C–H active compound in Mannich reactions. Konovalov et al.,<sup>103</sup> synthesized a glycine functionalized resorcinarene in the absence of a protic acid catalyst. Acceptable yields were indeed obtained by heating the reaction at reflux in a benzene/ethanol 1:1 mixture.

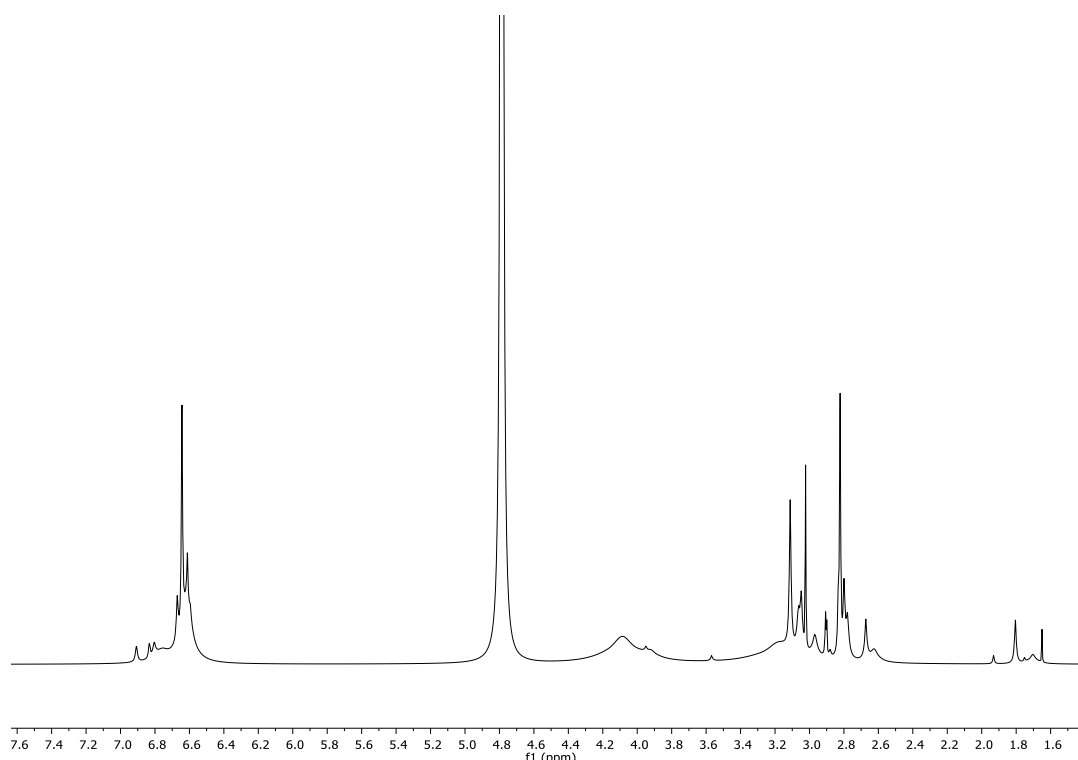
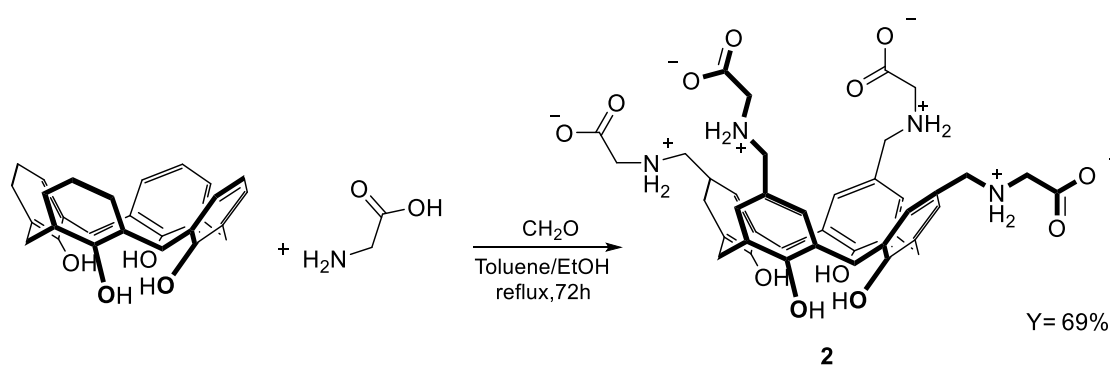


**Fig. 7:**  $^1\text{H-NMR}$  ( $\text{D}_2\text{O} + 20\mu\text{L NaOD}$ ,  $400\text{MHz}$ ,  $25^\circ\text{C}$ ) of the crude product of the “classical” ( $\text{THF}/\text{H}_2\text{O}$ ,  $\text{CH}_3\text{COOH}$ ) Mannich reaction with glycine.

Taking inspiration from this works we also tested these conditions in an attempt to obtain product **2** with glycine. The reaction was carried out in a Toluene/Ethanol 1:1 mixture without the addition of protic acids as catalyst. A white precipitate began to form a few hours after the reaction started. After 72 hours, the reaction was cooled to room temperature and the white solid in suspension was filtered.



**Scheme 3:** Modified reaction conditions for the synthesis of compound **2**

The precipitate is poorly soluble in water alone and the  $^1\text{H}$  NMR spectrum (Figure 8) was recorded in a solution of  $\text{D}_2\text{O}$  with the addition of a  $20\mu\text{L}$  of  $\text{NaOD}$ . The  $^1\text{H-NMR}$  spectrum

of **2** is quite similar to that of the sarcosino **8** since the only difference in the structure of the two molecules is the presence of methyl on the nitrogen atom for sarcosine.

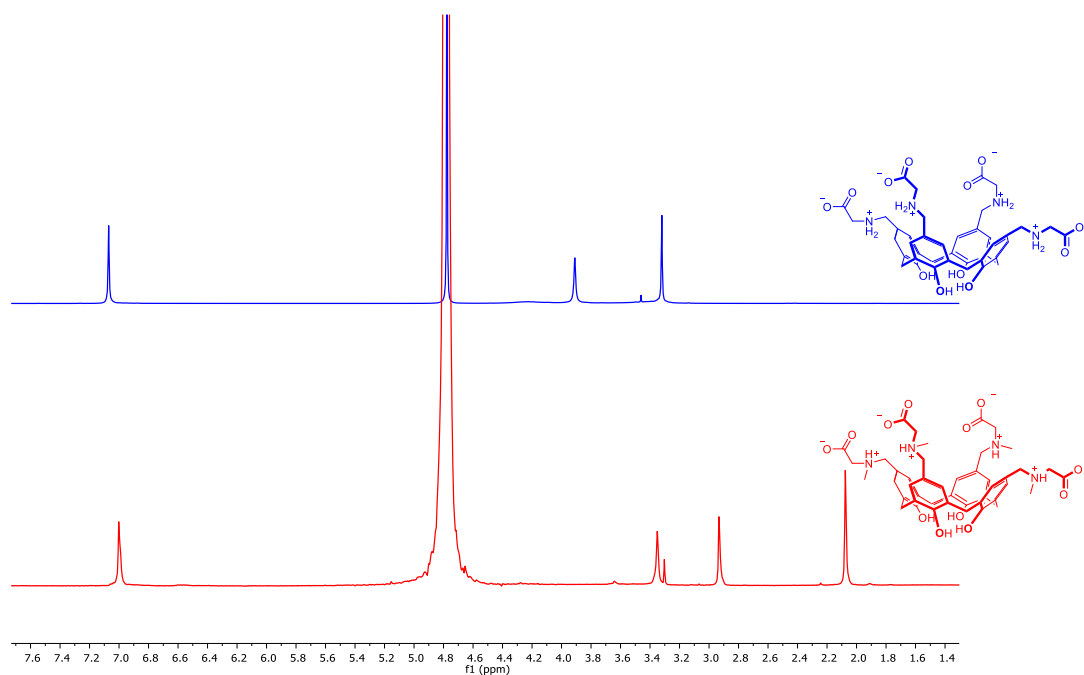


**Fig. 8:** Stacked  $^1\text{H-NMR}$  ( $450\ \mu\text{L D}_2\text{O}+20\ \mu\text{L NaOD}$ ,  $400\text{MHz}$ ,  $25^\circ\text{C}$ ) of compounds **2** (top) and **8** (bottom)

Furthermore, XRD analysis of a crystal of **2** (Figure 9) obtained in a  $\text{H}_2\text{O}/\text{MeOH}/\text{DMF}$  mixture shows that a DMF molecule is included within the cavity of calix[4]arene **2**. The DMF molecule is complexed within the calixarene cavity thanks to the formation of a  $\text{CH}\text{-}\pi$  interaction between one of the methyl groups of DMF that points inside the cavity and an aromatic nucleus of the calixarene.

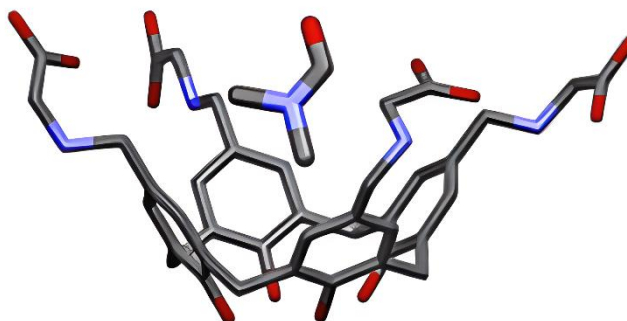



**Fig. 9:** Crystal structure of compound **2** shows inclusion of one DMF molecule

The Mannich reaction thus proved to be efficient for link amino acids to the upper rim of calix[4]arenes via a methylene group in only one synthetic step. In the case of all the products


obtained, the tetra substituted compound, once formed, spontaneously precipitates from the reaction mixture. This characteristic makes separation of the product easy as it can be isolated simply by filtration. Given the poor solubility of these compounds in a wide range of organic solvents and in water, purification from any unreacted amino acid is performed by trituration in different solvents. A preliminary analysis of the reaction yields shows that there appears to be a relationship between the water solubility of the amino acid used and the yields of the reaction. In fact, when proline, glycine and sarcosine are used, the reaction leads to acceptable yields. On the other hand, when amino acids with apolar side residues such as valine, leucine and phenylalanine are used, the reaction yield is significantly lower and sometimes even half of those with the previous amino acids.

### 3.9 STD NMR experiments

As already explained in the introduction of this chapter the STD-NMR experiment relies on the fact that, for a weak-binding ligand, there is exchange between the bound and the free ligand state. STD experiments were carried out on a suspension of bacteria in a solution of the calixarene ligand and implies subtracting an on-resonance spectrum (a spectrum where the bacteria cell wall was selectively saturated in a region with no signals of the ligand) from an off-resonance spectrum (no saturation of the bacteria cell wall) of the same sample. In the resulting difference spectrum, only the signals of the ligands that experience a saturation transfer from the biomolecules (through spin diffusion and/or nuclear Overhauser effect) appear.<sup>104</sup> The feasibility of on-cell STD NMR experiment for the detection of the ability of ligands **1**, **2** and **3** to interact with bacteria were carried out on samples containing the three following different bacteria as representatives of Gram-negative, Mycobacteria and Gram-positive bacteria:

 *Pseudomonas putida* (Gram-negative bacteria)

 *Mycobacterium smegmatis* (Mycobacteria)

 *Staphylococcus epidermidis* (Gram-positive bacteria)



In this preliminary studies only calix[4]arenes **1**, **2** and **3** were employed for the class of zwitterionic calix[4]arenes. For further analysis, positively charged calix[4]arene **9** functionalised at the upper rim with four methyl guanidinium units and calix[4]arene **5** functionalised at the upper rim with 4 methyl sulfonate groups were also tested.

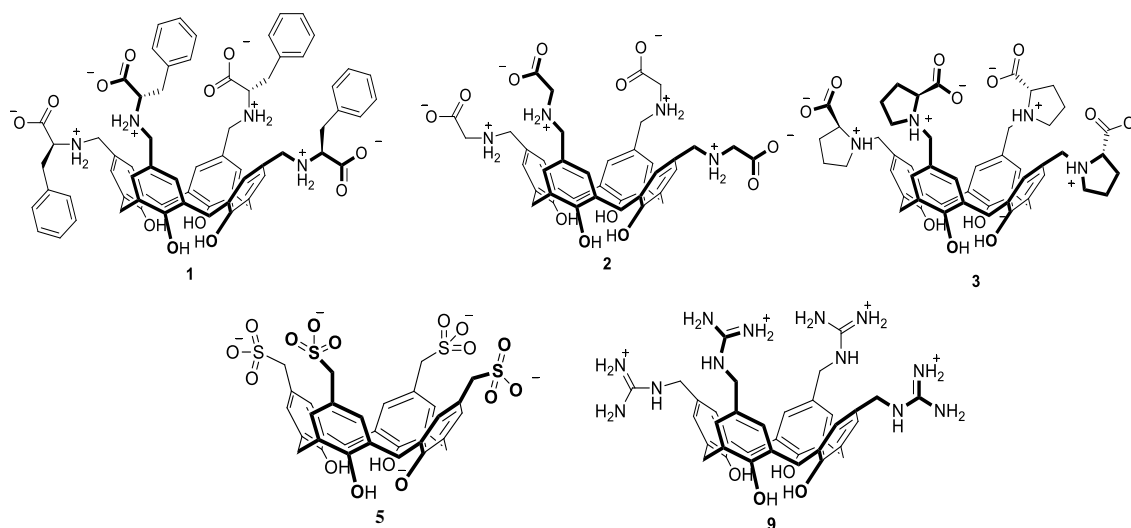


**Fig.10:** Structure of the ligands studied in this chapter for bacteria cell wall recognition

Ligands were employed in the millimolar range of concentration (2 mM) and dissolved in a mixture composed by *d*-PBS and *d*<sub>6</sub>-DMSO. For experiments with bacteria cells, 2 aliquots of freeze-dried cells ( $OD_{600nm} = 1.5$  in 750  $\mu$ L) were resuspended in distilled water and then washed in *d*-PBS 10 mM, by centrifugation. Pellets were reunited and suspended in 32  $\mu$ L of *d*-PBS and added to the disposable insert. The best on-resonance selective irradiation frequency, assuring a good saturation transfer from the receptor to ligands without the direct saturation of its resonances were 5.15, 0.5 or -1.0 ppm. Notably, a high signal-to-noise ratio was achieved with a very low number of scans (256), implying acquisition times of about 30 min. These acquisition times are short enough to assure that cell integrity and viability are preserved during measurements.

### 3.9.1 On-cell STD NMR experiments with ligands **1**, **2** and **3**

The screening of the recognition properties of calixarenes **1**, **2** and **3** towards different bacteria strains were studied using on-cell STD NMR experiments by Professor Cristina Airoidi group at University Milano Bicocca.

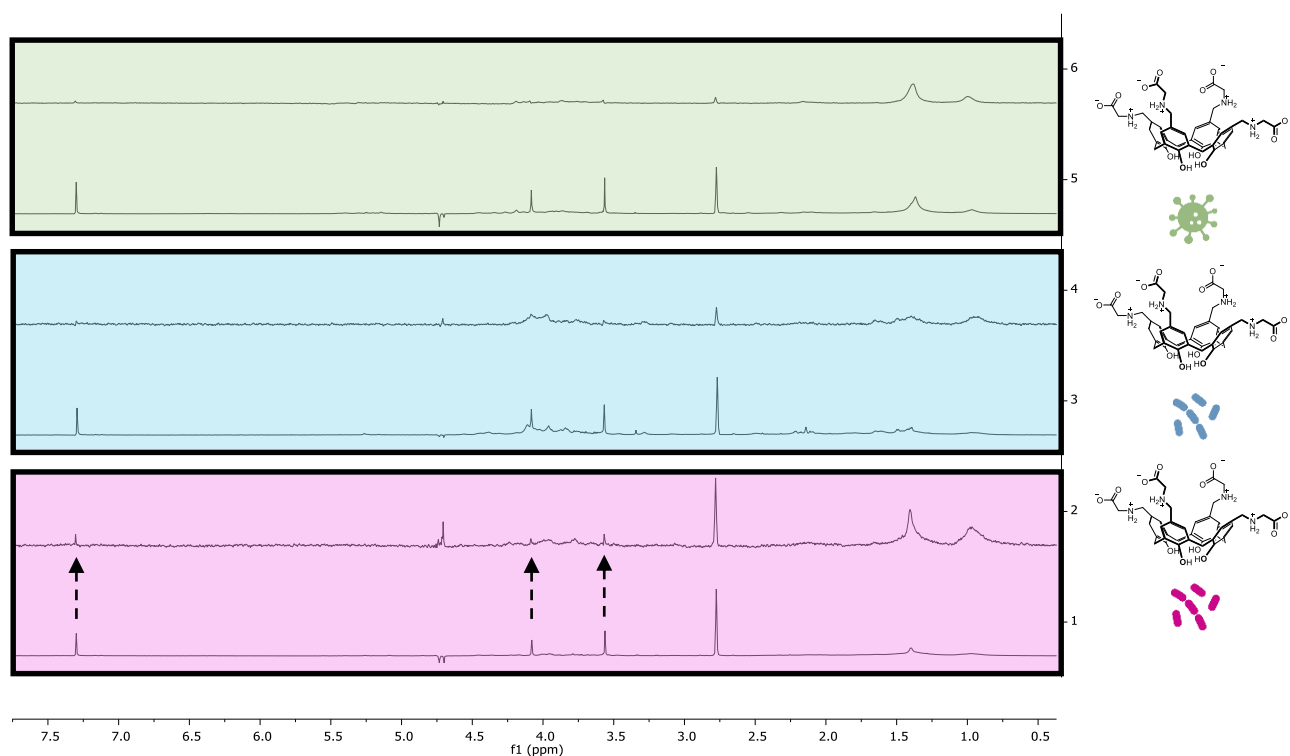


**Fig.11:**  $^1\text{H-NMR}$  ( $d\text{-PBS} + 20\% d_6\text{-DMSO}$ ) on-resonance spectra of a sample containing calixarene **2** (2 mM) and *Pseudomonas putida* (OD 1 in  $750\mu\text{L} \times 2$  pelleted resuspended in  $25\mu\text{L}$  of  $d\text{-PBS}$ ) (trace 1), *Staphylococcus epidermidis* (OD 1 in  $750\mu\text{L} \times 2$  pelleted resuspended in  $25\mu\text{L}$  of  $d\text{-PBS}$ ) (trace 3), *Mycobacterium smegmatis* (OD 1 in  $750\mu\text{L} \times 2$  pelleted resuspended in  $25\mu\text{L}$  of  $d\text{-PBS}$ ) (trace 5). STD NMR spectra (trace 2, 4 and 6) acquired in presence of ligand **2** and the three different bacterial strains. Ligand **2** interact only with the surface of gram-negative cells, as some of the compound resonances appeared in the STD spectrum (trace 2).

STD spectra acquired of calixarene **2** in presence of the different bacteria strain are shown in Figure 11. STD spectra showed that neither *Mycobacterium smegmatis* (Figure 11, trace 6), nor *Staphylococcus epidermidis* (Figure 11, trace 4) interact with this ligand, as no resonances of these ligands appears in the resulting STD spectra. In stark contrast, the STD experiment with the *Pseudomonas putida* would appear to show an interaction with calixarene **2** as evidenced by the appearance of ligand signals in the corresponding STD spectrum. From this STD spectrum it can also be seen that both the aromatic signals related to the calixarene scaffold and the singlet signals related to glycine are present suggesting that both are involved in the molecular recognition process and that the scaffold could contribute to stabilize the interaction with the bacteria cell wall constituents. The same experiment was then repeated for calixarene **1** and **3** to evaluate the degree of the interaction when other groups are present on the calixarene scaffold. STD spectra acquired of calixarene **1** in presence of the different bacteria strain are shown in Figure 12.

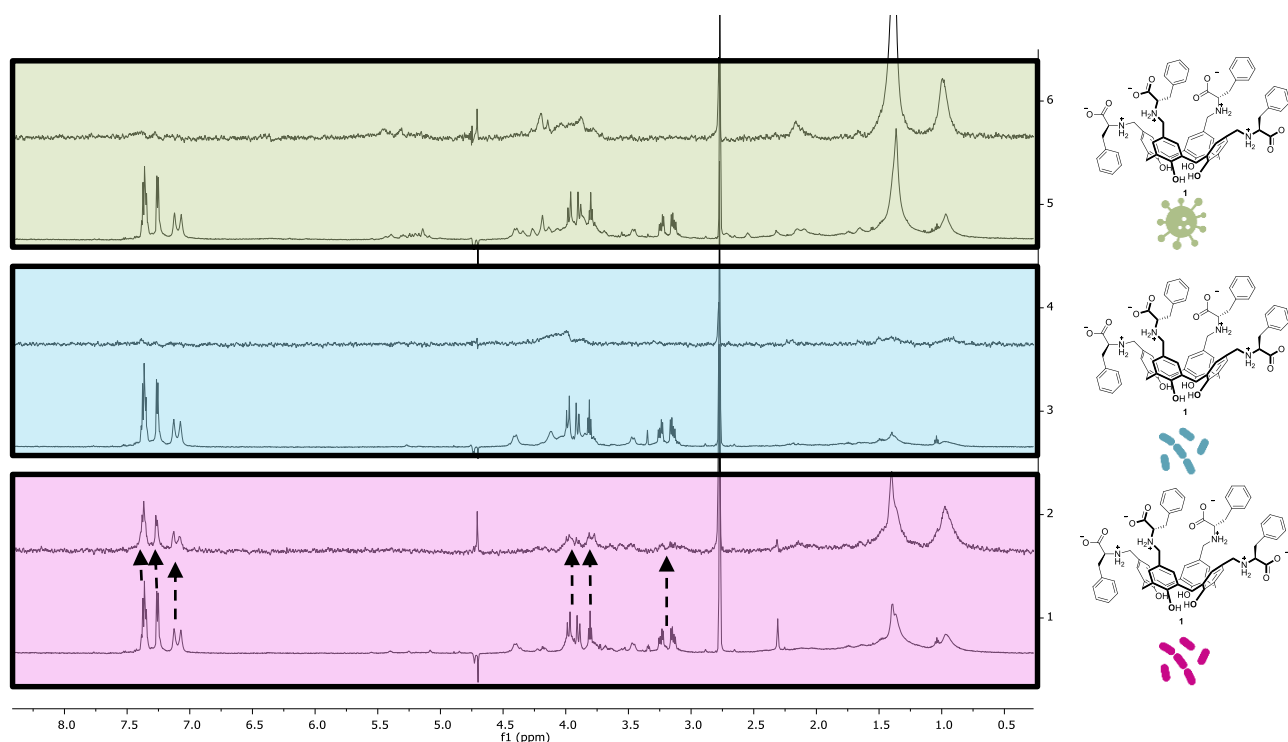


**Fig.12:**  $^1\text{H-NMR}$  ( $d\text{-PBS} + 20\% d_6\text{-DMSO}$ ) on-resonance spectra of a sample containing calixarene **1** (2 mM) and *Pseudomonas putida* (OD 1 in  $750\mu\text{L}$  x 2 pelleted resuspended in  $25\mu\text{L}$  of  $d\text{-PBS}$ ) (trace 1), *Staphylococcus epidermidis* (OD 1 in  $750\mu\text{L}$  x 2 pelleted resuspended in  $25\mu\text{L}$  of  $d\text{-PBS}$ ) (trace 3), *Mycobacterium smegmatis* (OD 1 in  $750\mu\text{L}$  x 2 pelleted resuspended in  $25\mu\text{L}$  of  $d\text{-PBS}$ ) (trace 5). STD NMR spectra (trace 2, 4 and 6) acquired in presence of ligand **1** and the three different bacterial strains. Ligand **1** interact only with the surface of gram-negative cells, as compound resonances appeared in the STD spectrum (trace 2).

Also in this experiment it is possible to note how calixarene **1** selectively interacts only with the cell wall of the *Pseudomonas putida* bacterium as demonstrated by the appearance of the ligand signals in the resulting STD spectrum (Figure 12, trace 2). As in the previous case, also in this case in the experiments conducted with *Staphylococcus epidermidis* (Figure 12, trace 4) and *Mycobacterium smegmatis* (Figure 12, trace 6), no ligand signals can be seen in the STD experiments because of the absence of interaction with these cell walls. Unlike the previous case (Figure 11, trace 2), in the STD NMR experiment with **1**, the ligand signals appear clearer and more intense. As already explained in the introduction the hydrogen atoms closest to the cell surfaces will have stronger signals due to a more effective saturation transfer. Given the greater intensity in the STD spectra of the signals relating to **1** compared to **2**, it can be concluded that the binding between the bacterial surface and the ligand is stronger in the case of **1**. From the STD spectrum it can also be seen that the aromatic signals related to the calixarene scaffold and the signals related to phenylalanine are present

suggesting that both are involved in the molecular recognition process. Finally calix[4]arene **3** was also tested with the three different bacteria strain.

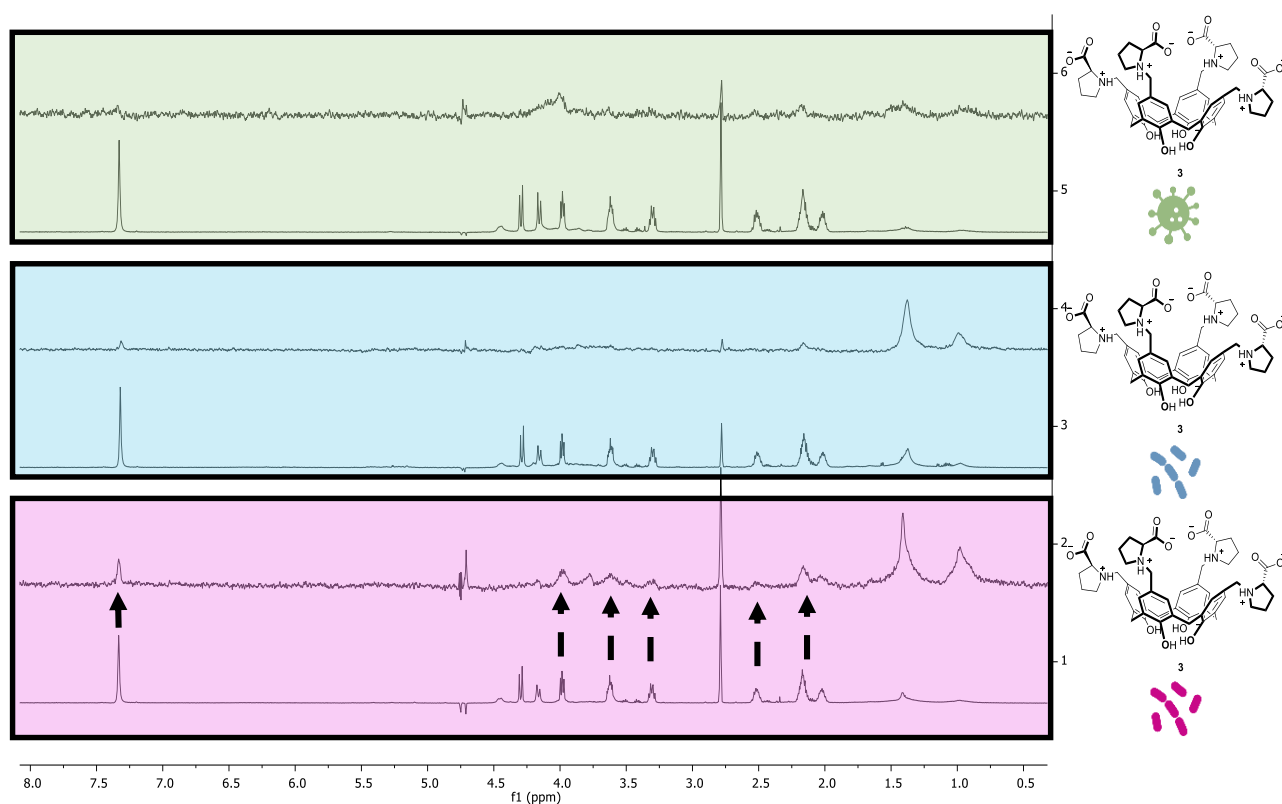


**Fig.13:**  $^1\text{H-NMR}$  ( $d\text{-PBS} + 20\% d_6\text{-DMSO}$ ) on-resonance spectra of a sample containing calixarene **3** (2 mM) and *Pseudomonas putida* (OD 1 in  $750\mu\text{L} \times 2$  pelleted resuspended in  $25\mu\text{L}$  of  $d\text{-PBS}$ ) (trace 1), *Staphylococcus epidermidis* (OD 1 in  $750\mu\text{L} \times 2$  pelleted resuspended in  $25\mu\text{L}$  of  $d\text{-PBS}$ ) (trace 3), *Mycobacterium smegmatis* (OD 1 in  $750\mu\text{L} \times 2$  pelleted resuspended in  $25\mu\text{L}$  of  $d\text{-PBS}$ ) (trace 5). STD NMR spectra (trace 2, 4 and 6) acquired in presence of ligand **3** and the three different bacterial strains. Ligand **3** interact only with the surface of gram-negative cells, as compound resonances appeared in the STD spectrum (trace 2).

The results of this experiments are shown in Figure 13. Also in this case, it seems that there is a preferential interaction with the gram-negative bacterium (Figure 13, trace 2). As in the previous case, it appears to be a greater interaction of **3** with the bacterial cell wall compared to calixarene **2**.

In parallel to zwitterionic calixarenes **1-3**, similar experiments were also performed with the p-methylsulfonato calixarene **5** and the p-methylguanidino calixarene **9**. The STD experiments with these families of calixarenes are not reported here. However, it has been shown that calixarene **5** shows a complete lack of affinity towards all three bacterial families (no ligands signals appear in the STD spectra). This may not be surprising since the cell wall

of gram-positive and -negative bacteria expose negative charges of the phosphate groups thus unfavourably interfering in the binding of the negative charged ligand.

In the case of positively calix[4]arene **9** the situation is quite different. In fact, this ligand is totally aspecific towards gram-positive and -negative bacteria as it recognizes both of them with high affinity. This is not surprising considering the high affinity that guanidinium groups possess towards phosphate groups.<sup>105</sup>

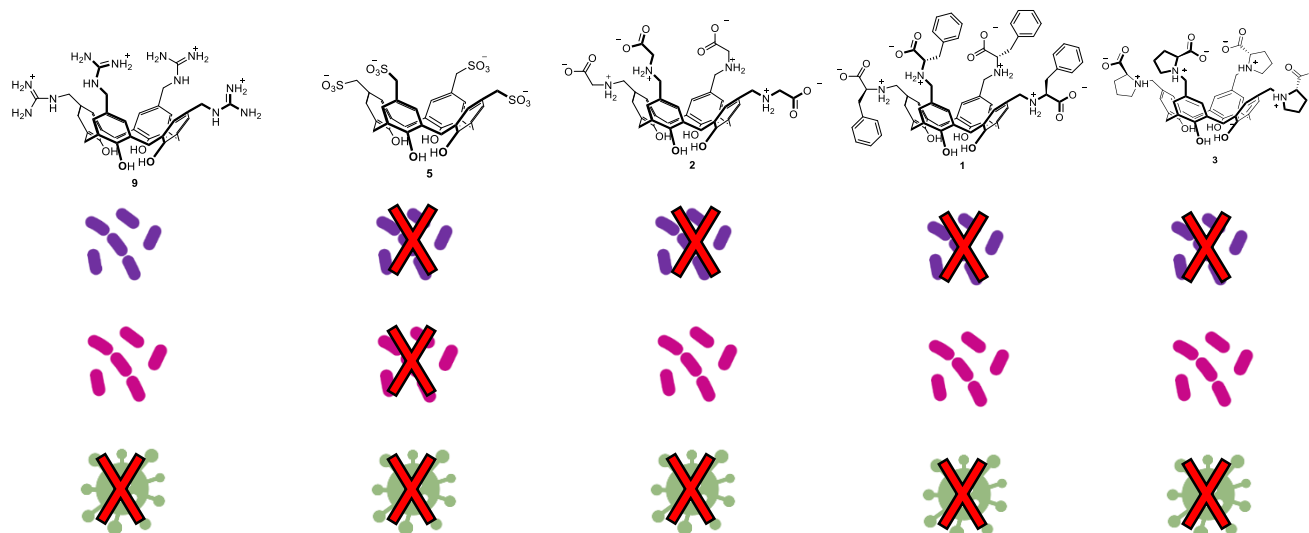


**Fig.14** Schematic and qualitative representation of the results obtained from the screening experiments between the three different bacteria classes and the calixarenes **1**, **2**, **3**, **5** and **9**. The red crosses on the cartoon of the bacteria strains mean very weak or no binding

### 3.9.2 STD NMR experiments with ligands **1**, **2** and **3** and LPS

As already mentioned in the introduction, the principal and more typical component of the cell wall of gram-negative bacteria is LPS. Lipopolysaccharides (LPS) are large molecules consisting of a lipid and a polysaccharide (Figure 15).

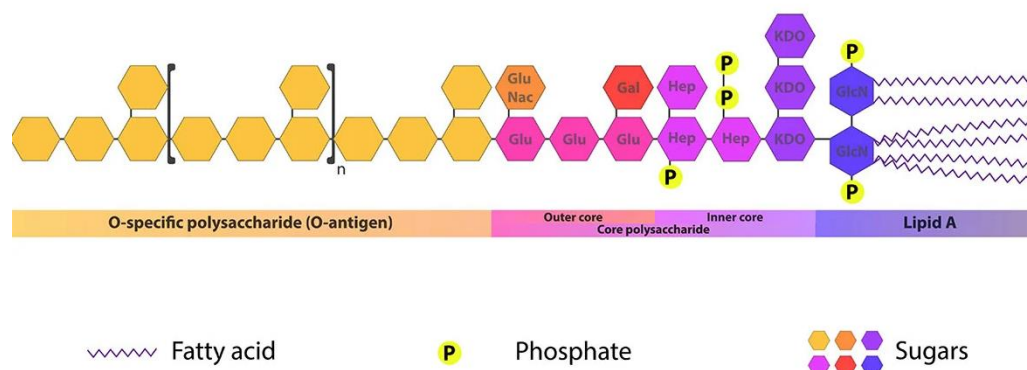


**Fig.15** Schematic representation of a generic LPS structure

It was hypothesised that LPS, being the principal component exposed on the cell wall of gram-negative bacteria was also the component responsible for the interaction with zwitterionic ligands. To shed lights on this point, STD NMR experiments with calixarene **3** and LPS from *Escherichia coli* were carried. Two different experiments were conducted, shown in Figure 15. In the first case, a 10 mM stock solution in d-PBS of LPS from *E. coli* was added to a solution of **3** (2mM) in d-PBS. In the second STD experiment, LPS was dispersed in d-SDS (deutero Sodium Dodecyl Sulfate) micelles in an attempt to mimic the bacteria cell wall conditions. These two experiments together seem to confirm the presence of an interaction between LPS and calixarene **3**. In fact, the ligand signals emerged in STD experiment with both free LPS (Figure 15, *trace 2*) and LPS dispersed in d-SDS micelles (Figure 15, *trace 4*)

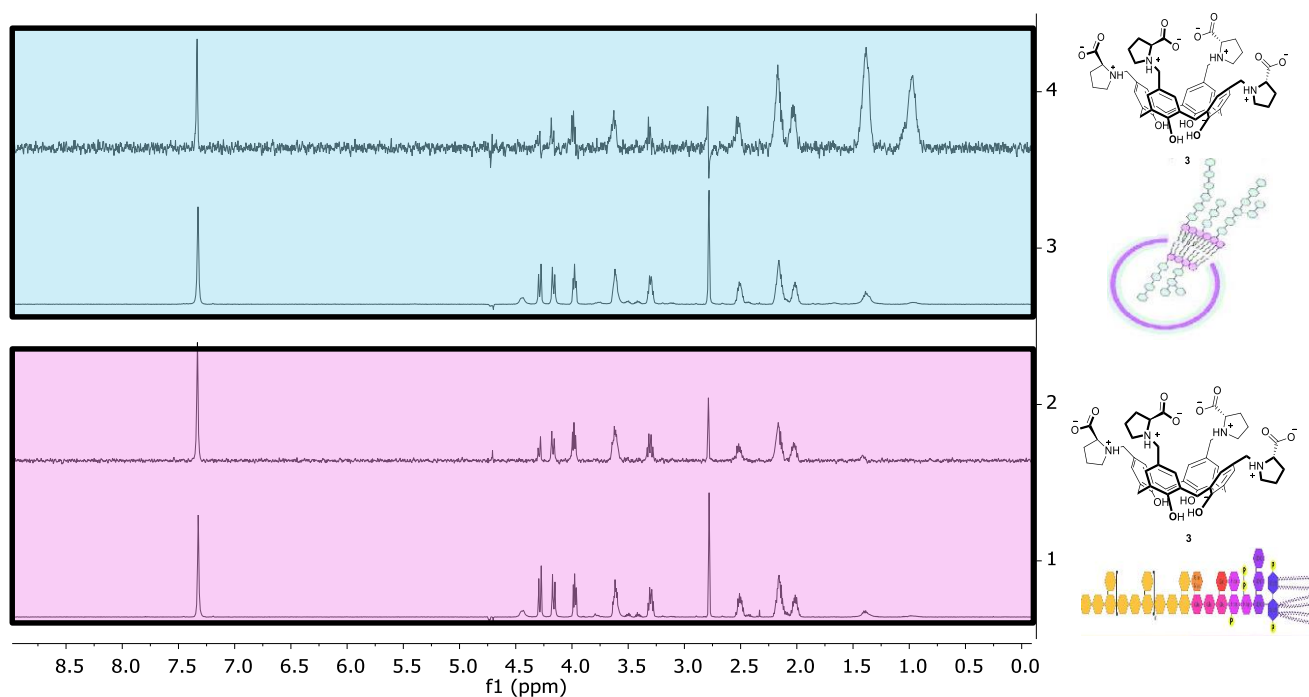


**Fig.15:**  $^1\text{H-NMR}$  (trace 1 and 3) and STD NMR (trace 2 and 4) spectra of a sample containing calixarene **3** (2 mM) and LPS (0.2 mg/mL) in d-PBS +20%  $d_6$ -DMSO (trace 1 and 2) and LPS (0.8 mg/mL) d-PBS +20%  $d_6$ -DMSO+ d-SDS (10 mM) (trace 3 and 4).

### 3.10 Conclusion

Amino acids were attached to the upper rim of calixarenes, preserving their zwitterionic structure, thanks to the general and fast methods of the Mannich reaction. In this work, it was further extended the previous reported study, applied only to proline, by using also other

natural amino acids. This reaction provided a relatively easy access to zwitterionic calixarenes, but only when Glycine, Sarcosine, Valine, Leucine and Phenylalanine were used. The X-ray structure of **2** was obtained showing the inclusion of a DMF molecule in the calixarene cavity.

The screening of the recognition properties of these calixarenes towards different bacteria strains were studied using on-cell STD NMR experiments by Professor Airoidi group at University Milano Bicocca. Calixarene **1**, **2** and **3** were proved to have greater affinity and selectivity with *Pseudomonas putida*, a gram-negative bacterium while calixarene **9** show affinity with both Gram-positive and Gram-negative bacteria. It was finally shown that the zwitterionic calixarene **3** binds to LPS, exposed on Gram-negative bacteria cell wall, and might therefore be the component recognized by this class of zwitterionic calixarene ligands in the “on-cell experiments”.





# Experimental Part

## 3.11 General information

$^1\text{H}$ -NMR and  $^{13}\text{C}$ -NMR spectra were recorded on Bruker AV400 spectrometers and partially deuterated solvents were used as internal standards to calculate the chemical shifts ( $\delta$  values in ppm). All  $^{13}\text{C}$ -NMR spectra were performed with proton decoupling. Electrospray ionization (ESI) mass analysis were performed with a Waters single-quadrupole spectrometer in positive mode using MeOH or  $\text{CH}_3\text{CN}$  as solvents. High resolution mass spectra were recorded on a LTQ Orbitrap XL instrument in positive mode using MeOH as solvent. Melting points were determined on an Gallenkamp apparatus in closed capillaries.

## 3.12 Bacterial strains and media

*Pseudomonas putida* (ATCC® 47054™), *Escherichia coli* MG1655 (ATCC® 700926™) and *Mycobacterium smegmatis* (ATCC® 700084™) were grown in LB broth at 37 °C aerobically under agitation in orbital shaker at 150 rpm, for 24 hours; *Staphylococcus epidermidis* (ATCC® 12228™) was grown in Nutrient Broth at 37 °C aerobically under agitation in orbital shaker at 150 rpm, for 24 hours. Bacterial cells were harvested and washed 2 times with PBS 10 mM at 1500  $\times g$  for 15 minutes at 4°C. Pellets were resuspended in PBS 10 mM ( $\text{OD}_{600\text{nm}} = 1.5$ ) and freeze-dried in 750  $\mu\text{L}$  aliquots.

## 3.13 On-cell STD NMR experiments

### - Sample preparation

8  $\mu\text{L}$  of 10 mM stock solution in  $\text{d}_6$ -DMSO of test molecule were added to Disposable Kel-F inserts for 4 mm  $\text{ZrO}_2$  MAS rotor (final concentration 2 mM).

For experiments with ligand alone, 32  $\mu\text{L}$  of deuterated PBS 10 mM were added to the disposable insert (total volume 40  $\mu\text{L}$ ).

For experiments with cells, 2 aliquots of freeze-dried cells ( $\text{OD}_{600\text{nm}} = 1.5$  in 750  $\mu\text{L}$ ) were resuspended in distilled water and then washed in d-PBS 10 mM, by centrifuging for 7.5 min

at 3000 ×g. Pellets were reunited and suspended in 32 μL of d-PBS and added to the disposable insert (total volume 40 μL).

For experiments with LPS, 3.2 or 6.4 μL of 5 mg/mL in d-PBS 10 mM stock solution of LPS from *E. coli* were added to the disposable insert (final LPS concentration 0.4 or 0.8 mg/mL). 28.8 or 25.6 μL of d-PBS 10 mM were then added to the disposable insert to reach the total volume of 40 μL.

For experiments with LPS dispersed in d-SDS micelles, 3.2 or 6.4 μL of stock solution 5 mg/mL in d-PBS 10 mM of LPS from *E. coli*, and 4 μL of 100 mM in d-PB (20 mM) stock solution of d-SDS, were added to the disposable insert (final LPS concentration 0.4 or 0.8 mg/mL; final d-SDS concentration 10 mM). 24.8 or 21.6 μL of d-PBS 10 mM were then added to the disposable insert to reach the total volume of 40 μL.

#### - NMR spectra acquisition

NMR spectra were acquired by using a Bruker Avance III 600 MHz NMR spectrometer, equipped with a HR-MAS probe. <sup>1</sup>H-NMR spectra were acquired with 16 scans. STD NMR spectra were acquired with 256 scans, selective irradiation frequency 5.15, 0.5 or -1.0 ppm, saturation time 3.0 s, off-resonance irradiation frequency 30 ppm, at 310 K and at a spinning rate of 3 kHz.

#### Synthesis of p-(L-proline-N-methyl)calix[4]arene 3

In a round bottom flask calix[4]arene (2 g, 4.8 mmol), tetrahydrofuran (45 mL), L-proline (6 mmol for each aromatic of the scaffold) dissolved in water (7 mL), glacial acetic acid (5.6 mL) and formaldehyde (2.0 mL, 37% w/v, 27 mmol) were combined and left stirring at room temperature for 96 hours. The liquid was decanted and drained well from the product that deposited on the flask wall. The flask was triturated with acetone and the solution then filtered. The precipitate was washed with acetone and then recrystallised from water/ethanol acetone (1:1:2)- to yield a white solid (3.7 g; yield 77%). <sup>1</sup>H NMR (D<sub>2</sub>O): δ (ppm) 7.03 (s, 8H, ArH), 3.88-3.83 (broad s, 8H, ArCH<sub>2</sub>Ar), 3.82-3.67 (s, 8H, ArCH<sub>2</sub>N), 3.67-3.54 (broad t, 4H, NCH), 3.35-3.18 (broad m, 4H, CH<sub>2</sub>N), 2.98-2.75 (broad m, 4H, CH<sub>2</sub>N), 2.20-1.82 (broad m, 4H, CHCH<sub>2</sub>), 1.82-1.40 (broad m, 12H CHCH<sub>2</sub>). The compound showed the same physico-chemical properties as those reported in literature.<sup>106</sup>

### General procedure for the Mannich reaction to form the zwitterionic calix[4]arenes 1, 6, 7 and 8

In a round bottom flask calix[4]arene (1mmol), tetrahydrofuran (15 mL), aminoacids (6 mmol for each aromatic of the scaffold) dissolved in water (2 mL), glacial acetic acid (2.8 mL) and formaldehyde (0.5 mL, 37% w/v, 7 mmol) were combined and left stirring at room temperature for 96 hours. The precipitated solid was filtered and washed with cold water.

#### Synthesis of p-(L-phenylalanine-N-methyl)calix[4]arene 1

The pure product was obtained by trituration with tetrahydrofuran then methanol to give a pale-yellow solid (0.450g, yield 35%) mp >320°C dec; <sup>1</sup>H NMR (400 MHz, D<sub>2</sub>O+NaOD) δ (ppm) 6.69-6.66 (broad m, 28 H, ArH), 4.11(broad s, 4H, ArCH<sub>ax</sub>Ar), 3.15-2.97 (broad m, 16H, ArCH<sub>2</sub>N+ArCH<sub>eq</sub>Ar+NCHCOOH), 2.43-2.63 (m, 8H, CH<sub>2</sub> Phe); <sup>13</sup>C NMR (100 MHz, D<sub>2</sub>O+NaOD) 181.3 (C=O), 151.8 (C–OH), 137.8 (Ar), 130.9 (Ar), 129.5 (Ar), 128.6 (Ar), 128.1 (Ar), 126.2 (Ar), 63.1 (N-CH-COOH), 50.2 (Ar-C-N), 38.6 (Ar-CH<sub>2</sub>-CH), 31.6 (Ar-CH<sub>2</sub>-Ar). ESI-MS m/z calcd for C<sub>68</sub>H<sub>69</sub>N<sub>4</sub>O<sub>12</sub> [(1+H)<sup>+</sup>] 1134.29, found 1134.51, calcd for C<sub>68</sub>H<sub>67</sub>N<sub>4</sub>O<sub>12</sub>Na [(1+Na)<sup>+</sup>] 1155.27, found 1155.51, calcd for C<sub>68</sub>H<sub>67</sub>N<sub>4</sub>O<sub>12</sub>K [(1+K)] 1171.38 found 1171.52

#### Synthesis of p-(L-valine-N-methyl)calix[4]arene 7

The pure product was obtained by trituration with methanol then acetone to give a white solid (0.350g, yield 31%) mp >300°C dec; <sup>1</sup>H NMR (400 MHz, D<sub>2</sub>O+NaOD) δ (ppm) 6.89 (s, 8H, ArH), 4.78 (broad s, 4H, ArCH<sub>ax</sub>Ar), 3.37-3.11 (m, 12H, ArCH<sub>2</sub>N+ArCH<sub>eq</sub>Ar), 2.67 (d, J= 6 Hz, 4H, NHCHCOOH), 1.67-1.60 (m, 4H, CH(CH<sub>3</sub>)<sub>2</sub>), 0.73-0.79 (dd, J= 7 Hz, 24H, (CH<sub>3</sub>)<sub>2</sub>); <sup>13</sup>C NMR (100 MHz, D<sub>2</sub>O+NaOD) δ (ppm) 181.5 (C=O), 152.2 (C–OH), 130.6 (Ar), 129.7 (Ar), 128.4 (Ar), 68.1 (N-CH-COOH), 50.4 (Ar-CH<sub>2</sub>-N), 31.6 (Ar-CH<sub>2</sub>-Ar), 30.3 (CH(CH<sub>3</sub>)<sub>2</sub>), 18.6 (CH<sub>3</sub>), 18.3 (CH<sub>3</sub>). ESI-MS: m/z calcd for C<sub>52</sub>H<sub>69</sub>N<sub>4</sub>O<sub>12</sub> [(7+H)<sup>+</sup>] 941.12, found 941.43, calcd for C<sub>52</sub>H<sub>67</sub>N<sub>4</sub>O<sub>12</sub>Na[(7+Na)<sup>+</sup>] 963.10 found 963.79

#### Synthesis of p-(L-leucine-N-methyl)calix[4]arene 6

The pure product was obtained by trituration with methanol then tetrahydrofuran to give a white solid (0.320g, yield 29%) mp >310°C dec, <sup>1</sup>H NMR (400 MHz, D<sub>2</sub>O+NaOD) δ (ppm) 6.73 (s, 8H, ArH), 4.06 (broad s, 4H, ArCH<sub>ax</sub>Ar), 3.24-2.99 (m, 12H, ArCH<sub>2</sub>N+ArCH<sub>eq</sub>Ar),

2.73 (t,  $J = 7$  Hz, 4H,  $\text{NHCHCOOH}$ ), 1.10-0.98 (m, 8H,  $\text{CH}_2(\text{CH}_3)_2$ ), 0.47 (d,  $J = 6.3$  Hz, 12H,  $\text{CH}_3$ ), 0.24 (d,  $J = 6.3$  Hz, 12H,  $\text{CH}_3$ );  $^{13}\text{C}$  NMR (100 MHz,  $\text{D}_2\text{O} + \text{NaOD}$ )  $\delta$  (ppm) 183.1 ( $\text{C}=\text{O}$ ), 152.8 ( $\text{C}-\text{OH}$ ), 130.3 (Ar), 129.1 (Ar), 128.3 (Ar), 61.1 (N-CH-COOH), 50.3 (Ar- $\text{CH}_2$ -N), 42.2 (CH- $\text{CH}_2$ -CH( $\text{CH}_3$ ) $_2$ ), 31.1 (Ar- $\text{CH}_2$ -Ar), 24.4 (CH( $\text{CH}_3$ ) $_2$ ), 21.8 ( $\text{CH}_3$ ), 21.4 ( $\text{CH}_3$ ); ESI-MS:  $m/z$  calcd for  $\text{C}_{56}\text{H}_{77}\text{N}_4\text{O}_{12}$  [(6+H) $^+$ ] 997.22, found 997.65, calcd for  $\text{C}_{56}\text{H}_{75}\text{N}_4\text{O}_{12}\text{Na}$  [(6+Na) $^+$ ] 1019.20, found 1019.67, calcd for  $\text{C}_{56}\text{H}_{75}\text{N}_4\text{O}_{12}\text{K}$  [(6+K) $^+$ ] 1035.31 found 1035.56

### Synthesis of p-(L-sarcosine-N-methyl)-calix[4]arene 8

The pure product was obtained by trituration with hot methanol and then acetone to give a white solid (0.200 g, yield 54%) mp  $>293$  °C dec,  $^1\text{H}$  NMR (400 MHz,  $\text{D}_2\text{O} + \text{NaOD}$ )  $\delta$  (ppm) 6.92 (s, 8H, ArH), 4.17 (broad s, 4H, Ar $\text{CH}_{ax}$ Ar), 3.27 (broad s, 12H, Ar $\text{CH}_2\text{N} + \text{ArCH}_{eq}$ Ar), 2.87 (s, 8H, N- $\text{CH}_2$ -COOH), 1.99 (s, 12H,  $\text{OCH}_3$ );  $^{13}\text{C}$  NMR (100 MHz,  $\text{D}_2\text{O} + \text{NaOD}$ )  $\delta$  (ppm) 178.6 ( $\text{C}=\text{O}$ ), 152.8 ( $\text{C}-\text{OH}$ ), 130.4 (Ar), 129.9 (Ar), 127.3 (Ar), 59.8 (N- $\text{CH}_2$ -COOH), 59.5 (Ar- $\text{CH}_2$ -N), 40.6 (N- $\text{CH}_3$ ), 31.5 (Ar- $\text{CH}_2$ -Ar); ESI-MS:  $m/z$  calcd for  $\text{C}_{44}\text{H}_{53}\text{N}_4\text{O}_{12}$  [(5+H) $^+$ ] 829.90, found 829.53, calcd for  $\text{C}_{44}\text{H}_{51}\text{N}_4\text{O}_{12}\text{Na}$  [(5+Na) $^+$ ] 850.89, found 850.98.

### Synthesis of p-(L-glycine-N-methyl)calix[4]arene 2

In a round bottomed flask calix[4]arene (0.5 g, 1.18 mmol), ethanol (3 mL), toluene (10 mL), glycine (5 mmol for each aromatic of the scaffold) dissolved in water (2 mL), and formaldehyde (0.5 mL, 37% w/v, 27 mmol) were combined and left stirring at 100 °C for 72 hours. After cooling to room temperature, the white solid was filtered and triturated with hot ethanol to give the pure product as a white solid (0.630g, yield 69%) mp  $>280$  °C dec,  $^1\text{H}$  NMR (400 MHz,  $\text{D}_2\text{O} + \text{NaOD}$ )  $\delta$  (ppm) 6.99 (s, 8H, ArH), 4.15 (broad s, 4H, Ar $\text{CH}_{ax}$ Ar), 3.83 (s, 8H, NH- $\text{CH}_2$ -COOH), 3.24 (broad s, 12H, Ar $\text{CH}_2\text{N} + \text{ArCH}_{eq}$ Ar);  $^{13}\text{C}$  NMR (100 MHz,  $\text{D}_2\text{O} + \text{NaOD}$ )  $\delta$  (ppm) 171.1 ( $\text{C}=\text{O}$ ), 153.5 ( $\text{C}-\text{OH}$ ), 131.3 (Ar), 129.8 (Ar), 122.1 (Ar), 49.9 (NH- $\text{CH}_2$ -COOH), 47.7 (Ar- $\text{CH}_2$ -N), 31.4 (Ar- $\text{CH}_2$ -Ar). ESI-MS:  $m/z$  calcd for  $\text{C}_{40}\text{H}_{45}\text{N}_4\text{O}_{12}$  [(6+H) $^+$ ] 773.80, found 773.22, calcd for  $\text{C}_{40}\text{H}_{43}\text{N}_4\text{O}_{12}\text{Na}$  [(6+Na) $^+$ ] 794.78, found 794.24, calcd for  $\text{C}_{40}\text{H}_{43}\text{N}_4\text{O}_{12}\text{K}$  [(6+K) $^+$ ] 810.89 found 811.02.

**Table 1 Crystal data and structure refinement for 2**

Empirical formula  $\text{C}_{42.25}\text{H}_{62.06}\text{N}_{4.75}\text{NaO}_{19.95}$

### Chapter 3: Zwitterionic calix[4]arene for bacteria cell wall detection

Formula weight	978.76
Temperature/K	200.0
Crystal system	monoclinic
Space group	P2 <sub>1</sub> /n
a/Å	9.8654(3)
b/Å	27.7900(9)
c/Å	17.9538(6)
$\alpha$ /°	90
$\beta$ /°	102.504(2)
$\gamma$ /°	90
Volume/Å <sup>3</sup>	4805.5(3)
Z	4
$\rho_{\text{calc}}/\text{cm}^3$	1.353
$\mu/\text{mm}^{-1}$	0.988
F(000)	2078.0
Crystal size/mm <sup>3</sup>	0.08 × 0.07 × 0.02
Radiation	CuK $\alpha$ ( $\lambda$ = 1.54184)
2 $\Theta$ range for data collection/°	6.362 to 140.732
Index ranges	-12 ≤ h ≤ 12, -33 ≤ k ≤ 33, -21 ≤ l ≤ 18
Reflections collected	89011
Independent reflections	9122 [R <sub>int</sub> = 0.1094, R <sub>sigma</sub> = 0.0404]
Data/restraints/parameters	9122/6/698
Goodness-of-fit on F <sup>2</sup>	1.027
Final R indexes [I ≥ 2 $\sigma$ (I)]	R <sub>1</sub> = 0.0697, wR <sub>2</sub> = 0.1938
Final R indexes [all data]	R <sub>1</sub> = 0.1027, wR <sub>2</sub> = 0.2231
Largest diff. peak/hole / e Å <sup>-3</sup>	0.75/-0.41

## References

- (1) Zhang, Y.-J.; Li, S.; Gan, R.-Y.; Zhou, T.; Xu, D.-P.; Li, H.-B. Impacts of Gut Bacteria on Human Health and Diseases. *Int J Mol Sci* **2015**, *16* (12), 7493–7519. <https://doi.org/10.3390/ijms16047493>.
- (2) Hu, R.; Zhou, F.; Zhou, T.; Shen, J.; Wang, Z.; Zhao, Z.; Qin, A.; Tang, B. Z. Specific Discrimination of Gram-Positive Bacteria and Direct Visualization of Its Infection towards Mammalian Cells by a DPAN-Based AIEgen. *Biomaterials* **2018**, *187*, 47–54. <https://doi.org/10.1016/j.biomaterials.2018.09.019>.
- (3) Jeong, M.-C.; Jeon, D.; Shin, A.; Jin, S.; Shin, S. Y.; Park, Y. S.; Kim, Y. Effects of Hydrophobic Peptoid Substitutions on the Bacterial Cell Selectivity and Antimicrobial Activity of Piscidin 1. *Bull Korean Chem Soc* **2016**, *37* (10), 1545–1551. <https://doi.org/10.1002/bkcs.10959>.
- (4) Nikaido, H. Molecular Basis of Bacterial Outer Membrane Permeability Revisited. *Microbiology and Molecular Biology Reviews* **2003**, *67* (4), 593–656. <https://doi.org/10.1128/MMBR.67.4.593-656.2003>.
- (5) Mai-Prochnow, A.; Clauson, M.; Hong, J.; Murphy, A. B. Gram Positive and Gram Negative Bacteria Differ in Their Sensitivity to Cold Plasma. *Sci Rep* **2016**, *6* (1), 38610. <https://doi.org/10.1038/srep38610>.
- (6) Thanassi, D. G.; Bliska, J. B.; Christie, P. J. Surface Organelles Assembled by Secretion Systems of Gram-Negative Bacteria: Diversity in Structure and Function. *FEMS Microbiol Rev* **2012**, *36* (6), 1046–1082. <https://doi.org/10.1111/j.1574-6976.2012.00342.x>.
- (7) Scott, J. R.; Barnett, T. C. Surface Proteins of Gram-Positive Bacteria and How They Get There. *Annu Rev Microbiol* **2006**, *60* (1), 397–423. <https://doi.org/10.1146/annurev.micro.60.080805.142256>.
- (8) Scott, J. R.; Barnett, T. C. Surface Proteins of Gram-Positive Bacteria and How They Get There. *Annu Rev Microbiol* **2006**, *60* (1), 397–423. <https://doi.org/10.1146/annurev.micro.60.080805.142256>.
- (9) Thanassi, D. G.; Bliska, J. B.; Christie, P. J. Surface Organelles Assembled by Secretion Systems of Gram-Negative Bacteria: Diversity in Structure and Function. *FEMS Microbiol Rev* **2012**, *36* (6), 1046–1082. <https://doi.org/10.1111/j.1574-6976.2012.00342.x>.
- (10) Brennan, P. J. Structure, Function, and Biogenesis of the Cell Wall of Mycobacterium Tuberculosis. *Tuberculosis* **2003**, *83* (1–3), 91–97. [https://doi.org/10.1016/S1472-9792\(02\)00089-6](https://doi.org/10.1016/S1472-9792(02)00089-6).
- (11) Ramírez-Castillo, F.; Loera-Muro, A.; Jacques, M.; Garneau, P.; Avelar-González, F.; Harel, J.; Guerrero-Barrera, A. Waterborne Pathogens: Detection Methods and Challenges. *Pathogens* **2015**, *4* (2), 307–334. <https://doi.org/10.3390/pathogens4020307>.
- (12) Mirmajlessi, S. M.; Destefanis, M.; Gottsberger, R. A.; Mänd, M.; Loit, E. PCR-Based Specific Techniques Used for Detecting the Most Important Pathogens on Strawberry: A Systematic Review. *Syst Rev* **2015**, *4* (1), 9. <https://doi.org/10.1186/2046-4053-4-9>.
- (13) Fox, R. T. V. The Present and Future Use of Technology to Detect Plant Pathogens to Guide Disease Control in Sustainable Farming Systems. *Agric Ecosyst Environ* **1997**, *64* (2), 125–132. [https://doi.org/10.1016/S0167-8809\(97\)00030-3](https://doi.org/10.1016/S0167-8809(97)00030-3).
- (14) Rohde, A.; Hammerl, J. A.; Appel, B.; Dieckmann, R.; al Dahouk, S. FISHing for Bacteria in Food – A Promising Tool for the Reliable Detection of Pathogenic Bacteria? *Food Microbiol* **2015**, *46*, 395–407. <https://doi.org/10.1016/j.fm.2014.09.002>.
- (15) Agüero-Rosenfeld, M. E.; Kalantarpour, F.; Baluch, M.; Horowitz, H. W.; McKenna, D. F.; Raffalli, J. T.; Hsieh, T.; Wu, J.; Dumler, J. S.; Wormser, G. P. Serology of Culture-Confirmed Cases of Human Granulocytic Ehrlichiosis. *J Clin Microbiol* **2000**, *38* (2), 635–638. <https://doi.org/10.1128/JCM.38.2.635-638.2000>.

- (16) Foulds, I. v; Guy, R. A.; Kapoor, A.; Xiao, C.; Krull, U. J.; Horgen, P. A. Application of Quantitative Real-Time PCR with Dual-Labeled Hydrolysis Probes to Microbial Water Quality Monitoring. *J Biomol Tech* **2002**, *13* (4), 272–276.
- (17) Azeredo, J.; Azevedo, N. F.; Briandet, R.; Cerca, N.; Coenye, T.; Costa, A. R.; Desvaux, M.; di Bonaventura, G.; Hébraud, M.; Jaglic, Z.; Kačániová, M.; Knöchel, S.; Lourenço, A.; Mergulhão, F.; Meyer, R. L.; Nychas, G.; Simões, M.; Tresse, O.; Sternberg, C. Critical Review on Biofilm Methods. *Crit Rev Microbiol* **2017**, *43* (3), 313–351. <https://doi.org/10.1080/1040841X.2016.1208146>.
- (18) Sieuwerts, S.; de Bok, F. A. M.; Mols, E.; de Vos, W. M.; van Hylekama Vlieg, J. E. T. A Simple and Fast Method for Determining Colony Forming Units. *Lett Appl Microbiol* **2008**, *47* (4), 275–278. <https://doi.org/10.1111/j.1472-765X.2008.02417.x>.
- (19) Rajapaksha, P.; Elbourne, A.; Gangadoo, S.; Brown, R.; Cozzolino, D.; Chapman, J. A Review of Methods for the Detection of Pathogenic Microorganisms. *Analyst* **2019**, *144* (2), 396–411. <https://doi.org/10.1039/C8AN01488D>.
- (20) Chen, L.-K.; Arai, H.; Chen, L.-Y.; Chou, M.-Y.; Djauzi, S.; Dong, B.; Kojima, T.; Kwon, K. T.; Leong, H. N.; Leung, E. M. F.; Liang, C.-K.; Liu, X.; Mathai, D.; Pan, J. Y.; Peng, L.-N.; Poblete, E. R. S.; Poi, P. J. H.; Reid, S.; Tantawichien, T.; Won, C. W. Looking Back to Move Forward: A Twenty-Year Audit of Herpes Zoster in Asia-Pacific. *BMC Infect Dis* **2017**, *17* (1), 213. <https://doi.org/10.1186/s12879-017-2198-y>.
- (21) William B. Coleman. *Molecular Diagnostics*; Coleman, W. B., Tsongalis, G. J., Eds.; Humana Press: Totowa, NJ, 2005. <https://doi.org/10.1385/1592599281>.
- (22) Gensberger, E. T.; Gössl, E.-M.; Antonielli, L.; Sessitsch, A.; Kostić, T. Effect of Different Heterotrophic Plate Count Methods on the Estimation of the Composition of the Culturable Microbial Community. *PeerJ* **2015**, *3*, e862. <https://doi.org/10.7717/peerj.862>.
- (23) Cangelosi, G. A.; Meschke, J. S. Dead or Alive: Molecular Assessment of Microbial Viability. *Appl Environ Microbiol* **2014**, *80* (19), 5884–5891. <https://doi.org/10.1128/AEM.01763-14>.
- (24) Rajapaksha, P.; Elbourne, A.; Gangadoo, S.; Brown, R.; Cozzolino, D.; Chapman, J. A Review of Methods for the Detection of Pathogenic Microorganisms. *Analyst* **2019**, *144* (2), 396–411. <https://doi.org/10.1039/C8AN01488D>.
- (25) Fredericks, D. N.; Relman, D. A. Sequence-Based Identification of Microbial Pathogens: A Reconsideration of Koch's Postulates. *Clin Microbiol Rev* **1996**, *9* (1), 18–33. <https://doi.org/10.1128/CMR.9.1.18>.
- (26) Dincer, C.; Bruch, R.; Costa-Rama, E.; Fernández-Abedul, M. T.; Merkoçi, A.; Manz, A.; Urban, G. A.; Güder, F. Disposable Sensors in Diagnostics, Food, and Environmental Monitoring. *Advanced Materials* **2019**, 1806739. <https://doi.org/10.1002/adma.201806739>.
- (27) Khalilian, A.; Khan, Md. R. R.; Kang, S.-W. Highly Sensitive and Wide-Dynamic-Range Side-Polished Fiber-Optic Taste Sensor. *Sens Actuators B Chem* **2017**, *249*, 700–707. <https://doi.org/10.1016/j.snb.2017.04.088>.
- (28) Ivnitiski, D.; Abdel-Hamid, I.; Atanasov, P.; Wilkins, E. Biosensors for Detection of Pathogenic Bacteria. *Biosens Bioelectron* **1999**, *14* (7), 599–624. [https://doi.org/10.1016/S0956-5663\(99\)00039-1](https://doi.org/10.1016/S0956-5663(99)00039-1).
- (29) Bosch, M.; Sánchez, A.; Rojas, F.; Ojeda, C. Recent Development in Optical Fiber Biosensors. *Sensors* **2007**, *7* (6), 797–859. <https://doi.org/10.3390/s7060797>.
- (30) Diamantis, S. A.; Margariti, A.; Pournara, A. D.; Papaefstathiou, G. S.; Manos, M. J.; Lazarides, T. Luminescent Metal–Organic Frameworks as Chemical Sensors: Common Pitfalls and Proposed Best Practices. *Inorg Chem Front* **2018**, *5* (7), 1493–1511. <https://doi.org/10.1039/C8QI00090E>.
- (31) Mako, T. L.; Racicot, J. M.; Levine, M. Supramolecular Luminescent Sensors. *Chem Rev* **2019**, *119* (1), 322–477. <https://doi.org/10.1021/acs.chemrev.8b00260>.
- (32) Lehn, J.-M. Supramolecular Chemistry: Where from? Where To? *Chem Soc Rev* **2017**, *46* (9), 2378–2379. <https://doi.org/10.1039/C7CS00115K>.

- (33) Hein, R.; Beer, P. D.; Davis, J. J. Electrochemical Anion Sensing: Supramolecular Approaches. *Chem Rev* **2020**, *120* (3), 1888–1935. <https://doi.org/10.1021/acs.chemrev.9b00624>.
- (34) You, L.; Zha, D.; Anslyn, E. v. Recent Advances in Supramolecular Analytical Chemistry Using Optical Sensing. *Chem Rev* **2015**, *115* (15), 7840–7892. <https://doi.org/10.1021/cr5005524>.
- (35) Inouye, M.; Hashimoto, K.; Isagawa, K. Nondestructive Detection of Acetylcholine in Protic Media: Artificial-Signaling Acetylcholine Receptors. *J Am Chem Soc* **1994**, *116* (12), 5517–5518. <https://doi.org/10.1021/ja00091a085>.
- (36) Boerrigter, H.; Grave, L.; Nissink, J. W. M.; Chrisstoffels, L. A. J.; van der Maas, J. H.; Verboom, W.; de Jong, F.; Reinhoudt, D. N. (Thio)Urea Resorcinarene Cavitands. Complexation and Membrane Transport of Halide Anions. *J Org Chem* **1998**, *63* (13), 4174–4180. <https://doi.org/10.1021/jo9721271>.
- (37) Rather, I. A.; Wagay, S. A.; Ali, R. Emergence of Anion- $\pi$  Interactions: The Land of Opportunity in Supramolecular Chemistry and Beyond. *Coord Chem Rev* **2020**, *415*, 213327. <https://doi.org/10.1016/j.ccr.2020.213327>.
- (38) Ahmad Rather, I.; Ali, R. Anion- $\pi$  Catalysis: A Novel Supramolecular Approach for Chemical and Biological Transformations. In *Current Topics in Chirality - From Chemistry to Biology*; IntechOpen, 2021. <https://doi.org/10.5772/intechopen.95824>.
- (39) Wu, J.; Kwon, B.; Liu, W.; Anslyn, E. v.; Wang, P.; Kim, J. S. Chromogenic/Fluorogenic Ensemble Chemosensing Systems. *Chem Rev* **2015**, *115* (15), 7893–7943. <https://doi.org/10.1021/cr500553d>.
- (40) Zhu, L.; Shabbir, S. H.; Gray, M.; Lynch, V. M.; Sorey, S.; Anslyn, E. v. A Structural Investigation of the N–B Interaction in an *o*-(*N,N*-Dialkylaminomethyl)Arylboronate System. *J Am Chem Soc* **2006**, *128* (4), 1222–1232. <https://doi.org/10.1021/ja055817c>.
- (41) Phillips, R. L.; Miranda, O. R.; You, C.-C.; Rotello, V. M.; Bunz, U. H. F. Rapid and Efficient Identification of Bacteria Using Gold-Nanoparticle–Poly(Para-Phenyleneethynylene) Constructs. *Angewandte Chemie International Edition* **2008**, *47* (14), 2590–2594. <https://doi.org/10.1002/anie.200703369>.
- (42) Zhou, Q.; Swager, T. M. Fluorescent Chemosensors Based on Energy Migration in Conjugated Polymers: The Molecular Wire Approach to Increased Sensitivity. *J Am Chem Soc* **1995**, *117* (50), 12593–12602. <https://doi.org/10.1021/ja00155a023>.
- (43) Perret, F.; Coleman, A. W. Biochemistry of Anionic Calix[n]Arenes. *Chemical Communications* **2011**, *47* (26), 7303. <https://doi.org/10.1039/c1cc11541c>.
- (44) Sansone, F.; Baldini, L.; Casnati, A.; Ungaro, R. Calixarenes: From Biomimetic Receptors to Multivalent Ligands for Biomolecular Recognition. *New Journal of Chemistry* **2010**, *34* (12), 2715. <https://doi.org/10.1039/c0nj00285b>.
- (45) Dondoni, A.; Marra, A. Calixarene and Calixresorcurene Glycosides: Their Synthesis and Biological Applications. *Chem Rev* **2010**, *110* (9), 4949–4977. <https://doi.org/10.1021/cr100027b>.
- (46) Baldini, L.; Casnati, A.; Sansone, F.; Ungaro, R. Calixarene-Based Multivalent Ligands. *Chem. Soc. Rev.* **2007**, *36* (2), 254–266. <https://doi.org/10.1039/B603082N>.
- (47) Giuliani, M.; Morbioli, I.; Sansone, F.; Casnati, A. Moulding Calixarenes for Biomacromolecule Targeting. *Chemical Communications* **2015**, *51* (75), 14140–14159. <https://doi.org/10.1039/C5CC05204A>.
- (48) Galante, E.; Geraci, C.; Sciuto, S.; Campo, V. L.; Carvalho, I.; Sesti-Costa, R.; Guedes, P. M. M.; Silva, J. S.; Hill, L.; Nepogodiev, S. A.; Field, R. A. Glycoclusters Presenting Lactose on Calix[4]Arene Cores Display Trypanocidal Activity. *Tetrahedron* **2011**, *67* (33), 5902–5912. <https://doi.org/10.1016/j.tet.2011.06.065>.



- (49) Mourer, M.; Duval, R. E.; Finance, C.; Regnouf-de-Vains, J.-B. Functional Organisation and Gain of Activity: The Case of the Antibacterial Tetra-Para-Guanidinoethyl-Calix[4]Arene. *Bioorg Med Chem Lett* **2006**, *16* (11), 2960–2963. <https://doi.org/10.1016/j.bmcl.2006.02.072>.
- (50) Mourer, M.; Dibama, H. M.; Fontanay, S.; Grare, M.; Duval, R. E.; Finance, C.; Regnouf-de-Vains, J.-B. P-Guanidinoethyl Calixarene and Parent Phenol Derivatives Exhibiting Antibacterial Activities. Synthesis and Biological Evaluation. *Bioorg Med Chem* **2009**, *17* (15), 5496–5509. <https://doi.org/10.1016/j.bmc.2009.06.040>.
- (51) Mourer, M.; Psychogios, N.; Laumond, G.; Aubertin, A.-M.; Regnouf-de-Vains, J.-B. Synthesis and Anti-HIV Evaluation of Water-Soluble Calixarene-Based Bithiazolyl Podands. *Bioorg Med Chem* **2010**, *18* (1), 36–45. <https://doi.org/10.1016/j.bmc.2009.11.016>.
- (52) Dudic, M.; Colombo, A.; Sansone, F.; Casnati, A.; Donofrio, G.; Ungaro, R. A General Synthesis of Water Soluble Upper Rim Calix[n]Arene Guanidinium Derivatives Which Bind to Plasmid DNA. *Tetrahedron* **2004**, *60* (50), 11613–11618. <https://doi.org/10.1016/j.tet.2004.09.047>.
- (53) Takeuchi, T.; Bagnacani, V.; Sansone, F.; Matile, S. Amphiphilic Counterion Activators for DNA: Stimuli-Responsive Cation Transporters and Biosensors in Bulk and Lipid Bilayer Membranes. *ChemBioChem* **2009**, *10* (17), 2793–2799. <https://doi.org/10.1002/cbic.200900512>.
- (54) Bagnacani, V.; Sansone, F.; Donofrio, G.; Baldini, L.; Casnati, A.; Ungaro, R. Macrocyclic Nonviral Vectors: High Cell Transfection Efficiency and Low Toxicity in a Lower Rim Guanidinium Calix[4]Arene. *Org Lett* **2008**, *10* (18), 3953–3956. <https://doi.org/10.1021/ol801326d>.
- (55) Sansone, F.; Dudič, M.; Donofrio, G.; Rivetti, C.; Baldini, L.; Casnati, A.; Cellai, S.; Ungaro, R. DNA Condensation and Cell Transfection Properties of Guanidinium Calixarenes: Dependence on Macrocyclic Lipophilicity, Size, and Conformation. *J Am Chem Soc* **2006**, *128* (45), 14528–14536. <https://doi.org/10.1021/ja0634425>.
- (56) Lalor, R.; DiGesso, J. L.; Mueller, A.; Matthews, S. E. Efficient Gene Transfection with Functionalised Multicalixarenes. *Chemical Communications* **2007**, No. 46, 4907. <https://doi.org/10.1039/b712100h>.
- (57) Bagnacani, V.; Franceschi, V.; Bassi, M.; Lomazzi, M.; Donofrio, G.; Sansone, F.; Casnati, A.; Ungaro, R. Arginine Clustering on Calix[4]Arene Macrocycles for Improved Cell Penetration and DNA Delivery. *Nat Commun* **2013**, *4* (1), 1721. <https://doi.org/10.1038/ncomms2721>.
- (58) Gasparello, J.; Lomazzi, M.; Papi, C.; D'Aversa, E.; Sansone, F.; Casnati, A.; Donofrio, G.; Gambari, R.; Finotti, A. Efficient Delivery of MicroRNA and AntimiRNA Molecules Using an Argininocalix[4]Arene Macrocyclic. *Mol Ther Nucleic Acids* **2019**, *18*, 748–763. <https://doi.org/10.1016/j.omtn.2019.09.029>.
- (59) Gasparello, J.; Manicardi, A.; Casnati, A.; Corradini, R.; Gambari, R.; Finotti, A.; Sansone, F. Efficient Cell Penetration and Delivery of Peptide Nucleic Acids by an Argininocalix[4]Arene. *Sci Rep* **2019**, *9* (1), 3036. <https://doi.org/10.1038/s41598-019-39211-4>.
- (60) da Silva, C. M.; da Silva, D. L.; Magalhães, T. F. F.; Alves, R. B.; de Resende-Stoianoff, M. A.; Martins, F. T.; de Fátima, Â. Iminecalix[4]Arenes: Microwave-Assisted Synthesis, X-Ray Crystal Structures, and Anticandidal Activity. *Arabian Journal of Chemistry* **2019**, *12* (8), 4365–4376. <https://doi.org/10.1016/j.arabjc.2016.06.013>.
- (61) Bezouška, K. Design, Functional Evaluation and Biomedical Applications of Carbohydrate Dendrimers (Glycodendrimers). *Reviews in Molecular Biotechnology* **2002**, *90* (3–4), 269–290. [https://doi.org/10.1016/S1389-0352\(01\)00064-2](https://doi.org/10.1016/S1389-0352(01)00064-2).
- (62) Guo, D.-S.; Uzunova, V. D.; Su, X.; Liu, Y.; Nau, W. M. Operational Calixarene-Based Fluorescent Sensing Systems for Choline and Acetylcholine and Their Application to Enzymatic Reactions. *Chem Sci* **2011**, *2* (9), 1722. <https://doi.org/10.1039/c1sc00231g>.

- (63) Erfani, A.; Seaberg, J.; Aichele, C. P.; Ramsey, J. D. Interactions between Biomolecules and Zwitterionic Moieties: A Review. *Biomacromolecules* **2020**, *21* (7), 2557–2573. <https://doi.org/10.1021/acs.biomac.0c00497>.
- (64) Zhang, C.; Sun, Y.; Dong, X. Conjugation of a Zwitterionic Polymer with Dimethyl Chains to Lipase Significantly Increases the Enzyme Activity and Stability. *Chin J Chem Eng* **2022**, *47*, 48–53. <https://doi.org/10.1016/j.cjche.2021.04.023>.
- (65) Schlenoff, J. B. Zwitteration: Coating Surfaces with Zwitterionic Functionality to Reduce Nonspecific Adsorption. *Langmuir* **2014**, *30* (32), 9625–9636. <https://doi.org/10.1021/la500057j>.
- (66) Yuan, Y.-Y.; Mao, C.-Q.; Du, X.-J.; Du, J.-Z.; Wang, F.; Wang, J. Surface Charge Switchable Nanoparticles Based on Zwitterionic Polymer for Enhanced Drug Delivery to Tumor. *Advanced Materials* **2012**, *24* (40), 5476–5480. <https://doi.org/10.1002/adma.201202296>.
- (67) Huang, P.; Liu, J.; Wang, W.; Zhang, Y.; Zhao, F.; Kong, D.; Liu, J.; Dong, A. Zwitterionic Nanoparticles Constructed from Bioreducible RAFT–ROP Double Head Agent for Shell Shedding Triggered Intracellular Drug Delivery. *Acta Biomater* **2016**, *40*, 263–272. <https://doi.org/10.1016/j.actbio.2015.11.038>.
- (68) Cao, Z.; Zhang, L.; Jiang, S. Superhydrophilic Zwitterionic Polymers Stabilize Liposomes. *Langmuir* **2012**, *28* (31), 11625–11632. <https://doi.org/10.1021/la302433a>.
- (69) Becker, T.; Yong Goh, C.; Jones, F.; McIlldowie, M. J.; Mocerino, M.; Ogden, M. I. Proline-Functionalised Calix[4]Arene: An Anion-Triggered Hydrogelator. *Chemical Communications* **2008**, No. 33, 3900. <https://doi.org/10.1039/b807248e>.
- (70) Zhang, J.; Guo, D.-S.; Wang, L.-H.; Wang, Z.; Liu, Y. Supramolecular Binary Hydrogels from Calixarenes and Amino Acids and Their Entrapment–Release of Model Dye Molecules. *Soft Matter* **2011**, *7* (5), 1756–1762. <https://doi.org/10.1039/C0SM01041C>.
- (71) Oguz, M.; Gul, A.; Karakurt, S.; Yilmaz, M. Synthesis and Evaluation of the Antitumor Activity of Calix[4]Arene 1-Proline Derivatives. *Bioorg Chem* **2020**, *94*, 103207. <https://doi.org/10.1016/j.bioorg.2019.103207>.
- (72) Fu, D.; Lu, T.; Liu, Y.; Li, F.; Ogden, M. I.; Wang, Y.; Wu, Y.; Mocerino, M. Enantioselective Inhibition of Human Papillomavirus L1 Pentamer Formation by Chiral-Proline Modified Calix[4]Arenes: Targeting the Protein Interface. *ChemistrySelect* **2016**, *1* (19), 6243–6249. <https://doi.org/10.1002/slct.201601467>.
- (73) Yang, L.-M.; Zheng, Y.-S.; Huang, Z.-T. Nucleophilic Substitution of *P*-Halomethylcalix[4]Arene. *Synth Commun* **1999**, *29* (24), 4451–4460. <https://doi.org/10.1080/00397919908086609>.
- (74) Verkade, J. M. M.; Hemert, L. J. C. van; Quaedflieg, P. J. L. M.; Rutjes, F. P. J. T. Organocatalysed Asymmetric Mannich Reactions. *Chem. Soc. Rev.* **2008**, *37* (1), 29–41. <https://doi.org/10.1039/B713885G>.
- (75) Córdova, A. The Direct Catalytic Asymmetric Mannich Reaction. *Acc Chem Res* **2004**, *37* (2), 102–112. <https://doi.org/10.1021/ar030231l>.
- (76) Agababyan, A. G.; Gevorgyan, G. A.; Mndzhoyan, O. L. Aminoacids as the Amine Component in the Mannich Reaction. *Russian Chemical Reviews* **1982**, *51* (4), 387–396. <https://doi.org/10.1070/RC1982v051n04ABEH002848>.
- (77) Gutsche, C. David.; Nam, K. Chun. Calixarenes. 22. Synthesis, Properties, and Metal Complexation of Aminocalixarenes. *J Am Chem Soc* **1988**, *110* (18), 6153–6162. <https://doi.org/10.1021/ja00226a034>.
- (78) Atwood, J. L.; Szumna, A. Hydrogen Bonds Seal Single-Molecule Capsules. *J Am Chem Soc* **2002**, *124* (36), 10646–10647. <https://doi.org/10.1021/ja027191l>.
- (79) Atwood, J. L.; Orr, G. W.; Robinson, K. D.; Hamada, F. Calixarenes as Enzyme Models. *Supramol Chem* **1993**, *2* (4), 309–317. <https://doi.org/10.1080/10610279308029824>.
- (80) Barker, E. C.; Martin, A. D.; Garvey, C. J.; Goh, C. Y.; Jones, F.; Mocerino, M.; Skelton, B. W.; Ogden, M. I.; Becker, T. Thermal Annealing Behaviour and Gel to Crystal Transition of

- a Low Molecular Weight Hydrogelator. *Soft Matter* **2017**, *13* (5), 1006–1011. <https://doi.org/10.1039/C6SM02431A>.
- (81) Goh C. Y. Amino Acid Functionalised Calixarenes: Crystal Growth Modifiers and Low Molecular Weight Gelators, Curtin University, Perth, 2012.
- (82) Arduini, A.; Fabbi, M.; Mantovani, M.; Mirone, L.; Pochini, A.; Secchi, A.; Ungaro, R. Calix[4]Arenes Blocked in a Rigid Cone Conformation by Selective Functionalization at the Lower Rim. *J Org Chem* **1995**, *60* (5), 1454–1457. <https://doi.org/10.1021/jo00110a055>.
- (83) Gutsche, C. D. *Calixarenes Revisited*; Royal Society of Chemistry: Cambridge, 1998. <https://doi.org/10.1039/9781847550293>.
- (84) Lepre, C. A.; Moore, J. M.; Peng, J. W. Theory and Applications of NMR-Based Screening in Pharmaceutical Research. *Chem Rev* **2004**, *104* (8), 3641–3676. <https://doi.org/10.1021/cr030409h>.
- (85) Meyer, B.; Peters, T. NMR Spectroscopy Techniques for Screening and Identifying Ligand Binding to Protein Receptors. *Angewandte Chemie International Edition* **2003**, *42* (8), 864–890. <https://doi.org/10.1002/anie.200390233>.
- (86) Viegas, A.; Manso, J.; Nobrega, F. L.; Cabrita, E. J. Saturation-Transfer Difference (STD) NMR: A Simple and Fast Method for Ligand Screening and Characterization of Protein Binding. *J Chem Educ* **2011**, *88* (7), 990–994. <https://doi.org/10.1021/ed101169t>.
- (87) Viegas, A.; Manso, J.; Nobrega, F. L.; Cabrita, E. J. Saturation-Transfer Difference (STD) NMR: A Simple and Fast Method for Ligand Screening and Characterization of Protein Binding. *J Chem Educ* **2011**, *88* (7), 990–994. <https://doi.org/10.1021/ed101169t>.
- (88) Airoidi, C.; Colombo, L.; Manzoni, C.; Sironi, E.; Natalello, A.; Doglia, S. M.; Forloni, G.; Tagliavini, F.; del Favero, E.; Cantù, L.; Nicotra, F.; Salmona, M. Tetracycline Prevents A $\beta$  Oligomer Toxicity through an Atypical Supramolecular Interaction. *Org. Biomol. Chem.* **2011**, *9* (2), 463–472. <https://doi.org/10.1039/C0OB00303D>.
- (89) Airoidi, C.; Sommaruga, S.; Merlo, S.; Sperandeo, P.; Cipolla, L.; Polissi, A.; Nicotra, F. Targeting Bacterial Membranes: Identification of *Pseudomonas Aeruginosa*D-Arabinose-5P Isomerase and NMR Characterisation of Its Substrate Recognition and Binding Properties. *ChemBioChem* **2011**, *12* (5), 719–727. <https://doi.org/10.1002/cbic.201000754>.
- (90) Airoidi, C.; Sommaruga, S.; Merlo, S.; Sperandeo, P.; Cipolla, L.; Polissi, A.; Nicotra, F. Targeting Bacterial Membranes: NMR Spectroscopy Characterization of Substrate Recognition and Binding Requirements of D-Arabinose-5-Phosphate Isomerase. *Chemistry - A European Journal* **2010**, *16* (6), 1897–1902. <https://doi.org/10.1002/chem.200902619>.
- (91) Airoidi, C.; Palmioli, A.; D'Urzo, A.; Colombo, S.; Vanoni, M.; Martegani, E.; Peri, F. Glucose-Derived Ras Pathway Inhibitors: Evidence of Ras–Ligand Binding and Ras–GEF (Cdc25) Interaction Inhibition. *ChemBioChem* **2007**, *8* (12), 1376–1379. <https://doi.org/10.1002/cbic.200700185>.
- (92) Palmioli, A.; Sacco, E.; Airoidi, C.; di Nicolantonio, F.; D'Urzo, A.; Shirasawa, S.; Sasazuki, T.; di Domizio, A.; de Gioia, L.; Martegani, E.; Bardelli, A.; Peri, F.; Vanoni, M. Selective Cytotoxicity of a Bicyclic Ras Inhibitor in Cancer Cells Expressing K-RasG13D. *Biochem Biophys Res Commun* **2009**, *386* (4), 593–597. <https://doi.org/10.1016/j.bbrc.2009.06.069>.
- (93) Caraballo, R.; Dong, H.; Ribeiro, J. P.; Jiménez-Barbero, J.; Ramström, O. Direct STD NMR Identification of  $\beta$ -Galactosidase Inhibitors from a Virtual Dynamic Hemithioacetal System. *Angewandte Chemie International Edition* **2010**, *49* (3), 589–593. <https://doi.org/10.1002/anie.200903920>.
- (94) Claasen, B.; Axmann, M.; Meinecke, R.; Meyer, B. Direct Observation of Ligand Binding to Membrane Proteins in Living Cells by a Saturation Transfer Double Difference (STDD) NMR Spectroscopy Method Shows a Significantly Higher Affinity of Integrin  $\alpha_{IIb}\beta_3$  in Native Platelets than in Liposomes. *J Am Chem Soc* **2005**, *127* (3), 916–919. <https://doi.org/10.1021/ja044434w>.

- (95) Mari, S.; Serrano-Gómez, D.; Cañada, F. J.; Corbí, A. L.; Jiménez-Barbero, J. 1D Saturation Transfer Difference NMR Experiments on Living Cells: The DC-SIGN/Oligomannose Interaction. *Angewandte Chemie* **2005**, *117* (2), 300–302. <https://doi.org/10.1002/ange.200461574>.
- (96) Airoidi, C.; Giovannardi, S.; La Ferla, B.; Jiménez-Barbero, J.; Nicotra, F. Saturation Transfer Difference NMR Experiments of Membrane Proteins in Living Cells under HR-MAS Conditions: The Interaction of the SGLT1 Co-Transporter with Its Ligands. *Chemistry - A European Journal* **2011**, *17* (48), 13395–13399. <https://doi.org/10.1002/chem.201102181>.
- (97) Bruno, E.; Digilio, G.; Cabella, C.; de Reggi, A.; Baroni, S.; Mainero, V.; Aime, S. Water Exchange across the Erythrocyte Plasma Membrane Studied by HR-MAS NMR Spectroscopy. *Magn Reson Med* **2006**, *56* (5), 978–985. <https://doi.org/10.1002/mrm.21054>.
- (98) Eloisa Tosi. Methylsulfonate and Methylphosphonate Functionalized Calix[4]Arenes for the Complexation of Ammonium Salts, University of Parma, Parma, 2021.
- (99) Becker, T.; Yong Goh, C.; Jones, F.; McIldowie, M. J.; Mocerino, M.; Ogden, M. I. Proline-Functionalised Calix[4]Arene: An Anion-Triggered Hydrogelator. *Chemical Communications* **2008**, No. 33, 3900. <https://doi.org/10.1039/b807248e>.
- (100) Jaime, C.; de Mendoza, J.; Prados, P.; Nieto, P. M.; Sanchez, C. Carbon-13 NMR Chemical Shifts. A Single Rule to Determine the Conformation of Calix[4]Arenes. *J Org Chem* **1991**, *56* (10), 3372–3376. <https://doi.org/10.1021/jo00010a036>.
- (101) Arena, G.; Cali, R.; Lombardo, G. G.; Rizzarelli, E.; Sciotto, D.; Ungaro, R.; Casnati, A. Water Soluble Calix[4]Arenes. A Thermodynamic Investigation of Proton Complex Formation. *Supramol Chem* **1992**, *1* (1), 19–24. <https://doi.org/10.1080/10610279208027437>.
- (102) Buckley, B. R.; Boxhall, J. Y.; Page, P. C. B.; Chan, Y.; Elsegood, M. R. J.; Heaney, H.; Holmes, K. E.; McIldowie, M. J.; McKee, V.; McGrath, M. J.; Mocerino, M.; Poulton, A. M.; Sampler, E. P.; Skelton, B. W.; White, A. H. Mannich And O-Alkylation Reactions of Tetraalkoxyresorcin[4]Arenes – The Use of Some Products in Ligand-Assisted Reactions. *European J Org Chem* **2006**, *2006* (22), 5117–5134. <https://doi.org/10.1002/ejoc.200600590>.
- (103) Shatalova, N. I.; Gavrilova, E. L.; Sidorov, N. A.; Burilovb, A. R.; Pudovik, M. A.; Krasil'nikova, E. A.; Konovalov, A. I. Calix[4]Resorcinols Functionalized with Amino Acid Residues. *Russ J Gen Chem* **2009**, *79* (7), 1494–1498. <https://doi.org/10.1134/S1070363209070159>.
- (104) Viegas, A.; Manso, J.; Nobrega, F. L.; Cabrita, E. J. Saturation-Transfer Difference (STD) NMR: A Simple and Fast Method for Ligand Screening and Characterization of Protein Binding. *J Chem Educ* **2011**, *88* (7), 990–994. <https://doi.org/10.1021/ed101169t>.
- (105) Walrant, A.; Bechara, C.; Alves, I. D.; Sagan, S. Molecular Partners for Interaction and Cell Internalization of Cell-Penetrating Peptides: How Identical Are They? *Nanomedicine* **2012**, *7* (1), 133–143. <https://doi.org/10.2217/nnm.11.165>.
- (106) Becker, T.; Yong Goh, C.; Jones, F.; McIldowie, M. J.; Mocerino, M.; Ogden, M. I. Proline-Functionalised Calix[4]Arene: An Anion-Triggered Hydrogelator. *Chemical Communications* **2008**, No. 33, 3900. <https://doi.org/10.1039/b807248e>.



# Chapter 4

## **Calix[4]arenes-based ligands for protein surface recognition\***

\*This work has been carried out in the group of Prof. Peter B. Crowley at University of Galway (Ireland).

# Introduction

## 4.1 Protein

Proteins<sup>1</sup> are big macromolecules that have several roles in living organisms. They are made up of one or more polypeptide sequences that give them a complex and distinctive 3D structure known as protein folding<sup>2</sup> and define their specific biological function. Proteins are recognized to act as enzymes and antibodies in living organisms, catalysing many type of biological transformations<sup>3</sup> and overseeing immune response activation<sup>4</sup>, respectively. They also contribute in cell signaling<sup>5,6</sup> acting as selective receptors on the cell surface to regulate cell proliferation, growth, and differentiation<sup>7</sup>, and transporting or storing numerous types of chemicals across the cell membrane. Protein receptors are often also the targets of viruses and bacteria to attach the cell membrane<sup>7</sup>, and in cancer, where they may enhance metastasis growth and its spread.<sup>8,9</sup> Furthermore, proteins can play a variety of crucial mechanical and structural roles, since they are constituents of connective tissues, cell cytoskeletons, animal shells, and muscles.<sup>6,10,11</sup> The identification of particular counterparts, which can be macromolecules such as nucleic acids, polysaccharides, and other proteins, or tiny molecules such as oxygen, metal cations, peptides, and other forms of ligands<sup>12–14</sup>, is a property shared by all proteins. To properly understand how these processes occur, it is critical to get the most detailed characterization of the mechanism of the interactions involving the given protein-ligand pair, both energetically<sup>15,16</sup> and structurally.<sup>17,18</sup> Understanding the nature of these interactions will help medicinal chemists to propose drug to inhibit or, on the contrary, restore the (self)recognition functions lost as a result of alterations, aiding in the development of effective therapies. Indeed, many drugs are already on the market, which are often also mimics of their natural substrates and interact with target proteins to interfere with or control their function. In details, these interactions may either prevent protein aggregation<sup>19</sup> or particular protein-protein interactions<sup>20</sup>, which have a pathological effect on the human body, or they can promote, control, and maintain oligomerization processes<sup>20</sup>, which have a

favourable physiological effect. To improve the binding efficiency and selectivity of designed ligands, chemists try to optimize the complementarity of their lead compounds with the selected counterparts in protein structures, identifying hydrophobic domains, charged groups, polarized residues, hydrogen bonding donors and acceptors, and their reciprocal positions and distances. Moreover, for targets with relatively extended surfaces or multiple binding sites a powerful tool, multivalency, can be also taken in account to give a helpful contribution.

## 4.2 Multivalency

Multivalency<sup>21</sup> is the capacity of one entity, particle, or molecule to bind another entity, particle, or molecule at the same time, producing several binding site-ligand complexes or contacts, each governed by non-covalent interactions (Figure 1). Nature exploits multivalency as a potent tool to produce selective and strong, yet reversible interactions, especially when the single complex formed by the substrate and the corresponding binding site is relatively low ( $K_D$  in the millimolar range). One of the most fundamental characteristics of a multivalent interaction is that it increases the overall binding constant in comparison to the sum of the binding constants of the equivalent single monovalent events.

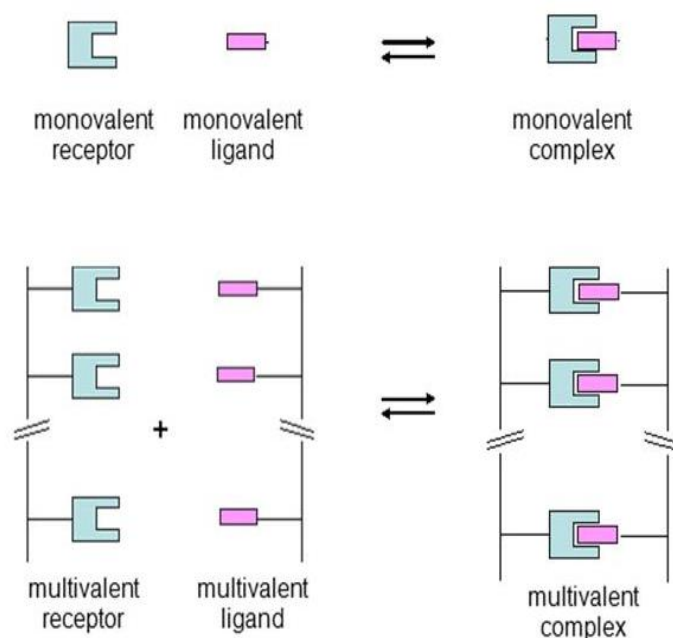


**Fig. 1:** monovalent and multivalent complex formation comparison<sup>22</sup>

A multivalent ligand can bind to a multivalent receptor in a variety of ways (Figure 1). The initial contact is obviously intermolecular. Following that, once a complexed form has been



created, both inter- and intra-binding events are possible. If the former is predominant, the binding results in intermolecular aggregates of varied stoichiometry; if the latter is predominant, the binding results in the creation of a 1:1 receptor-ligand multivalent complex. Multivalency is also typically associated with a positive avidity entropy, a statistical term that grows fast with complex valency, constantly favoring binding and compensating for the loss of conformational entropy that occurs during multivalent complex formation. According to Jenks<sup>23</sup>, the following formula may be used to a multivalent binding from a thermodynamic perspective:

$$\text{eq 1)} \quad \Delta G^{\circ}_{\text{multi}} = n \Delta G^{\circ}_{\text{mono}} + \Delta G^{\circ}_{\text{interaction}}$$

where  $\Delta G^{\circ}_{\text{mono}}$  is the standard free energy provided by a ligand monovalent binding to a receptor and  $\Delta G^{\circ}_{\text{multi}}$  is the standard free energy provided by a multivalent ligand in the interaction with the same receptor.  $\Delta G^{\circ}_{\text{multi}}$  takes into account avidity ( $\Delta G^{\circ}_{\text{interaction}}$ ), which is an extra free energy component that balances the positive and negative impacts of tethering. Kitov and Bundle<sup>24</sup> proposed a new parameter to simplify thermodynamic analysis by rearranging the terms in eq 1, based on the idea that multivalent interactions are the consequence of an initial intermolecular binding, followed by subsequent intramolecular interactions. As a result,  $\Delta G^{\circ}_{\text{mono}} = \Delta G^{\circ}_{\text{inter}}$ , which is distinct from the free energy of all future interactions  $(n-1) \Delta G^{\circ}_{\text{intra}} = (n-1) \Delta G^{\circ}_{\text{mono}} + \Delta G^{\circ}_{\text{interaction}}$ . As a consequence, the following eq.2 is valid:

$$\text{eq 2)} \quad \Delta G^{\circ}_{\text{multi}} = n \Delta G^{\circ}_{\text{inter}} + (n-1) \Delta G^{\circ}_{\text{intra}} - RT \ln \Omega_n$$

governed by the Boltzmann-like distribution law. A third term ( $- RT \ln \Omega_n$ ) was added to eq 2, which conforms with the generalized Boltzmann-Gibbs concept of entropy and is given in entropy units. This last element was given the label of "avidity entropy,"  $\Delta S^{\circ}_{\text{avidity}}$ , because it expresses the probability of the interaction rather than its strength. Furthermore, because it measures the chaos in the distribution of microscopically different complexes, this form of entropy is specific to multivalent interactions. When the number of binding sites per protein receptor and the number of ligand branches increase consistently,  $\Delta S^{\circ}_{\text{avidity}}$  may not always be favourable. In fact, Kitov and Bundle explore an interaction between an oligomeric protein receptor and a multivalent ligand under the two limiting circumstances. The first is that all of the  $n$  receptor binding sites and all of the branches of the multivalent ligand are independent but have similar binding characteristics. The second is that only one multivalent ligand may

attach to the oligomeric receptor at a time. If, upon formation of the complex, the steric crowding increases, it may happen that no additional interaction can occur or they take place less favourably than in the monovalent binding, even with vacant binding sites. As a consequence, the number of available binding sites decreases consistently and  $\Delta S^{\circ}_{\text{avidity}}$  becomes unfavourable.

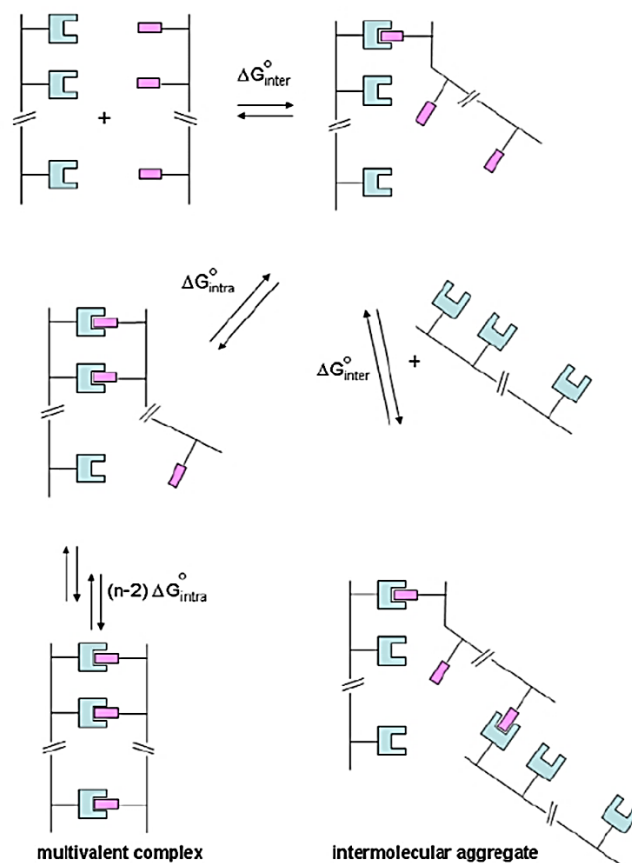


**Fig. 2:** Different ways in which a multivalent ligand can bind to a multivalent receptor<sup>22</sup>

To quantitatively evaluate multivalency, Whitesides and co-workers<sup>25</sup> created the enhancement factor  $\beta$ . This is the ratio between a multivalent ligand binding constant ( $K_{\text{multi}}$ ) for a multivalent binding to a multivalent receptor and a monovalent ligand binding constant ( $K_{\text{mono}}$ ) for monovalent binding to the same multivalent receptor:

$$\text{eq 3)} \quad \beta = K_{\text{multi}}/K_{\text{mono}}$$

When  $\beta \gg 1$  there is a clear positive effect in tethering monovalent ligands in a multivalent one. This enhancement factor has the advantage of being used even if the number of the

effective single binding interactions is unknown. One disadvantage is that it does not allow to properly evaluate the effects of cooperativity<sup>26</sup> and of the symmetry effect.

Another parameter often used to evaluate multivalency is the relative potency (rp), which is defined as the ratio of the IC<sub>50</sub> values of the monovalent ligand (IC<sub>50</sub> mono) and the multivalent ligand (IC<sub>50</sub> multi):

$$\text{eq 4) } \quad rp = IC_{50 \text{ mono}} / IC_{50 \text{ multi}}$$

where the IC<sub>50</sub> value of a substance is the concentration required to block the examined process by 50% and provides a measure of its efficacy. Also in this case if  $rp \gg 1$  there is a positive effect of the multivalent ligand.

When the cluster valency  $n$  is known, the enhancement factor and relative potency  $rp$  can both be normalised by dividing their values by  $n$ , yielding the  $\beta/n$  and  $rp/n$  parameters, which measure the gain of each ligating unit obtained by its multivalent presentation in comparison to the same ligating unit used alone in a monovalent interaction with the multivalent receptor. These characteristics are excellent tools for comparing the efficiency of clusters with varying valency, topology, and linker. Clusters with high  $\beta/n$  or  $rp/n$  values ( $\gg 1$ ) are more efficient ligands/inhibitors than their monovalent counterpart (the single ligating unit) and thus have a positive multivalent effect, whereas clusters with low  $\beta/n$  or  $rp/n$  values have a lower affinity/inhibition than the monovalent ligand and thus have a negative multivalent effect.  $\beta/n$  or  $rp/n$  values lower than 1 indicate there are only disadvantages in linking monovalent units together.

Based on these concerns and information, in recent years, numerous research groups interested in the creation of protein ligands have used multivalency to design and manufacture multivalent systems as potentially extremely effective protein modulators. Numerous copies of multivalent ligands have unique features because they can probe multivalent cell/protein surfaces with multiple binding events. They also offer several benefits since the scaffold structure, identity of binding elements, number of binding units, and linker joining ligating units to the scaffold may all be changed systematically based on the structural and chemical characteristics of the target proteins<sup>27</sup>. Furthermore, protein-protein or protein-ligand interactions need a high amount of preorganization in some circumstances. Multivalent ligands can exhibit many copies of the ligating units in a pre-organized manner, giving these

designed compounds unusual features. There are various scaffold families with varying structure, flexibility, and valency that are crucial in the synthesis of synthetic multivalent ligands for targeting protein-protein and protein-ligand interactions<sup>28</sup>. They differ chemically, but they often have a central core, the scaffold, that carries multiple covalent connections that determine the valency of the cluster, linkers or spacers, and peripheral functions or ligating units.

### **4.3 X-ray crystallography as a technique for the study of protein-ligand interactions**

Several experimental approaches may be used to investigate the various aspects of protein-ligand interactions. X-ray crystallography, nuclear magnetic resonance (NMR), Laue X-ray diffraction, small-angle X-ray scattering, transmission electron microscopy (TEM), scanning electron microscopy (SEM), and cryo-electron microscopy (cryo-EM) provide (near-)atomic-resolution of the structure of protein ligand-complexes and related larger aggregates while isothermal titration calorimetry (ITC) is the most effective method for obtaining a comprehensive thermodynamic characterization of the corresponding binding processes<sup>29</sup>. Among them one of the most dependable method for determining the structural characterisation of these processes in the solid state continues to be X-ray diffraction of protein-ligand co-crystals.<sup>30-32</sup> Since the three-dimensional structure of these macromolecules governs their functionality, protein crystallization is a potent technique to get definitive structural information. To create therapeutic treatments and novel medications, it is imperative to be able to see how proteins and ligands interact.

The stability of the protein-ligand complexes and the strength of the connections that permit the crystallization of the entire complex rather than just a single ligand or macromolecule are limiting factors for the structural determination of these complexes. Additionally, crystals containing both counterparts must be large enough and possess the correct physical quality to permit diffraction. The fundamental stages of the crystallization process are:

- **Nucleation**, in which a sufficient number of molecules combine to create the critical nucleus, which provides the surfaces essential for crystal formation.

- **Growth**, in which new molecules diffuse from the bulk solution to the surface of crucial nuclei and adhere to them to create the crystal lattice via particular and highly directed interactions.
- **End of growth**, occurs when the protein content in the bulk solution falls below the saturation level or when the developing lattice is destabilized by deformation-induced strain or the presence of contaminants.

The protein-ligand co-crystallization process can be described as a subset of protein crystallization in which the presence of the ligand is one of the variables that must be optimized to obtain the desired co-crystals, along with pH, temperature, protein concentration, precipitant agent concentration, and other additives.<sup>33–35</sup> Bi-dimensional phase diagrams, which are commonly used to describe standard protein crystallization (Figure 5)<sup>30,31,33</sup> can thus be used to conveniently represent this process. In these diagrams, the stable states of the protein (liquid, crystalline, and amorphous solid) are each shown as a function of only two of these parameters at a given time, with the initial protein concentration typically acting as one of these parameters.

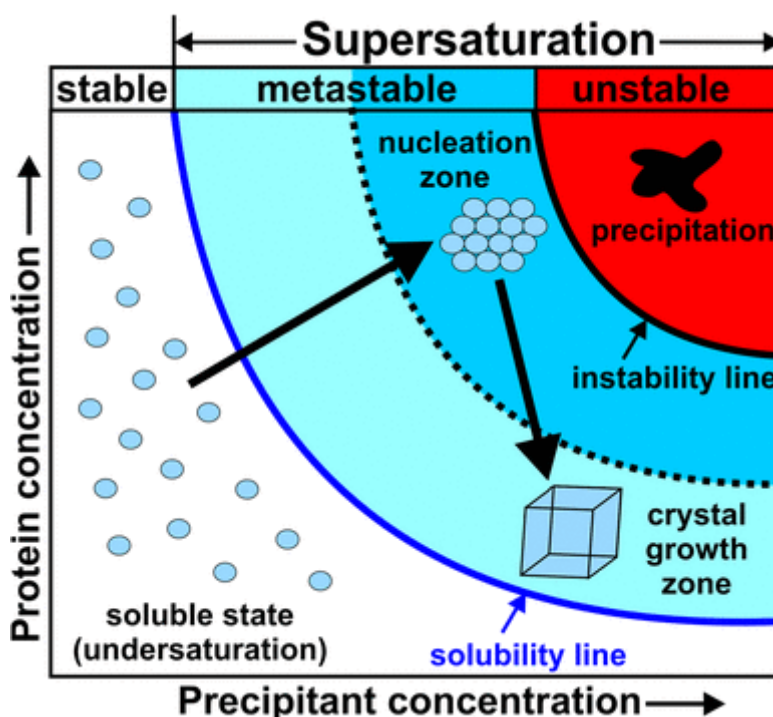


Fig.5: Schematic illustration of a protein crystallization phase diagram<sup>36</sup>

The following schematic regions may be identified: an *undersaturation* zone, which is bordered by the values of [P] (Protein concentration) and the other adjustable variable where

the protein is soluble in the examined medium, and a *supersaturation* zone. The latter region is further subdivided into three sections:

- the precipitation zone, when supersaturation levels are too high and amorphous aggregates form;
- the nucleation one, in which crystal formation around crucial nuclei begins and crystal growth begins;
- and the metastable zone, where nucleation is kinetically inhibited and only slowdown growth may occur.

To achieve ideal crystallization conditions, the many factors that influence the process should be modified to push the system as near to the border with the metastable nucleation zone as possible. As a result of the progressive drop in protein concentration during the process, once nucleation starts, the system will easily move into the metastable zone, where growth happens slowly and the final crystal will be of higher quality. Despite substantial research into the physicochemical principles that govern protein crystallization, a complete understanding of this phenomena has not yet been reached, and obtaining protein crystals appropriate for X-ray diffraction remains a difficult issue. When the goal is to crystallize the target protein together with its ligand, additional problems arise since the presence of the binding partner represents an additional parameter to be adjusted. However, according to the great interest connected to this topic, several methods for protein-ligand co-crystallization have been developed over the years. The vapour-diffusion experiment<sup>37,38</sup> which has also been employed in this thesis study, is by far the most widely used. This method involves equilibrating an aqueous droplet containing the protein, the ligand, the buffer, and the precipitating agents (typically inorganic salts or high molecular weight polyethylene glycols (PEGs)) against a reservoir solution made up of the same buffer and precipitant agents but in a higher concentration. Since they contain differing amounts of buffer and precipitants, water will slowly diffuse from the crystallization mixture to the reservoir solution, increasing the concentrations of the protein and ligand and, in certain situations, resulting in their co-crystallization. These tests are carried out on suitable plates with hermetically sealed wells, where the relative positions of the two solutions can vary. The crystallization mixture is placed on the cover slides that shut the wells and suspended above the reservoir solution in

the so-called *hanging drop design*, whereas in the *seated drop design* the crystallization mixture is placed in a dedicated compartment in direct communication with the reservoir (Figure 6).

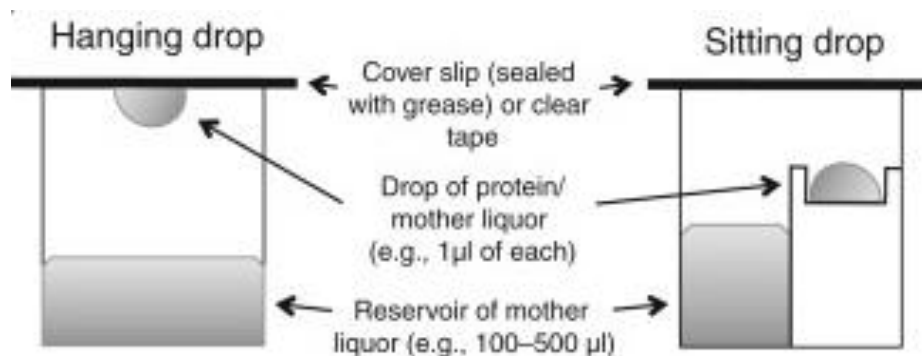


**Fig.6:** Schematic representation of vapour diffusion experiments in the hanging drop (left) and the sitting drop (right) configurations.

From a purely practical standpoint the seated drop studies are simpler to set up, but they occasionally have disadvantages since the crystals may stick to the support where they are positioned, making it difficult to collect them.<sup>34</sup> While the setup for the hanging drop experiments is more challenging, they frequently produce better results because the crystals do not adhere to the cover slide and the greater distance from the reservoir solution ensures a slower rate of droplet evaporation and, consequently, a higher quality of the crystals. The easy experiment setup and minimal protein and ligand requirements, which allow systematic exploration of a wide range of diverse experimental condition, are the most favourable aspects of the vapour diffusion approach in both of its possible configurations.<sup>34,35,39</sup> In fact, multi-well plates (Figure 7c) are commercially available and can be used to equilibrate very small droplets of protein and ligand in varying concentrations against reservoirs of various compositions. These reservoirs can be prepared manually or obtained from commercial crystallization kits. Crystallization screening kits are commercially accessible and may be acquired from numerous companies. These kits include a number of pre-made reservoir solutions (Figure 7a) that differ greatly from one another. In this approach, several tests may be completed quickly, simultaneously, without wasting any time, taking advantage of extremely diverse settings. Additionally, robotic technologies to automate the setup of the experiments have been developed for both the sitting drop and in the hanging drop

configurations (Figure 7b), allowing to further reduce the time and raw materials (droplets volume of less than 1 $\mu$ L) required to carry out the crystallization tests.<sup>40</sup>



**Fig.7:** a) commercial crystallization kits with 96 different reservoir solutions; b) robot for automatized hanging drop vapour diffusion screening; c) well plates commonly used to set up manual hanging drop vapour diffusion experiments

These facts are extremely important because protocols for the systematic co-crystallization of protein-ligand complexes have not yet been established, and the ability to quickly and easily screen in-depth for the various factors that affect these phenomena can be crucial to the success of their occurrence.

#### 4.4 Calixarene-based multivalent ligands for proteins

Ligands built on calixarenes have demonstrated very interesting capability to interact with proteins, evidencing high efficiency and selectivity in the studied recognition phenomena thanks to their intrinsic multivalent nature, the wide variety of functionalities that can be linked to their structure at different distances from the aromatic units, and the different geometries of presentation of the ligating units that they can furnish. Furthermore, since the synthesis of water-soluble derivatives of these macrocycles was reported, their use as ligands for biological macromolecules such as enzymes<sup>41-43</sup>, proteins, nucleic acids, and lypopolysaccharides has been investigated in order to test their potential use as anti-tumor agents, immune response effectors, gene- or drug-delivery systems, and anti-adhesion agents against viruses, bacteria, and bacterial toxins. The ability to exploit the various non-covalent interactions provided by both the lipophilic cavity<sup>44</sup> of these macrocycles and the wide variety of functional groups<sup>45</sup> that can be easily inserted at both its upper and lower rim is a powerful tool for achieving the desired binding events. Moreover, the ability to modulate the number



and orientation<sup>42,46,47</sup> of the binding units present on the calix[n]arene scaffold is especially advantageous for the development of multivalent ligands<sup>42</sup> tailored to fit the surfaces of target macromolecules.

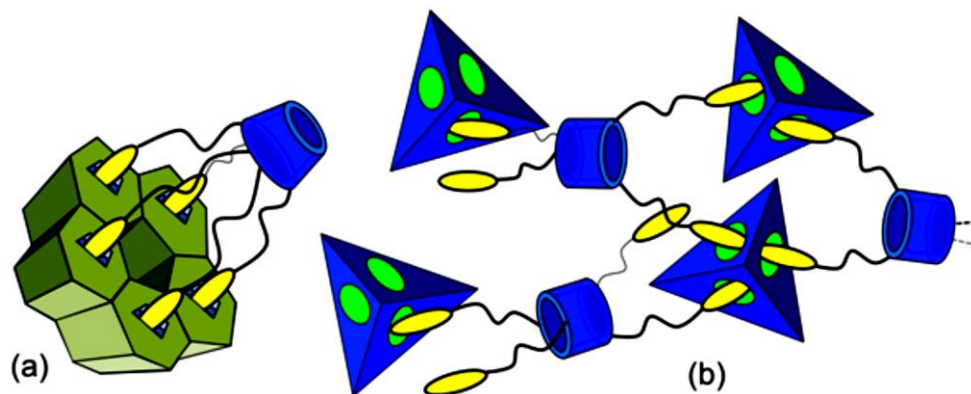


**Fig.8:** Different complexes formed with a) a cone calix[5]arene and cholera toxin and b) a 1,3-alternate glycolyx[4]arene and a tetrameric lectin of *Pseudomonas Aeruginosa*<sup>48</sup>

A comprehensive assessment of the literature on calix[n]arene-based ligands for biomacromolecules<sup>49–51</sup> is beyond the scope of this paragraph. Thus, in the following pages, a general description of the properties that allow these compounds to be effective ligands for proteins and, in some cases, to influence their biological activity will be reported, with a special emphasis on calix[4]arene derivatives, as they are the sub-family of these macrocycles on which this chapter has been focused. The many geometries that calixarene-based ligands can assume, result in a variety of mechanisms of binding to biomacromolecules. A cone derivative, for example, can interact with large surface areas or with species that have recognition domains very close to each other and convergent, resulting in multivalent 1:1 complexes (figure 8a). The 1,3-alternate shape, on the other hand, organizes the ligating units in two opposed directions of the space and is therefore more ideal for connecting various receptors, resulting in multivalent cross-linked aggregates, as illustrated in figure 8b. Instead, conformationally mobile calixarenes can benefit from the potential of an induced fit rearrangement of the ligating units in the presence of the protein, which can compensate for a larger loss in entropy. Proteins may interact with their counterparts via surface interactions, as seen above, exploiting large regions. In this regard, examples of calixarene compounds that can interact with protein surfaces via three distinct mechanisms of binding have been identified, as shown schematically in figure 9:

- 1) recognition of “*hot-spots*”;
- 2) single point recognition, that means substantial complexation of the side chain of a selected amino acid of the peptide sequence;
- 3) recognition and stoppage of lipophilic pockets.

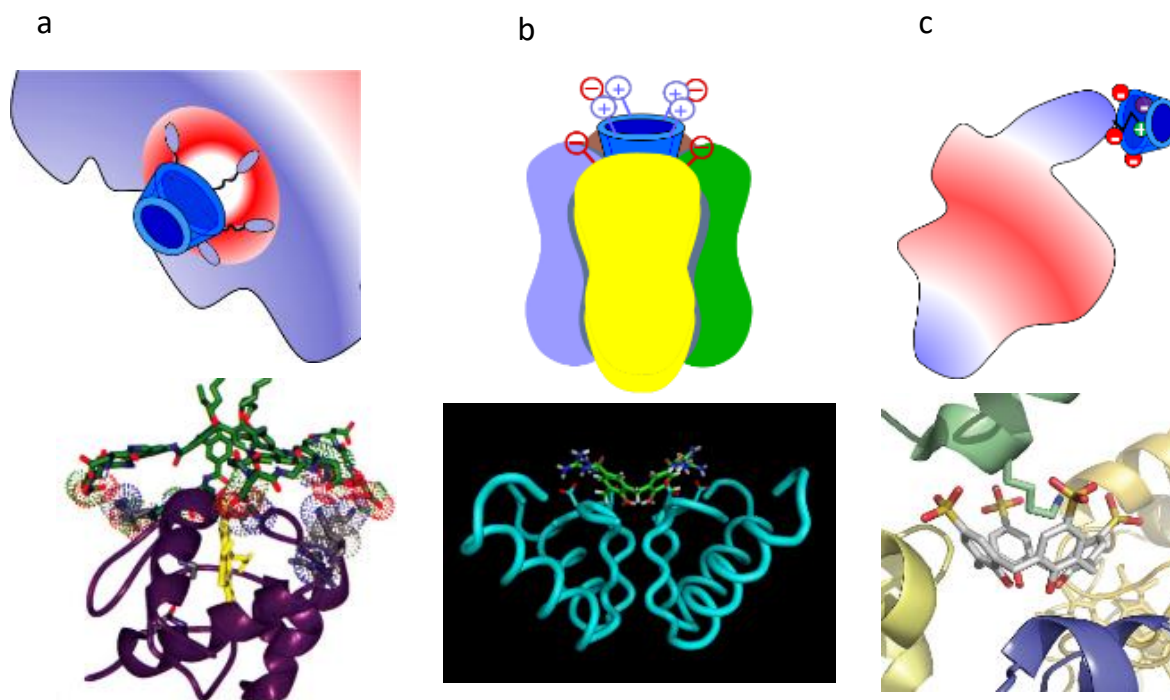


**Fig.9:** schematic representation of three different binding modes of calixarene-based multivalent ligands: a) recognition of “*hot spots*”; b) recognition and stoppage of pocket in a protein; c) interaction with a specific residue in the protein backbone.<sup>12</sup>

Cone-calix[4]arene derivatives, have been reported to be useful for the optimal orientation of binding units capable of interacting the *hot-spots* of proteins<sup>52</sup>. Hamilton et al. used this characteristic to create compounds **1** and **2** (Figure 10)<sup>53,54</sup>, which are adorned at the upper rim with four polypeptide loops. Taking inspiration from the function of antibodies, these derivatives were engineered to bind the target proteins by recognizing a vast portion of their surfaces by using both hydrophobic and electrostatic multiple contacts at the same time.

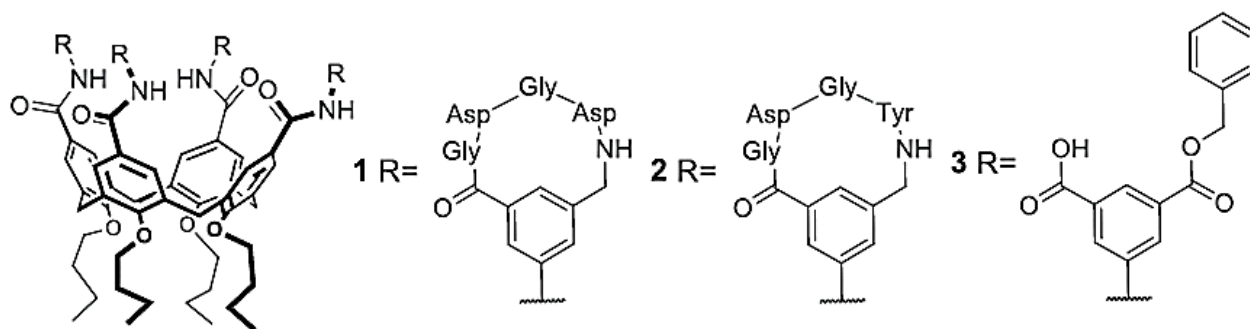


**Fig. 10:** Cone-calix[4]arene derivatives tested as ligands for cytochrome *c*.

The first protein-ligand system studied consisted of **1** and cytochrome *c* (cyt *c*). The catalytic heme group in cyt *c* is surrounded by a lipophilic area with a positively charged belt that may be covered by **1** to produce a very stable 1:1 complex ( $K_a 10^{-8} M^{-1}$ ). The binding process was proposed to take place due to the presence of four cyclic GlyAspGlyAsp loops containing hydrophobic and negatively charged amino acid residues at the upper rim of the calix[4]arene, which provide the complementary interactions required to recognize the protein hot spot. Furthermore, it was proposed that the 3-aminobenzoyl moieties present in each peptide sequence contribute to the recognition process by providing extra hydrophobic interactions with the protein surface. Because of the presence of **1**, the reduction of the Fe(III) ion present in the protein heme group by ascorbate was hindered, as was the interaction with its catalytic partner cyt *c* peroxidase.<sup>55</sup> Similarly, when evaluated as a ligand for  $\alpha$ -chymotrypsinase, **1** was shown to bind the target protein with a dissociation constant in the nanomolar range while avoiding complex formation with soybean trypsin<sup>56</sup>. The same authors also examined compound **2** as an inhibitor of growth factor binding to the relevant receptors implicated in angiogenesis and tumour development. More specifically, the capacity of this calix[4]arene to block the connection of platelet derived growth factor (PDGF) and its membrane receptor (PDGFR)<sup>53</sup>, which is a critical event for the maintenance of blood vessels in oncogenesis, was investigated. PDGF, like cytochrome *c* and  $\alpha$ -chymotrypsinase, has a hydrophobic area on its surface with a positively charged belt, and compound **2** was a significant inhibitor of the adhesion process ( $IC_{50}=250nM$ ). This appears to be detrimental to the development of many human cancers transplanted in nude mice. Inhibitor properties were also reported for calix[4]arene **3**,<sup>57</sup> where the upper rim was functionalized with monobenzylester isophthalic acid moieties to achieve the alternation of negatively charged and hydrophobic groups, and it has thus been presented as a simplified version of compounds **1** and **2**. Both PDGF and the

vascular endothelial growth factor VEGF were inhibited ( $IC_{50}$ = 190 and 480 nM, respectively). The in vivo administration of this chemical to mice resulted in the suppression of transplanted human cancers.

Cone-calix[4]arenes can also allow single-point recognition of studied target proteins by taking advantage of their aromatic cavity in combination with the action of appropriate functional groups at its upper rim, to host lipophilic or positively charged amino acid residues. Examples of protein-ligand interactions of this type have been described for the tetrasulfonato calix[4]arene **4**. (Figure 9c). This compound<sup>58</sup> is soluble in water and buffer solution and assumes a rigid cone conformation in these media at neutral pH, thanks to the instauration of a network of tight hydrogen bonding at its lower rim. Crowley et al.<sup>59</sup> established the capacity of **4** to bind cyt c via NMR titrations and the resolution of the X-ray crystal structure of the associated protein-ligand complex. More specifically, the X-ray diffraction data revealed that this compound can recognize three lysine residues by utilizing the insertion of the alkyl portion of the side chains into its hydrophobic cavity and the interaction of the ammonium group with the four sulfonate units at the upper rim. The three molecules of **4** were found at the interface of a cytochrome c dimer, whose aggregation was thought to be aided by the burying of the target lysine residues. Additional CH- $\pi$  and van der Waals contacts formed between the opposite protein monomer apolar amino acid side chains and, respectively, the external part of the calix[4]arene cavity and the phenolic/phenolate moieties at the lower rim were supposed to allow cyt c oligomerization during the co-crystallization process (*molecular glue effect*). Following the determination of the X-ray crystal structure of the related protein-ligand complex<sup>60</sup>, similar findings were reported for the lysozyme-**4** system. In this case, the calix[4]arene derivative **4** recognized the C-terminal Arg128 rather than lysine residues, but the binding characteristics were very similar to those observed for the **4**-cyt c couple, because the bound amino acid side chain sits in the macrocyclic cavity and the charged guanidinium head group established salt bridge interactions with the sulfonate groups. The preference for Arg128 over other arginine residues was attributed to the fact that it is the most exposed residue from the protein surface, making it the most accessible to the ligand. In this scenario, the ligand was also found to serve as molecular glue by causing the target protein to crystallize as a tetramer. A shift in selectivity was seen when the lysine side chains of lysozyme were bis-methylated in a subsequent study.<sup>61</sup> In this situation, **4** binds preferentially to the dimethylated

Lys116, the most accessible of the six lysine residues found in the protein backbone. The findings of NMR and X-ray diffraction tests revealed that, contrary to prior crystal structures, the dimethyl ammonium head group penetrates the cavity of the calix[4]arene to form a cation-interaction, while the remaining lysine side chain remains outside the cavity. The selectivity of **4** for dimethylated lysine side chains has been described as a mimic of the activity of proteins involved in gene regulation and signalling networks, such as chromodomains.

The cone-calix[4]arene scaffold has also been found to function as a stopper of lipophilic spaces derived from protein quaternary structure. De Mendoza et al.<sup>62</sup> provided a notable example of this action in a research study where compounds **5-9** (Figure 11) were investigated as inhibitors of the activity of voltage-dependent potassium channels.

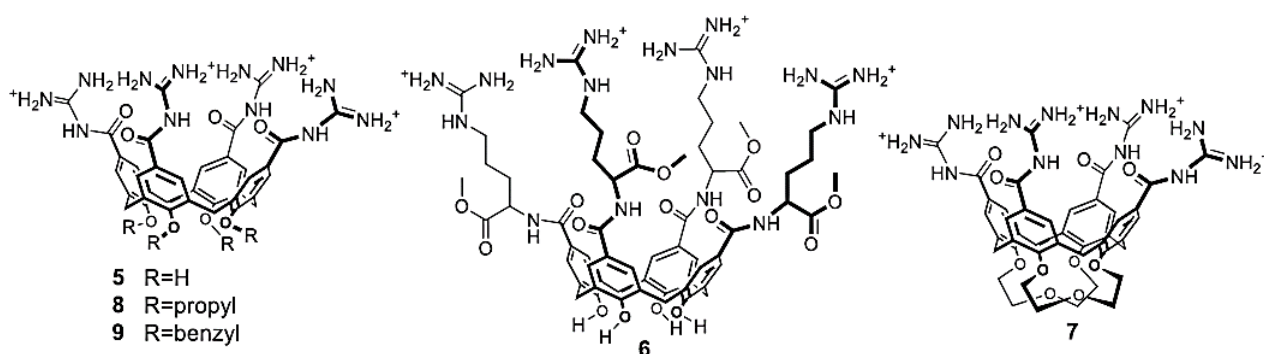


**Fig. 11:** Cone-calix[4]arene derivatives tested as stoppers of voltage-dependent ionic channels

The study hypothesis was that the cup-like form of the investigated compounds would fit the portals of these channels, while the guanidinium groups at their upper rim would be used to bind the carboxylate moieties present at the channel entry. The compounds tested were able to inhibit reversibly the action of the Shaker potassium channels, with **7** having the highest inhibitor activity due to its rigid-cone structure, which was imparted by the presence of crown ether-like motifs at its lower rim, allowing a better fit to the target channel surface. The presence of substituents at the lower rim of tested calix[4]arenes, on the other hand, was not always recognized as helpful to their biological activity. Compounds **8** and **9**, for example, were discovered to cause a significant, but irreversible, decrease in ionic current for the channels expressing oocytes, and this disadvantage was attributed to the ligand amphiphilic nature, as provided by their propyl and benzyl groups at the lower rim, respectively. In reality,

both calix[4]arene derivatives were designed to behave as a disruptive detergent against cell membranes containing the target ionic channels. Control experiments with carboxylate- or ammonium-bearing calix[4]arenes and a monofunctional model compound of **5** revealed no appreciable activity for the tested derivatives, confirming the importance of both the macrocyclic cavity and positively charged guanidinium groups in obtaining effective inhibitors.

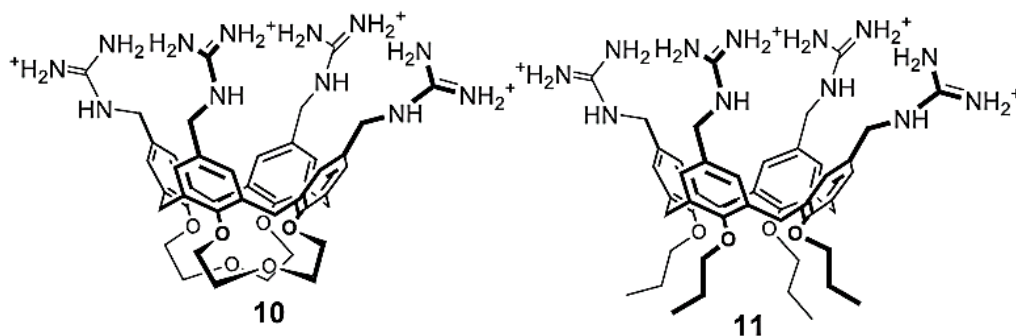


**Fig. 11:** Calix[4]arene derivatives used to restore the activity of p53 mutated form.

Compounds **10** and **11**, illustrated in Figure 12, were synthesized with a similar design by the same scientists and shown to restore the physiological function of a mutant variant of the tetrameric p53 transcription factor.<sup>63</sup>

The wild type version of p53 has significant anti-tumor effect in the human body, operating as a "genome guardian" when properly associated as a tetramer. Arg337 plays an important role in this process by recognizing equivalent Asp residues on opposing protein units and thereby maintaining the resultant oligomer. Unfortunately, p53 can occasionally be found in a mutant version in which Arg337 is replaced by a histidine residue, that, being not completely protonated at physiological pH, leads to the disruption of tetramers and to a consistent decrease of the anti-tumor efficacy. The presence of a Glu336 and Glu339 couple on the extremities of each of their four protein monomers, that provide a squared distribution of negative charges at the two bases of each oligomeric protein, is a common feature of the tetramers formed by the association of both the wild type and the mutated form of p53. This collection of negatively charged residues was shown to be an excellent anchoring site for the four guanidinium groups of **10**, which were predicted to approach each extremity of the tetrameric altered protein via its lower rim side. The inclusion of **10** at 400 mM concentration increased the stability of the resultant tetramer. ESI mass spectrometry was able to validate

the creation of a complex including two calix[4]arene molecules and the related protein. On the other hand, the addition of the ligand had no effect on the stability of the wild-type tetrameric protein, as predicted. Compound **11**, which was alkylated with simple propyl chains at the lower rim, was even more successful than its more rigid bis-crown-3 homologue **10** in holding the four units of mutant p53 together.<sup>64</sup> Indeed, DSC experiments revealed that a 25mM concentration of this chemical is adequate to restore target protein oligomerization, and this increase in activity was attributed to a distinct property of its molecular scaffold. More specifically, it was assumed that the residual flexibility of **11** allowed for better rearrangement of its guanidinium groups at the upper rim to fit the target Glu residues and that the propyl chains at the lower rim can penetrate the protein lipophilic pocket to establish additional hydrophobic interactions.

Other important instances of protein recognition by calix[4]arene-based ligands include the interactions of glycolixarenes (calixarenes adorned with glycosyl units) with sugar binding proteins, generally known as lectins<sup>42,43</sup>. Lectins play an important role in a variety of physiological and pathological processes by acting as receptors for specified glycosylated binding partners/ligands. This type of binding mechanism may be defined as a specific form of multivalency known as the *glycoside cluster effect*.<sup>65</sup> Several calix[n]arene derivatives have been functionalized with saccharide units in order to interact with lectins and alter the biological processes in which they are engaged. Focusing on calix[4]arenes, important examples of glycolix[4]arenes, are compounds **12-14** (Figure 12)<sup>66,67</sup>, which are blocked in different macrocyclic geometries and functionalized with distinct glycoside units at the lower rim. The tetrameric galactose-binding lectins PA-IL from *Pseudomonas aeruginosa* (a bacterium responsible for chronic respiratory illnesses) were chosen as the target for the galactosylated ligands **12** and **13**, and their inhibitor action was shown to be dependent on their structural characteristics. ITC titrations revealed that the 1,3-alternate calix[4]arene **13** outperformed the equivalent conical isomer **12** in binding the target protein, with dissociation constants of 176 nM and 420 nM and stoichiometry of 1:4 and 1:3, respectively. As a result of the complex stoichiometries, the reduced binding affinity of **12** comes from the fact that only three out of four binding units may interact with PA-IL. Because the binding sites of this protein are known to be located two by two in the minor faces of its parallelepipedon-like structure, it was proposed that **13** provides an orientation of its four galactoside groups

suitable to bridge two protein tetramers at the same time, whereas for the cone-calix[4]arene derivative **12** the geometry of complexation is disadvantaged because all its binding groups are disposed on the same side of the macrocycle.

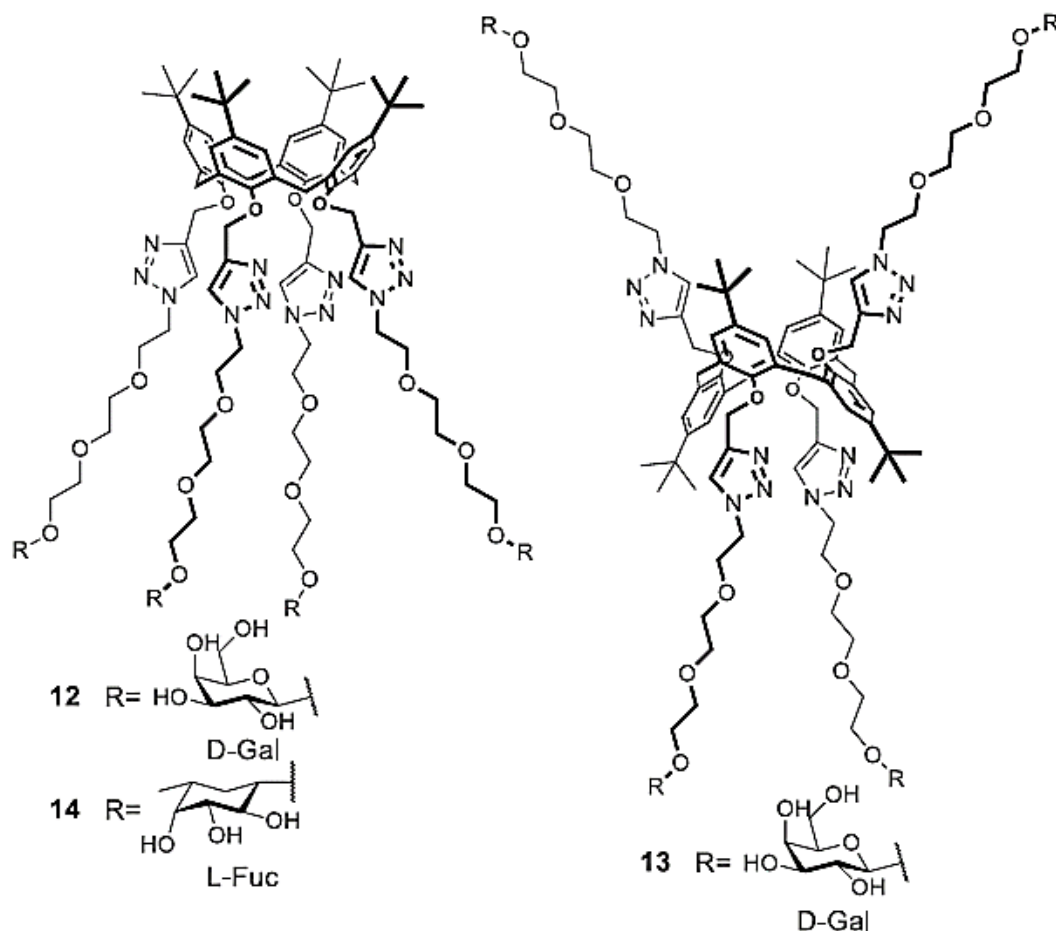


**Fig.12:** Glycolix[4]arenes of different conformation tested as inhibitors of PA-IL and/or PA-IIL lectines.

The *in vivo* investigations on mice revealed a block in bacterial growth after administration with both calix[4]arene-based ligands, validating the suppression of the target lectins function. In contrast to the **13**-PA-IL system, it has been postulated that fucosylated cone calix[4]arene **14** interacts with PA-IIL by binding four separate protein tetramers rather than bridging two of them at a time. Despite the fact that the structures of PA-IL and PA-IIL are quite similar, it is known that the binding sites for fucose in the latter protein tetramer are further apart, and so an interaction with two of them by the same calix[4]arene derivative was thought to be unlikely.

All the examples provided demonstrate the use of calixarenes as interesting ligands for protein identification and inhibition. Several of these important proteins have been demonstrated to interact with calixarenes with high affinity and selectivity via surface recognition or via



interaction with binding sites or single residues. The success shown by calixarene in protein binding is essentially due to the high versatility of these macrocycles that can be properly manipulated to modulate their structural characteristics such as the valency and the stereochemical disposition of their ligating units in the space.

#### 4.5 Aim of this work

The rational design of ligands as inhibitors for specific proteins is a critical step in the development of new drugs, while the ability to restore the activity of other types of proteins by using synthetic molecules capable of reinforcing and stabilizing their oligomeric structure has been reported as a promising approach for the same purpose. Since of the variable orientation of the binding groups supplied by the aromatic scaffold, calix[4]arenes deserve special attention because they can be blocked in different conformations, which might induce a strong selectivity even towards very comparable target proteins. Of course, the type of the substituent present on the calix[4]arene scaffold, which collaborates with the aromatic cavity of these compounds to generate distinct modalities of binding, influences how target proteins are recognized. Crowley et al., for example, reported that the sulfonato-calix[4]arene **4** is able to recognize single positively charged amino acid residues on the surface of both cytochrome c and lysozyme, owing to the synergistic action of the negatively charged groups at its upper rim and the macrocyclic cavity, which can host a portion of the bound amino acid side chains.<sup>59,60,68</sup> Furthermore, this compound has been shown to stimulate the crystallization of target proteins as oligomers. Based on these discoveries, we decided to conduct research with the same group to investigate the interaction between two protein *Ralstonia solanacearum lectin* (RSL) or his counterpart dimethylated on the lysine motif (RSL-KMe2) and the ligands shown in Figure 13. Particularly, derivatives belonging to two classes of calixarenes were studied: the methylsulfonate **5** and the zwitterionic calix[4]arenes **1,2,3,6,7** and **8**. The lower rim of these compounds was left unfunctionalised to exploit the array of H-bonds which keeps the structure rigid at physiological pH. In fact, at this value of pH, one of the four hydroxyl groups at the lower rim is deprotonated and the network of H-bond is strengthened and keep the structure in its cone conformation.

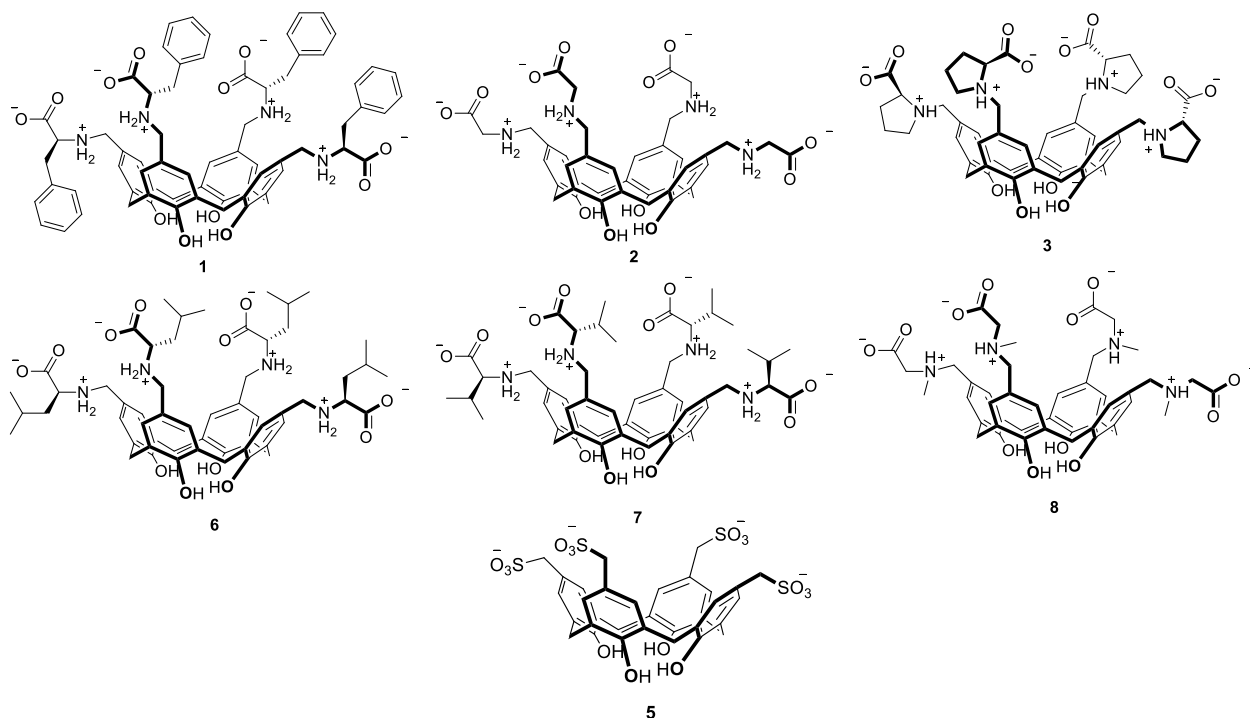


**Fig.13:** structure of the ligands studied in this chapter as surface protein

The derivative **5** is functionalised at the upper rim with four methyl sulfonate groups. As mentioned in the introduction to this chapter, calixarene functionalised with sulfonate groups gave good results in the recognition of lysine residues on protein surfaces. With intermediate **5**, the aim is to study how the greater conformational freedom of the group responsible for the surface recognition influences its binding capacity and thus its ability to act as a molecular glue. As already mentioned in the previous section, there are numerous examples of recognition of biological surfaces by negatively charged calix[4]arenes in the literature. However, the recognition ability of calixarenes bearing zwitterionic motifs remains unexplored. Part of the work shown in this chapter involves the study of zwitterionic calix[4]arenes and their possible interaction with proteins. Unfortunately, due to the low solubility of these ligands in water at physiological pH, only the intermediates **2**, **3** and **8** were used for crystallisation trials.



# Results and Discussion

## 4.6 Target proteins

Protein-protein and protein-ligand interactions are the heart of many pathological and physiological processes. As a result, these macromolecules are the prime targets of novel bioactive chemicals. These latter ones might be developed to restore activities lost by a protein due to genetic or post-translational changes or, in other cases, they may be inhibitors of protein-protein interactions, which are at the origin of illnesses. Using crystallization techniques, we investigated the capacity of several multivalent calix[4]arenes to bind to protein surfaces, side chain residues, and recognition sites during a term spent in Professor Crowley's laboratory at the National University of Galway (Ireland).

In the next paragraph it is reported the description of one of the proteins selected for these studies, that is *Ralstonia solanacearum* lectin (RSL). The protein was chemically dimethylated<sup>69,70</sup> onto the  $\epsilon$ -NH<sub>2</sub> group of Lysine to yield RSL-KMe<sub>2</sub> with four modified sites, K25Me<sub>2</sub>, K34Me<sub>2</sub>, K83Me<sub>2</sub> and the N-terminus S1Me<sub>2</sub>.

### 4.6.1 *Ralstonia solanacearum* lectin (RSL): Carbohydrate binding proteins (CBS)

*Ralstonia solanacearum* lectin come from this bacterium, which is found all over the world and causes deadly wilt in many agricultural crops. *Ralstonia solanacearum* is a soil-borne plant pathogen that belongs to the  $\beta$ -proteobacteria family.<sup>71</sup> *R. solanacearum* generates three distinct soluble lectins: RSL (9.9 kDa), RS-IIL (11.6 kDa), and RS20L. (20 kDa). However, in this chapter, the focus is on the first protein: RSL. This is a tiny protein of 90 amino acids with a tandem repeat in its amino acid sequence that is a powerful L-fucose-binding lectin with high affinity for fucose residues, particularly Fuc1-2Gal and Fuc1-6Gal links. The sugar affinity order, in particular, is as follows: L -fucose > L -galactose > D -arabinose > D -fructose > D -mannose.<sup>72</sup> This protein's 3D structure is well-known, and RSL crystal analysis revealed a symmetrical trimeric structure, producing a so-called six-bladed -propeller, with

each monomer composed of two tiny four-stranded anti-parallel  $\beta$ -sheets (see figure below). The resultant hexavalent trimer can bind fucosylated glycolipid-containing lipid membranes.<sup>73</sup> RSL was also co-crystallized with two sugars (methylfucose and 2-fucosyllactose). Co-crystallization with methylfucose indicated the presence of two sugar binding pockets in each monomer: one in the monomer itself and one at the interface where two monomers meet, for a total of six binding sites in a trimer.<sup>74</sup> Therefore the discovery of ligands with higher affinity with this protein than natural carbohydrates, might prevent native interactions and shed light on the use of this novel ligands to fight the plant diseases.

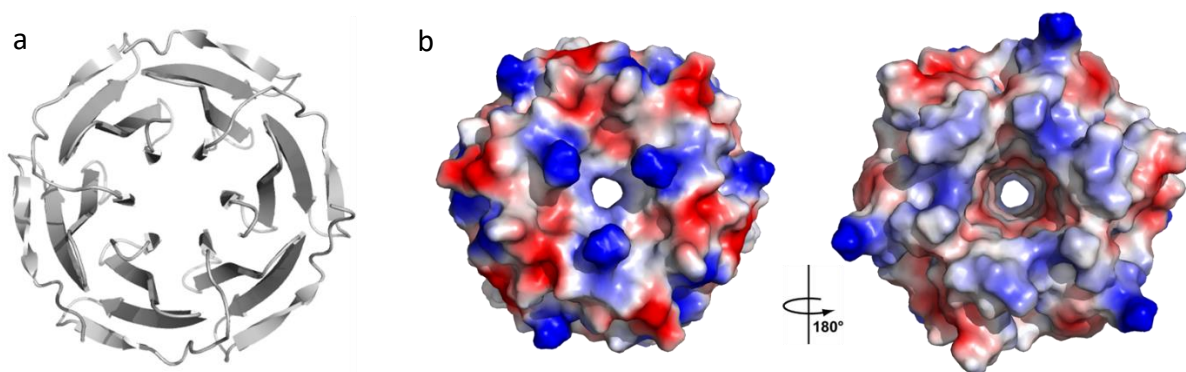


**Fig.1:** a) Cartoon representation of RSL and b) electrostatic potential of the protein surfaces with blue and red areas corresponding to positively and negatively charged regions, respectively

#### 4.6.2 Dimethylated *Ralstonia solanacearum* lectin (RSL-KMe<sub>2</sub>)

Methylation of amino acid side chains is a post-translational modification (PTM) that is essential for gene regulation and developmental signaling pathways.<sup>75-78</sup> Lysine residues that have been selectively mono-, di-, and trimethylated by methyltransferase enzymes serve as recruitment sites for new protein-protein interactions. The study field was made even more interesting by the finding that lysine side chains are methylated at high levels in hundreds of nonhistone proteins.<sup>79-81</sup> Additionally, uncontrolled levels of methylation have been linked to a number of cancer types.<sup>82</sup>

It has been shown that the well-known host p-sulfonatocalix[4]arene **4** may bind ammonium ions in pure water exploiting its rigid multiaromatic cavity and the assistance of charge complementary sulfonate head groups.<sup>83-89</sup> Hof et al demonstrated that the affinity of **4** for lysine peptides increases with the increasing of their methylation degree, with an overall 70-fold selectivity for Lys(Me<sub>3</sub>) versus Lys.<sup>90</sup> Moreover, the increase of the methylation degree

of lysine is accompanied by significant increases in enthalpic driving force and smaller favourable changes in entropy. Moreover, unlike acylation, the methylation of Lys does not change the charge of the protein and is often non-perturbing its overall structure. In fact, the majority of spectroscopic and crystallographic studies have found that although protein crystallization properties may be significantly altered, lysine dimethylation results in only minor structure perturbations.<sup>91-95</sup> So the methylation of RSL was performed in order to increase the affinity of the ligands for this protein.

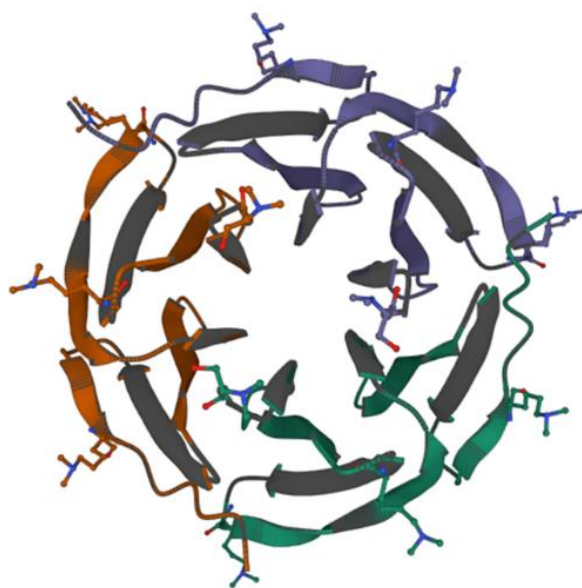


**Fig.2:** *Cartoon representation of RSL-KMe2*

Methylated lysines (LysMe<sub>n</sub>) present a unique hotspot for recognition by reader proteins that possess an aromatic cage motif. As a result, artificial receptors that can identify LysMe<sub>n</sub> have enormous promise as system probes for methylated lysines and as inhibitors of protein-protein interactions.<sup>90,96-101</sup>

## 4.7 The ligands

### 4.7.1 p-methylsulfonatocalix[4]arene

The p-methylsulfonatocalix[4]arene **5** was previously synthesised in our group.<sup>102</sup> Its ability to bind cytochrome c lysine cation residues has already been investigated by another PhD student in Ireland. The use of **5** appears to induce much more efficient crystallisation and better quality crystals than p-tetrasulfonato calix[4]arene **4** (Figure 3). Crystallisation tests with **5** leads to crystal formation in 25 out of 96 cases while with **4** in only 1 out of 96 cases.

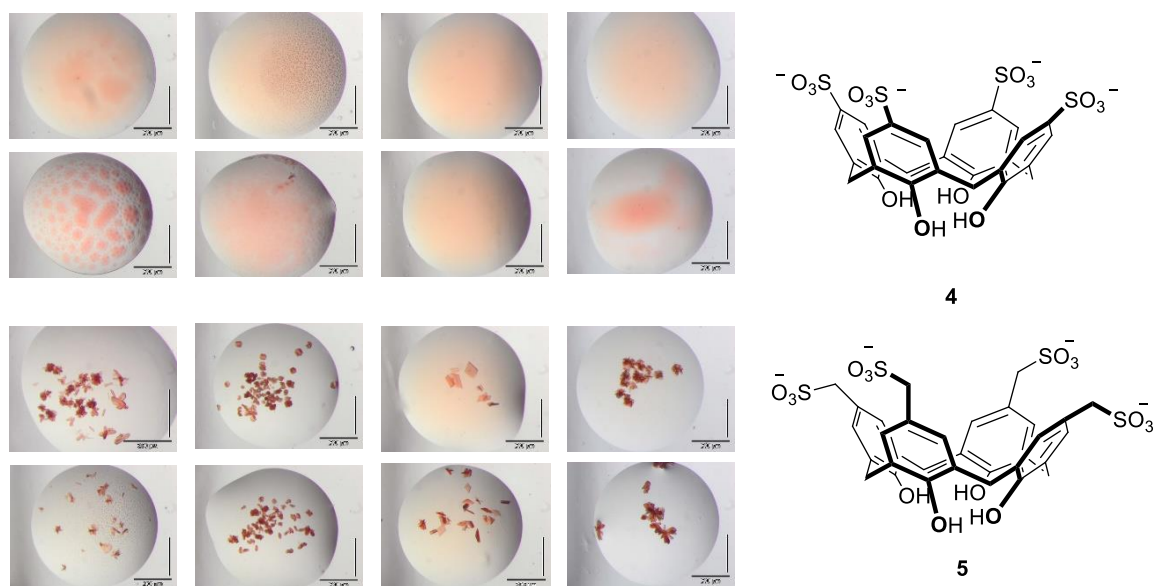


**Fig.3:** Photographs of crystallisation tests using the same conditions (1mM cyt-c and 2mM calixarene) in the presence of *sclx4* (above), and in the presence of *smclx4* (below). Each condition is differentiated by a different reservoir composition.

Crowley and his research team were also able to solve the X-ray structure (Figure 5) of one of these crystals. The unit cell contains two proteins and three ligands **5**. Each calixarene includes a single lysine unit and, in particular, on protein unit A Lys54 and Lys86 are included, while on unit B only Lys86 is included. The conformation of the CH<sub>2</sub>SO<sub>3</sub><sup>-</sup> groups generally projects the anionic groups outwards from the macrocycle. Only in some calixarenes the CH<sub>2</sub>SO<sub>3</sub><sup>-</sup> group is facing inwards to form a salt bridge with the lysine ammonium cation. The inclusion of the lysine side chains has many similarities with the resolved structures of the calix[4]arene **4** and of the tetramethylphosphonate calix[4]arene **9**<sup>35</sup>, whereby cation- $\pi$  and CH- $\pi$  bond interactions with the CH<sub>2</sub> groups in  $\epsilon$  of the lysine are observed

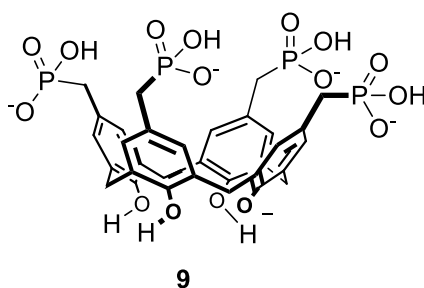


**Fig.4:** Structure of the tetramethylphosphonate calix[4]arene **9**

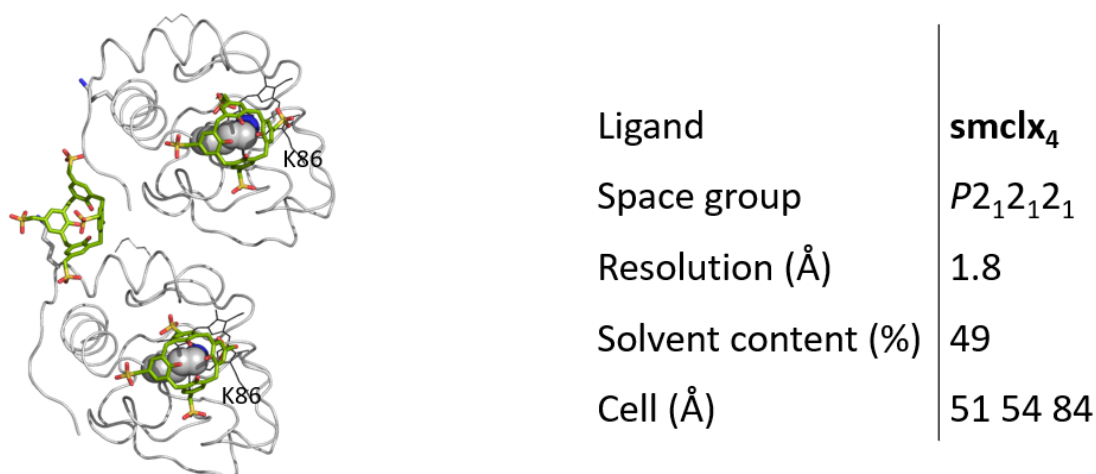


**Fig.5:** X-ray structure of the complex *cyt c smclx 4*

The encapsulation of the lysines by **5** leads to a coverage of approximately 300 Å<sup>2</sup> of protein surface area, which is equivalent to almost 10% of the total available surface area. Furthermore, in addition to the masking effect of the side groups of the included lysines, the calixarene increases the total surface area of the particle by approximately 600 Å<sup>2</sup> and provides numerous other non-covalent interactions with adjacent proteins in the crystal, thus leading to the typical 'molecular glue' effect and promoting crystallisation. The resulting structure is also similar to that previously obtained by Parma Galway collaboration with tetramethylphosphonato calix[4]arene **9**, in which the ligand complexes the same lysine residues (Lys54 and Lys86), but with a slightly different crystal packing.<sup>103</sup> Thus, **5** would appear to act as a better molecular glue than its **4** analogue, at least in the case of cytochrome c. Part of the work carry out in the group of professor Crowley regarded the use of **5** as a molecular glue also for the case of a symmetrical and neutral proteins such as RSL and RSL-KMe<sub>2</sub>

#### 4.7.2 Zwitterionic calix[4]arenes

As already been thoroughly explained in the previous chapter amines and amino acids can be attached to the upper rim of calixarenes, preserving their zwitterionic structure, thanks to the general and fast methods of the Mannich reaction.<sup>104</sup> The Mannich reaction provided a relatively easy access to zwitterionic calix[4]arenes and we have further extended the previous reported study, which exploited only proline, by using also other natural amino acids. In this way we were able to obtain several new products, shown in Figure 5.



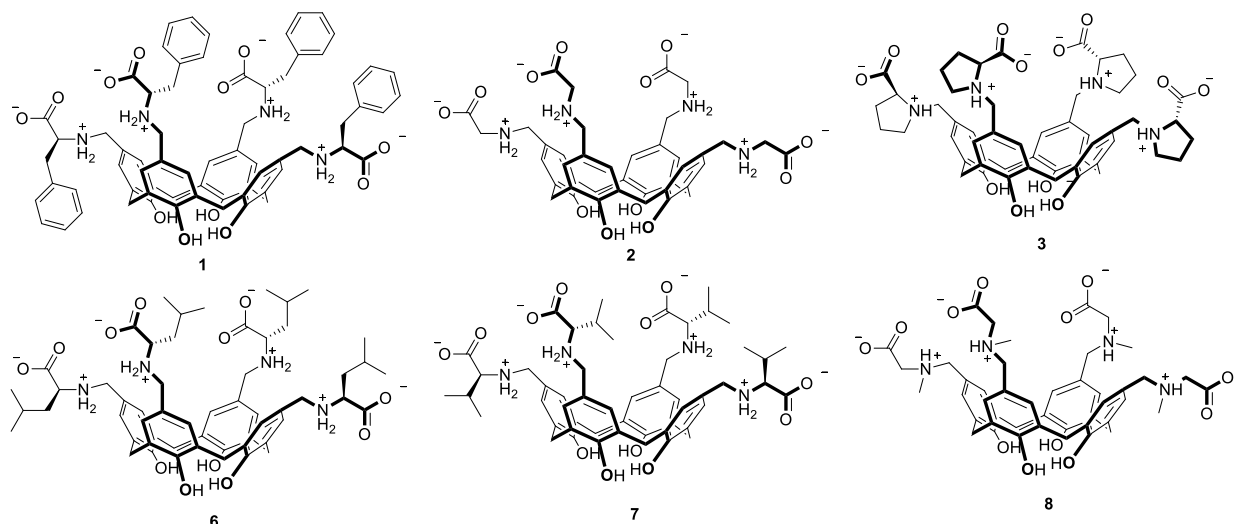


**Fig.6:** Compounds obtained via Mannich reaction.

This reaction gave good results only when using lipophilic amino acids such as: proline, valine, leucine and phenylalanine. We were also able to obtain good results with glycine and sarcosine but changing the reaction condition previously reported in the literature for compound **3**.<sup>103</sup> In this work we wanted to study this new class of calix[4]arenes as a potential ligands for protein.

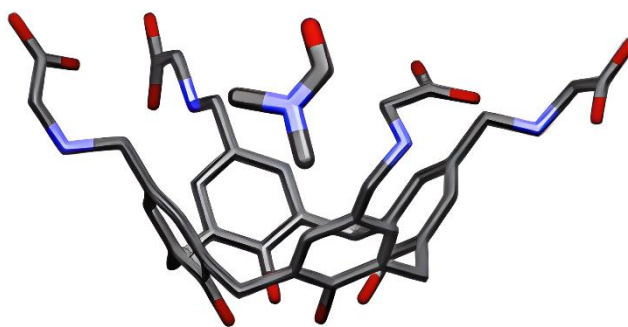


**Fig.7:** Crystal structure of compound **2** shows inclusion of one DMF molecule

The inclusion of a DMF molecule within the calixarene cavity in the X-ray structure of compound **2** (Figure 7) encouraged us to think that this class of calixarenes could also host amino acid side chains. Due to the poor solubility under physiological conditions of ligands **1**, **6** and **7**, we were able to study only compounds **2**, **3** and **8**. In fact, compounds **2** and **8** are completely soluble only at pH=8.5 and 9.5 respectively. Only ligand **3** is instead completely

soluble at pH=7. It was therefore decided to test these three calixarene derivatives with RSL due to its high chemical stability and low isoelectric point.

#### 4.8 Crystallization tests between zwitterionic calix[4]arenes and RSL

For RSL, co-crystallization experiments<sup>105,106</sup> with **2**, **3** and **8** were carried out in an effort to gain information about this system concerning their reciprocal interactions from the solid state structure of the corresponding complex. The sitting drop vapour diffusion method was then used to perform a robot screening over a commercially available kit of 96 different reservoir solutions. We also decided to adopt the “three drops experiment” where in one of the three drops is present only the ligand and this is used as a control. In fact, since these ligands were not tested before for protein crystallisation, the control drop allows to exclude the possibility that the ligand alone crystallizes in those conditions. The other two drops contained the ligands at different concentrations and the protein at 1 mM concentration. Firstly, we tried calixarene **3** with this set up. Crystals were obtained in several different conditions. The most promising conditions were easily replicated in manual hanging drop tests where the same protein and ligand concentrations of the experiment performed with robot trials were tested. The best results were obtained in the conditions in which the reservoir solutions were composed by:

- 20 % w/v polyethylene glycol 3350, 200 mM ammonium formate; pH 6.6 (Figure 8)
- 10 % w/v polyethylene glycol 8000, 100 mM TRIS; pH 7.0, 200 mM magnesium chloride (Figure 13)
- 10 % w/v polyethylene glycol 3000, 100 mM TRIS; pH 7.0, 200 mM zinc acetate (Figure 15)
- 10 % w/v polyethylene glycol 8000, 300mM magnesium chloride (Figure 16)



**Fig.8:** Crystal formation observed during crystallization tests for the RSL-**3** complex performed by a robot sitting drop. The first drop is the control with only compound **3** without protein. The other two drops are

*made by 1 mM protein + 1mM and 10 mM of ligand, respectively). The crystallization mixtures were equilibrated over reservoir solutions composed of 20 % w/v Polyethylene glycol 3350, 200 mM Ammonium formate; pH 6.6*

It was considered useful to perform some cycles of optimization of the experimental conditions to prompt the system to afford better crystalline precipitates and to test the reproducibility of these crystals. In case of the first reported condition (20 % w/v Polyethylene glycol 3350, 200 mM Ammonium formate; pH 6.6) we decided firstly to change the concentration of the precipitant in the reservoir solution. These investigations pointed out that the crystallization process was promoted between pH 8 and 9 and in the presence of 20-22% PEG 3350 and at both 1 or 10 mM **3**, while it was prevented at acid pH or by increasing the PEG concentration. In fact, at higher concentration of the latter, some precipitant starts to appear in the drops (Figure 9).

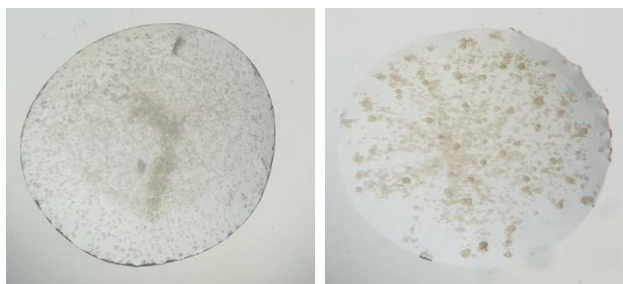


**Fig.9:** *Precipitation formation observed during crystallization tests for the RSL-3 complex. The two drops are made by 1 mM protein + 1mM and 10mM of ligand respectively. The crystallization mixtures were equilibrated over reservoir solutions composed of 200 mM Ammonium formate; pH 6.6 and 24 % and 26%w/v Polyethylene glycol 3350, respectively*

We then tested different buffer composition and different pH to evaluate the effect of the different protonation state of the ligand on the capability to promote crystallization (Figure 10). We keep constant the concentration of both the precipitant and salt. As in the previous case we tested two different concentrations of ligand. A control drops of the only **3** and the protein only were also tested.

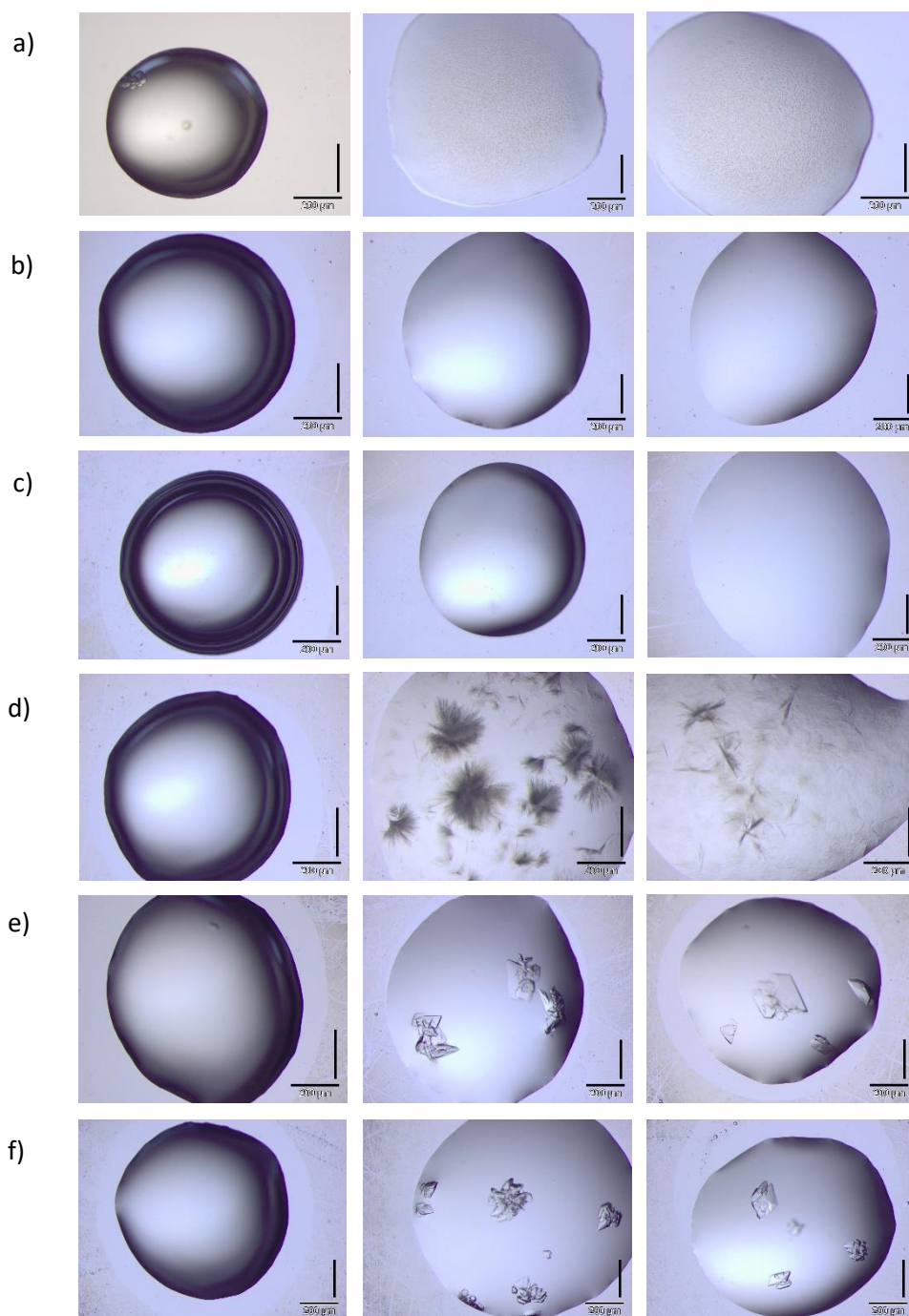


**Fig.10:** Crystal formation observed during crystallization tests for the RSL-3 complex varying the buffer composition. The first drop for each row is the control with only compounds **3** without protein. The other two drops are made by 1 mM protein + 1mM and 10mM of ligand respectively. The crystallization mixtures were equilibrated over reservoir solutions composed of 20 % w/v Polyethylene glycol 3350, 200 mM Ammonium formate and a) 100mM sodium citrate pH=3, b) 100mM sodium citrate pH=4, c) 100mM sodium citrate pH=5, d) 100mM TRIS pH=7, e) 100mM TRIS pH=8, f) 100mM TRIS pH=9

From the resulting pictures in Figure 10 it is possible to see how increasing the pH is possible to promote the crystal growth. The crystals growth in the presence of TRIS at pH=8 and 9 appears to be the most promising regarding the quality and the dimension. To rule out the possibility that the crystals formed were protein-only crystals, a crystallisation test was

conducted with the protein alone under conditions *d* and *f* shown in Figure 12. In both of the conditions tested the drop remains clear. So, it seems that is the presence of the ligand to promote the crystallization. Finally, we tested if different concentration of the ligand could promote the formation of different morphology in the crystals obtained using the reported condition at pH=8 and 9 (Figure 11).

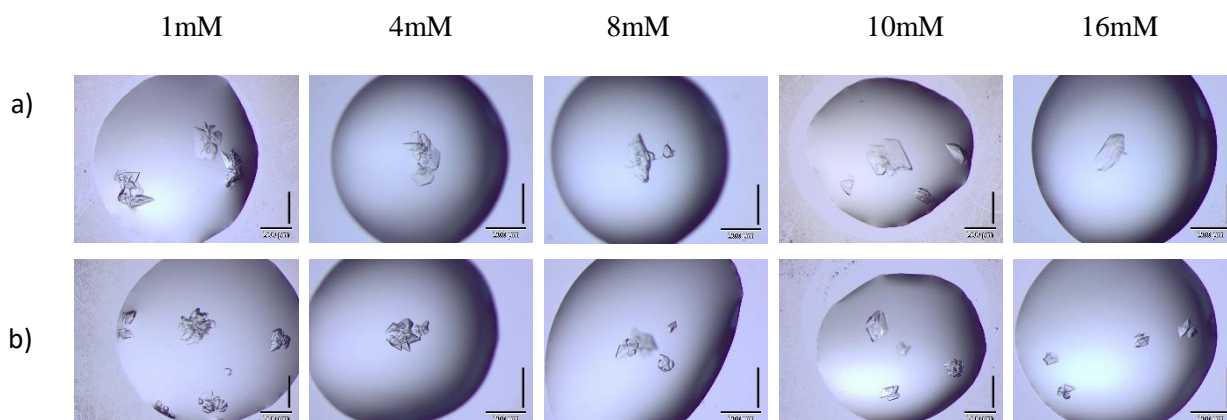


**Fig.11:** Crystal formation observed during crystallization tests for the RSL-3 complex varying the ligand concentration. The crystallization mixtures were equilibrated over reservoir solutions composed of 20 % w/v Polyethylene glycol 3350, 200 mM Ammonium formate and a) 100mM TRIS pH=8, b) 100mM TRIS pH=9.

It can be seen from Figure 11 that by increasing the ligand concentration, the morphology of the resulting crystal does not change significantly. The crystals in Figure 12 were sent to be analysed in Paris at the SOLEIL synchrotron, but the structure obtained revealed the presence of the protein alone. Since crystallisation tests with the protein alone did not result in the formation of any crystals, it can be concluded that under these conditions the addition of calixarene **3** probably promoted the crystallisation of the protein due to the increased ionic strength of the solution upon addition of **3**.

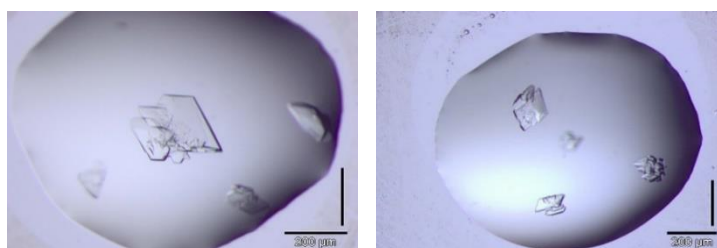


**Fig.12:** Crystals chosen to be analysed by synchrotron in Paris. The drops are made by 1 mM protein + 10mM of ligand **3**. The crystallization mixtures were equilibrated over reservoir solutions composed of 20 % w/v Polyethylene glycol 3350, 200 mM Ammonium formate and 100mM TRIS pH=8 (left) and 100mM TRIS pH=9 (right).

In the second promising reported condition (10 % w/v Polyethylene glycol 8000, 100 mM TRIS; pH 7.0, 200 mM Magnesium chloride) we were able to see crystal growth in the sitting drop vapour diffusion experiment performed by the robot but only when the concentration of the ligand was raised from 10 mM to 25 mM. Unfortunately, this crystal forms a sort of cluster that are difficult to use for the data acquisition (Figure 13, left)

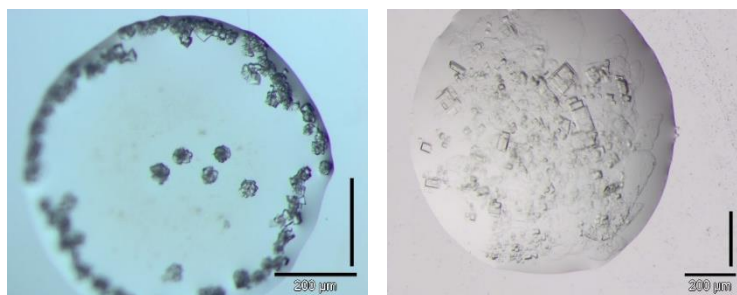


**Fig.13:** Images obtained by optical microscopy of the crystallization tests performed by robot (left) and using manual hanging drop (right) between RSL and **3**. The drop is made by 1mM protein + 25mM of ligand. The crystallization mixtures were equilibrated over reservoir solution composed of 10 % w/v Polyethylene glycol 8000, 100 mM TRIS; pH 7.0, 200 mM Magnesium chloride

Also in this case, it was considered useful to perform some cycles of optimization of the experimental conditions in order to improve the quality of the crystals. Firstly, a manual hanging drop tests was carried to test the reproducibility of the crystals keeping the same experimental conditions. Thanks to the manual experiment, it was possible to obtain crystals of better quality as shown in Figure 13 (right). To rule out the possibility that the crystals formed are protein-only or ligand-only crystals, crystallisation test was conducted for both the protein and the ligand alone. The resulting drops remain clear also after several weeks so it can be concluded that is the presence of the ligand to promote the crystallization. As in the previous experiment we tested different buffer composition and different pH to evaluate the effect of the different protonation state of **3** on the capability to promote crystallization.

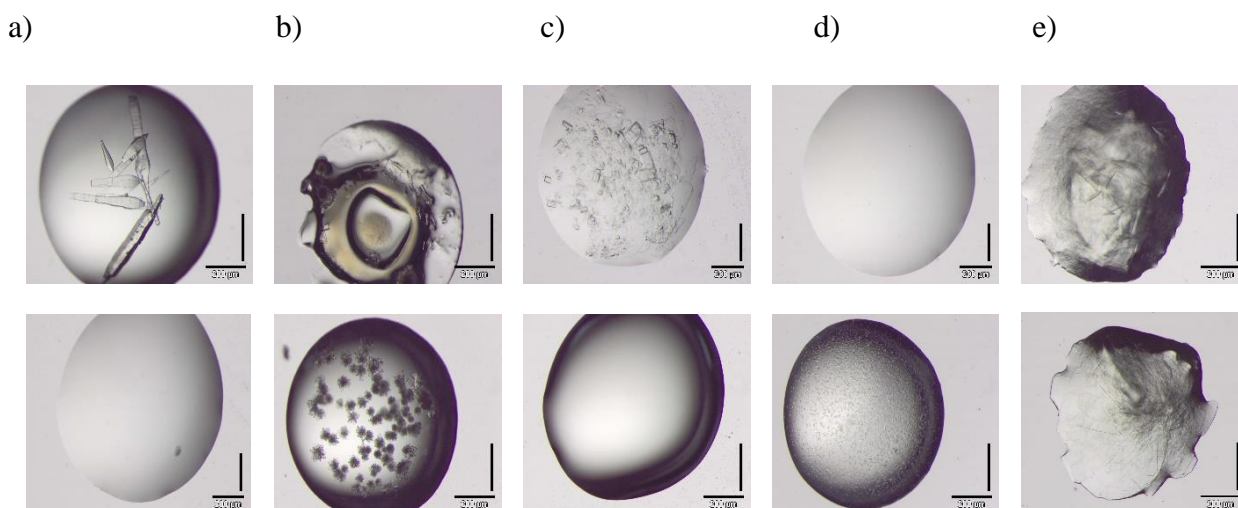


**Fig.14:** Images obtained by optical microscopy of the crystallization tests for the RSL-**3** complex varying the buffer composition and the pH. The drops contain 1 mM protein + 25mM of ligand. The crystallization mixtures were equilibrated over reservoir solutions composed of 10 % w/v Polyethylene glycol 8000, 200 mM Magnesium chloride and a) without buffer, b) 100mM sodium citrate pH=3, c) 100mM TRIS pH=7, d) 100mM TRIS pH=8, e) 100mM TRIS pH=9. Under each drop of the RSL-**3** solution are reported the crystallisation tests done in the same experimental conditions but in the presence of **3** only.

From the resulting pictures in Figure 14 it is possible to see the different behaviour between the drops containing the RSL-**3** solution (Figure 14, top) and the calixarene **3** alone in the same experimental condition (Figure 14, bottom). From these images it can be seen that at basic pH, no crystal growth is noticeable (Figure 14 d and e) but, on the other hand, crystal grow when the buffer is composed of sodium citrate buffer at pH=3. Interestingly, under the same conditions, calixarene **3** alone crystallized with a different crystal morphology. Furthermore, under these conditions, it can be seen that when both protein and **3** are present, the solution evolves into the formation of a gel (Figure 14b) in which, however, crystalline material is dispersed. If no buffer is added to the reservoir composed of PEG and Magnesium chloride tubular-shaped crystals grow (Figure 14a). This marked difference in the properties of the protein-ligand systems could be probably ascribed to the different degree of protonation of **3**. All the three crystals shows in Figure 14 a,b and c were sent to be analysed in Paris by the SOLEIL synchrotron. Unfortunately, the crystals obtained in the absence of buffers are degraded during transport and the acquisition of the crystals obtained with sodium citrate buffer gave a low-resolution data and it was impossible to identify the electron density of **3** in the complex. Finally, the third crystal obtained revealed the presence of the protein alone. Using the third promising condition (10 % w/v Polyethylene glycol 3000, 100 mM TRIS; pH 7.0, 200 mM Zinc acetate), we were able to see crystal growth in the sitting drop vapour

diffusion experiment performed by the robot but these crystals were too small to be used. They grew under the conditions reported but only when **3** was added to the protein solution at the 10mM concentration. Higher concentrations of ligand were tested but resulted in the formation of precipitates while with lower concentrations of **3** no crystal formation was observed. Thanks to the manual experiment, it was possible to obtain crystals of better quality as shown in Figure 15.

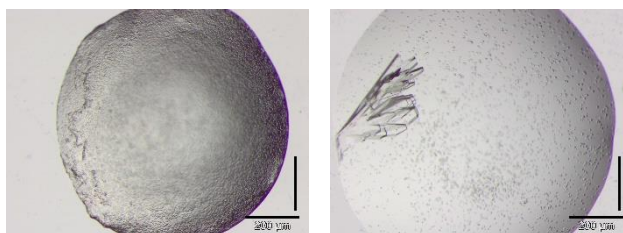


**Fig.15:** Images obtained by optical microscopy of the crystallization tests performed by robot (left) and using manual hanging drop using a paraffin barrier (right) between RSL and **3**. The drop is made by 1mM protein and 10mM of ligand. The crystallization mixtures were equilibrated over reservoir solution composed of 10 % w/v Polyethylene glycol 3000, 100 mM TRIS; pH 7.0, 200 mM Zinc acetate

In an attempt to improve the quality of the crystal and to obtain some crystals suitable for X-ray studies, other manual hanging drop test were prepared using paraffin oil as a barrier to reduce the evaporation rate of the reservoir, in order to reduce the nucleation rate. In this way we were able to produce crystals bigger and with different morphology in respect of the crystal obtained with the robot trials (Figure 15). As it is possible to observe the reservoir solution contain zinc salt and, when the reported conditions were varied by adding different salts with cations different from zinc, the resulting solutions did not result in the formation of crystalline material indicating an important role of zinc cation in the crystals formation. Unfortunately, even in this case, after analysis at the Paris synchrotron, the structure of the crystals, shows in the right side of Figure 17, was demonstrated to be the only protein. The last promising condition (10 % w/v Polyethylene glycol 8000, 300mM Magnesium chloride) obtained from the robot crystals trials between RSL and **3** led to the formation of tiny crystals impossible to use to solve the structure.

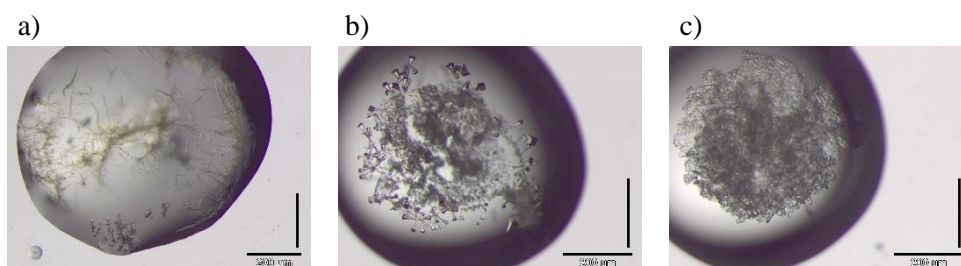




**Fig.16:** Images obtained by optical microscopy of the crystallization tests performed by a) robot and b-c) using manual hanging drop between RSL and **3**. The drop is made by 1mM protein and a) 10mM of ligand b) 25mM of **3**, c) 50mM of **3**. The crystallization mixtures were equilibrated over reservoir solution composed of 10 % w/v Polyethylene glycol 8000, 300 mM Magnesium chloride

It was considered useful to perform some cycles of optimization of the experimental conditions to improve the quality of the crystals changing the concentration of the ligand and the concentration of the salt. The best results were obtained by increasing the concentration of **3** to 25mM. In fact, thanks to this method, crystals of excellent quality were obtained, and they seem to maintain the same morphology as those obtained with the robot (Figure 16). In this case, a test was also done by increasing the ligand concentration from 25 to 50 mM, and again, crystals with very different morphology grew from the resulting solution than those obtained with **3** concentrations of 25mM. Unfortunately, the crystals were not analysed at the synchrotron because of the difficulty encountered in taking a high-quality crystal from the solution. In contrast, it was possible to obtain the structure relative to the crystals obtained when the ligand is present at 25mM concentration (Figure 16b), but the size of the unit cell led to the conclusion that the crystal is of calixarene **3** alone.



**Fig.17:** Images obtained by optical microscopy of the heavy precipitant formed during the crystallization between RSL and **2** (top) or **8** (bottom).

We decided also to test calixarens **2** and **8** as ligands for interaction with RSL but, probably because of the poor solubility of these compounds at pH below 8.5, the crystallization tests done resulted in the formation of heavy precipitates under most conditions (Figure 17). It was possible to observe crystals formation only in two conditions both composed by 10mM of **8** and 1mM of RSL equilibrating over a reservoir solution composed by 20% PEG 3350, TRIS pH=8 and 9 and 200mM Ammonium formate.

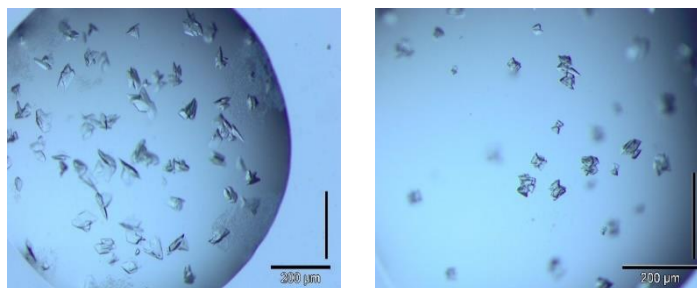


**Fig.18:** Images obtained by optical microscopy of the crystallization tests performed by manual hanging drop between RSL and **8**. The drop is made by 1mM protein and 10mM of ligand. The crystallization mixtures were equilibrated over reservoir solution composed of 10 % w/v Polyethylene glycol 3000, 200 mM Zinc acetate and 100 mM TRIS; pH 8.0 (left) or 100 mM TRIS; pH 9.0 (right)

These crystals were also sent to the synchrotron in Paris, and thanks to the structure obtained, it was possible to conclude that the crystals were also of the protein alone.

Given the excellent results obtained using compound **5** to co-crystallise cytochrome c, our interest shifted to evaluating the use of this ligand for other proteins as well. We therefore decided to try to use compound **5** to obtain complex structures with more neutral and symmetrical proteins than cytochrome c. We therefore tried to use this ligand to obtain a co-crystal with RSL. Although numerous crystallisation tests have been performed between compound **5** and RSL, none have resulted in crystal growth even when trying different ratios between **5** and the protein.

As already explained in the previous section Hof et al demonstrated that the affinity of **4** for lysine derivatives increases with increasing methylation. Since compounds **4** and **5** are very similar, we imagined that this higher affinity of **4** for methylated lysine residues might also be valid for compound **5**. So, the methylation of RSL was performed to increase the affinity of the ligands for this protein. Following a known protocol, lysine and N-terminal methylation were obtained (Figure 19). The process involves reductive methylation, which is done when formaldehyde and a reducing agent such sodium cyanoborohydride or dimethylamino borane (DMAB) complex are present. Depending on the stoichiometric ratios of the reagents, this procedure produces mono-methyl and di-methyl lysine. In fact, RSL may be completely converted to RSL-LysMe<sub>2</sub> by applying excess of formaldehyde.

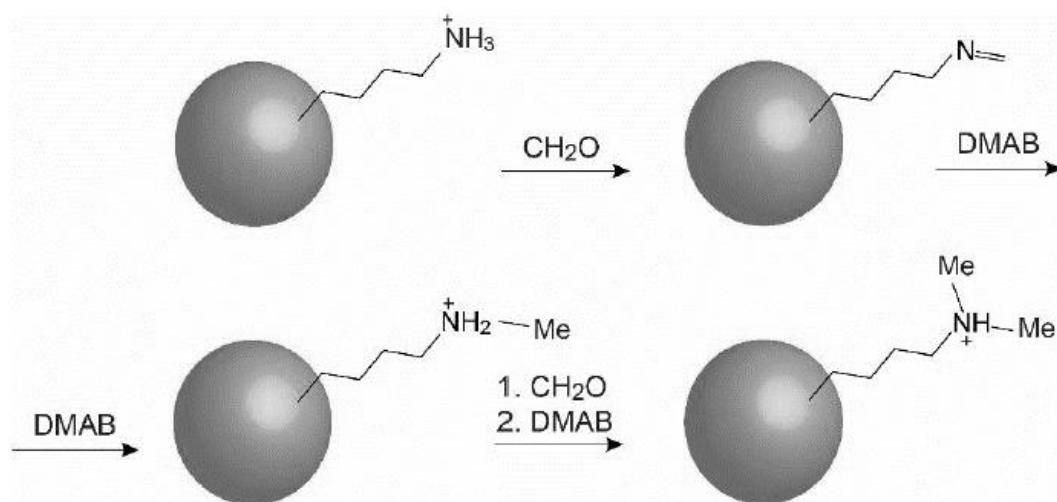


**Fig.19:** Schematic representation of the methylation reaction. The protein is represented as a grey sphere.  
(DMAB = dimethylamino borane)

To verify that the reaction was successful,  $^1\text{H}$ - $^{15}\text{N}$  HSQC NMR measurements were taken (Figure 20) by comparing the assigned backbone amide NHs resonances to native RSL. Overall, resonances did not seem to be much shifted, supporting the conclusion that the modification had little impact on RSL folding. Small chemical shift perturbations in lysines were present, supporting that the modification had taken place. The N-terminal end, or Ser1 cannot be detected by NMR as well as Ser2. Therefore, the closest probe to N-terminus is valine 3 (Val3). Chemical shift perturbation at Val3 corroborates methylation of the N-termini.

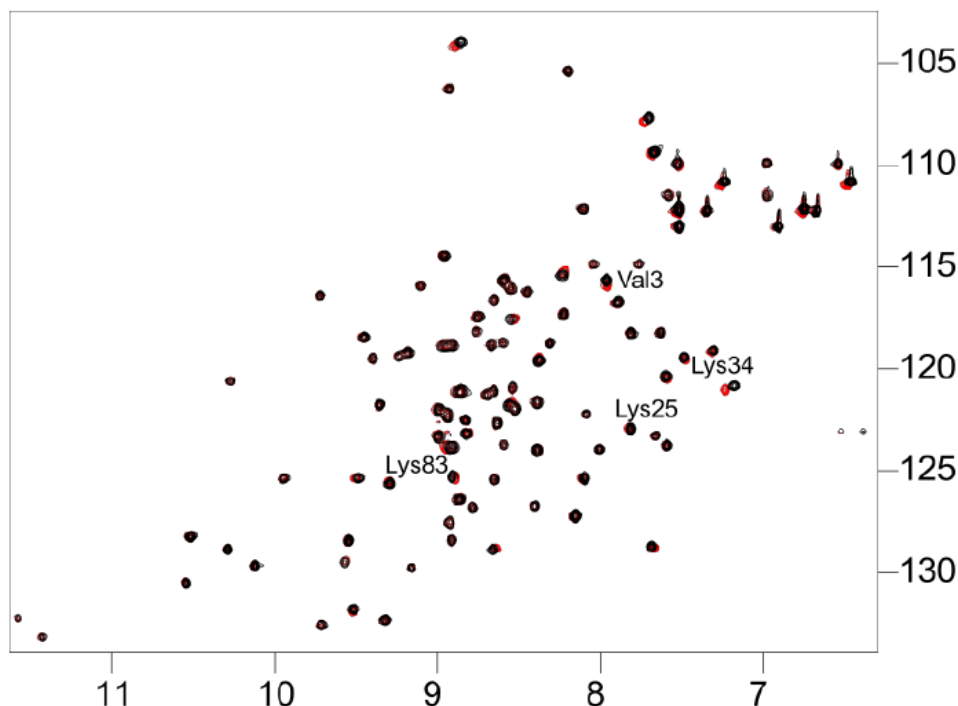


**Fig.20:** Overlaid  $^1\text{H}$ - $^{15}\text{N}$  HSQC spectra of original RSL (black outlines) and modified RSL (red) exhibited small chemical shift disturbances caused by dimethylation.

After the methylation process, the new RSL-KMe<sub>2</sub> was used for the crystallization tests with calixarene **5**. Although the protein was methylated, the sitting drop vapour diffusion method tests resulted in the formation of promising crystals in only two out of 96 different conditions and only when **5** is in a concentration between 1mM and 10mM. The best results were obtained in the conditions in which the reservoir solutions were composed by:

-20% w/v polyethylene glycol 8000, 100mM CHES pH=9.5

-20% w/v polyethylene glycol 6000, 100mM tri-sodium citrate pH=4.0, 1M Lithium chloride

The first condition was easily replicated in manual hanging drop tests where the same protein and ligand concentrations of the experiment performed with robot trials were tested. We also tested if the calixarene or the protein alone can crystallize in the same experimental condition. While the protein alone does not lead to crystal formation even after several weeks (Figure 21e), crystals begin to form after a few days in the solution containing calixarene **5** alone in the concentration of 10mM (Figure 21d). However, the crystals of the ligand alone are completely different in morphology to those obtained when RSL-KMe<sub>2</sub> is present (Figure 21 a, b and c). These crystals were also sent to the synchrotron in Paris, and thanks to the structure

obtained, it was possible to conclude that also in this case the crystals were composed of the protein alone.

Finally, the last promising condition (20% w/v Polyethylene glycol 6000, 100mM tri-Sodium citrate pH=4.0, 1M Lithium chloride) was also replicated in manual hanging drop tests. The experiment, carried out keeping the protein concentration at 1mM, evidenced that the presence of 10 or 20 mM ligand (Figure 22) caused the formation of crystals. Furthermore, by reducing the PEG percentage below 12%, crystal growth is not observed.

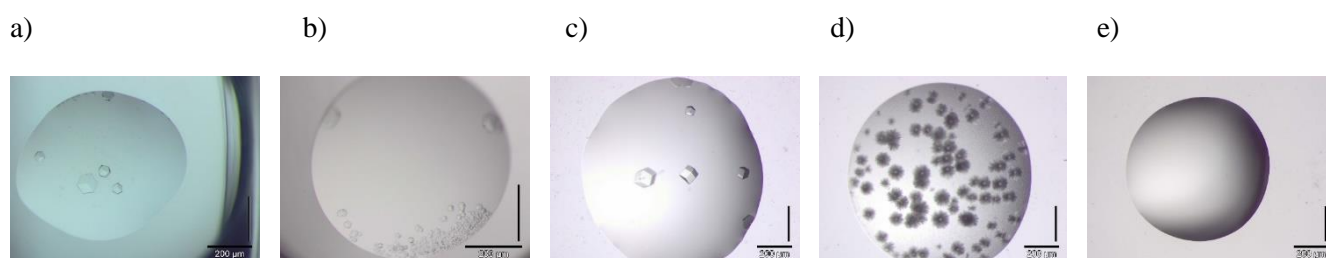


**Fig.21:** Images obtained by optical microscopy of the crystallization tests performed by a) robot and b-e) using manual hanging drop between RSL-KMe<sub>2</sub> and **5**. The drop were made by 1mM protein and a)10mM of **5**, b) 15mM of **5**, c)10mM of **5**. Drop d) is the control with **5** alone and drop e) is the control with the protein alone. The crystallization mixtures were equilibrated over reservoir solution composed of 20% w/v polyethylene glycol 8000, 100mM CHES pH=9.5

The concentration of LiCl would also seem to be important for crystal growth. In fact, when this concentration is brought below 800mM, the solution does not lead to the formation of any crystals (Figure 23). We then tested the importance of the cation by testing the standard condition but varying the salt composition using magnesium chloride instead of lithium chloride while keeping the ionic strength of the solvent constant.

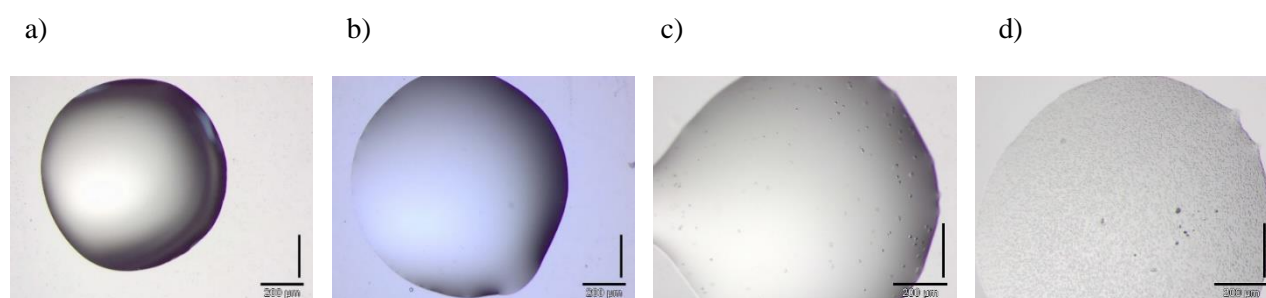


**Fig.22:** Images obtained by optical microscopy of the crystallization tests performed by using manual hanging drop between RSL-KMe<sub>2</sub> and **5**. The drop were made by 1mM protein and c)10mM of **5**, d) 20mM of **5**. Drop a) is the control with **5** alone and drop b) is the control with the protein alone. The crystallization mixtures were equilibrated over reservoir solution composed of 20% w/v polyethylene glycol 6000, 100mM tri-sodium citrate pH=4.0, 1M lithium chloride

We then performed an experiment keeping constant the polyethylene glycol 6000 and the tri-sodium citrate but replacing the 1M solution of LiCl with a 330mM solution of MgCl<sub>2</sub>. In this way, we can evaluate the effect of the cation on the crystals growth while keeping the ionic strength of the solution constant (Figure 24). The presence of salts cations can help crystallization forming salt bridges with the proteins. We then decided also to test the crystal growth between RSL-KMe<sub>2</sub> and **5** with a lower amount of MgCl<sub>2</sub> (Figure 24b).

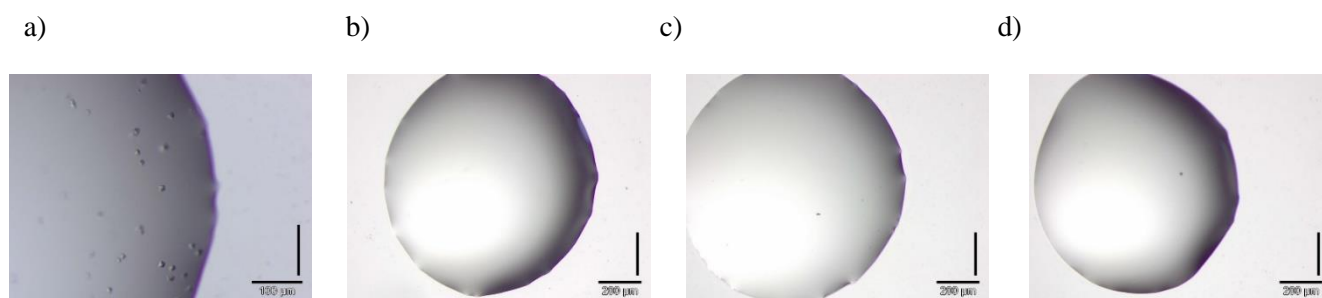


**Fig.23:** Images obtained by optical microscopy of the crystallization tests performed by using manual hanging drop between RSL-KMe<sub>2</sub> and **5**. The drop were made by 1mM protein and 10mM of **5**. The crystallization mixtures were equilibrated over reservoir solution composed of 20% w/v polyethylene glycol 6000, 100mM tri-sodium citrate pH=4.0 and a) 800mM lithium chloride, b) 600mM lithium chloride, c) 400mM lithium chloride, d) 200mM lithium chloride

As can be seen from Figure 24, it appears that the cation does not play a major role in crystal formation. In fact, when replacing 1M lithium chloride with 330mM magnesium chloride, the crystals grow in solution with a morphology very similar to those obtained with LiCl (Figure 24b). Furthermore, nucleation is favoured when magnesium chloride is present at a lower concentration (Figure 24a), resulting in the formation of many more crystals. This could be encouraging because in a complexation study, salts are used in lower concentration in respect of the crystallization of the free protein, in order to facilitate the interaction between the macromolecule and a charged ligand and then, to favour the crystallization of the complex.

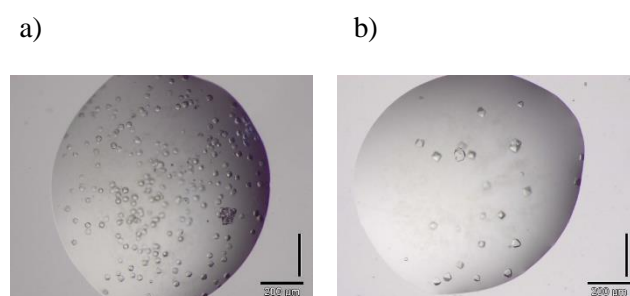


**Fig.24:** Images obtained by optical microscopy of the crystallization tests performed by using manual hanging drop between RSL-KMe<sub>2</sub> and **5**. The drop were made by 1mM protein and 10mM of **5**. The

*crystallization mixtures were equilibrated over reservoir solution composed of 20% w/v polyethylene glycol 6000, 100mM tri-sodium citrate pH=4.0 and a) 200mM magnesium chloride, b) 330mM magnesium chloride*

From a preliminary analysis it appears that crystal growth is pH dependent. In fact, for pH higher than 5.5 there is no growth of crystals. This could be explained because of the isoelectric point of this protein that is 6.5. This means that by increasing the pH we progressively deprotonate the protein and this could weaken the interaction with the anionic ligand.

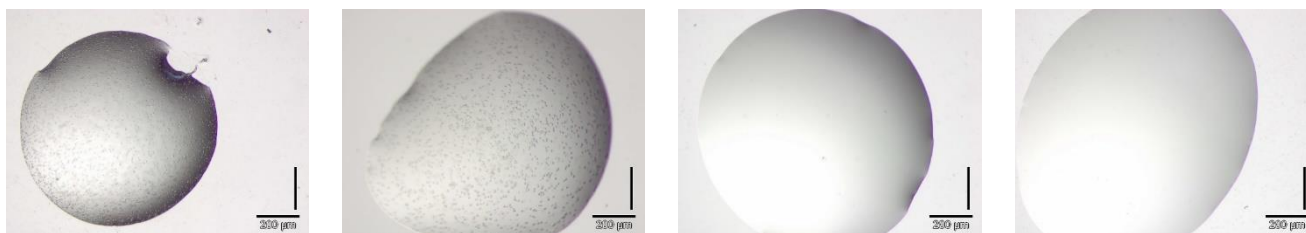


**Fig.25:** Images obtained by optical microscopy of the crystallization tests performed by using manual hanging drop between 1mM RSL-KMe<sub>2</sub> and 20mM **5**. The drops were made by 1mM protein and 10mM of **5**. The crystallization mixtures were equilibrated over reservoir solution composed of 20% w/v polyethylene glycol 6000, 1M lithium chloride and a) 100mM tri-sodium citrate pH=5, b) 100mM tri-sodium citrate pH=5.5, c) 100mM tri-sodium citrate pH=6, d) 100mM TRIS pH=8

In an attempt to improve the quality of the crystal and to obtain some of them suitable for X-ray studies, other manual hanging drop test were prepared using paraffin oil as a barrier to reduce the evaporation rate of the reservoir, in order to reduce the nucleation rate and obtained bigger crystals. In this way we obtained bigger crystals promising for the X-ray studies (Figure 26)

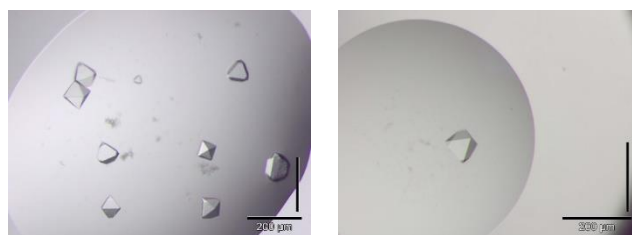


**Fig.26:** Images obtained by optical microscopy of the crystallization tests performed using a paraffin barrier between RSL-KMe<sub>2</sub> and **5**. The drop is made by 1mM protein and 20mM of ligand. The crystallization mixtures were equilibrated over reservoir solution composed of 20 % w/v polyethylene glycol 8000, 100mM tri-sodium citrate pH=6, 1M lithium chloride

We finally sent some of the crystal shown in the left picture of Figure 26 to the synchrotron in Paris and after the collection of diffraction data the structure was solved. A preliminary

study shows that the asymmetric unit comprised a trimer and a monomer of RSL-LysMe<sub>2</sub> and only one calixarenes (Figure 27). Surprisingly calixarene **5** seems to interact only with one (Lys34) out of four lysine residues. This could be due to the higher flexibility of the SO<sub>3</sub><sup>-</sup> group in **5** compared to **4** because of the presence of methylene groups between the aryl units and the SO<sub>3</sub><sup>-</sup> groups. This feature could disadvantage ligand **5** to fix the binding units according to a spatial disposition suitable to crystallize with RSL-KMe<sub>2</sub>, thus rendering trickier the complexation. Lys34 from a symmetry mate forms a cation-pi bond with the exterior of an aromatic nucleus of the calixarene. This can be seen in Figure 28 in which the symmetry mate is shown as light pink.

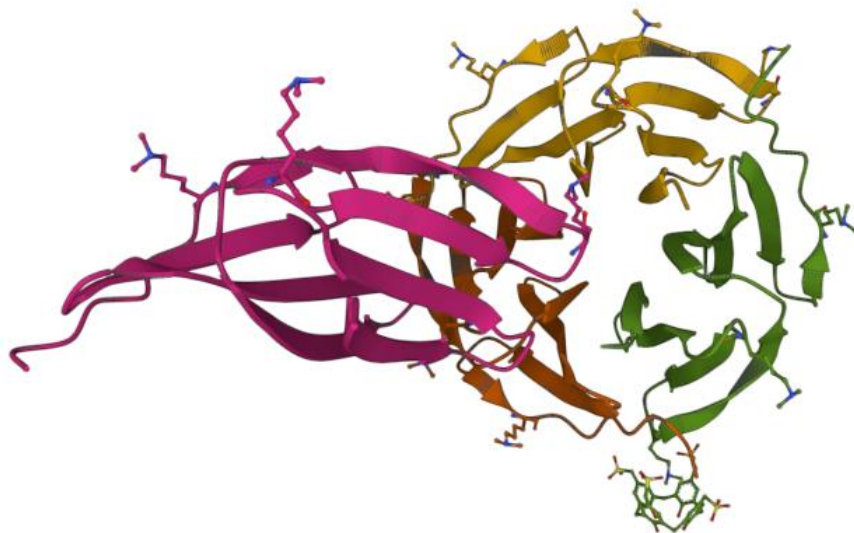


**Fig.27:** *Cartoon representation of the asymmetric unit of the complex between RSL-KMe<sub>2</sub> and **5**. Only Lys34 is encapsulated*

The encapsulated Lys34 forms cation-pi bonds with one of the aromatic rings of the calixarene and, in addition a salt bridge interaction with the two sulfonates pointing inward the cavity. Of all the lysine residues exposed on the protein surface, residue Lys34 is the most accessible one so it is not surprising that calixarene encapsulated that residue, at least.



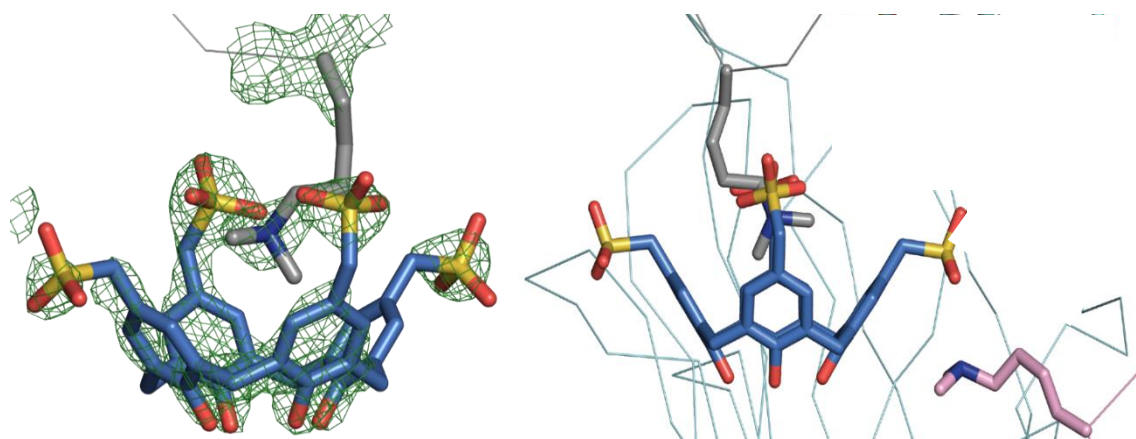


**Fig.28:** Detailed view of the **5**-LysMe<sub>2</sub> complex. a) electron density of the calixarene and Lys34Me<sub>2</sub>, b) **5** is acting as a molecular glue between two RSL-LysMe<sub>2</sub> and Lys34 from a symmetry mate forms a cation-pi bond with the calixarene **5**. The symmetry mate Lys is shown as light pink.

In another PhD thesis<sup>107</sup> the structure of a co-crystal obtained between RSL-KMe<sub>2</sub> and p-sulfonato calix[4]arene **4** was obtained. The structure (unpublished result) was solved in space group P2<sub>1</sub>2<sub>1</sub>2<sub>1</sub> by molecular replacement using PDB entry 2bt9 as a search model. Comparing the two asymmetric unit of the co-crystal obtained with **5** and that obtained with **4** shows that the latter would appear to act as better molecular glue. In fact, the asymmetric unit comprised a trimer of RSL-LysMe<sub>2</sub> and 6 units of **4** (Figure 29). Calixarene **4** mediated the interface between two protein trimers, by interacting with backbone NHs of Lys83Me<sub>2</sub> and Trp81 chain A from the symmetry related molecule



**Fig. 29.** The asymmetric unit comprises a trimer of RSL-LysMe<sub>2</sub> and 6 molecules of **4**. LysMe<sub>2</sub> and an entrapped PEG fragment and **4** are represented as sticks.

## 4.9 Conclusion

In this chapter the results obtained in the crystallizations trials between zwitterionic calix[4]arene **2,3** and **8** and RSL were shown. Unfortunately, no crystals of complexes were obtained, although a rather large screening testing different conditions was tried. In fact, all the crystals obtained during this tests proved to be either calixarene alone or ligand alone.

The use of p-methyl sulfonato calix[4]arene **5** appears to induce much more efficient crystallisation and better quality crystals than p-tetrasulfonato calix[4]arene **4** when cytochrome c was used as a model proteins. In an attempt to study the difference in solid-state binding between these two calixarene and a less cationic and more symmetrical protein, crystallization tests with RSL and **5** were performed. Unfortunately, even in this case the trials did not result in obtaining crystals from the complex. In an attempt to increase the affinity of the ligand **5** for the protein a lysine residue dimethylation reaction was carry out on the RSL. The obtained RSL-KMe<sub>2</sub> was then tested as a model protein in crystallization tests with **5**. Nice crystals were obtained in the condition fomed by 20% w/v polyethylene glycol 6000, 100mM tri-sodium citrate pH=4.0, 1M lithium chloride. After the collection of diffraction data the structure was solved. A preliminary study shows that the asymmetric unit comprised a trimer and a monomer of RSL-LysMe<sub>2</sub> and only one calixarenes. Surprisingly calixarene **5** seems to interact only with one (Lys34) out of four lysine residues. Comparing the two asymmetric unit of the co-crystal of RSL-KMe<sub>2</sub> obtained with **5** and that obtained with **4** shows that the latter would appear to act as better molecular glue. In fact, the asymmetric unit comprised a trimer of RSL-LysMe<sub>2</sub> and 6 units of **4**. Future studies will also be conducted in solution by titration NMR to see if this particular behavior is also adopted in solution as well as in solid phase.



# Experimental Part

## 4.10 Protein production

Unlabelled and  $^{15}\text{N}$ -labeled RSL were over-expressed in *Escherichia coli* BL21 and purified according to literature methods<sup>108-110</sup>. The concentration and purity of the protein were estimated by using 15% SDS polyacrylamide gel electrophoresis (SDS-PAGE) and UV-vis spectroscopy (Perkin Elmer Lambda 35). Luria-Bertani (LB) medium was prepared by dissolving in 1L of water 10 g yeast extract, 10 g N-Z amine, 5 g NaCl and then by adjusting pH to 7. LB Agar plates were prepared according to same procedure, but with the addition of 15 g Agar and 2 mM  $\text{MgSO}_4$ .  $^{15}\text{N}$  labelled minimal medium (MM) was produced with 50 mM  $\text{Na}_2\text{HPO}_4$ , 50 mM  $\text{KH}_2\text{PO}_4$ , 2g/L D-glucose, 1 g/L  $(^{15}\text{NH}_4)_2\text{SO}_4$ , 20 mM citrate, 20 mM succinate pH 7.0, 20 mL/L 50x5052, 30 mg/L Thiamine, 1  $\mu\text{L}/\text{mL}$  Carbenicillin (75 mg/mL), where 50x5052 contains 25 g glycerol, 7 mL water, 2.5 g glucose, 10 g lactose monohydrate. According to known procedures, the amino groups were dimethylated using formaldehyde and dimethylaminoborane complex<sup>111,112</sup>.

## 4.11 Stock solutions of the ligands and proteins

Stock solutions of the ligand **3** was prepared in water at pH 7.0 at a concentration of 100 mM. For ligands **2** and **8** the stock solutions were prepared in water at pH=9.5 and 8 respectively. In this way we were able to prepare a 11mM solution of **2** and a 35 mM solution of **8**. For ligand **5** a stock solution was prepared in water at pH=7 at a concentration of 50 mM. Stock solution of the proteins were prepared in a 4.5 mM solution to avoid precipitation phenomenon.

## 4.12 NMR spectroscopy

$^{15}\text{N}$ -labelled RSL-LysMe<sub>2</sub> samples were prepared to a concentration of 0.1 mM in 20mM potassium phosphate, 50 mM sodium chloride, 1.2 mM  $\alpha$ -methyl-Lfucose, 10 % D<sub>2</sub>O at pH

6.0.  $^1\text{H}$ - $^{15}\text{N}$  HSQC spectra of  $^{15}\text{N}$ -labelled RSL-LysMe<sub>2</sub> were acquired at 25 °C on a 600 MHz Varian NMR spectrometer with a HCN cold probe.

### 4.13 General experiment for the crystallization tests

The sitting drop vapour diffusion methods<sup>113-115</sup> were used for crystallization tests at 20°C. Drops for the former experimental configuration were prepared manually in 24-well plates, by mixing 1 µL volumes of the protein, the ligand and the reservoir solution. Control drops were obtained by replacing the solution of the ligand with 1 µL of water. For the general screening of all the 96 conditions we used a sparse matrix screen (JCSG++, Jena Bioscience) in sitting drop vapour diffusion format, prepared with an Oryx 8 robot (Douglas Instruments), with same strategy, but by decreasing the volumes of the combined solutions to 0.3 µL.

### 4.14 SDS-PAGE

A total of 20 µL cell/protein extract was mixed with SDS buffer and boiled at 95°C for 5 min. The purity of denatured, reduced samples were tested on 15% SDS polyacrylamide gel electrophoresis (80 minutes, 140 V). As a protein size marker 5 µL of EZ-Run™ Pre-Stained Rec Protein Ladder (Fisher BioReagents) were loaded. Coomassie Blue staining was performed as reported in literature<sup>108</sup>.

### 4.15 General procedure for the dimethylation of lysine residues on RSL

To 1 mM RSL in 50 mM KPi, 50 mM NaCl buffer pH 7.5, 20 eq of DMAB 1M is added, followed by 40 eq of a 1M H<sub>2</sub>CO solution. The reaction is left to proceed at 4°C, with some gentle mixing. After 2 h, the above additions are repeated, and the reaction is left at 4°C. After another 2 h, 10 eq of DMAB 1M is added and the reaction is left to proceed overnight (18 h) at 4°C. The reaction is quenched with 125 µL of 1M TRIS buffer, pH 7.5, and left to equilibrate for 15 minutes. The mixture is then transferred to a filtration tube, centrifuged 4 times at 4000 rpm for 30 min while topping up with distilled water, in order to get rid of the salts. Mass analysis (Agilent 6460 Triple Quadrupole LC/MS) of RSL (9726 Da) of the dimethylated protein (9838 Da) allowed to verify the complete dimethylation of all 3 lysines and of the N-terminus.

#### **4.16 X-ray diffraction and structure determination**

Crystals were transferred to the reservoir solution supplemented with 20 % glycerol as cryoprotectant. Data were collected at the SWING beamline (SOLEIL Synchrotron) using the direct injection mode. The structure was solved by molecular replacement in Phaser<sup>116</sup>.

The presence of **5** was clear in the unbiased electron density map. Iterative model building and refinement in COOT<sup>116</sup> and REFMAC<sup>117</sup> were performed

## References

- (1) Berg, J.; John L. *Biochemistry*; 2002; Vol. 5.
- (2) Gething, M.-J.; Sambrook, J. Protein Folding in the Cell. *Nature* **1992**, 355 (6355), 33–45. <https://doi.org/10.1038/355033a0>.
- (3) Herries, D. Enzyme Structure and Mechanism (Second Edition). *Biochem Educ* **1985**, 13 (3), 146. [https://doi.org/10.1016/0307-4412\(85\)90213-4](https://doi.org/10.1016/0307-4412(85)90213-4).
- (4) Medzhitov, R. Recognition of Microorganisms and Activation of the Immune Response. *Nature* **2007**, 449 (7164), 819–826. <https://doi.org/10.1038/nature06246>.
- (5) Pawson, T. Specificity in Signal Transduction. *Cell* **2004**, 116 (2), 191–203. [https://doi.org/10.1016/S0092-8674\(03\)01077-8](https://doi.org/10.1016/S0092-8674(03)01077-8).
- (6) Kim, S.-H.; Turnbull, J.; Guimond, S. Extracellular Matrix and Cell Signalling: The Dynamic Cooperation of Integrin, Proteoglycan and Growth Factor Receptor. *Journal of Endocrinology* **2011**, 209 (2), 139–151. <https://doi.org/10.1530/JOE-10-0377>.
- (7) Norton, J. D. ID Helix-Loop-Helix Proteins in Cell Growth, Differentiation and Tumorigenesis. *J Cell Sci* **2000**, 113 (22), 3897–3905. <https://doi.org/10.1242/jcs.113.22.3897>.
- (8) Varambally, S.; Dhanasekaran, S. M.; Zhou, M.; Barrette, T. R.; Kumar-Sinha, C.; Sanda, M. G.; Ghosh, D.; Pienta, K. J.; Sewalt, R. G. A. B.; Otte, A. P.; Rubin, M. A.; Chinnaiyan, A. M. The Polycomb Group Protein EZH2 Is Involved in Progression of Prostate Cancer. *Nature* **2002**, 419 (6907), 624–629. <https://doi.org/10.1038/nature01075>.
- (9) Morin, P. J. Claudin Proteins in Human Cancer: Promising New Targets for Diagnosis and Therapy. *Cancer Res* **2005**, 65 (21), 9603–9606. <https://doi.org/10.1158/0008-5472.CAN-05-2782>.
- (10) Soejima, T.; Morikawa, M.; Kimizuka, N. Holey Gold Nanowires Formed by Photoconversion of Dissipative Nanostructures Emerged at the Aqueous-Organic Interface. *Small* **2009**, 5 (18), 2043–2047. <https://doi.org/10.1002/sml.200900348>.
- (11) Cai, R.; Hashimoto, K.; Itoh, K.; Kubota, Y.; Fujishima, A. Photokilling of Malignant Cells with Ultrafine TiO<sub>2</sub> Powder. *Bull Chem Soc Jpn* **1991**, 64 (4), 1268–1273. <https://doi.org/10.1246/bcsj.64.1268>.
- (12) Giuliani, M.; Morbioli, I.; Sansone, F.; Casnati, A. Moulding Calixarenes for Biomacromolecule Targeting. *Chemical Communications* **2015**, 51 (75), 14140–14159. <https://doi.org/10.1039/C5CC05204A>.
- (13) Stites, W. E. Protein–Protein Interactions: Interface Structure, Binding Thermodynamics, and Mutational Analysis. *Chem Rev* **1997**, 97 (5), 1233–1250. <https://doi.org/10.1021/cr960387h>.
- (14) Pecuh, M. W.; Hamilton, A. D. Peptide and Protein Recognition by Designed Molecules. *Chem Rev* **2000**, 100 (7), 2479–2494. <https://doi.org/10.1021/cr9900026>.
- (15) Janin, J. Protein–Protein Recognition. *Prog Biophys Mol Biol* **1995**, 64 (2–3), 145–166. [https://doi.org/10.1016/S0079-6107\(96\)00001-6](https://doi.org/10.1016/S0079-6107(96)00001-6).
- (16) Perozzo, R.; Folkers, G.; Scapozza, L. Thermodynamics of Protein–Ligand Interactions: History, Presence, and Future Aspects. *Journal of Receptors and Signal Transduction* **2004**, 24 (1–2), 1–52. <https://doi.org/10.1081/RRS-120037896>.
- (17) Chothia, C.; Janin, J. Principles of Protein–Protein Recognition. *Nature* **1975**, 256 (5520), 705–708. <https://doi.org/10.1038/256705a0>.

- (18) Stites, W. E. Protein–Protein Interactions: Interface Structure, Binding Thermodynamics, and Mutational Analysis. *Chem Rev* **1997**, *97* (5), 1233–1250. <https://doi.org/10.1021/cr960387h>.
- (19) Yin, H.; Hamilton, A. D. Strategies for Targeting Protein-Protein Interactions With Synthetic Agents. *Angewandte Chemie International Edition* **2005**, *44* (27), 4130–4163. <https://doi.org/10.1002/anie.200461786>.
- (20) Sheng, C.; Dong, G.; Miao, Z.; Zhang, W.; Wang, W. State-of-the-Art Strategies for Targeting Protein–Protein Interactions by Small-Molecule Inhibitors. *Chem Soc Rev* **2015**, *44* (22), 8238–8259. <https://doi.org/10.1039/C5CS00252D>.
- (21) Fasting, C.; Schalley, C. A.; Weber, M.; Seitz, O.; Hecht, S.; Kokschi, B.; Dervede, J.; Graf, C.; Knapp, E.-W.; Haag, R. Multivalency as a Chemical Organization and Action Principle. *Angewandte Chemie International Edition* **2012**, *51* (42), 10472–10498. <https://doi.org/10.1002/anie.201201114>.
- (22) Baldini, L.; Casnati, A.; Sansone, F.; Ungaro, R. Calixarene-Based Multivalent Ligands. *Chem. Soc. Rev.* **2007**, *36* (2), 254–266. <https://doi.org/10.1039/B603082N>.
- (23) Jencks, W. P. On the Attribution and Additivity of Binding Energies. *Proceedings of the National Academy of Sciences* **1981**, *78* (7), 4046–4050. <https://doi.org/10.1073/pnas.78.7.4046>.
- (24) Kitov, P. I.; Bundle, D. R. On the Nature of the Multivalency Effect: A Thermodynamic Model. *J Am Chem Soc* **2003**, *125* (52), 16271–16284. <https://doi.org/10.1021/ja038223n>.
- (25) Kadam, R. U.; Bergmann, M.; Hurley, M.; Garg, D.; Cacciarini, M.; Swiderska, M. A.; Nativi, C.; Sattler, M.; Smyth, A. R.; Williams, P.; Cámara, M.; Stocker, A.; Darbre, T.; Reymond, J.-L. A Glycopeptide Dendrimer Inhibitor of the Galactose-Specific Lectin LecA and of *Pseudomonas Aeruginosa* Biofilms. *Angewandte Chemie International Edition* **2011**, *50* (45), 10631–10635. <https://doi.org/10.1002/anie.201104342>.
- (26) Ercolani, G. Assessment of Cooperativity in Self-Assembly. *J Am Chem Soc* **2003**, *125* (51), 16097–16103. <https://doi.org/10.1021/ja038396c>.
- (27) Kiessling, L. Synthetic Multivalent Ligands in the Exploration of Cell-Surface Interactions. *Curr Opin Chem Biol* **2000**, *4* (6), 696–703. [https://doi.org/10.1016/S1367-5931\(00\)00153-8](https://doi.org/10.1016/S1367-5931(00)00153-8).
- (28) Harris, D. C.; Saks, B. R.; Jayawickramarajah, J. Protein-Binding Molecular Switches via Host–Guest Stabilized DNA Hairpins. *J Am Chem Soc* **2011**, *133* (20), 7676–7679. <https://doi.org/10.1021/ja2017366>.
- (29) Du, X.; Li, Y.; Xia, Y.-L.; Ai, S.-M.; Liang, J.; Sang, P.; Ji, X.-L.; Liu, S.-Q. Insights into Protein–Ligand Interactions: Mechanisms, Models, and Methods. *Int J Mol Sci* **2016**, *17* (2), 144. <https://doi.org/10.3390/ijms17020144>.
- (30) Russo Krauss, I.; Merlino, A.; Vergara, A.; Sica, F. An Overview of Biological Macromolecule Crystallization. *Int J Mol Sci* **2013**, *14* (6), 11643–11691. <https://doi.org/10.3390/ijms140611643>.
- (31) Gavira, J. A. Current Trends in Protein Crystallization. *Arch Biochem Biophys* **2016**, *602*, 3–11. <https://doi.org/10.1016/j.abb.2015.12.010>.
- (32) McPherson, A. Review Current Approaches to Macromolecular Crystallization. In *EJB Reviews 1990*; Springer Berlin Heidelberg: Berlin, Heidelberg, 1990; pp 49–71. [https://doi.org/10.1007/978-3-642-76168-3\\_4](https://doi.org/10.1007/978-3-642-76168-3_4).
- (33) Raaijmakers, H. C. A.; Versteegh, J. E.; Uitdehaag, J. C. M. The X-Ray Structure of RU486 Bound to the Progesterone Receptor in a Destabilized Agonistic Conformation. *Journal of*



- Biological Chemistry* **2009**, *284* (29), 19572–19579. <https://doi.org/10.1074/jbc.M109.007872>.
- (34) Bolanos-Garcia, V. M.; Chayen, N. E. New Directions in Conventional Methods of Protein Crystallization. *Prog Biophys Mol Biol* **2009**, *101* (1–3), 3–12. <https://doi.org/10.1016/j.pbiomolbio.2009.12.006>.
- (35) Luft, J. R.; Collins, R. J.; Fehrman, N. A.; Lauricella, A. M.; Veatch, C. K.; DeTitta, G. T. A Deliberate Approach to Screening for Initial Crystallization Conditions of Biological Macromolecules. *J Struct Biol* **2003**, *142* (1), 170–179. [https://doi.org/10.1016/S1047-8477\(03\)00048-0](https://doi.org/10.1016/S1047-8477(03)00048-0).
- (36) Bijelic, A.; Rompel, A. Polyoxometalates: More than a Phasing Tool in Protein Crystallography. *ChemTexts* **2018**, *4* (3), 10. <https://doi.org/10.1007/s40828-018-0064-1>.
- (37) Chayen, N. E. Comparative Studies of Protein Crystallization by Vapour-Diffusion and Microbatch Techniques. *Acta Crystallogr D Biol Crystallogr* **1998**, *54* (1), 8–15. <https://doi.org/10.1107/S09074444997005374>.
- (38) Benvenuti, M.; Mangani, S. Crystallization of Soluble Proteins in Vapor Diffusion for X-Ray Crystallography. *Nat Protoc* **2007**, *2* (7), 1633–1651. <https://doi.org/10.1038/nprot.2007.198>.
- (39) Cudney, R.; Patel, S.; Weisgraber, K.; Newhouse, Y.; McPherson, A. Screening and Optimization Strategies for Macromolecular Crystal Growth. *Acta Crystallogr D Biol Crystallogr* **1994**, *50* (4), 414–423. <https://doi.org/10.1107/S09074444994002660>.
- (40) Korczyńska, J.; Hu, T.-C.; Smith, D. K.; Jenkins, J.; Lewis, R.; Edwards, T.; Brzozowski, A. M. Microscale Vapour Diffusion for Protein Crystallization. *Acta Crystallogr D Biol Crystallogr* **2007**, *63* (9), 1009–1015. <https://doi.org/10.1107/S09074444907037857>.
- (41) Giuliani, M.; Morbioli, I.; Sansone, F.; Casnati, A. Correction: Moulding Calixarenes for Biomacromolecule Targeting. *Chemical Communications* **2015**, *51* (82), 15208–15208. <https://doi.org/10.1039/C5CC90427G>.
- (42) Sansone, F.; Baldini, L.; Casnati, A.; Ungaro, R. Calixarenes: From Biomimetic Receptors to Multivalent Ligands for Biomolecular Recognition. *New Journal of Chemistry* **2010**, *34* (12), 2715. <https://doi.org/10.1039/c0nj00285b>.
- (43) Nimse, S. B.; Kim, T. Biological Applications of Functionalized Calixarenes. *Chem. Soc. Rev.* **2013**, *42* (1), 366–386. <https://doi.org/10.1039/C2CS35233H>.
- (44) Danylyuk, O.; Suwinska, K. Solid-State Interactions of Calixarenes with Biorelevant Molecules. *Chemical Communications* **2009**, No. 39, 5799. <https://doi.org/10.1039/b910331g>.
- (45) Casnati, A.; Sansone, F.; Ungaro, R. Peptido- and Glycocalixarenes: Playing with Hydrogen Bonds around Hydrophobic Cavities. *Acc Chem Res* **2003**, *36* (4), 246–254. <https://doi.org/10.1021/ar0200798>.
- (46) Groenen, L. C.; Ruël, B. H. M.; Casnati, A.; Verboom, W.; Pochini, A.; Ungaro, R.; Reinhoudt, D. N. Synthesis of Monoalkylated Calix[4]Arenes via Direct Alkylation. *Tetrahedron* **1991**, *47* (39), 8379–8384. [https://doi.org/10.1016/S0040-4020\(01\)96179-4](https://doi.org/10.1016/S0040-4020(01)96179-4).
- (47) van Duynhoven, J. P. M.; Janssen, R. G.; Verboom, W.; Franken, S. M.; Casnati, A.; Pochini, A.; Ungaro, R.; de Mendoza, J.; Nieto, P. M. Control of Calix[6]Arene Conformations by Self-Inclusion of 1,3,5-Tri-O-Alkyl Substituents: Synthesis and NMR Studies. *J Am Chem Soc* **1994**, *116* (13), 5814–5822. <https://doi.org/10.1021/ja00092a036>.

- (48) Giuliani, M.; Morbioli, I.; Sansone, F.; Casnati, A. Correction: Moulding Calixarenes for Biomacromolecule Targeting. *Chemical Communications* **2015**, *51* (82), 15208–15208. <https://doi.org/10.1039/C5CC90427G>.
- (49) Zadnarm, R.; Alavijeh, N. S. Protein Surface Recognition by Calixarenes. *RSC Adv.* **2014**, *4* (78), 41529–41542. <https://doi.org/10.1039/C4RA05181E>.
- (50) *Calixarenes and Beyond*; Neri, P., Sessler, J. L., Wang, M.-X., Eds.; Springer International Publishing: Cham, 2016. <https://doi.org/10.1007/978-3-319-31867-7>.
- (51) Perret, F.; Coleman, A. W. Biochemistry of Anionic Calix[n]Arenes. *Chemical Communications* **2011**, *47* (26), 7303. <https://doi.org/10.1039/c1cc11541c>.
- (52) Bogan, A. A.; Thorn, K. S. Anatomy of Hot Spots in Protein Interfaces. *J Mol Biol* **1998**, *280* (1), 1–9. <https://doi.org/10.1006/jmbi.1998.1843>.
- (53) Sebti, S. M.; Hamilton, A. D. Design of Growth Factor Antagonists with Antiangiogenic and Antitumor Properties. *Oncogene* **2000**, *19* (56), 6566–6573. <https://doi.org/10.1038/sj.onc.1204121>.
- (54) Hamuro, Y.; Calama, M. C.; Park, H. S.; Hamilton, A. D. A Calixarene with Four Peptide Loops: An Antibody Mimic for Recognition of Protein Surfaces. *Angewandte Chemie International Edition in English* **1997**, *36* (23), 2680–2683. <https://doi.org/10.1002/anie.199726801>.
- (55) Wei, Y.; McLendon, G. L.; Case, M. A.; Purring, C. B.; Yu, T.; Hamilton, A. D.; Lin, Q.; Park, H. S.; Lee, C.-S. Disruption of Protein–Protein Interactions: Design of a Synthetic Receptor That Blocks the Binding of Cytochrome c to Cytochrome c Peroxidase. *Chemical Communications* **2001**, No. 17, 1580–1581. <https://doi.org/10.1039/b104142h>.
- (56) Takashima, H.; Shinkai, S.; Hamachi, I. Ru(Bpy)<sub>3</sub>-Based Artificial Receptors toward a Protein Surface: Selective Binding and Efficient Photoreduction of Cytochrome c. *Chemical Communications* **1999**, No. 23, 2345–2346. <https://doi.org/10.1039/a907642e>.
- (57) Sun, J.; Wang, D.; Jain, R. K.; Carie, A.; Paquette, S.; Ennis, E.; Blaskovich, M. A.; Baldini, L.; Coppola, D.; Hamilton, A. D.; Sebti, S. M. Inhibiting Angiogenesis and Tumorigenesis by a Synthetic Molecule That Blocks Binding of Both VEGF and PDGF to Their Receptors. *Oncogene* **2005**, *24* (29), 4701–4709. <https://doi.org/10.1038/sj.onc.1208391>.
- (58) Ikeda, A.; Shinkai, S. Novel Cavity Design Using Calix[ n ]Arene Skeletons: Toward Molecular Recognition and Metal Binding. *Chem Rev* **1997**, *97* (5), 1713–1734. <https://doi.org/10.1021/cr960385x>.
- (59) McGovern, R. E.; Fernandes, H.; Khan, A. R.; Power, N. P.; Crowley, P. B. Protein Camouflage in Cytochrome c–Calixarene Complexes. *Nat Chem* **2012**, *4* (7), 527–533. <https://doi.org/10.1038/nchem.1342>.
- (60) McGovern, R. E.; McCarthy, A. A.; Crowley, P. B. Protein Assembly Mediated by Sulfonatocalix[4]Arene. *Chem. Commun.* **2014**, *50* (72), 10412–10415. <https://doi.org/10.1039/C4CC04897K>.
- (61) McGovern, R. E.; Snarr, B. D.; Lyons, J. A.; McFarlane, J.; Whiting, A. L.; Paci, I.; Hof, F.; Crowley, P. B. Structural Study of a Small Molecule Receptor Bound to Dimethyllysine in Lysozyme. *Chem Sci* **2015**, *6* (1), 442–449. <https://doi.org/10.1039/C4SC02383H>.
- (62) Martos, V.; Bell, S. C.; Santos, E.; Isacoff, E. Y.; Trauner, D.; de Mendoza, J. Calix[4]Arene-Based Conical-Shaped Ligands for Voltage-Dependent Potassium Channels. *Proceedings of*

- the National Academy of Sciences* **2009**, *106* (26), 10482–10486. <https://doi.org/10.1073/pnas.0813396106>.
- (63) Joerger, A. C.; Fersht, A. R. The Tumor Suppressor P53: From Structures to Drug Discovery. *Cold Spring Harb Perspect Biol* **2010**, *2* (6), a000919–a000919. <https://doi.org/10.1101/cshperspect.a000919>.
- (64) Gordo, S.; Martos, V.; Vilaseca, M.; Menéndez, M.; de Mendoza, J.; Giralt, E. On the Role of Flexibility in Protein-Ligand Interactions: The Example of P53 Tetramerization Domain. *Chem Asian J* **2011**, *6* (6), 1463–1469. <https://doi.org/10.1002/asia.201000938>.
- (65) Lee, R. T.; Lee, Y. C. Affinity Enhancement by Multivalent Lectin-Carbohydrate Interaction. *Glycoconj J* **2000**, *17* (7/9), 543–551. <https://doi.org/10.1023/A:1011070425430>.
- (66) Cecioni, S.; Lalor, R.; Blanchard, B.; Praly, J.-P.; Imberty, A.; Matthews, S.; Vidal, S. Achieving High Affinity towards a Bacterial Lectin through Multivalent Topological Isomers of Calix[4]Arene Glycoconjugates. *Chemistry - A European Journal* **2009**, *15* (47), 13232–13240. <https://doi.org/10.1002/chem.200901799>.
- (67) Boukerb, A. M.; Rousset, A.; Galanos, N.; Méar, J.-B.; Thépaut, M.; Grandjean, T.; Gillon, E.; Cecioni, S.; Abderrahmen, C.; Faure, K.; Redelberger, D.; Kipnis, E.; Dessein, R.; Havet, S.; Darblade, B.; Matthews, S. E.; de Bentzmann, S.; Guéry, B.; Cournoyer, B.; Imberty, A.; Vidal, S. Antiadhesive Properties of Glycoclusters against *Pseudomonas Aeruginosa* Lung Infection. *J Med Chem* **2014**, *57* (24), 10275–10289. <https://doi.org/10.1021/jm500038p>.
- (68) McGovern, R. E.; Snarr, B. D.; Lyons, J. A.; McFarlane, J.; Whiting, A. L.; Paci, I.; Hof, F.; Crowley, P. B. Structural Study of a Small Molecule Receptor Bound to Dimethyllysine in Lysozyme. *Chem Sci* **2015**, *6* (1), 442–449. <https://doi.org/10.1039/C4SC02383H>.
- (69) Larda, S. T.; Bokoch, M. P.; Evanics, F.; Prosser, R. S. Lysine Methylation Strategies for Characterizing Protein Conformations by NMR. *J Biomol NMR* **2012**, *54* (2), 199–209. <https://doi.org/10.1007/s10858-012-9664-z>.
- (70) McGovern, R. E.; Snarr, B. D.; Lyons, J. A.; McFarlane, J.; Whiting, A. L.; Paci, I.; Hof, F.; Crowley, P. B. Structural Study of a Small Molecule Receptor Bound to Dimethyllysine in Lysozyme. *Chem Sci* **2015**, *6* (1), 442–449. <https://doi.org/10.1039/C4SC02383H>.
- (71) Rodriguez-Valera, F.; Lillo, J. G. Halobacteria as Producers of Polyhydroxyalkanoates. *FEMS Microbiol Lett* **1992**, *103* (2–4), 181–186. <https://doi.org/10.1111/j.1574-6968.1992.tb05836.x>.
- (72) Sudakevitz, D.; Kostlánová, N.; Blatman-Jan, G.; Mitchell, E. P.; Lerrer, B.; Wimmerová, M.; Katcoff, D. J.; Imberty, A.; Gilboa-Garber, N. A New *Ralstonia Solanacearum* High-Affinity Mannose-Binding Lectin RS-IIL Structurally Resembling the *Pseudomonas Aeruginosa* Fucose-Specific Lectin PA-IIL. *Mol Microbiol* **2004**, *52* (3), 691–700. <https://doi.org/10.1111/j.1365-2958.2004.04020.x>.
- (73) Arnaud, J.; Tröndle, K.; Claudinon, J.; Audfray, A.; Varrot, A.; Römer, W.; Imberty, A. Membrane Deformation by Neolactins with Engineered Glycolipid Binding Sites. *Angewandte Chemie International Edition* **2014**, *53* (35), 9267–9270. <https://doi.org/10.1002/anie.201404568>.
- (74) Kostlánová, N.; Mitchell, E. P.; Lortat-Jacob, H.; Oscarson, S.; Lahmann, M.; Gilboa-Garber, N.; Chambat, G.; Wimmerová, M.; Imberty, A. The Fucose-Binding Lectin from *Ralstonia Solanacearum*. *Journal of Biological Chemistry* **2005**, *280* (30), 27839–27849. <https://doi.org/10.1074/jbc.M505184200>.
- (75) Beshara, C. S.; Jones, C. E.; Daze, K. D.; Lilgert, B. J.; Hof, F. A Simple Calixarene Recognizes Post-Translationally Methylated Lysine. *ChemBioChem* **2009**, *11* (1), 63–66. <https://doi.org/10.1002/cbic.200900633>.

- (76) Bernstein, B. E.; Mikkelsen, T. S.; Xie, X.; Kamal, M.; Huebert, D. J.; Cuff, J.; Fry, B.; Meissner, A.; Wernig, M.; Plath, K.; Jaenisch, R.; Wagschal, A.; Feil, R.; Schreiber, S. L.; Lander, E. S. A Bivalent Chromatin Structure Marks Key Developmental Genes in Embryonic Stem Cells. *Cell* **2006**, *125* (2), 315–326. <https://doi.org/10.1016/j.cell.2006.02.041>.
- (77) Taverna, S. D.; Li, H.; Ruthenburg, A. J.; Allis, C. D.; Patel, D. J. How Chromatin-Binding Modules Interpret Histone Modifications: Lessons from Professional Pocket Pickers. *Nat Struct Mol Biol* **2007**, *14* (11), 1025–1040. <https://doi.org/10.1038/nsmb1338>.
- (78) Huang, J.; Sengupta, R.; Espejo, A. B.; Lee, M. G.; Dorsey, J. A.; Richter, M.; Opravil, S.; Shiekhhattar, R.; Bedford, M. T.; Jenuwein, T.; Berger, S. L. P53 Is Regulated by the Lysine Demethylase LSD1. *Nature* **2007**, *449* (7158), 105–108. <https://doi.org/10.1038/nature06092>.
- (79) Mafacki, J.; Aileni, V. K.; Ho, A. Y. Y.; Schwarz, J.; Moen, A.; Sørensen, V.; Nilges, B. S.; Jakobsson, M. E.; Leidel, S. A.; Falnes, P. Ø. The Novel Lysine Specific Methyltransferase METTL21B Affects MRNA Translation through Inducible and Dynamic Methylation of Lys-165 in Human Eukaryotic Elongation Factor 1 Alpha (EEF1A). *Nucleic Acids Res* **2017**, gkx002. <https://doi.org/10.1093/nar/gkx002>.
- (80) Lee, J.; Perez, L.; Liu, Y.; Wang, H.; Hooley, R. J.; Zhong, W. Separation of Methylated Histone Peptides via Host-Assisted Capillary Electrophoresis. *Anal Chem* **2018**, *90* (3), 1881–1888. <https://doi.org/10.1021/acs.analchem.7b03969>.
- (81) Carlson, S. M.; Gozani, O. Nonhistone Lysine Methylation in the Regulation of Cancer Pathways. *Cold Spring Harb Perspect Med* **2016**, *6* (11), a026435. <https://doi.org/10.1101/cshperspect.a026435>.
- (82) Yi, X.; Jiang, X.-J.; Li, X.-Y.; Jiang, D.-S. Histone Methyltransferases: Novel Targets for Tumor and Developmental Defects. *Am J Transl Res* **2015**, *7* (11), 2159–2175.
- (83) Crowley, P. B. Protein–Calixarene Complexation: From Recognition to Assembly. *Acc Chem Res* **2022**, *55* (15), 2019–2032. <https://doi.org/10.1021/acs.accounts.2c00206>.
- (84) Arena, G.; Casnati, A.; Contino, A.; Magrì, A.; Sansone, F.; Sciotto, D.; Ungaro, R. Inclusion of Naturally Occurring Amino Acids in Water Soluble Calix[4]Arenes: A Microcalorimetric and <sup>1</sup>H NMR Investigation Supported by Molecular Modeling. *Org. Biomol. Chem.* **2006**, *4* (2), 243–249. <https://doi.org/10.1039/B514896K>.
- (85) Douteau-Guével, N.; Perret, F.; Coleman, A. W.; Morel, J.-P.; Morel-Desrosiers, N. Binding of Dipeptides and Tripeptides Containing Lysine or Arginine by P-Sulfonatocalixarenes in Water: NMR and Microcalorimetric Studies. *Journal of the Chemical Society, Perkin Transactions 2* **2002**, No. 3, 524–532. <https://doi.org/10.1039/b109553f>.
- (86) Memmi, L.; Lazar, A.; Brioude, A.; Ball, V.; Coleman, A. W. Protein–Calixarene Interactions: Complexation of Bovine Serum Albumin by Sulfonatocalix[n]Arenes. *Chemical Communications* **2001**, No. 23, 2474–2475. <https://doi.org/10.1039/b109190p>.
- (87) Douteau-Guével, N.; Coleman, A. W.; Morel, J.-P.; Morel-Desrosiers, N. Complexation of the Basic Amino Acids Lysine and Arginine by Three Sulfonatocalix[n]Arenes (n = 4, 6 and 8) in Water: Microcalorimetric Determination of the Gibbs Energies, Enthalpies and Entropies of Complexation. *Journal of the Chemical Society, Perkin Transactions 2* **1999**, No. 3, 629–634. <https://doi.org/10.1039/a806855k>.
- (88) Buschmann, H.-J.; Mutihac, L.; Schollmeyer, E. Complexation of Some Amino Acids and Peptides by P-Sulfonatocalix[4]Arene and Hexasodium p-Sulfonatocalix[6]Arene in Aqueous Solution. *J Incl Phenom Macrocycl Chem* **2003**, *46* (3/4), 133–137. <https://doi.org/10.1023/A:1026361017680>.
- (89) Mutihac, L.; Buschmann, H.-J.; Mutihac, R.-C.; Schollmeyer, E. Complexation and Separation of Amines, Amino Acids, and Peptides by Functionalized Calix[n]Arenes. *J Incl Phenom Macrocycl Chem* **2005**, *51* (1–2), 1–10. <https://doi.org/10.1007/s10847-004-5098-x>.
- (90) Beshara, C. S.; Jones, C. E.; Daze, K. D.; Lilgert, B. J.; Hof, F. A Simple Calixarene Recognizes Post-Translationally Methylated Lysine. *ChemBioChem* **2009**, *11* (1), 63–66. <https://doi.org/10.1002/cbic.200900633>.

- (91) Rypniewski, W. R.; Holden, H. M.; Rayment, I. Structural Consequences of Reductive Methylation of Lysine Residues in Hen Egg White Lysozyme: An x-Ray Analysis at 1.8-Å Resolution. *Biochemistry* **1993**, *32* (37), 9851–9858. <https://doi.org/10.1021/bi00088a041>.
- (92) White, H. D.; Rayment, I. Kinetic Characterization of Reductively Methylated Myosin Subfragment 1. *Biochemistry* **1993**, *32* (37), 9859–9865. <https://doi.org/10.1021/bi00088a042>.
- (93) Rayment, I. [12] Reductive Alkylation of Lysine Residues to Alter Crystallization Properties of Proteins; 1997; pp 171–179. [https://doi.org/10.1016/S0076-6879\(97\)76058-0](https://doi.org/10.1016/S0076-6879(97)76058-0).
- (94) Moore, G. R.; Cox, M. C.; Crowe, D.; Osborne, M. J.; Rosell, F. I.; Bujons, J.; Barker, P. D.; Mauk, M. R.; Mauk, A. G. N Epsilon,N Epsilon-Dimethyl-Lysine Cytochrome c as an NMR Probe for Lysine Involvement in Protein-Protein Complex Formation. *Biochem J* **1998**, *332* ( Pt 2), 439–449. <https://doi.org/10.1042/bj3320439>.
- (95) Zhang, M.; Thulin, E.; Vogel, H. J. Reductive Methylation And pKa Determination of the Lysine Side Chains in Calbindin D9k. *J Protein Chem* **1994**, *13* (6), 527–535. <https://doi.org/10.1007/BF01901534>.
- (96) Gober, I. N.; Waters, M. L. Supramolecular Affinity Labeling of Histone Peptides Containing Trimethyllysine and Its Application to Histone Deacetylase Assays. *J Am Chem Soc* **2016**, *138* (30), 9452–9459. <https://doi.org/10.1021/jacs.6b02836>.
- (97) Beaver, J. E.; Waters, M. L. Molecular Recognition of Lys and Arg Methylation. *ACS Chem Biol* **2016**, *11* (3), 643–653. <https://doi.org/10.1021/acscchembio.5b00996>.
- (98) McGovern, R. E.; Snarr, B. D.; Lyons, J. A.; McFarlane, J.; Whiting, A. L.; Paci, I.; Hof, F.; Crowley, P. B. Structural Study of a Small Molecule Receptor Bound to Dimethyllysine in Lysozyme. *Chem Sci* **2015**, *6* (1), 442–449. <https://doi.org/10.1039/C4SC02383H>.
- (99) Minaker, S. A.; Daze, K. D.; Ma, M. C. F.; Hof, F. Antibody-Free Reading of the Histone Code Using a Simple Chemical Sensor Array. *J Am Chem Soc* **2012**, *134* (28), 11674–11680. <https://doi.org/10.1021/ja303465x>.
- (100) Bontempi, N.; Biavardi, E.; Bordiga, D.; Candiani, G.; Alessandri, I.; Bergese, P.; Dalcanale, E. Probing Lysine Mono-Methylation in Histone H3 Tail Peptides with an Abiotic Receptor Coupled to a Non-Plasmonic Resonator. *Nanoscale* **2017**, *9* (25), 8639–8646. <https://doi.org/10.1039/C7NR02491F>.
- (101) Faggi, E.; Pérez, Y.; Luis, S. v.; Alfonso, I. Supramolecular Protection from the Enzymatic Tyrosine Phosphorylation in a Polypeptide. *Chemical Communications* **2016**, *52* (52), 8142–8145. <https://doi.org/10.1039/C6CC03875A>.
- (102) Eloisa Tosi. Methylsulfonate and Methylphosphonate Functionalized Calix[4]Arenes for the Complexation of Ammonium Salts, University of Parma, Parma, 2021.
- (103) Alex, J. M.; Rennie, M. L.; Volpi, S.; Sansone, F.; Casnati, A.; Crowley, P. B. Phosphonated Calixarene as a “Molecular Glue” for Protein Crystallization. *Cryst Growth Des* **2018**, *18* (4), 2467–2473. <https://doi.org/10.1021/acs.cgd.8b00092>.
- (104) Goh, C. Y.; Becker, T.; Brown, D. H.; Skelton, B. W.; Jones, F.; Mocerino, M.; Ogden, M. I. Self-Inclusion of Proline-Functionalised Calix[4]Arene Leads to Hydrogelation. *Chemical Communications* **2011**, *47* (21), 6057. <https://doi.org/10.1039/c1cc11286d>.
- (105) McPherson, A. Current Approaches to Macromolecular Crystallization. *Eur J Biochem* **1990**, *189* (1), 1–23. <https://doi.org/10.1111/j.1432-1033.1990.tb15454.x>.
- (106) Hassell, A. M.; An, G.; Bledsoe, R. K.; Bynum, J. M.; Carter, H. L.; Deng, S.-J. J.; Gampe, R. T.; Grisard, T. E.; Madauss, K. P.; Nolte, R. T.; Rocque, W. J.; Wang, L.; Weaver, K. L.; Williams, S. P.; Wisely, G. B.; Xu, R.; Shewchuk, L. M. Crystallization of Protein–Ligand Complexes. *Acta Crystallogr D Biol Crystallogr* **2007**, *63* (1), 72–79. <https://doi.org/10.1107/S09074444906047020>.
- (107) Francesca Guagnini. Molecular Recognition, Metal Coordination and Self-Assembly with Macrocyclic Receptors and Multidentate Pyridine Ligands, University of Parma, Parma, 2018.

- (108) Studier, F. W. Protein Production by Auto-Induction in High-Density Shaking Cultures. *Protein Expr Purif* **2005**, *41* (1), 207–234. <https://doi.org/10.1016/j.pep.2005.01.016>.
- (109) Volkov, A. N.; Vanwetswinkel, S.; van de Water, K.; van Nuland, N. A. J. Redox-Dependent Conformational Changes in Eukaryotic Cytochromes Revealed by Paramagnetic NMR Spectroscopy. *J Biomol NMR* **2012**, *52* (3), 245–256. <https://doi.org/10.1007/s10858-012-9607-8>.
- (110) Crowley, P. B.; Chow, E.; Papkovskaia, T. Protein Interactions in the Escherichia Coli Cytosol: An Impediment to In-Cell NMR Spectroscopy. *ChemBioChem* **2011**, *12* (7), 1043–1048. <https://doi.org/10.1002/cbic.201100063>.
- (111) Larda, S. T.; Bokoch, M. P.; Evanics, F.; Prosser, R. S. Lysine Methylation Strategies for Characterizing Protein Conformations by NMR. *J Biomol NMR* **2012**, *54* (2), 199–209. <https://doi.org/10.1007/s10858-012-9664-z>.
- (112) Rypniewski, W. R.; Holden, H. M.; Rayment, I. Structural Consequences of Reductive Methylation of Lysine Residues in Hen Egg White Lysozyme: An x-Ray Analysis at 1.8-Å Resolution. *Biochemistry* **1993**, *32* (37), 9851–9858. <https://doi.org/10.1021/bi00088a041>.
- (113) Russo Krauss, I.; Merlino, A.; Vergara, A.; Sica, F. An Overview of Biological Macromolecule Crystallization. *Int J Mol Sci* **2013**, *14* (6), 11643–11691. <https://doi.org/10.3390/ijms140611643>.
- (114) McPherson, A. Review Current Approaches to Macromolecular Crystallization. In *EJB Reviews 1990*; Springer Berlin Heidelberg: Berlin, Heidelberg, 1990; pp 49–71. [https://doi.org/10.1007/978-3-642-76168-3\\_4](https://doi.org/10.1007/978-3-642-76168-3_4).
- (115) Hassell, A. M.; An, G.; Bledsoe, R. K.; Bynum, J. M.; Carter, H. L.; Deng, S.-J. J.; Gampe, R. T.; Grisard, T. E.; Madauss, K. P.; Nolte, R. T.; Rocque, W. J.; Wang, L.; Weaver, K. L.; Williams, S. P.; Wisely, G. B.; Xu, R.; Shewchuk, L. M. Crystallization of Protein–Ligand Complexes. *Acta Crystallogr D Biol Crystallogr* **2007**, *63* (1), 72–79. <https://doi.org/10.1107/S0907444906047020>.
- (116) Emsley, P.; Cowtan, K. *Coot* : Model-Building Tools for Molecular Graphics. *Acta Crystallogr D Biol Crystallogr* **2004**, *60* (12), 2126–2132. <https://doi.org/10.1107/S0907444904019158>.
- (117) Murshudov, G. N.; Skubák, P.; Lebedev, A. A.; Pannu, N. S.; Steiner, R. A.; Nicholls, R. A.; Winn, M. D.; Long, F.; Vagin, A. A. *REFMAC 5* for the Refinement of Macromolecular Crystal Structures. *Acta Crystallogr D Biol Crystallogr* **2011**, *67* (4), 355–367. <https://doi.org/10.1107/S0907444911001314>.